Redesigning the Austroads creep procedure for the evaluation of permanent deformation of asphalt pavements in Australia

A Thesis submitted by

Esmaeil Ahmadinia

B Eng (Civil Engineering)

M Eng (Civil Engineering – Highway and Transportation)

For the award of

Doctor of Philosophy at the

University of Southern Queensland

School of Civil Engineering and Surveying

2017

ABSTRACT

The broad spectrum of dynamic creep tests developed over the last decade around the world is one of the more significant innovations in the prediction and analysis of the behaviour of asphalt pavements. Although current laboratory creep test methods have good potential for evaluating permanent plastic deformation of asphalt mixtures, there are serious concerns about their abilities to provide any precise prediction of asphalt susceptibility to permanent plastic deformation. These concerns have arisen when creep test outcomes have been unsuccessfully compared with data from field assessments.

In response to the critical questions about the adequacy of the various unconfined creep tests to predict permanent plastic deformation of asphalt, many researchers have been attempting to develop methods to improve laboratory test methods. It has been hypothesised that by providing a lateral pressure around the laboratory specimens, it would be possible to better simulate field conditions and obtain more relevant creep test outcomes.

In this study, a new methodology is explored to provide effective confinement for asphalt creep specimens. The proposed methodology is founded on the current Australian test, adapted to provide simulated field conditions. Finite Element Method (FEM) modelling is employed in the study to provide a formative view about the overall study. It is used to develop a correlation between the new confined test and in situ pavement conditions.

It has been established that the new confined dynamic creep test method (CDCT) is a superior test for duplicating in-situ conditions than the existing test methods. Outcomes of the study indicate that the CDCT will significantly decrease existing shortcomings associated with the existing Australian creep test. It is concluded that the CDCT is a much improved test method that better represents in-situ conditions and it

can be used as a methodology for evaluating permanent deformation of asphaltic pavements.

Certification of Thesis

This thesis is entirely the work of *Esmaeil Ahmadinia* except where otherwise acknowledged. The work is original and has not previously been submitted for any other award, except where acknowledged.

Student and supervisors signatures of endorsement are held at USQ.

Professor Frank Bullen

Principal Supervisor

Professor Ron Ayers

Associate Supervisor

Professor John Yeaman

Associate Supervisor

ACKNOWLEDGEMENTS

First I would like to thank my supervisors Professor Frank Bullen, Professor Ron Ayers, and Professor John Yeaman for giving me the opportunity to work under their supervision, valuable advice, supporting assistance and continued guidance during this research.

My thanks also go to the Brisbane City Council and the Eagle Farm Asphalt Plant, especially Dr Gregory John Stephenson and Troy Akers for their assistance throughout my experimental works. I acknowledge Professor John Worden for the professional proofreading advice.

I appreciate my family, to whom I owe a big debt of gratitude for their support during my entire life.

TABLE OF CONTENTS

LIST OF FIGURES

LIST OF TABLES

LIST OF SYMBOLS

$\dot{\varepsilon_0}$	Basis strain rate
ε_1	Delayed deformation at recovery phase
ε_0	Instantaneous deformation at recovery phase
$\dot{\varepsilon}$	Shear rate
ε_i	Strain amplitude at load cycle i
ε_t	The tensile strain at the bottom of the asphalt layer
ε_v	The compressive vertical strain on the surface of subgrade
ε_p	Total plastic strain
ε_e	Elastic strain (recoverable and time-independent)
ε_o	Creep strain
ε_{pn}	Permanent strain due to single load application
ε_r	Resilient strain
ε_{sum}	Elastic deformations summation
ε_{ve}	Viscoelastic strain (recoverable and time-dependent)
ε_{vp}	Viscoelastic strain (irrecoverable and time-dependent)
$\varepsilon_{vp,ini}^{0}$	The initial permanent strain
ε_0, ρ, b	Regression coefficients
ρ_w	Water density at 25°C
ρ_{bulk}	Bulk density of the compacted mix (t/m^3)
ρ_{max}	Maximum density of the mix (t/m^3)
σ_0	Constant shear stress

σ_d	Deviator stress (psi) determined at the middle layer depth
σ_i	Stress amplitude at load cycle i
λ_2	Retardation time
η_1, η_2	Viscosity of two dashpot parts in the Burgers model
$\theta_1 \; and \; \theta_3$	Primary and tertiary strain
$\frac{d\varepsilon}{dt}$	Time derivative of strain
ϕ_i	Phase angle between the stress and strain wave signals
$\delta(T)$	Temperature function
A_a	Material property, function of resilient modulus and applied
C_f	The final crack length
C_o	The starter flaw
D_o	Instantaneous compliance
D′	Viscoelastic compliance component at any time
D(t)	Total compliance component at any time
E_1 , E_2	Elastic moduli of two spring parts in the Burgers model
f_1 , f_2 , f_3 , f_4 , f_5	The regression coefficients.
G_0 and K_0	Instantaneous shear and volumetric modulus, respectively
G_i, K_i, and τ_i	Prony series parameters stress
H_{ini}	The initial hardening of a specimen
h_{ac}	Thickness of asphalt concrete layer
$I_H(t_l, t_r, \sigma_d)$	Incremental hardening due to one load cycle
$I_{vp}(t_l, t_r, \sigma_d)$	Incremental permanent strain due to one load cycle
k_1, k_2, k_3	Regression coefficients

m_1	The mass of the pycnometer and lid (grams)
m_2	Mass in air of the saturated specimen (grams)
m_3	Mass in water of the specimen (grams)
m_4	The mass of the pycnometer, lid, test portion and water (grams)
n_p	Slope of the creep compliance curve
N_f	Number of load repetitions to cracking
N_r	The permissible load cycles number for preventing rutting
P_{eff}	Effective asphalt volume
t_l	Load time
t_2	Time at the end of recovery phase
t_r	Rest period
V_a	Air voids (%)
V_b	Effective binder content (%)
V_v	Volume of air voids
Vis	Viscosity at 21^{O}C (in poises $\times 10^6$) water at 25^{o}C
W_i	Dissipated energy at load cycle i
$\bar{x}$	The mean of values

ABBREVIATIONS

AAPA	Australian Asphalt Pavement Association
AC	Asphalt Concrete
ADINA	Automatic Dynamic Incremental Nonlinear Analysis
ALF	Accelerated Loading Facilities
ARRB	Australian Road Research Board
AS	Australian Standard
BCC	Brisbane City Council
BISAR	Bitumen Stress Analysis in Road
BS	British Standard
CAMA	Computer Aided Mixture Design
CDCT	Confined Dynamic Creep Test
CFD	Computational Fluid Dynamics
CV	Coefficient of Variation
DEM	Discrete Element Method
EDCT	Existing Australian Dynamic Creep Test
ELSYM	Elastic Layered System computer program
EN	European Standard
EVA	Ethyl-Vinyl-Acetate
FEM	Finite Element Method
FHWA	Federal Highway Administration
HMA	Hot Mix Asphalt
IPC	Industrial Process Controls
M-E	Mechanistic-Empirical
MG	Multigrade
MLET	Multilayer Elastic Theory
OBC	Optimum Bitumen Content
PG	Performance Grade

PMB	Polymer Modified Bitumen
PTT	Partial Triaxial Test
PV	Plateau Value
Q	Queensland Department of Transport and Main Roads specifications
RAP	Reclaimed Asphalt Pavement
RLPD	Repeated Load Permanent Deformation
SBR	Styrene-Butadiene Rubber
SBS	Styrene-Butadiene-Styrene
SCDCT	Semi-Confined Dynamic Creep Test
SHRP	Strategic Highway Research Program
TRL	Transport Research Laboratory
TRTs	Triaxial Repeated load Tests
UK	United Kingdom
USA	United States of America
UTS	Universal Testing Machine
VESYS	Viscoelastic layered-pavement analysis program
VFB	Voids Filled with Bitumen
VIM	Voids In the Mix
VMA	Voids In Mineral Aggregate

CHAPTER 1

INTRODUCTION

1.1 Introduction

Australia has 1,690,000 kilometres of public accessible roads, which is one of the largest networks in the world, especially on a per capita head basis. Governments spend significant amounts of funding (in present values more than $4.7 billion) for maintaining road networks (Shrapnel 2011). Asphalt is used widely in the urban environment parts of the network and for example over 10 million tonnes of asphalt has been produced yearly at a price of over $1 billion (Huang & Zhang 2010). A decrease in asphalt maintenance costs will provide significant saving to the country.

The continuing growth in the quantity and magnitude of vehicle axle loads on road pavements has resulted in increased stresses in pavements. One of the major modes of pavement distress is creep deformation as illustrated in figure 1.1. Creep deformation of a flexible pavement is the time-dependent accumulation of strain generated by repeated traffic loads, especially when heavy and slow vehicular loads occur (Öztürk 2007). After a load is removed from a pavement, some portion of the deformation may be recovered while another portion accumulates in the asphalt as creep.

The development of creep in asphalt is associated with a range of factors including ambient temperature, load duration, stress levels, material properties and mix design. To adequately cater for asphalt deformation in the mix design process potential, field performance of a mix must be able to be evaluated within the laboratory and predictive relationships established. The laboratory test conditions need to comply as closely as possible with the conditions of the pavement in the field.

The broad spectrum of dynamic creep tests developed over the last decade around the world is one of the more recent significant innovations in the prediction and analysis of behaviour of asphalt pavements. For any creep test to be widely attractive and

accepted it must be reasonably simple to execute and also incorporate repeated loading that simulates traffic effects.

Figure: 1.1 Permanent deformation of asphalt mixture (Building-Science 2016)

However, several questions have been raised around the world about the capability of existing creep tests to effectively predict asphalt susceptibility to permanent deformation in-situ. The source of such questioning emanates from the different estimations of dynamic creep from laboratory tests compared to the collected data from in-situ pavement monitoring (Butcher & Lindsell 1996). One problem with using existing dynamic creep tests is that they do not accurately simulate the conditions of the pavement in the field (Aksoy & Iskender 2008; Huang & Zhang 2010). The main cause of a dynamic creep test's inability to adequately predict asphalt in-situ behaviour is attributed to its use of an unconfined sample condition compared to an in-situ asphalt mixture being confined by the surrounding asphalt that provides lateral restraint (Butcher & Lindsell 1996).

It is considered that by providing a measure of confinement around dynamic creep samples it would be possible to provide improved results, which will correlate better with field tests, permitting better prediction of rut resistance. Several ways of providing lateral resistance have been tried in previous studies. For example, triaxial cells have been used to provide a pulsed (cyclic) vertical stress with either a static or pulsed lateral pressure. However, these tests often have proved either too difficult and time consuming to run, or did not yield results that differed significantly from the standard unconfined test (Butcher & Lindsell 1996).

This research aims to improve the suite of existing dynamic creep test methodologies by providing an appropriate confining pressure. Confining pressure will be provided by applying a hoop stress via a ring arrangement around the sample, augmented by using smaller loading platen sizes (figure 1.2), which create a restraint annulus of asphalt. These conditions will provide a much improved simulation of field conditions.

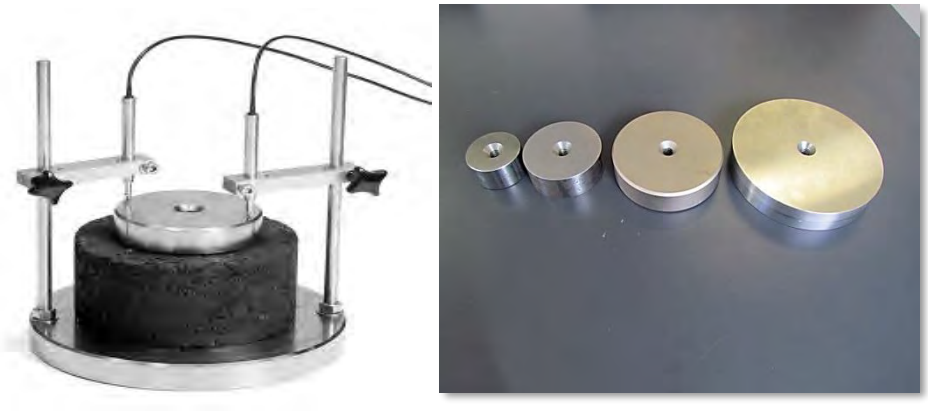

Figure: 1.2 Different platen sizes

Creep deformation is one prevalent failure of asphalt pavements. It has very undesirable effects on road performance, such as safety of road users (e.g. loss of control of vehicles) and riding comfort (Sohm et al. 2012). This type of pavement distress has necessitated the expenditure of millions of dollars on repairing and maintaining roads. While there is an existing range of techniques to evaluate and analyse permanent deformation of an asphalt mixture, all have their own disadvantages. The lack of precise methods to evaluate rut potential and design asphalt mixtures has created a challenge for road designers and researchers. Hence, new research to advance and redesign laboratory permanent deformation assessment of asphalt mixture is required.

1.2 Research hypothesis

The overarching research hypothesis is: “The existing Australian dynamic creep test can be redesigned to more accurately predict in-situ permanent deformation of asphalt”.

The hypothesis is first examined through an exhaustive stand alone, international literature summary that is also embedded throughout the thesis to provide context and relevance. The literature review was scrutinised to identify the deficiencies within the current creep testing methodologies and a new innovative stress responsive confinement system conceived. The system's authenticity was validated through finite element modelling and an extensive series of laboratory testing followed which involved the development of new criteria for evaluating creep potential.

1.3 The research

The study investigated the permanent deformation of asphalt mixtures by redesigning the existing Australian dynamic creep test procedure. In order to increase the accuracy of the test, this study was intended to replicate field conditions (confining pressure) in the laboratory. The research introduced a new method of applying lateral pressure for the dynamic creep test by employing a stress responsive confining ring around the sample, and different platen and sample sizes to provide a confining annulus of asphalt. The research would provide a new and improved laboratory evaluative procedure for industry to investigate and design creep resistant asphalt mixes.

The research extended the use of the existing Australian standard by the use of a full or quasi confining stress to better replicate field conditions. Quasi-confinement by use of smaller platen on an oversize asphalt sample has been explored with mixed success previously by Bullen and Preston (Bullen & Preston 1992) and Austroads (Oliver et al. 1995). Later Nunn (Nunn et al. 1998) proposed the extension of the Nottingham Asphalt Tester using a similar approach. That work has been encapsulated in the current European standard EN12697-25A using a 96 mm diameter platen with 150 mm diameter specimens. It is worth noting that Austroads (Oliver et al. 1995) found that radial splitting (bursting) occurred for the arrangement recommended in EN 12697-25A due to the lack of an adequate confining annulus of asphalt.

The intent of this research was to extend the earlier research by exploring the platen to sample diameter effects through modelling and experimental work. This work was augmented by the use of a hoop stress applied through a confining ring, similar in geometry to that used in Geomechanics for odometer testing (soil consolidation).

Similar to asphalt fatigue modelling, the complex stress distributions within the small laboratory specimens, and the different loading types and magnitudes in the field make it difficult to replicate field rutting in the laboratory. With appropriate numerical modelling it was considered that it would be possible to develop a calibrated model that would assist with field rutting prediction similar to that now widely used in fatigue analysis and mechanistic design.

The study also involved modelling of laboratory and in-situ conditions using Abaqus modelling software. This part modelled in-situ and laboratory test situations, including the effects of variable factors such as loads, confining conditions and boundary conditions.

1.4 Format of the thesis

The research is presented as follows:

- Chapter one: The chapter introduces the study topic and scope of the study. This includes the problem statement and motivations for the study, and the main aims of the study are presented.

- Chapter two: This chapter is an overview on the performance of asphalt as a structural layer, while including terminology, asphalt composition, factors affecting pavement service life, asphalt failures modes and mix design.

- Chapter three: The related literature on the permanent deformation of asphalt is discussed with emphasis on creep parameters. Here, several mathematical and mechanical models for explaining viscoelastic behaviour of asphalt are presented.

- Chapter four: In this chapter, a new methodology is explored to provide confinement for asphalt specimens. The chapter first considers key relevant previous research related to the adopted methodology and then progresses to a more detailed explanation of laboratory testing methods for aggregates,

bitumen, and developing a new prototype for providing a stress responsive confinement are discussed.

- Chapter five: Here the author discusses the FEM models employed for the study. A brief review on FEM and Abaqus modelling software has provided for the processes employed to create the models required for the research. Finally, outcomes of the models are discussed compared to each other and to those outcomes of experimental tests.

- Chapter six: This chapter provides details of the experimental work undertaken including the effects of test parameters such as air voids, sample/platen diameter ratios, asphalt mix type and confining conditions on creep.

- Chapter seven: This chapter considers the modelling and laboratory relationships. Stress distribution on the confined laboratory specimens were evaluated and stresses compared with the stresses in the geometrically corresponding point of the models.

- Chapter eight: In this chapter, an overarching discussion is provided on the outcomes. Some of the more significant modelling and laboratory outcomes have been effectively discussed in this chapter.

- Chapter nine: In this chapter the main findings of the study have been presented. A summary of study outcomes with some recommendations for further work are presented.

CHAPTER 2

ASPHALT AS A STRUCTURAL PAVEMENT ELEMENT

2.1 Introduction

The optimal performance of an asphaltic concrete (asphalt) as a structural pavement layer is a function of its components, the operating environment and its functional design within the pavement structure. A precise selection of materials and accurate design of the asphalt mixture, with due consideration of environmental conditions, is essential to maximise service life of the mixture.

Asphalt is a manufactured engineering composite material consisting of aggregate, fillers, bituminous binder, air voids and some specific additives. It is manufactured by a range of methods dependent on it being a “hot” or “cold” mix. Hot mixed asphalt is produced in batch or continuous mixing plants and placed and compacted in a hot plastic state. Cold mixed products are typically manufactured using emulsion and used for maintenance activities, although materials such as Grave are used in structural layers. In-situ recycling can also be undertaken to produce a form of asphalt. This thesis is concerned with hot mix asphalt.

2.2 Terminology

A wide spectrum of terms and definitions is used within road engineering science around the world and it is worth setting out same key definitions here. In this thesis, the terms normally used in Australia are depicted in figure 2.1 (Sharp 2009). Definitions and roles of some important pavement elements are discussed below (AS-1348.1 1986; Stephenson 2002):

- *Road*. A way trafficable by motor-powered vehicles, including footpaths and the public right-of-way between abutting property boundaries.

- *Pavement*. That section of a roadway located above the subgrade level for the support of, and to form a running surface for, vehicular traffic.

- *Course*. Any single layer within pavement structure.

- *Layer*. The portion of one pavement material placed and compacted as a unit.

- *Wearing course (or surface course).* The uppermost section of the road pavement structure which directly accommodates the traffic.

- *Binder course or (intermediate course)*. A course between the surface course and basecourse.

- *Basecourse (or base or roadbase).* The structural course of a pavement composed of one or more layers of materials. Basecourse typically consists of natural gravel, stabilized materials, crushed stone, fine broken rock, and for heavy duty pavements, Portland cement or asphalt concrete.

- *Sub-base*. The materials between the subgrade and the basecourse that enables efficient and effective load transfer.

-*Subgrade (or basement or roadbed or substrate)*. The prepared and trimmed formation on which the pavement is built.

- *Formation*. The finished earthworks surface, without cutting or filling batters.

-*Asphalt*. The mixture of aggregate and bituminous binder, with or without additives, blended through heating. Some other names for the same product around the globe are "hot mix asphalt (HMA)", "asphalt concrete (AC)", and "asphalt mix", "asphalt paving mix" "bituminous mixture (BC)", "bituminous concrete", "bituminous paving mix".

-*Binder (or asphaltic binder, or asphalt cement).* A coherent material used for holding solid particles together in the asphalt mixture. It is usually straight run bitumen, polymer modified bitumen (PMB), or multigrade bitumen.

- *Bitumen*. Defined as a black sticky liquid or solid material that is both viscoelastic and non-corrosive. It essentially consists of hydrocarbons and their derivatives and softens steadily while heated. Bitumen is extracted from natural asphalt or by refinery processes of crude oil.

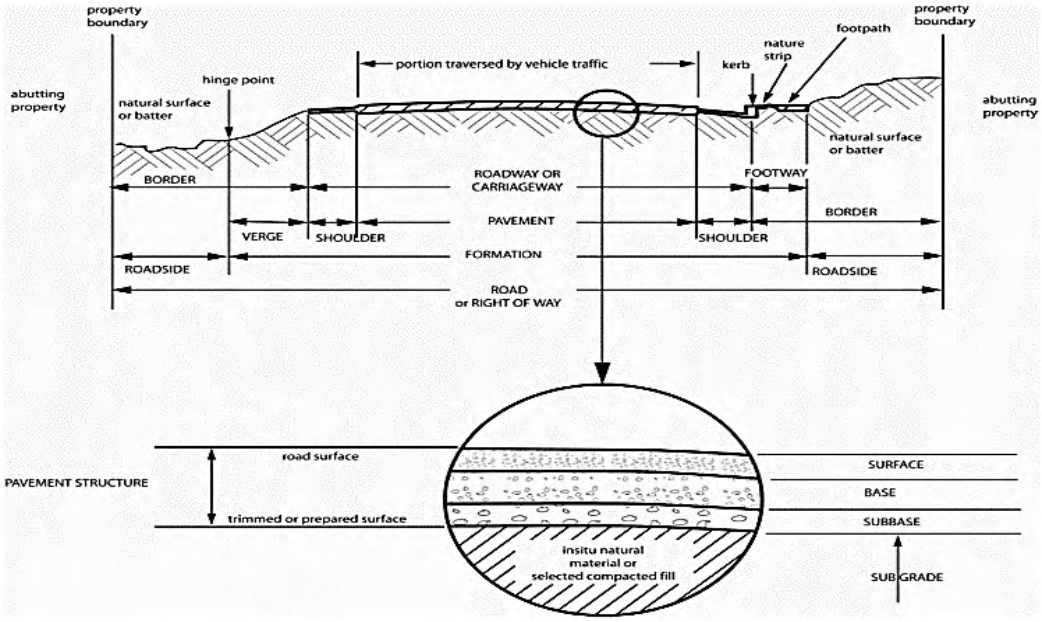

Figure: 2.1 Pavement elements (Sharp 2009)

2.3 Road pavements

A road pavement should be a strong and durable structure, designed for bearing high vehicular loads. Road pavements are categorized into the main groups of flexible and rigid. A flexible pavement consists of aggregate, and bitumen/asphalt and its total structure deflects under loading. A rigid pavement usually contains a Portland cement concrete slab. Flexible pavements are more widely employed throughout the globe as they have good riding quality and are usually cheaper to construct in comparison to concrete pavements for low to medium design traffic.

Flexible pavements, with thin surfacing, transfer vehicular loads to the lower layers by particle-to-particle load transfer within the pavement granular structure. Traffic stresses are then distributed over a wider area, which result in a pressure decrease with depth in flexible pavements. Conventional granular layered flexible pavement, and full-depth asphalt pavement are both types of flexible pavements albeit that the load transfer mechanisms vary.

In a rigid pavement, axle loads are transmitted by a concrete slab action. The concrete's high modulus of elasticity, flexural strength and rigidity enables it to distribute traffic loads over a wider area of subgrade. Figure 2.2 shows the axle load distribution for flexible and rigid pavements. Some of the main types of rigid pavements are; jointed plain concrete pavement, jointed reinforced concrete pavement, and pre-stressed concrete pavement.

As outlined above the main difference between flexible and rigid pavements is in their method of stress redistribution. Wheel stresses are transmitted based on a layered system in flexible pavements, while maximum portion of loads in rigid pavements are carried by slab action (Mathew & Rao 2007). The use of stabilised road pavements and full depth composite asphalt has led to the application of new terms such as semi-rigid or semi-flexible pavements (Transport engineering 2013).

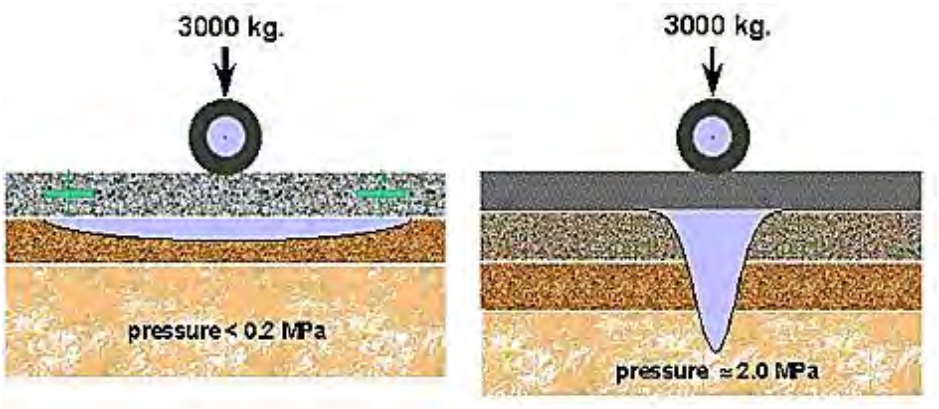

Figure: 2.2 Load distribution in layers of flexible (right) and rigid pavement (left) (Smith et al. 2001)

2.4 Asphalt composition

Asphalt component materials in a flexible pavement may either be mixed in hot or cold state. In hot mix (HMA) aggregates and bitumen binder are mixed through heating and then placed and compacted while the mixture is in a plastic state (elevated temperature).

Hot mix asphalt typically consists of 95% aggregate by weight, while bitumen binder makes up around 5% of the mixture. By volume, a typical asphalt mixture contains approximately 85% mineral aggregate, 10% bitumen binder and around 5% air voids (NCHRP 2011). Figure 2.3 shows a compacted asphalt mixture proportion by weight and volume.

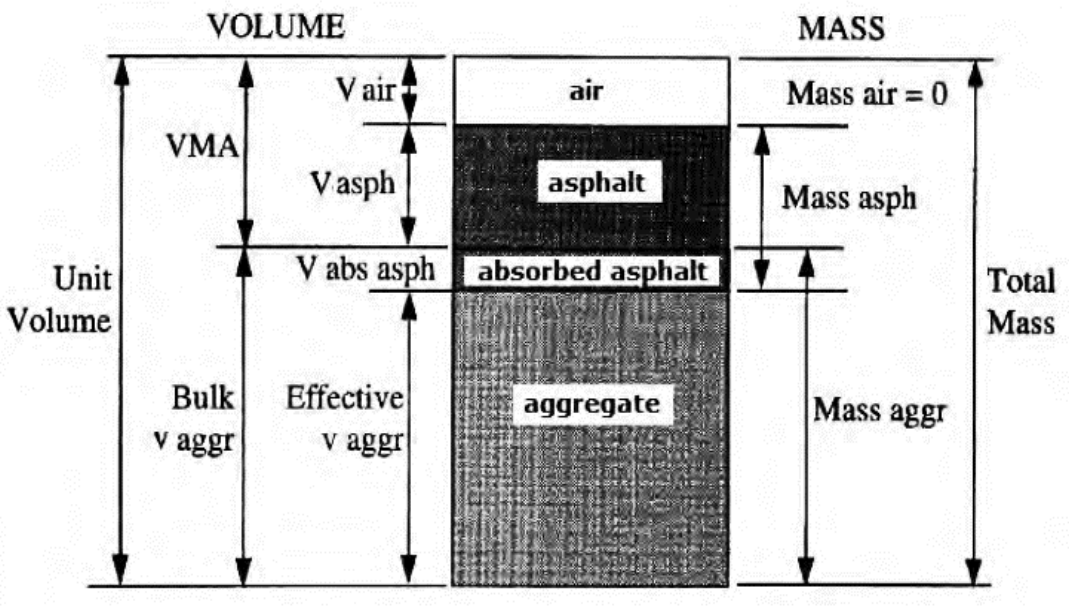

Figure: 2.3 Volume/ Weight relationships in an asphalt mixture (Vazquez et al. 2010)

2.4.1 Aggregate

As previously mentioned, aggregates constitute up to 95% of the mass of an asphalt mixture, therefore its quality and characteristics exert considerable influence on performance of the mixture. Primary functions of the aggregate are; ensuring stability to the asphalt mixture via interlocking between its particles, providing an appropriate surface texture with suitable polish and skid resistance, appropriate spreading of traffic loads to the lower layers of the pavement, and providing a durable pavement without degradation and failure under wheel loads (Rebbechi 2014). The quality control of aggregate for asphalt mixture can generally be specified by the particle grading, particle size and shape, surface texture, angularity, absorption, particle density, abrasion resistance, resistance to polishing, toughness and durability, and cleanliness (Rebbechi 2014).

Aggregate are categorised into the two main groups of coarse aggregate and fine aggregate. The portion of aggregate remaining on the sieve 4.75 mm (sieve no 4) is defined as coarse aggregate, and the portion passing the sieve 4.75 mm and remaining on the sieve 0.075 mm (sieve no 200) is defined as fine aggregate. The main roles of the coarse aggregate are to carry and transmit traffic loads to other layers, and provide a deformation-resistance in the mixture, while fine aggregates particles complete the overall aggregate structure by generating a support structure for void spaces in the mixture. Without inclusion of fine aggregate, many air voids would remain in the asphalt mixture (Vavrik 2000).

The most common source for providing aggregate is igneous rocks that include dolerite, granite, basalt, andesite, rhyolite, diorite, and porphyry. Metamorphic rocks such as, schists, hornfels, gneisses, and quartzites are also employed as asphalt mixture aggregates. Aggregate can be gained through some recycling of materials, and by-products of some industrial processes, such as calcined bauxite, and industrial slag. Reclaimed asphalt pavement (RAP), crushed recycled concrete, crumb rubber, and crushed glass are some examples of recycled materials used as asphalt mixture aggregate (Rebbechi 2014).

2.4.2 Bitumen

Bitumen is a visco-elastic material produced from crude oil distillation in the petroleum refinement process. Adhesive, impermeable, modifiable, recyclable, and durable, are some interesting properties of bitumen that make it a capable engineering material. As appraised by Eurobitumen and Asphalt Institute, the recent production of bitumen in the world is around 87 million tonnes yearly (Asphalt-Institute 2015). As depicted in the figure 2.4 around 85% percent of the produced bitumen in the world is used for paving the surfaces of roads. The features that have made bitumen such an ideal material in the road engineering sector are waterproofing, ductility, flexibility, weathering resistance and good adhesion for bonding materials in the asphalt mixture (Rebbechi 2014; Asphalt-Institute 2015). Bitumen needs to be temporarily altered to a liquid form to be mixed, placed and compacted.

There are many types of bitumens used in asphalt. Whilst conventional unmodified bitumen is the most common type of binder, multigrade bitumen, polymer modified bitumen (PMBs), cutback bitumen and bituminous emulsions are also important types of bituminous binders. Multigrade bitumen is less sensitive to temperature fluctuations and classified based on a range of features expected at both low and high service temperatures. In PMBs, various types of polymers can be added in the bitumen for enhancing pavement performance under traffic loads. In cutback bitumen, cutter and flux oils are employed for extending available time between manufacturing and compacting the asphalt (Rebbechi 2014). Asphalt manufactured with emulsion can be placed cold.

In the United States and Europe, bitumen specifications were primarily based on hardness and viscosity tests until the 1990s. After that, the performance grade (PG) system for grading bitumen was introduced as an outcome of the Strategic Highway Research Program (SHRP) (Monographs 2013). Penetration grading system still applies in Europe and in some other nations such as New Zealand, bitumen is graded by a penetration test at 25 °C. In Australia, bitumen is classified based on its viscosity at 60 °C as shown in Table 2.1.

Table: 2.1 Bitumen classes (AS 2008)

Formal grade designation	Informal name	Viscosity at 60 °C (Pa.s)	
		Pre RTFO treatment	Post RTFO treatment
Class 170	C170	140–200	N/A
Class 240	C240	190–280	N/A
Class 320	C320	260–380	N/A
Class 450	C450	N/A	750–1150
Class 600	C600	500–700	N/A
Multigrade 500	M500	400–600	N/A
Multigrade 1000	M1000	N/A	3500–6500

Figure: 2.4 Bitumen use in the world (Asphalt-Institute 2015)

2.4.3 Fillers

Filler refers to the portion of aggregate particles passing the 0.075mm sieve (sieve no 200) and retain on pan (Zulkati et al. 2012; Rebbechi 2014). Fillers are primary employed for reducing voids in the mixture. Small particles of the filler blend with the bitumen and provide a stiff mastic that can improve the stiffness of the mixture. The greater portion of the filler works as aggregate and fills voids in the mixture (Mahan 2013).

There is a range of reasons for adding fillers. Some of the most significant effects of filler are: reducing optimum binder content, increasing final mixture stability, increasing resilient modulus of mixture, improving bond between aggregate and binder, increasing the resistance of the binder mortar to flow and meeting aggregate gradation (Zulkati et al. 2012; Mahan 2013; Rebbechi 2014). However, the excessive use of filler can be a negative as it increases the proportion of binder required for coating aggregates, resulting in a too stiff mixture and decreasing workability of the mixture (Zulkati et al. 2012).

Typically fillers are mineral aggregate powders, waste material powders and industrials material powders. The most common available fillers are hydrated lime, rock flour, cement kiln dust, limestone powder, Portland cement, mineral sludge, ground slag, fly ash, recycled brick powder, and baghouse dust (Zulkati et al. 2012; Rebbechi 2014).

2.4.4 Additives

In many environments an unmodified bituminous binder does not offer the required performance for asphalt pavements that are subjected to heavy wheel loads and extreme climatic conditions. In order to enable asphalt mixtures to gain specific engineering characteristics, additives can be either added to the bitumen binder or the asphalt mixture. Bitumen modification commenced in Europe in the early 1930s, and was first employed in America in the 1950s (Ahmadinia 2012).

The main reasons for using modified bitumen in asphalt are to obtain a softer mixture (less brittle) at low ambient temperatures for minimising cracking and improving fatigue life of the pavements, and for providing a stiffer mixture at high ambient temperatures to resist rutting. Increasing stiffness and strength can also enable a reduction in the thickness of the pavement and is another important reason to consider the use of additives in the mixture.

Additives can be categorised according to their compositions, such as polymers (elastomeric and plastomeric), anti-stripping agents and hydrocarbons. Table 2.2 provides a list of common asphalt modifiers and their purposes.

2.4.5 Air voids

Air voids in an asphalt mixture are very small air spaces trapped between coated aggregate particles in the mixture. The optimal amount of air voids in an asphalt mixture is vital to certify that a durable mixture is constructed. Too low a quantity of air voids can lead to asphalt mixture deterioration such as rutting, flushing or shoving. Too high an amount of air voids can result in water damage, air damage, ravelling, rutting and cracking in the mixture. The percentage of air voids for dense- graded asphalt mixture should not be less than 3% and also should not be more than 8% (Brown et al. 2004).

Table: 2.2 Types of additives (after (Roque et al. 2005)

Type of Modifier	Purpose	Example
Elastomers	- Increase stiffness at higher temperatures. -Increase elasticity at medium range temperatures to resist fatigue cracking. - Decrease stiffness at lower temperatures to resist thermal cracking.	-Natural rubber -Styrene-butadiene-styrene (SBS) -Styrene-butadiene rubber (SBR).
Fiber	-Improves tensile strength -Improve cohesion -Allow for higher asphalt content without drain down	- Polyester -Fiber glass
Plastomers (Thermoplast)	-Increase high temperature performance -Increase structural strength -Increase resistance to rutting	-Polyvinyl chloride (PVC) -Ethyl-vinyl-acetate(EVA) -Ethylene propylene (EPDM)
Oxidant	Increased stiffness after placement	- Manganese salts
Hydrocarbons (Natural Asphalts)	- Restore aged asphalts - Increase stiffness	- Oils - Natural asphalts (Lake Asphalt) - Gilsonite
Anti-strippers	- Minimize binder stripping	- Lime - Amines
Antioxidant	- Increase durability by retarding oxidation	- Carbons - Calcium salts
Extender	- Decreases the amount of asphalt cement needed (typically 20 - 35% of total asphalt binder)	- Sulphur - Lignin

Figures 2-5 to 2-7 show the effects of air void contents on fatigue life (or mixture resistance to cracking under traffic loads), rutting resistance and structural strength of asphalt mixture. As shown in figure 2.5, fatigue life is a function of air content of the

mixture and may be reduced by 50% by increasing air voids from 5% to 8%. Figure 2.6, shows that low and high air void content may greatly impact on the permanent deformation of asphalt. As shown in figure 2.7, the structural strength of a mixture, as measured by its modulus (an indication of stiffness) has a direct relationship with air content of the mixture and a 20% reduction in asphalt stiffness (or load-carrying capacity) may occur by increasing air voids from 5% to 8% (Austroads 2013).

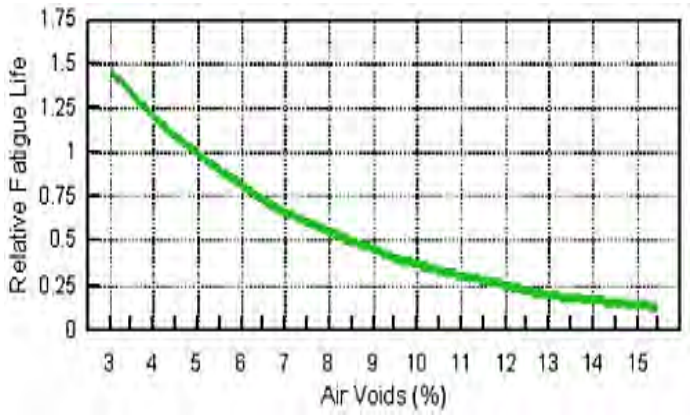

Figure: 2.5 Relative Fatigue Life vs. Air Voids (Austroads 2013)

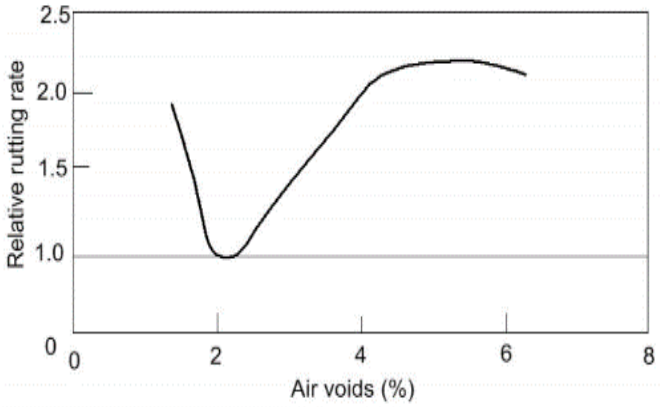

Figure: 2.6 Relative Rutting Rate vs. Air Voids (Austroads 2013)

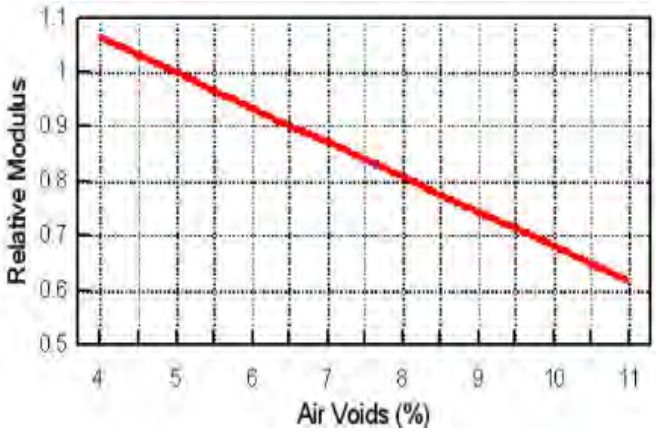

Figure: 2.7 Relative Modulus vs. Air Voids (Austroads 2013)

2.5 Asphalt pavement deterioration and failure modes

Deterioration in asphalt mixtures is very common and all asphalt pavements experience some type of distress during their service life. Asphalt failures can start immediately after paving a road, and even with ideal construction conditions, failures can arise after the first months. Many various reasons exist for pavement deterioration where the most significant are; temperature fluctuations, high axle/wheel loads, weather conditions, construction deficiencies and using improper materials. The common types of asphalt pavement failure are described below:

Fatigue cracking (or crocodile cracking); appears at the asphalt pavement caused by fatigue cracking as a result of heavy and repeated wheel loads. It manifested as a series of interconnected cracks (like the skin of a *crocodile*).

Edge cracking; is a longitudinal crack that take place typically within 0.5m of the edge of a pavement. Insufficient lateral support from the shoulder, inadequate drainage, and growing vegetation around the edge of pavement are the main reasons for edge cracking in the pavement.

Block cracking; is a series of large interconnected rectangular shape cracks on the surface of the asphalt pavement. The spacing of block cracks range in size typically

from under 0.5m up to 3m. Shrinkage due to temperature fluctuations and stiff pavement surface is the most important reason of block cracking.

Longitudinal and Transverse cracking; Longitudinal cracking is a linear crack parallel to the centreline axis of the pavement, while transverse cracks are predominantly perpendicular to the centreline axis. Harsh climates, shrinkage in asphalt mixes, poor constructions and underlying layer cracks are causes of these types of pavement distresses.

Slippage cracking; this type of crack has a crescent shape and develops on the part of the pavement that is subjected to more automobile stopping or turning. This distress is caused mostly by poor bonding between pavement layers and materials.

Ravelling; appears as a wearing away of the asphalt pavement surface. Losing bitumen binder in the asphalt mixture can lead to separation between mixture particles and consequently dislodging of aggregate. Poor quality of the mixture and excessively stiff bitumen binder are said to be the main reasons for ravelling.

Potholes; pothole failure is a bowl shaped hole appearing in the surface of the pavement. Potholes can be a continuation of other deterioration of the pavement such as fatigue cracks and ravelling over a long period of time.

Stripping; is attributed to breaking of the bond and a loss of adhesion between the bitumen binder and aggregate due to moisture in the asphalt mixture.

Bleeding or Flushing; is an accumulation of a thin film of bitumen binder on the surface of the road pavement. Excessive binder content in the mixture is the main reason for bleeding.

Rutting; it is discussed in detail later.

2.6 Fatigue

Fatigue cracking is one of the primary failure modes in asphaltic mixtures that is basically caused by repeated traffic loads. Over more than 40 years of asphalt technology, it was assumed that because of the bending function of the asphalt layer while developing flexural stresses, fatigue cracking merely commences at the bottom of the asphalt layer and then spreads up the layer (bottom-up fatigue cracking). Recent studies (NCHRP 2004; Chiangmai 2010; Behiry 2012), have determined that fatigue cracking could also be initiated from the top of the surface and transfer down (top-down fatigue cracking). This model of fatigue cracking could be due to critical tensile and/ or shear stresses established at the top of asphalt layer and caused by significantly greater contact pressures at the tyre edge-pavement interface. Fatigue cracking may also result from a greatly aged (stiff) thin asphalt layer that has become oxidized (NCHRP 2004).

2.6.1 Fatigue models for asphalt

Commonly experimental approaches are applied for evaluating fatigue performance of asphalt mixes. The phenomenological method, the energy-based method, and the fracture mechanics method are the most appropriate approaches for evaluating fatigue properties of asphalt mixes.

The phenomenological method investigates the correlation between repeated stress or strain in asphalt specimens and the number of cycling loads to cause failure. This method is based on the theory of Miner's linear law linked with accumulated deterioration of the asphalt pavement. According to standard methods such as AASHTO T321-03 (AASHTO 2003) and the European Standard (EN12697-24 2004), failure is defined as the number of load cycles to produce 50% reduction in mix stiffness. According to this relationship, many fatigue models have been developed for predicting fatigue cracking. Studies have indicated that there is a correlation between the number of applied loads on asphalt and strain at the bottom of the asphalt layer as follows (Chiangmai 2010):

$$N_f = K(\frac{1}{\varepsilon})^a$$ Equation 2.1

Where;

N_f= number of load repetitions to cracking,
ε = predicted asphalt strain (mm/mm),
K and a = factors depending on the composition and properties of the asphalt mixture.

The energy-based method for assessing fatigue is based on the theory of dissipated energy. This approach assumes that fatigue damage is a depletion of dissipated energy from one load cycle to the next (Carpenter & Jansen 1997). The concept of this method is that by applying cyclic loading to a material, damage will accumulate in the material. Hence, this approach involves evaluating deterioration that takes place in the material before failure. The dissipated energy in a viscoelastic material, such as an asphalt mixture in a flexural fatigue test, can calculated from the following equation (Chiangmai 2010);

$$W_i = \pi\, \sigma_i\, \varepsilon_i\, Sin\, \phi_i$$ Equation 2.2

Where;

W_i = dissipated energy at load cycle i,
σ_i = stress amplitude at load cycle i,
ε_i = strain amplitude at load cycle i,
ϕ_i= phase angle between the stress and strain wave signals,

The constant amount of dissipated energy which generates deterioration in the material under cycles is defined as the Plateau Value (PV). The PV is a function of stress, strain, initial load and dissipated energy. The fatigue performance of an asphalt mixture based on the energy-based method can be predicted as follows (Chiangmai 2010);

$$N_f = C(PV)^b$$ Equation 2.3

Where;

N_f= number of load repetitions to cracking,
PV= plateau value of dissipated ratio (ΔDE/DE),
C and b = factors depending on the composition and properties of the asphalt mixture.

The fracture mechanics method is based on the theory of fracture mechanics and, investigates the occurrence and propagation of fatigue cracks. The growth of a crack in asphalt usually has three stages of, crack initiation, a propagation stage, and an unstable fracture. This method uses a relationship between crack propagation characteristics in asphalt and fracture elements such as the stress intensity factor (KIC). Paris' law can be applied to determine crack growth rate in asphalt as follows (Chiangmai 2010);

$$N_f = \int_{C_o}^{C_f} \frac{1}{AK^n}\, dc \qquad \text{Equation 2.4}$$

Where;

N_f = the number of cycles to failure,
C_o = the starter flaw,
C_f = the final crack length
A, n = material parameters,
K = stress intensity factor (in N/$mm^{1.5}$).

The Shell Oil Company has introduced a model for predicting fatigue in asphalt which is based on the relation between stress conditions and damage mechanisms. The following are the equations for predicting fatigue performance of asphalt mixes. Constant stress and constant strain are the two common approaches used for controlling the applied load in the laboratory for the fatigue test (NCHRP 2004).

Constant Strain;

$$N_f = A_f[0.17\,PI - 0.0085\,PI\,(V_b) + 0.0454\,V_b - 0.112]^5\,\varepsilon_t^{-5}\,E^{-1.8}$$

Equation 2.5

Constant Stress;

$$N_f = A_f[0.0252\ PI - 0.00126\ PI\ (V_b) + 0.0673\ V_b - 0.0167]^5\ \varepsilon_t^{-5}\ E^{-1.4}$$

Equation 2.6

Where PI is the penetration index and is calculated as follows;

$$PI = \frac{20 - 500\ A}{1 + 50\ A}$$

Equation 2.7

'A' is the temperature susceptibility i.e. logarithm slope of penetration plotted versus temperature. A is calculated as following;

$$A = \frac{\log(pen\ at\ T_1) - \log(\ pen\ at\ T_2)}{T_1 - \ T_2}$$

Equation 2.8

$where\ T_1\ and\ T_2$ are centigrade temperatures at which penetrations are measured.

The Asphalt Institute has introduced a fatigue equation for asphalt. This model is based on modifying the constant stress of the laboratory fatigue test developed by Witczak and Shook (NCHRP 2004). The equations for evaluating fatigue performance of asphalt mixes is as follows:

$$N_f = 0.00432\ C\ (\frac{1}{\varepsilon_t})^{3.291}\ (\frac{1}{E})^{0.854}$$

Equation 2.9

$$C = \ 10^M$$

$$M = 4.84\ (\frac{V_b}{V_a - \ V_b} - 0.69)$$

Equation 2.10

Where;

V_b = effective binder content (%)
V_a = air voids (%)

2.7 Rutting

The accumulation of permanent deformation in the form of longitudinal depressions is termed rutting. This mode of failure, which usually appears in the wheel path is caused by densification and/ or shear deformation phenomena (Xu & Huang 2012). Based on the strength of layers and also the magnitude of traffic loads, rutting can take place in any asphalt or unbound layers within the pavement (White et al. 2002). Severe rutting can result in pavement structural failure and have significant effects on road safety (Xu & Huang 2012).

Current pavement design systems, such as the mechanistic-empirical methods have been developed and include fatigue and rutting criteria for designing pavements to minimise the potential of fatigue cracking and rutting in the pavement. It is often considered that there is a conflict between addressing fatigue and rutting susceptibility of asphalt. For example, increasing the binder content can result in increased fatigue life and decreased rutting resistance. It is essential to have a desirable balance in the design stage between rutting and fatigue modes of distress. Applying traffic loads on the surface of the pavement induces strains which are used for designing rutting and fatigue. The vertical compressive strain (ε_v) on top of the subgrade, and horizontal tensile strain (ε_t) at the bottom of asphalt layer as shown in the figure 2.8 are the two critical strains for designing for rutting and fatigue. High values of ε_t, results in fatigue cracking occurring in the asphalt. High values of ε_v produces rutting of the pavement. It should be noted here that this model refers to rutting within the subgrade rather than the asphalt. Various models have been developed around the world for presenting the relationship among modulus of asphalt, strain and number of load cycles to pavement failure. Two forms of models are as below (Behiry 2012):

Fatigue model:

$$N_f = f_1 \varepsilon_t^{-f_2} E_1^{-f_3} \qquad \text{Equation 2.11}$$

Rutting model:

$$N_r = f_4 (\varepsilon_v)^{-f_5}$$ Equation 2.12

Where;

N_f; is the permissible load cycles number for preventing fatigue cracking;
N_r; is the permissible load cycles number for preventing rutting;
ε_t: is the tensile strain at the bottom of the asphalt layer;
ε_v; is the compressive vertical strain on the surface of the subgrade;
E_1; *is the* asphalt elastic modulus;
f_1, f_2, f_3, f_4, f_5 ; are regression coefficients.

Additionally, Oglesby and Hicks have presented a relationship between compressive strain at the top of subgrade and rutting failure in the asphalt as follows (Behiry 2012):

$$N_r = 1.365 \times 10^{-9} (1/\varepsilon_v)^{4.477}$$ Equation 2.13

Where;

N_r; denotes the load applications number to prevent rutting

ε_v; is the compressive vertical strain on the surface of subgrade.

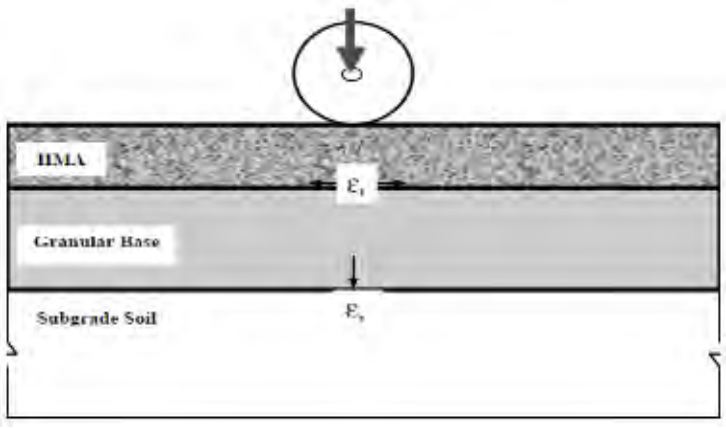

Figure: 2.8 vertical and horizontal strains in the pavement layers (White et al. 2002)

Only a brief description of the available models for rutting is presented here. A more comprehensive review is provided in the chapter 3.

2.8 Asphalt mixture design overview

Designing an asphalt mixture includes the careful proportioning and selection of the mixture component substances in a way that the final product has optimal fatigue and creep properties. For example, optimising fatigue performance by increasing bitumen content and filler with decreased air voids may reduce its creep resistance. However, the principal aim of the design process is to achieve a mixture with the following characteristics (Abdelaziz 2008):

1. Adequate volume of bitumen binder in the mixture, that ensures a stable and durable pavement.

2. An adequate quantity of air voids in the compacted mixture that allows for a minimised further compaction beneath heavy wheel loads without vulnerability to damage caused by flushing and bleeding. The air voids must be minimised to avoid exposure to any damaging moisture and air, which can affect the bitumen film.

3. Adequate stability to protect the asphalt mixture from movement and distortion in the case of heavy loads.

4. Sufficient workability permitting efficient mixture paving without separation.

Numerous systems and methods for designing asphalt have been used around the world. Some of the most popular methods are as follow.

2.8.1 Marshall method

The Marshall Method is one of the oldest conventional systems utilised for designing trial asphalt mixtures to find the optimum bitumen content (OBC). It was initially proposed by Bruce Marshall, a pavement engineer cooperating with the Mississippi State Highway Department (Tarakji 1992). The modus operandi for heating, blending, and compacting the combination of aggregates and bitumen is determined by the Marshall Method, that is afterwards subjected to a Marshal stability-flow test (Garber & Hoel 1997; Ahmadinia 2012).

2.8.2 Superpave mix design

Superpave mix design was introduced by the Strategic Highway Research Program (SHRP). Superpave stands for Superior Performing Pavements, and describes features of the material in relation to the traffic loads and ambient climatic considerations (Huang 2004). Primary elements employed in Superpave are as follows:

- A specification for bitumen according to climate (with a suitable database for climactic factors) and vehicular loadings.
- A special way for analysing volumetric properties of mixes.
- Environment and performance models.

However, one of the most innovative elements of Superpave could be its novel system for grading bitumen. Bitumen grading is connected with performance of the asphalt pavement (Huang 2004). Accordingly, Superpave is a mixture design method based on performance.

Superpave allows pavement engineers to design a finely-tuned asphalt pavement and adjust it to traffic stresses and different climates. Asphalt pavement built in this way has been shown to have superior durability and a lower probability of rutting in hot climates or cracking in cold climates (Ahmadinia 2012).

2.8.3 Australian asphalt mix design

In the late 1990's, Austroads, the Australian Road Research Board (ARRB) and the Australian Asphalt Pavement Association (AAPA), commenced work on a project to develop a performance-based mix design. The new approach measured fundamental mix properties, used newly-developed test equipment, and largely replaced the Marshall and the Hubbard Field procedures. The new mix design was intended to design affordable asphalt mixes for all sets of performance requirements and also provide more precise data for mechanistic pavement design. The purpose of the Australian method is a mix design procedure (Rebbechi & Liddle 2006) that:

- is performance-related

- enables the in-service performance of mixes to be predicted
- is relatively affordable (in terms of new equipment cost)
- is rapid and easy to use

Figure 2.9 details the Australian mix design procedure for dense graded mixes. As shown in the figure, a mix can be designed at three levels. In the first level, the type of mix and materials are selected and the mix is compacted by a gyratory compactor, and volumetric properties and optimum binder content determined. Some performance tests are undertaken in order to define structural performance properties of the mix in the second level. The rutting resistance of the mix is determined in the third level by the wheel tracking test.

Mixes are designed for different traffic situations. Gyratory compaction is applied at a rate of 50 cycles for light traffic; 80 cycles for medium and 120 cycles for very heavy traffic situations. For a light traffic situation, the mix design ends once the volumetric properties have been satisfactory achieved. For medium and heavy traffic situations, volumetric properties and performance testing are considered. For a very heavy traffic situations, the asphalt specimen is subjected to compaction to refusal density (350 gyratory compactor cycles) and further performance tests (Stephenson 2002).

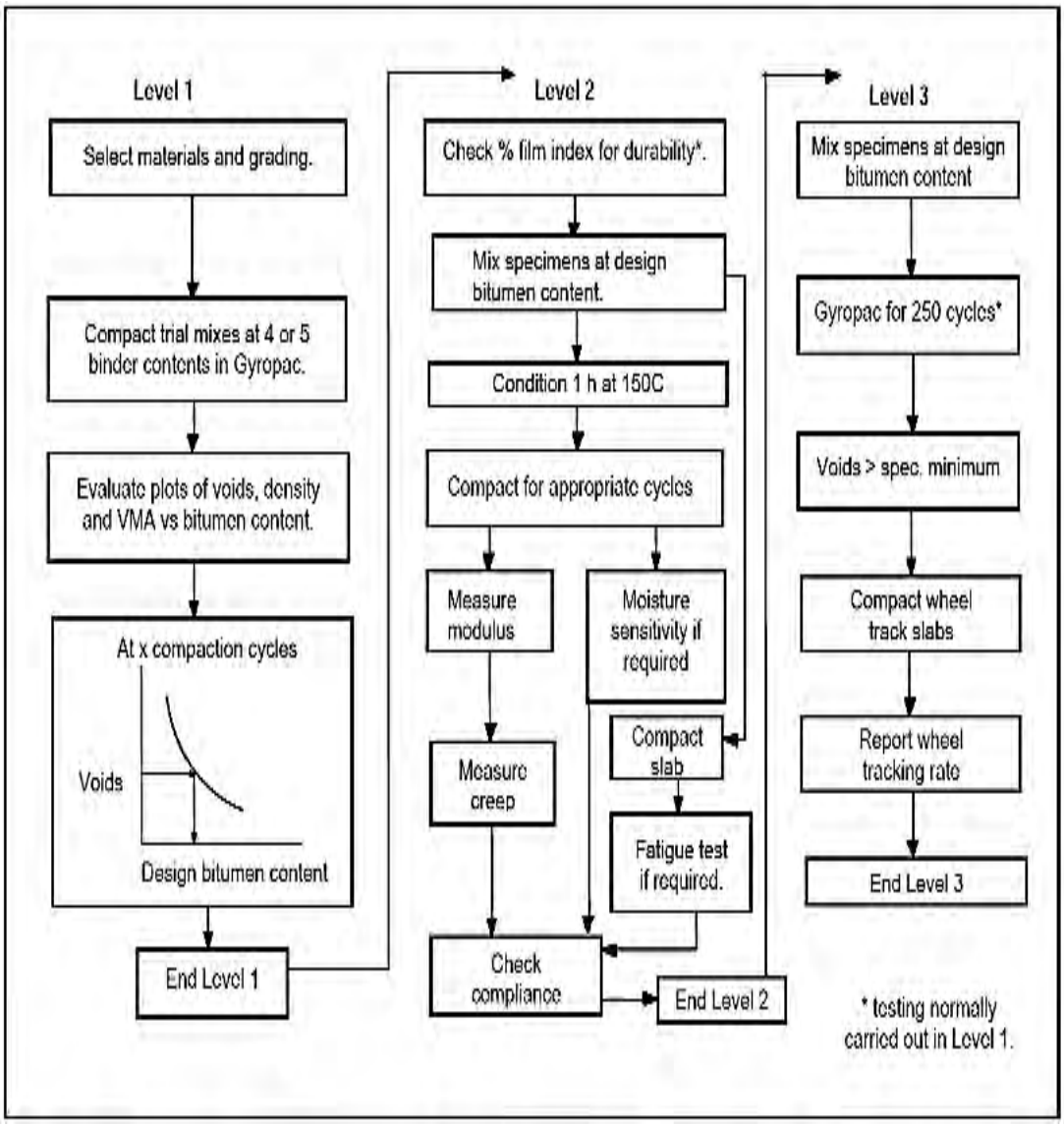

Figure: 2.9 Australian mix design procedure (Rebbechi & Liddle 2006)

2.8.4 Mechanistic pavement design

Mechanistic pavement design is a method to evaluate responses of the pavement to traffic loads. The method is based on a mathematical model to calculate stresses and strains in the pavement when exposed to traffic loads. By calculating stresses and strains, the method is theoretically able to predict and analyse pavement failures under vehicular loads.

A flow chart of the mechanistic design procedure is shown in figure 2.10. The mechanistic design includes two important parts, i.e. response and performance

models. The response model calculates the stresses and strains when the pavement is subjected to loads. The most common response models are: elastic and visco-elastic response models. Essential input items for response models are: thickness of the layers, properties of materials in the layers and load conditions. The performance model considers the pavement's response under stress over time such as estimating start and development time of cracks and rutting (as discussed in the sections 2.6 and 2.7). The required input parameters for the response model are; accurate stresses, rate of vehicular load, and strains as obtained in the response model part (Transport engineering 2013).

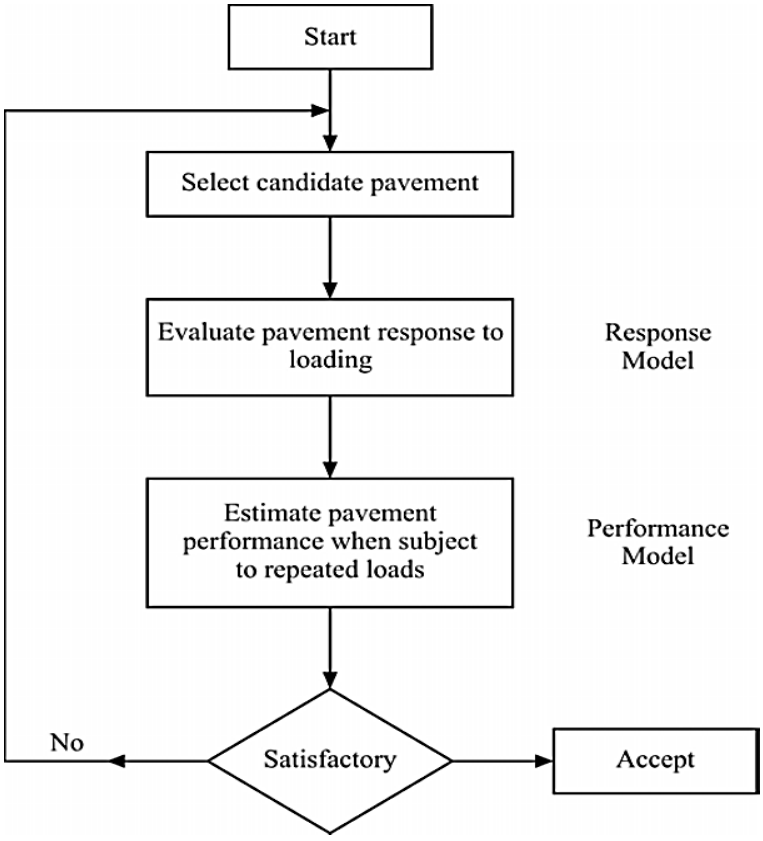

Figure: 2.10 Procedure of mechanistic pavement design (Transport engineering 2013)

2.9 Operating environment of road pavements

External loads and environmental conditions are two critical factors which significantly affect the service life of road pavements. The main environmental

elements affecting pavements are; ambient temperature gradient, rainfall, wind and solar radiation (Ongel & Harvey 2004). Figure 2.11 depicts the balance of energy on the pavement surface.

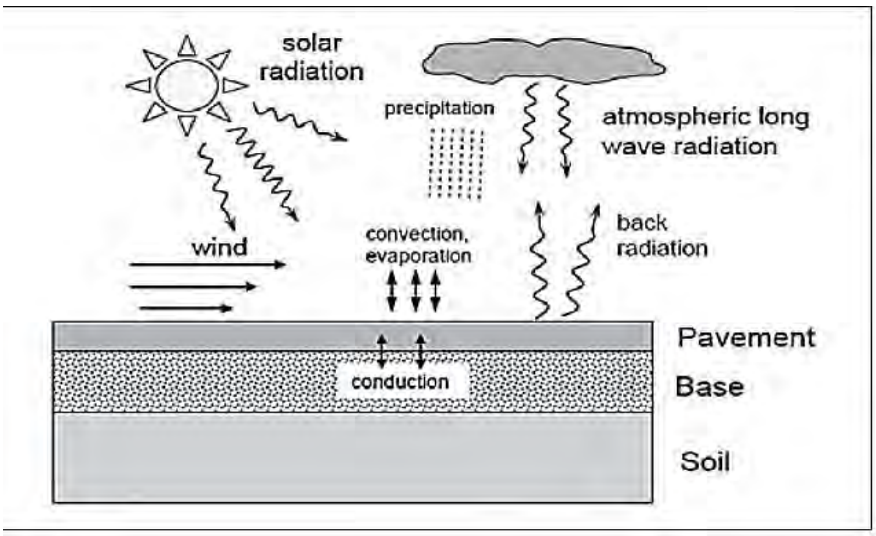

Figure: 2.11 Energy balance on the surface of the pavement (Matić et al. 2013)

2.9.1 Temperature

High temperature results in a loss of stiffness for the asphalt due to the bitumen's viscoelastic properties. Asphalt similarly becomes stiffer, relatively more brittle and tends to shrink at lower temperatures (below 10ºC), while at higher temperatures a mix becomes softer and susceptible to creep deformation (Ongel & Harvey 2004; Merbouh 2012). The principal thermal related failures in a flexible pavement are; fatigue cracking, thermal cracking, reflection cracking and rutting (Ongel & Harvey 2004).

Asphalt pavement performance is temperature dependent and thus a function of ambient temperature. In a section of a pavement, different depths can have different temperatures on different days and even hours during a day. In a hot climate, the surface of a pavement is much hotter than lower depths and thermal gradients are positive in the daytime. At night-time, the surface is cooler and thermal gradients are negative (Ongel & Harvey 2004). Figures 2.12 and 2.13 illustrate temperature distributions at different depths of a pavement. As the graphs show, in the winter by increasing depth of the pavement, temperatures inside the pavement increase. The

summer situation is a bit more complex with surface temperatures mostly higher than lower depths. The main ways that heat transfer occurs are solar radiation, thermal radiation between sky and surface of the pavement, convection between air and surface of the pavement, and also conduction inside the pavement. Generally, temperature in a pavement is controlled by three main elements: thermal conductivity, specific heat capacity, and convection (Xu & Solaimanian 2010).

Conventional flexible pavement design typically uses an average temperature equivalent. Repeated temperature fluctuation during daytimes and night-times produces many defects in asphalt pavement. Therefore, inclusion of a temperature fluctuation variable for designing flexible pavements is preferred (Merbouh 2012). Some approaches for estimation of temperature gradients inside flexible pavements based on numerical and presumptive techniques have been established based on collected climate and pavement data , however, many concerns remain about their accuracy and validity (Matić et al. 2013).

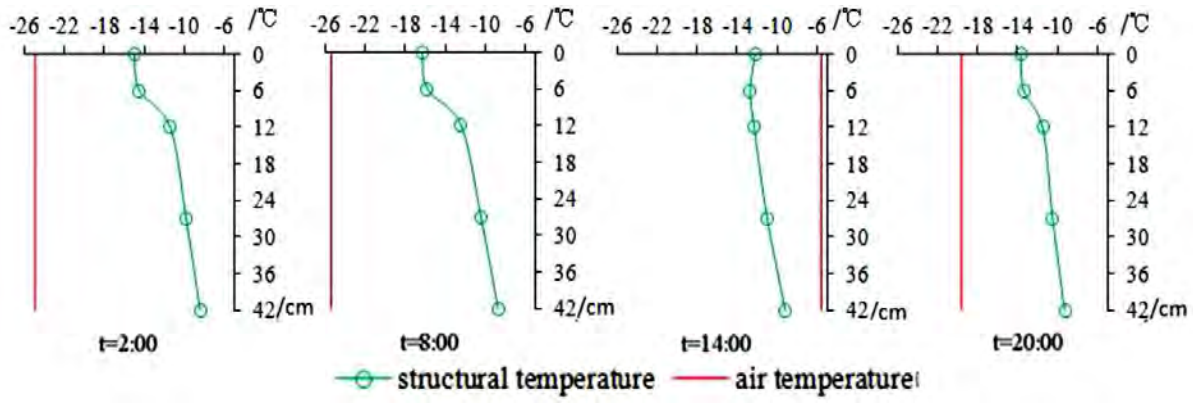

Figure: 2.12 temperature distribution in a pavement at different depth in winter (Ma et al. 2012)

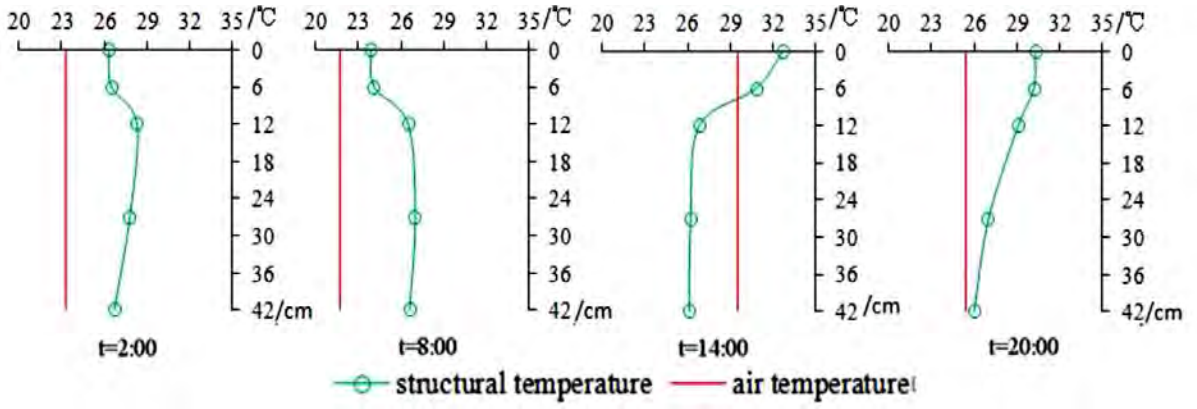

Figure: 2.13 Temperature distribution in a pavement at different depth in summer (Ma et al. 2012)

2.9.2 Moisture

As shown in the figure 2.14, water is another important environmental factor that has significant impacts on pavements. Water or moisture damage in the asphalt mixture can reduce pavement strength and durability. Penetrating moisture in the asphalt mixture affects cohesion (strength) by stripping which is a loss of internal adhesion (bond) between aggregate particles and bitumen binder. This can result in serious asphalt mixture deterioration such as degradation of aggregate particles, permanent deformation and fatigue cracking (Scholz & Rajendran 2009; Pavement-Interactive 2011).

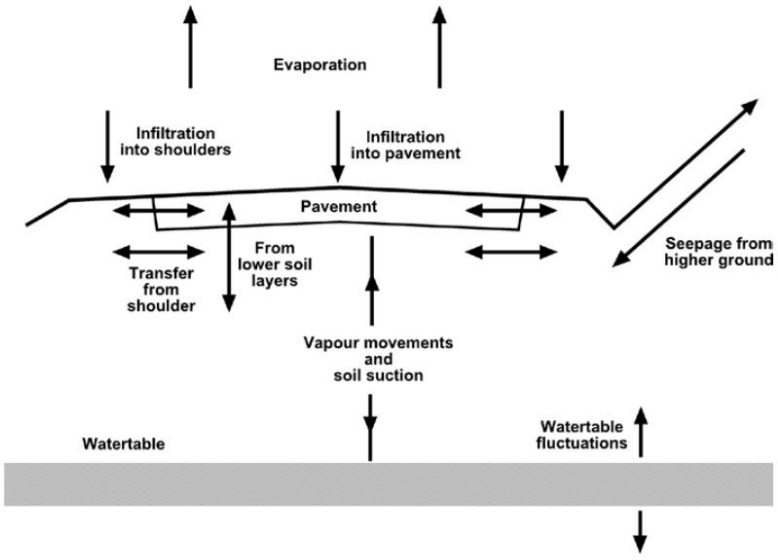

Figure: 2.14 Moisture movement in the road pavement (Austroads 2012)

Moisture susceptibility of an asphalt mixture is a complex phenomenon and depends on mechanisms affecting aggregate-bitumen adhesion such as mechanical properties, chemical composition, adhesion and tension characteristics, and molecular orientation features. The interaction of these factors complicates any precise prediction about the role of each factor when specifying the moisture susceptibility of a pavement. In fact, each variable affects the moisture susceptibility of the pavement to some degree, but no single factor provides a sure approach to predict pavement moisture susceptibility. Generally, moisture susceptibility of an asphalt pavement is increased by any element which causes increasing moisture content in the pavement, or a decrease in the bond between the aggregate and bitumen binder (Pavement-Interactive 2011). Table 2.3 summarizes the various elements affecting susceptibility of asphalt mixture to water damage (Scholz & Rajendran 2009).

In order to avoid and minimise permeability effects, a number of actions can be taken that range from initial pavement design and materials selection to construction of the pavement Moisture susceptibility of the asphalt pavements can be decreased by, the use of anti- striping agents -a is very common and popular solution. Some types of anti- striping additives are; hydrated lime, amines, Portland cement, sodium aluminosilicate, liquid antistripping agents, and polymers (Scholz & Rajendran 2009).

2.10 Traffic loads

The very obvious reason for the existence of a road pavement is to carry traffic loads. The imposed axle/wheel loads from heavy vehicles are the primary reason for road pavement deterioration, i.e. fatigue damage and creep deformation (Shuiyou 2003; Chatti et al. 2004).

Recent decades have seen a dramatic increase in the number and weight of large-sized heavy vehicles and containers with higher wheel pressures and axle loads that have high impact on pavements (Ahmadinia 2012). Research by Austroads has confirmed that since 1950 onwards, permissible gross loads have increased at the rate of around 0.45 tonnes per annum (Pearson & Foley 2001). The current design tyre pressure for designing and analysing asphalt pavement adopted by Austroads is 750 kPa, although

it can be vary between 500 and 1000 kPa (Youdale 1996; Gribble & Patrick 2008; Austroads 2012).

Table: 2.3 Elements effecting moisture damage (Scholz & Rajendran 2009)

Major Factors	Description
Aggregate Properties	▪ Composition (degree of acidity or pH, surface chemistry, type of minerals, source of aggregate) ▪ Physical characteristics (angularity, surface roughness, surface area, gradation, porosity, and permeability) ▪ Dust and clay coatings ▪ Moisture content ▪ Resistance to degradation
Asphalt Binder Properties	▪ Grade or stiffness ▪ Chemical composition ▪ Crude source and refining process
HMA Mixture Characteristics	▪ Air void level and compaction ▪ Type of HMA (dense-graded, gap-graded, open-graded)
Environmental Factors	▪ Temperature ▪ Freeze-thaw cycles ▪ Moisture vapor ▪ Dampness ▪ Pavement age ▪ Micro organisms ▪ Presence of ions in the water
Traffic	▪ Percent of trucks ▪ Gross vehicle weight of trucks ▪ Truck tire pressure
Construction of HMA Pavements	▪ Compaction ▪ Drainage ▪ Weather ▪ Segregation ▪ Contractor experience
Design of HMA Pavements	▪ Air void content ▪ Subsurface drainage ▪ HMA mix selection ▪ Designer experience ▪ Designer site visit

The distribution of stress at the tyre/pavement interface can considerably change as a function of tyre inflation pressure, type and configuration of tyre, wheel load and also tread patterns of tyres (figure 2.15 and 2.16). Moreover, the distribution of interfacial pressure between asphalt pavement and tyre is non-uniform, noncircular, and discontinuous. Many pavement design producers adopt the simplistic approach of

using a circular uniform pressure for analysing the response of pavements to axle loads (Shuiyou 2003).

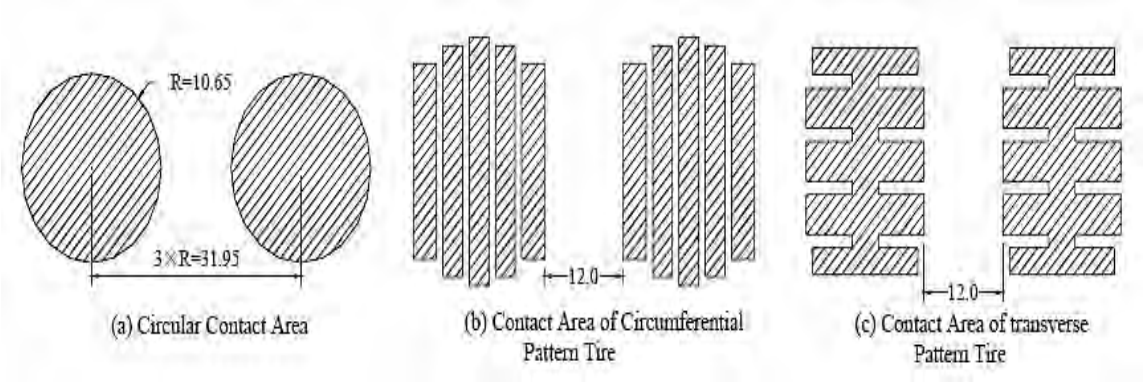

Figure: 2.15 Different contact zone pattern for dual tyre, unit: cm (Shuiyou 2003)

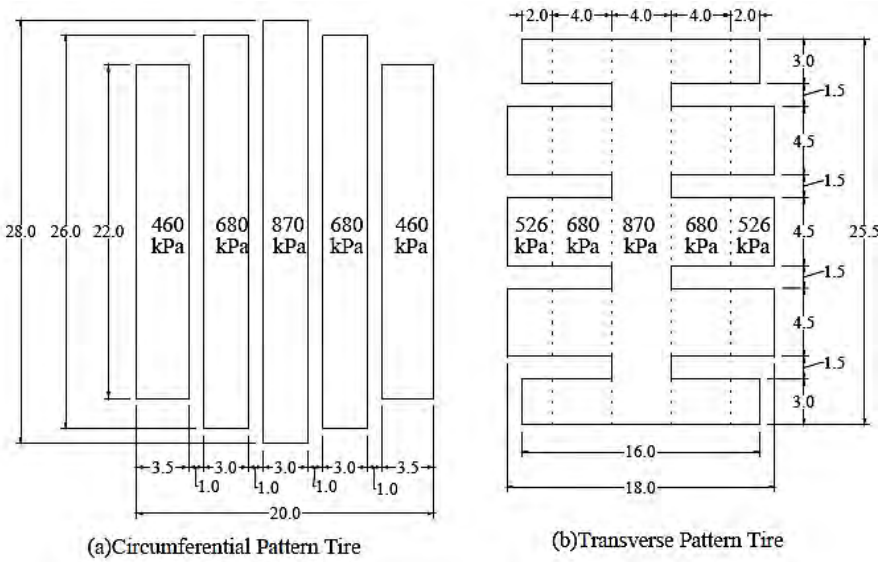

Figure: 2.16 Streamlined tyre contact zone and pressure (by 25 KN load), unit: cm (Shuiyou 2003)

2.11 Summary

This chapter has provided an overarching introduction to the thesis. It considered asphalt mix components including aggregates, bitumens, and fillers, outlining how mix

design can optimise in-situ performance by addressing the mix parameters that impact on performance, and subsequent pavement life.

The two key failure modes of asphalt fatigue and creep were explored and it was noted how designing for each is addressed through different processes. For example very high tyre pressure on hot days can result in severe asphalt surfacing rutting, but may have no impact on fatigue life.

The research literature suggests that the fatigue design of asphalt uses well established testing regimes and the application of proven predicative relaxations. The literature also suggests that designing for creep however, largely remains unaddressed in mechanistic design. Many pavement design methods adopt a subgrade deformation model, accompanied by a mix design approach for the asphalt.

CHAPTER 3

A LITERATURE REVIEW OF ASPHALT PERMANENT DEFORMATION: CREEP

3.1 Introduction

As outlined in the previous chapter, asphalt can exhibit structural failure in the form of creep deformation and/or fatigue cracking. Fatigue models such as those related to the Shell criteria, are well established (Austroads 2012) and are used in mechanistic pavement design. However, there has been little progress with the development of predictive creep correlations for incorporation in the mechanistic pavement design process. This chapter provides an overview on permanent deformation of asphalt with emphasis on creep parameters.

3.2 Permanent deformation or rutting

Failure types such as permanent deformation (rutting) are more serious and acute in hot climates, where increases in asphalt pavement temperatures significantly reduce the stiffness of asphalt, leading to permanent deformation. Rutting accrues mostly within the wheel paths resulting from high axle loads on the roads (Yang et al. 2005). This deformation is typically the earliest distress exhibited and can sometimes manifest itself after only a few days postdating construction. Subgrade rutting can be covered by an effective pavement design, while surface rutting can usually be covered by a precise selection of asphalt materials.

Permanent deformations are generated by two main mechanisms, which are densification and shear deformation. Densification (volume decrease, and /or density increase) can be due to poor specifications and /or inadequate compaction of pavements during the construction and usually happens early in the life of a pavement. In this process, aggregates tend to pack more closely under traffic pressures (post construction compaction) and a reduction of air voids in the mixture occurs. Shear

deformation (or lateral movement of materials) can be the more important factor for permanent deformation in asphalt mixtures. In this process, materials are compressed under tyre pressure, displaced laterally and pressed up into upheavals on either side of the tyre path (figure 3.1) (Aksoy & Iskender 2008; Cai 2013). Research undertaken by Eisenmann and Hilmar (1987) to evaluate mechanisms of permanent deformation, concluded that although in the initial stages densification or traffic compaction is the primary factor for developing rutting, shear deformation is considered as the main factor to develop permanent deformation during the pavement's lifetime. It should be also noted that the densification process may cause initial ruts that can result in accelerated deformation.

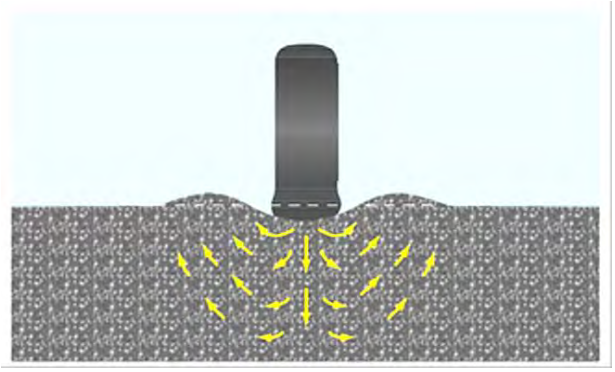

Figure: 3.1 Densification and shear deformation

The permanent deformation of asphalt mixtures depicted in figure 3.2 has three stages termed the primary stage, secondary stage and tertiary stage (Oscarsson 2011). This behaviour can be observed in any type of permanent deformation repeated load test. In the primary stage, permanent strain develops quickly due to initial densification. The majority of asphalt pavement life is often considered to be in the secondary stage, where there is an almost constant rate for developing rutting. There may be accelerated rutting in the tertiary stage.

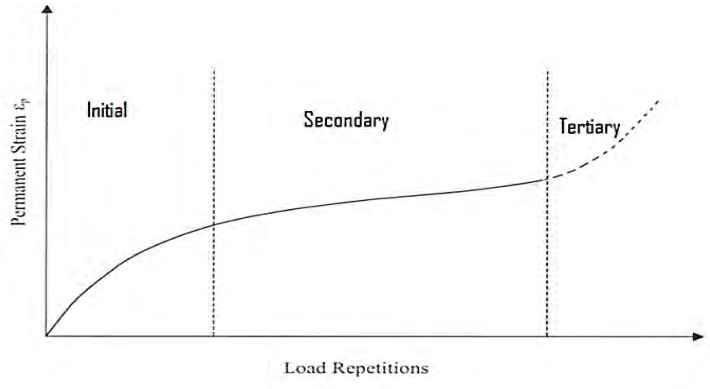

Figure: 3.2 Schematic permanent deformation curve (Oscarsson 2011)

The permanent deformation behaviour of asphalt mixtures can be affected by several factors such as: type and gradation of aggregate, type and content of binder in the mixture, degree and method of compaction (the air voids), temperature, and the frequency and magnitude of traffic loading.

3.3 Permanent deformation models

Permanent deformation of asphalt is most often modelled through three methods, being empirical models, mechanistic-empirical (M-E) models, and fully mechanistic models. Empirical models are based on observation and recorded distress data, while site factors and related materials properties are not considered. Empirical models have serious limitations and typically only used in some particular areas such as pavement management systems. In M-E models, an association of a mechanistic prediction technique (such as elasticity concept), and an empirical distress model is employed for predicting the permanent deformation of the asphalt. M-E models are said to be able to include repeated traffic loads and environmental conditions for predicting rutting and fatigue performance of asphalt. Fully mechanistic models include more complex constitutive techniques to incorporate various aspects of loading conditions (such as frequency, magnitude, and duration), environmental conditions and also material behaviour, into the predicting model. Fully mechanistic models are able to analyse imposed stresses and subsequent strains, by external loads without needing empirical transfer functions. Fully mechanistic models are typically complicated and can also be expensive to implement and calibrate (Carvalho 2012).

Table 3.1 is a brief summary of some existing M-E models based on power-laws for describing asphalt behaviour under frequency loading tests such as the creep test. These models are derived from repeated load permanent deformation (RLPD) tests with different forms to involve different parameters and fitting with experimental data. Figure 3.3 is an illustration of the comparative accuracy of these models with an accepted repeated load tests. As is evident from the figure, the second stage of permanent deformation is typically well predicted by the models, while most are inaccurate in the primary stage (Choi 2013).

Several structural analysis programs exist for assessing and predicting behaviour of pavements. For instant, BISAR (Bitumen Stress Analysis in Road) and ELSYM5 (Elastic Layered System computer program), introduced by Shell and the Federal Highway Administration (FHWA) respectively, for analysing pavements based on the elastic layer theory. VESYS (viscoelastic layered-pavement analysis program) has been developed by the FHWA based on viscoelastic layer theory, and CAMA (Computer Aided Mixture Design) has been developed by the Asphalt Institute to predict pavement behaviour based on in-situ stresses. CIRCLY is the most popular and widely pavement design tool used in Australia. The CAMA and VESYS models are discussed in greater detail as they represent contemporary computer modelling (Uzarowski et al. 2007).

CAMA is reported to be able to predict cracking and permanent deformation of asphalt under traffic loads. In this program, stresses are determined according to the elastic response of the pavement under wheel loads and also from asphalt mixture stiffness. In order to predict permanent deformation, equation 3.1 is utilized by CAMA (Uzarowski et al. 2007) as follows:

Table: 3.1 A brief summary of some existing M-E models based on power-law (reference to specific models included within (Choi 2013))

Model	Model Form	Variables
Classical Power	$\varepsilon_p = aN^b$	N = load cycle numbers a, b = regression coefficients
Monismith et al.	$\varepsilon_p = \delta(T)N^{\alpha}\sigma^{n-1}[\sigma_z - 0.5 \times (\sigma_x + \sigma_y)]$	$\delta(T)$= temperature function α = coefficient N = load cycles numbers T = load time σ = equivalent stress defined as a function of principal stress
Incremental	$\varepsilon_{vp} = \frac{A + BN}{(C + N)^{\alpha}}$	α = hardening evolution parameter $A = \frac{\varepsilon^0_{vp,ini}}{(I_H(t_l, t_r, \sigma_d))^{\alpha}}$ $B = \frac{I_{vp}(t_l, t_r, \sigma_d)}{(I_H(t_l, t_r, \sigma_d))^{\alpha}}$ $C = \frac{H_{ini}}{I_H(t_l, t_r, \sigma_d)}$ $I_{vp}(t_l, t_r, \sigma_d)$ = incremental permanent strain due to one load cycle $I_H(t_l, t_r, \sigma_d)$ = incremental hardening due to one load cycle t_l = load time t_r = rest period σ_d = deviatoric stress H_{ini} = the initial hardening of a specimen $\varepsilon^0_{vp,ini}$ = the initial permanent strain
Brown and Bell	$\varepsilon_p = (q/a)^b N$	ε_p= permanent shear strain q = deviatoric stress a, b = coefficient N = load cycle numbers

Model	Model Form	Variables
Khedr (Ohio State Univ.)	$\varepsilon_p/N = A_a N^{-m}$	A_a= material property, function of resilient modulus and applied stress m = material parameter N = load cycle numbers
Wilshire and Evans	$\varepsilon_p = \theta_1(1 - e^{\theta_2 N}) + \theta_3(e^{-\theta_4 N} - 1)$	ε_p= creep strain θ_1 and θ_3= primary and tertiary strain θ_1 and θ_4= rate parameters quantifying the curvature of the primary and tertiary stages
Francken	$\varepsilon_p = AN^B + C(e^{DN} - 1)$	A, B, C, and D = coefficients N = load cycle numbers
MEPDG (Mechanical-Empirical Pavement Design Guide)	$\frac{\varepsilon_p}{\varepsilon_r} = 10^{k_1} T^{k_2} N^{k_3}$	ε_r = resilient strain N = load cycle numbers T = temperature k_1, k_2, k_3 = regression coefficients

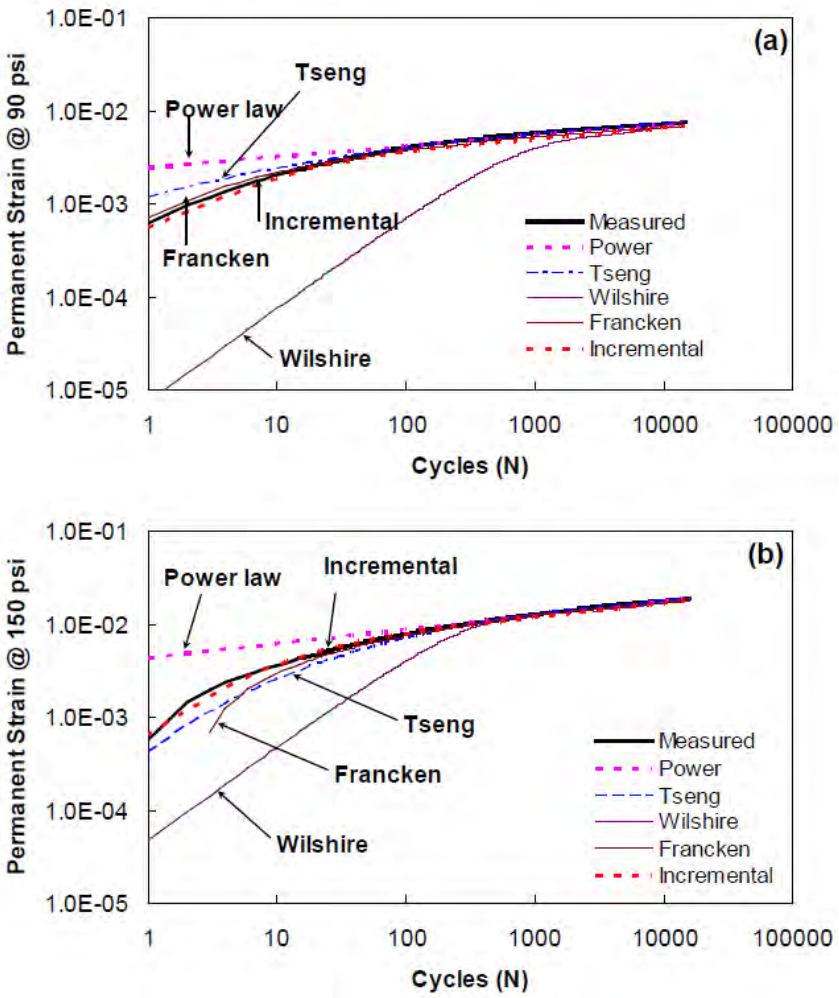

Figure: 3.3 Comparing permanent deformation models with a repeated load test at different stress (a] 90 psi, b] 150 psi) (Choi 2013)

$$\log \varepsilon_p = -14.97 + 0.408 \log (N) + 6.85 \log (T) + 1.107 \log (\sigma_d) - 0.117 \log(Vis) + 1.908 \log(P_{eff}) + 0.971 \log(V_v)$$

(Equation 3.1)

ε_p = permanent strain

P_{eff} = effective asphalt volume

V_v = volume of air voids

σ_d = deviator stress (psi) determined at the middle layer depth

N = load applications number

Vis = viscosity at 21^{O}C (in poises $\times 10^6$)

T = temperature of pavement

In the VESYS model, it is assumed that plastic strain of the asphalt is proportional to its resilient strain. Then equation 3.2 is used in the VESYS model as follows (Öztürk 2007);

$$\varepsilon_{pn} = \mu\, \varepsilon_r\, n^{-\alpha} \qquad \text{(Equation 3.2)}$$

ε_{pn} = permanent strain due to single load application
μ = a plastic deformation factor representing the constant of proportionally between plastic strain and elastic strain
ε_r = resilient strain
n = load applications
α = a plastic deformation factor representing the rate of reduction in the incremental plastic deformation as the number of load repetitions increases.

3.4 Mechanical models for simulating viscoelastic behaviour of asphalt

The behaviour of asphalt as a type of viscoelastic material can be simulated and predicted by some mechanical models. These models are able to determine relationships between stress and strain or load and deformation with their time dependencies in the viscoelastic materials. In the mechanical models, a combination of springs and dashpots (dampers) are employed to model material responses under loading conditions. Springs are able to be fitted in the elastic phase (as equation 3.3), and the viscous phase is simulated by dashpots (equation 3.4). A combination of springs and dashpots are able to simulate a material's linear viscoelastic behaviour (figure 3.4 and 3.5) (Abbas 2004; Liao 2007; Öztürk 2007).

$$\sigma = E\, \varepsilon \qquad \text{(Equation 3.3)}$$

σ =stress
E = spring constant or elastic modulus
ε = strain

$$\sigma = \eta \frac{d\varepsilon}{dt} \qquad \text{(Equation 3.4)}$$

σ =stress
η =coefficient of viscosity
$\frac{d\varepsilon}{dt}$ = time derivative of strain

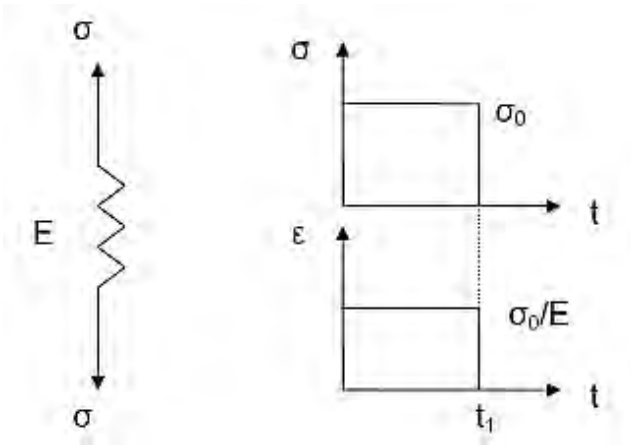

Figure: 3.4 Spring as an elastic element (Öztürk 2007)

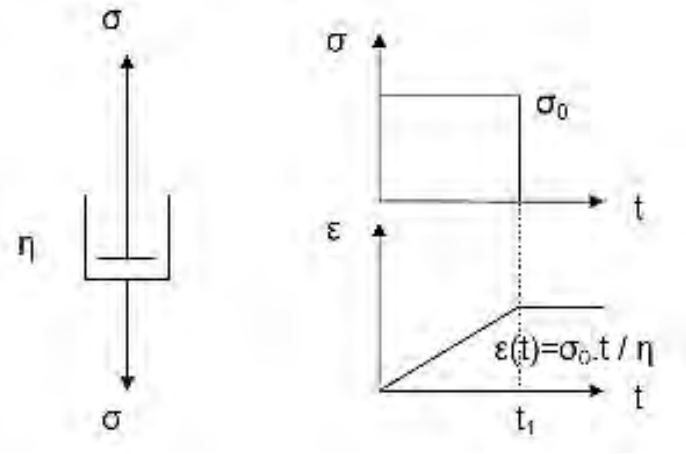

Figure: 3.5 Dashpot as an element (Öztürk 2007)

Based on these fundamental elements (spring and dashpot), various viscoelastic models have been introduced for evaluating the response of asphalt under traffic loads and for inclusion in mechanistic models (Liao 2007) . The number and arrangement of springs and dashpots are varied for each model. All models can also be equally modelled as electrical circuits wherein stress can be indicated by voltage, rate of strain by current, spring's elastic modulus by the circuit's capacitance, and dashpot viscosity by the circuit's resistance (McCrum et al. 1997; Vliet & Ortiz 2006).

3.4.1 Maxwell model

The Maxwell model is a plane viscoelastic model (i.e. diagram 3.6), as a Hookean spring and a Newtonian dashpot connected in series. In this figure, E is assigned for elastic modulus and η is the viscosity coefficient of the material. This model does not provide a good prediction for creep. Total stress (σ_{Total}) and total strain(ε_{Total}) are as per the following equations (3.5 and 3.6), and the Maxwell model can be expressed as equation 3.7 (McCrum et al. 1997; Vliet & Ortiz 2006).

$$\sigma_{Total} = \sigma_D = \sigma_S \qquad \text{(Equation 3.5)}$$

$$\varepsilon_{Total} = \varepsilon_D + \varepsilon_S \qquad \text{(Equation 3.6)}$$

where,
D indicates stress/ strain in the damper and the subscript S indicates the stress/strain in the spring. By taking derivation of strain with respect to time, the following equation is obtained (McCrum et al. 1997; Vliet & Ortiz 2006).

$$\frac{d\varepsilon_{Total}}{dt} = \frac{d\varepsilon_D}{dt} + \frac{d\varepsilon_S}{dt} = \frac{\sigma}{\eta} + \frac{1}{E}\frac{d\sigma}{dt} \qquad \text{(Equation 3.7)}$$

where;
E: elastic modulus
η: viscosity coefficient of the material.

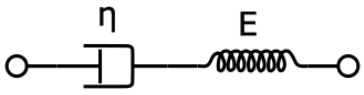

Figure: 3.6 Maxwell Model

3.4.2 Kelvin/ Voigt model

The Kelvin or Voigt model is another plain viscoelastic model combining a Hookean spring and a Newtonian dashpot in a parallel connection. Figure 3.7 depicts a Kelvin

model where E is assigned for elastic modulus and η is the viscosity coefficient of the material. The Kelvin model is able to provide a proper creep model for viscoelastic materials ,however, it does not produce an acceptable relaxation model (Liao 2007; Viscoelasticity 2016). In the Kelvin model, total stress (σ_{Total}) and total strain (ε_{Total}) are expressed in the following equations (equation 3.8, and 3.9), while the Kelvin model itself is given by equation 3.10 (McCrum et al. 1997; Vliet & Ortiz 2006).

$$\varepsilon_{Total} = \varepsilon_D = \varepsilon_S \quad \text{(Equation 3.8)}$$

$$\sigma_{Total} = \sigma_D + \sigma_s \quad \text{(Equation 3.9)}$$

where,
D indicates stress/ strain in the damper and S indicates the stress/strain in the spring (Viscoelasticity 2016).

$$\sigma\,(t) = E\varepsilon(t) + \eta\,\frac{d\varepsilon(t)}{dt} \quad \text{(Equation 3.10)}$$

where;
E: elastic modulus
η: viscosity
σ (t) ; stress and its changing rates by time
ε (t) : strain and its changing rates by time
t : time

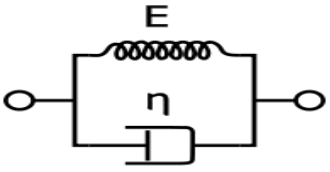

Figure: 3.7 Kelvin/ Voigt Model

3.4.3 Burgers model

As indicated previously the Maxwell and Kelvin models are often considered to be overly simple in providing a precise prediction of a materials' viscoelastic behaviour (Liao 2007; Öztürk 2007). Therefore, some more advanced viscoelastic models have

been built by combinations of these two basic models such as, the Burgers model, the Generalized Maxwell model, and the Generalized Kelvin model (Abbas 2004).

The Burgers model is one of the favourite rheological models for predicting and evaluating deformations in viscoelastic materials under a constant loading (creep) phase and also in the recovery phase (unloading). Figure 3.8 substantiates this that it is a combination of Maxwell and Kelvin models. The Burgers equations for the creep and recovery phases are presented in the equation 3.11, and 3.12 respectively (Geber et al. 2014).

Creep (loading) phase;

$$\varepsilon_{sum}(t) = \frac{\sigma_0}{E_1} + \frac{\sigma_0}{\eta_1}.t + \frac{\sigma_0}{E_2}.\left(1 - e^{-\frac{E_2}{\eta_2}.t}\right) \qquad \text{(Equation 3.11)}$$

where:

ε_{sum}: is the elastic deformations summation
σ_0: the constant shear stress
E_1 , E_2: elastic moduli of two spring parts in the Burgers model
η_1, η_2: viscosity of two dashpot parts in the Burgers model
t: loading time

Recovery phase;

$$\varepsilon_{sum} = \varepsilon_0 + \dot{\varepsilon}.t_2 + \varepsilon_1.(1 - e^{\frac{-t_2}{\lambda_2}}) \qquad \text{(Equation 3.12)}$$

Where:

ε_{sum}: represents the elastic deformations summation
ε_0 : is the instantaneous deformation at recovery phase
ε_1 : delayed deformation at recovery phase
$\dot{\varepsilon}$: shear rate
t_2 : the time at the end of recovery phase
λ_2 : the retardation time

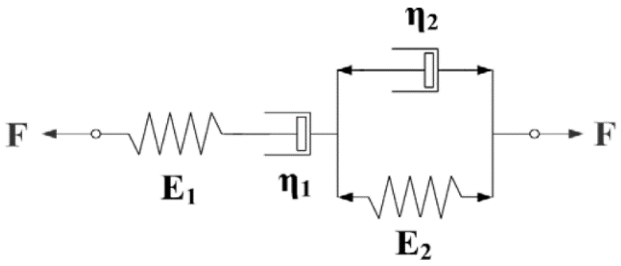

Figure: 3.8 Schematic of Burgers model (Öztürk 2007; Geber et al. 2014)

3.4.4 Generalized Maxwell model

The Generalized Maxwell model, also known as the Wiechert model, is one of the most promising existing models for modelling asphalt. The model assumes that the relaxation phase happens at a distribution of times, but not at a particular single time. The model is represented in this feature by including a spring and as many as required Maxwell elements for a precise response indication (Liao 2007). The Generalized Maxwell model is represented in figure 3.9 below:

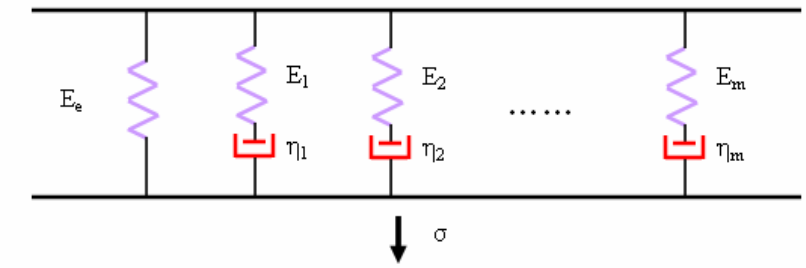

Figure: 3.9 Schematic of Maxwell–Wiechert model (Liao 2007)

3.5 Existing test methods to evaluate permanent deformation of asphalt mixtures

In order to evaluate permanent deformations of asphalt mixtures, many test methods have been used around the world. These methods can be classified into the three main groups of: Empirical tests, Fundamental tests and Simulative or Wheel track tests (Brown et al. 2001; Liao et al. 2013). More information and a comparison of the various test methods employed for evaluating the permanent deformation of asphalt mixtures is provided in Table 1 in the Appendix.

3.5.1 Empirical tests

Empirical tests are the oldest test methods used to evaluate permanent deformation of asphalt mixtures. Nowadays, empirical tests are considered to provide only a poor assessment of the performance of asphalt mixtures. The main reason is that test results do not correlate well with results from observed field situations. Consequently, the use of such methods to assess the permanent deformation of asphalt mixtures has decreased sharply. Some of the more well-known empirical tests are the Marshall Test, and the Hveem Test.

3.5.2 Fundamental tests

Fundamental tests to evaluate permanent deformation of asphalt mixtures are more theoretical and newer than empirical tests. The test outcomes provide better correlations between laboratory assessments and real field situations than empirical testing. This feature has made fundamental tests popular for performance evaluations of asphalt mixtures. In general, fundamental tests can be divided into the three main groups as follows (Brown et al. 2001; Liao et al. 2013):

- Uniaxial and Triaxial tests: unconfined (uniaxial) and confined (triaxial) cylindrical specimens in repeated loading test, strength test, and creep test.
- Shear loading tests
- Diametric tests: cylindrical specimens in creep tests, repeated loading test, and strength test.

However, these tests have their own inherent disadvantages. The most significant disadvantage of these tests is the lack of a confining pressure, or a uniform pressure applied to specimens, which thereby does not replicate in-situ tyre pressures. Moreover, a small laboratory sample (without proper confining pressure) cannot duplicate the field conditions of a pavement. Another disadvantage, which is related to diametric tests in the fundamental test group, is that indirect tensile tests are used to predict permanent deformation of asphalt pavements (Liao et al. 2013). The creep test, which is one of the fundamental tests, is explained in detail in the next section.

3.5.3 Simulative or wheel track tests

Wheel tracking tests attempt to simulate traffic conditions on a road in the laboratory in order to evaluate permanent deformation of asphalt mixtures. These tests mainly measure rut depth created by repeated passing of a wheel over an asphalt mixture sample over time. The generated rut depth is used as an indicator to evaluate the susceptibility of the asphalt mixture to permanent deformation. Wheel tracking tests do not calculate stress, and they cannot be used to determine asphalt mixture modulus; therefore these tests cannot be used in mechanistic pavement analysis (Aksoy & Iskender 2008). However, wheel tracking tests are popular around the world and experimental procedures are available to evaluate rutting properties of asphalt mixtures. Some of the more well-known simulative methods include the Hamburg Wheel-Tracking Device, the Nottingham Pavement wheel tracker, the French Rutting Tester (LCPC Wheel tracker) and the Asphalt Pavement Analyser.

3.6 Classical creep

When a solid material is subjected to mechanical stress, especially at elevated temperatures, it tends to move slowly and begins to irreversibly deform. This phenomenon is known as “creep” in materials science. Creep of a material is distinguished as the consequence of long-term exposure to high levels of stress below the material’s yield stress. The creep rate is always increased by increased load duration and increased temperature (figure 3.10). The creep deformation rate is also a function of material properties, duration and magnitude of applied loads, and the duration and magnitude of temperature changes. Creep is a time-dependent phenomenon and it does not occur abruptly when a load is applied.

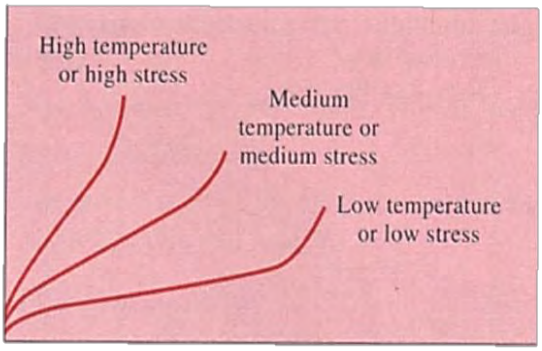

Figure: 3.10 Effect of temperature & stress

3.6.1 Classical creep curve

Creep behaviour in a material is divisible into three stages, namely primary creep, secondary creep and tertiary creep (Brown et al. 2001). Figure 3.11 shows a classical creep curve of a material, where strain is plotted against time (or log time). The primary creep occurs in the early stage of loading, and starts at a high rate, which slows with time. For metals in this stage, microstructural changes take place in the material and make it gradually harder to deform. Secondary creep is the steady state region where strain has a comparatively even rate. The secondary creep state (which is sometimes called steady state creep) is the most important part of creep, because primary and tertiary creep stages do not contribute significantly to total strain and service life of the material. In tertiary creep, strain has an accelerated rate, flaws increase quickly in the microstructure, and continue until the material ruptures. Tertiary creep may be only less than 1% of the total life time, but typically include a high percentage of the deformation life. Creep in metals and asphalt occurs through entirely different mechanisms.

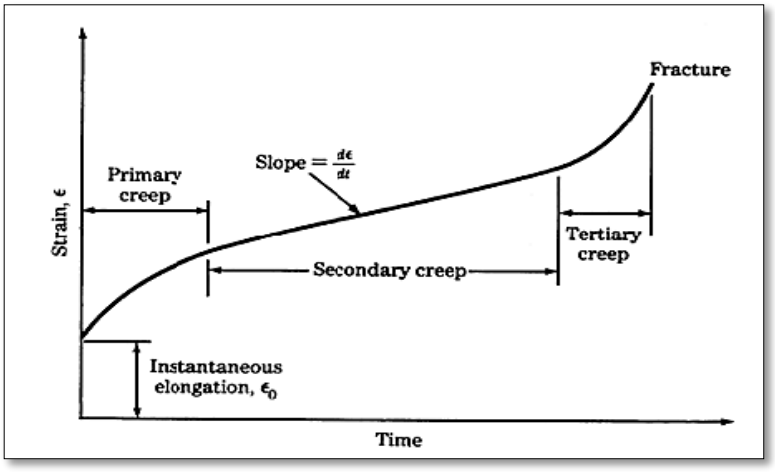

Figure: 3.11 Classical Creep Curve

3.6.2 Creep in asphalt

Asphalt undergoes intermittent traffic loads and temperature fluctuations during its service life, and this makes it susceptible to creep deformation. Creep deformation in asphalt is the continuous time-dependent accumulation of strain produced by repeated

traffic loads, especially when heavy slow vehicular loads exist (Brown & Foo 1994; Öztürk 2007).

According to many researchers (Lai & Hufferd 1976; Abdulshafi 1983; Perl et al. 1983), the creep deformation of an asphalt mixture can be resolved into four components which are: elastic strain (recoverable and time-independent), plastic strain (irrecoverable and time-independent), viscoelastic strain (recoverable and time-dependent), and viscoplastic strain (irrecoverable and time-dependent).

Typical asphalt mixture creep behaviour for a load cycle is depicted in Figure 3.12. The ε_o is elastic and plastic strain, which occurs immediately by applying load (at t= t_0), viscoelastic and viscoplastic strains happen during loading (t_0 until t_1), elastic strain is recovered as soon as the load is removed (t= t_1), and viscoelastic strain is recovered during rebound or rest time (during t_1 to t_2). Therefore, as shown in the equation 3.13, total permanent creep deformation is the sum of plastic and viscoelastic strain.

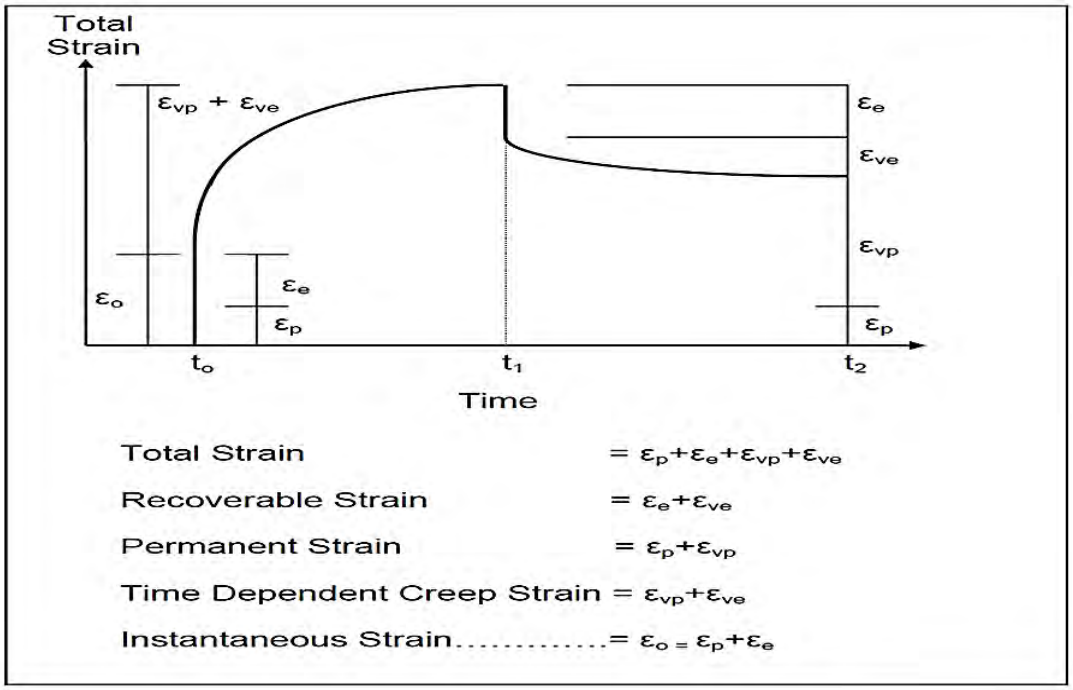

Figure: 3.12 Creep behaviour of an asphalt mixture (Perl et al. 1983)

$$\varepsilon_o = \varepsilon_e + \varepsilon_p + \varepsilon_{ve} + \varepsilon_{vp} \quad \text{(Equation 3.13)}$$

where:

ε_o = *is the* creep strain

ε_e = elastic strain (recoverable and time-independent)

ε_p = *is the* plastic strain (irrecoverable and time-independent)

ε_{ve} = viscoelastic strain (recoverable and time-dependent)

ε_{vp} = viscoelastic strain (irrecoverable and time-dependent)

3.6.3 Creep test method (static and dynamic)

Laboratory creep testing is one of the most common methods for predicting and evaluating the rutting potential of asphalt. The creep test is performed by applying either a static load, or dynamic cyclic loads. In a static creep test, the specimen is exposed to an axial compressive static load. This test is performed at low stress and moderate temperature (Sousa et al. 1991), and where the magnitude of the load is around 100 kPa, with loading time around 1 hour and test temperature around 40°C. After unloading, the deformation is plotted as a function of time to obtain an indication of the rutting potential of the asphalt mixture. As shown in figure 3.13, a repeated load is applied in the dynamic creep test to simulate traffic loads and provide recovery time for the asphalt mixture. The dynamic creep test can be performed at higher stresses and temperatures than the static creep test (Brown et al. 2001; Aksoy & Iskender 2008).

Both static and dynamic creep tests can be performed in confined and unconfined test situations. In the unconfined or uniaxial creep test, there is no confining pressure around the sample and the specimen is only subjected to compressive axial load. However, for better field simulation, sometimes a confining pressure (usually 130 to 140 kPa) is applied to the specimens. In general, the results of confined dynamic creep tests (or the triaxial dynamic creep test) exhibit better correlation with field performance than the results from the static or unconfined tests (Brown et al. 2001).

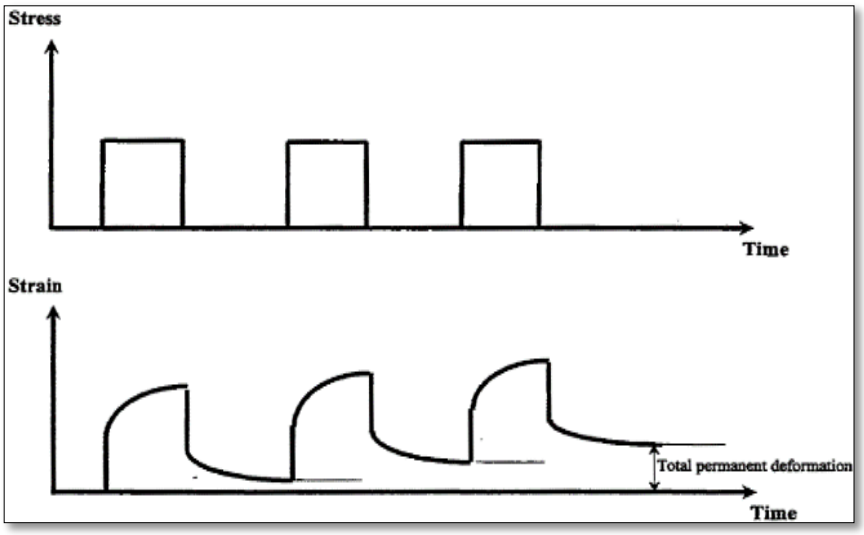

Figure: 3.13 Accumulation of permanent deformation under repeated loading (Khanzada 2000)

Typically, the linear part (secondary phase) of the creep curve is considered for analysing outcomes of a static creep test. The linear part can be modelled by the power-law model as per the following (equation 3.14) (Ebrahimi 2015);

$$D' = D(t) - D_o = at^m \qquad \text{(Equation 3.14)}$$

where,

D' = Viscoelastic compliance component at any time
$D(t)$ = Total compliance component at any time
D_o = Instantaneous compliance
t = Loading time
a, m = Materials regression coefficients

Similarly to the static creep test, the linear zone of the creep diagram is used for evaluating a dynamic creep test. The Power-law is able to provide permanent deformation parameters including intercept (a) and slope (b), as in equation 3.15 (Ebrahimi 2015);

$$\varepsilon_p = aN^b \qquad \text{(Equation 3.15)}$$

Alternatively, a mathematical model is obtained by employing permanent strain per load repetition as expressed in equation 3.16 (Ebrahimi 2015);

$$\frac{\delta\varepsilon_p}{\delta N} = \varepsilon_{pn} = \frac{\delta(aN^b)}{\delta N} \quad or \quad \varepsilon_{pn} = abN^{b-1} \qquad \text{(Equation 3.16)}$$

3.6.4 Creep models used to explain laboratory phenomena

The Cross Model is a non-linear rheological model that has been developed by Cheung, Cebon and Deshpande (2005), and later extended by Ossa et al (2010). To characterize the asphalt monotonic behaviour at both creep test conditions i.e. constant stress and constant strain creep tests. The developed Cross Model defines stress (σ) and the strain rate ($\dot{\varepsilon}$) relationship as presented in the equation 3.17 (Bai et al. 2014);

$$\frac{\sigma}{\sigma_0} = \frac{\dot{\varepsilon}}{\dot{\varepsilon_0}(\varepsilon,T)} \frac{1}{1+\left(\frac{\dot{\varepsilon}}{\dot{\varepsilon}_0(\varepsilon,T)}\right)^m} \qquad \text{(Equation 3.17)}$$

where:

σ_0; is the Basis stress

$\dot{\varepsilon_0}$; the Basis strain rate.

ε ; Total strain

T; temperature, and

m; the strain rate sensitivity exponent

Lai (1973) performed an unconfined creep test (uniaxial) on asphalt under a variety of loading conditions, i.e. constant loading system, multiple-step loading system and repeated loading system, to explore the plastic strain of an asphalt mixture. It was concluded that the total irrecoverable creep strain can be expressed as per the following equation (3.18) (Uzarowski et al. 2007);

$$\varepsilon_p(t) = (b_1\sigma + b_2\sigma^2)\, t^{n_p} \qquad \text{(Equation 3.18)}$$

where;

ε_p= total plastic strain

and the plastic strain rate is as below (equation 3.19);

$$\varepsilon_p(t) = n_p(b_1\sigma + b_2\sigma^2)\, t^{n_p-1} \qquad \text{(Equation 3.19)}$$

where;

ε_p = total plastic strain rate

σ = loading stress

t = time

n_p = slope of the creep compliance curve

b_1 and b_2 = parameters of the stress-strain curve

As the creep behaviour of the asphalt includes various phases i.e. consolidation, deformation and plastic failure, Beckedahl et al. (1992) in (Öztürk 2007) have developed a mathematical model to fit these stages of the creep curve. The model is presented in equation 3.20 below:

$$\varepsilon(n) = E0 + An^k + B(e^{mC} + 1) \qquad \text{(Equation 3.20)}$$

where;

$\varepsilon(n)$ = Strain after n loading application

n = number of applied loading

E0, A, B, C, k = model constant parameters which are obtained by regression analysis.

In this model, E0 represents the consolidation, An^k is the creep deformation, and $B(e^{mC} + 1)$ is the plastic failure part of the mixture. These parameters have been plotted in the figure 3.14 (Öztürk 2007).

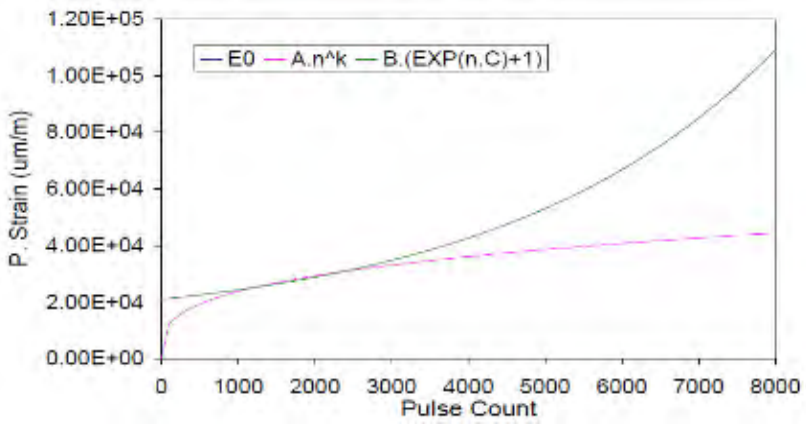

Figure: 3.14 Bechedahl model parts (Öztürk 2007)

3.6.5 Evaluating and measuring creep in Australia

The Australian creep test was issued as the Australian Standard, AS 2891.12.1995 in November 1995. The test procedure was improved in 2008 in accordance with the Austroads mix design procedures. The Australian creep test procedure uses two specimen sizes, i.e. 100 mm diameter for mixtures with a maximum particle size of 20 mm and 150 mm diameter for mixtures with a maximum particle size of 40 mm. According to the test procedure the cyclic loading stress is 200 kPa, termination strain is 3,000 microstrain, and/or a termination pulse count of 40,000. The main parameter derived from the creep test curve in this procedure is the minimum slope of the accumulative strain versus number of load cycles (figure 3.15). The minimum slope is the point of inflection of the curve. The Austroads mix design procedure was published by Austroads (Alderson, Allan & Hubner, David 2008) and also as Australian Standard (AS-2891.12.1 1995).

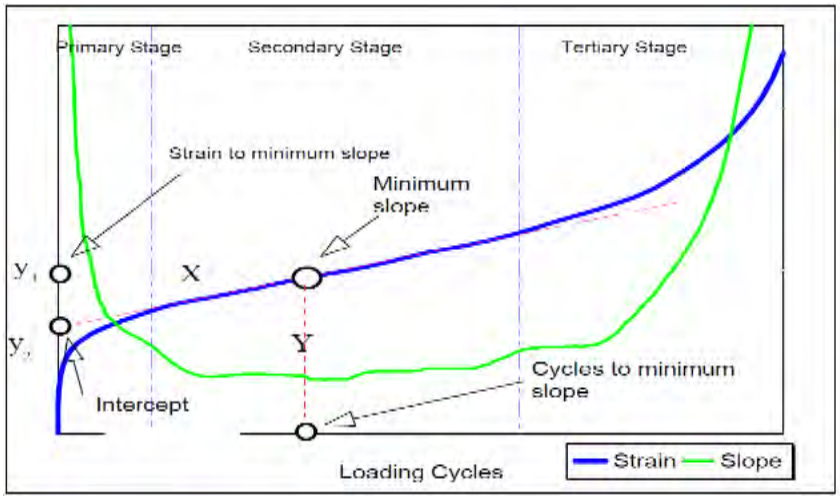

Figure: 3.15 Dynamic creep diagram (Alderson, Allan & Hubner, David 2008)

3.7 Summary

The literature review undertaken outlines the numerous tests and models that are available to be applied to explain the visco-elastic behaviour of asphalt under applied traffic loading. Behaviour of an asphalt mixture as a viscoelastic material can be modelled under vehicular loads by various mechanical techniques. Moreover, it is possible to model creep deformation of asphalt and to describe asphalt behaviour when it is subjected to repeated loads. The approaches vary from the simplistic elastic and mechanical models to the more complex ones employed in many of the computer programs used to predict the viscoelastic behaviour of asphalt. The models developed are normally based on laboratory data, which is dependent upon the actual testing procedure and replication of field in-situ stress conditions.

The review has indicated that there is much scope for improving laboratory testing methodologies that will generate superior models that can be used to evaluate in-situ behaviour. The key factor appears to be the use of a confining stress that is generated in response to the load cycle, thereby better simulating in-situ conditions. This is therefore the focus of this research.

CHAPTER 4

RESEARCH METHODOLOGY

4.1 Introduction

Many countries around the world, including the United States of America (USA), the United Kingdom (UK), and Australia, employ failure criteria as key input parameters for the mechanistic design of asphaltic pavements. While fatigue is a very commonly used criterion, creep is also an important factor, but not commonly considered due to a lack of well accepted and proven laboratory test methodologies. A laboratory creep test should replicate field stress and strain conditions in the test asphalt specimens to ensure that it is an appropriate option for including as a permanent deformation indicator in mechanistic pavement design.

A laboratory creep test should be able to be employed for predicting the resistance of an asphalt pavement to permanent deformation under repetitive trafficking. Although current laboratory creep test methods have good potential for evaluating permanent deformation of asphalt mixtures, there are serious concerns about their abilities to provide any precise prediction of asphalt susceptibility to permanent deformation. These concerns have arisen when creep test outcomes have been compared with data from field assessments. One reason for poor correlation appears to be a lack of an appropriate lateral confinement around the laboratory creep specimens. In other words a true 3D stress field is not generated. In an unconfined creep test, resistance to permanent deformation of the specimen is mainly dependent on the binder flow (rheology), while the role of the aggregate skeleton and its internal friction is minimised.

In this chapter, a new methodology is explored which will provide effective confinement for asphalt creep specimens. The proposed methodology is founded on the current Australian test, adapted to provide simulated field conditions. Sample

confinement is provided by a resin/ PVC composite ring that provides lateral support while operating within its elastic range under the generated hoop stresses. The chapter first considers key relevant previous research related to the adapted methodology before providing a detailed description of the new methodology. The following diagram (figure 4.1) provides an indication of the parameters that needed to be considered in establishing a testing regime for this investigation.

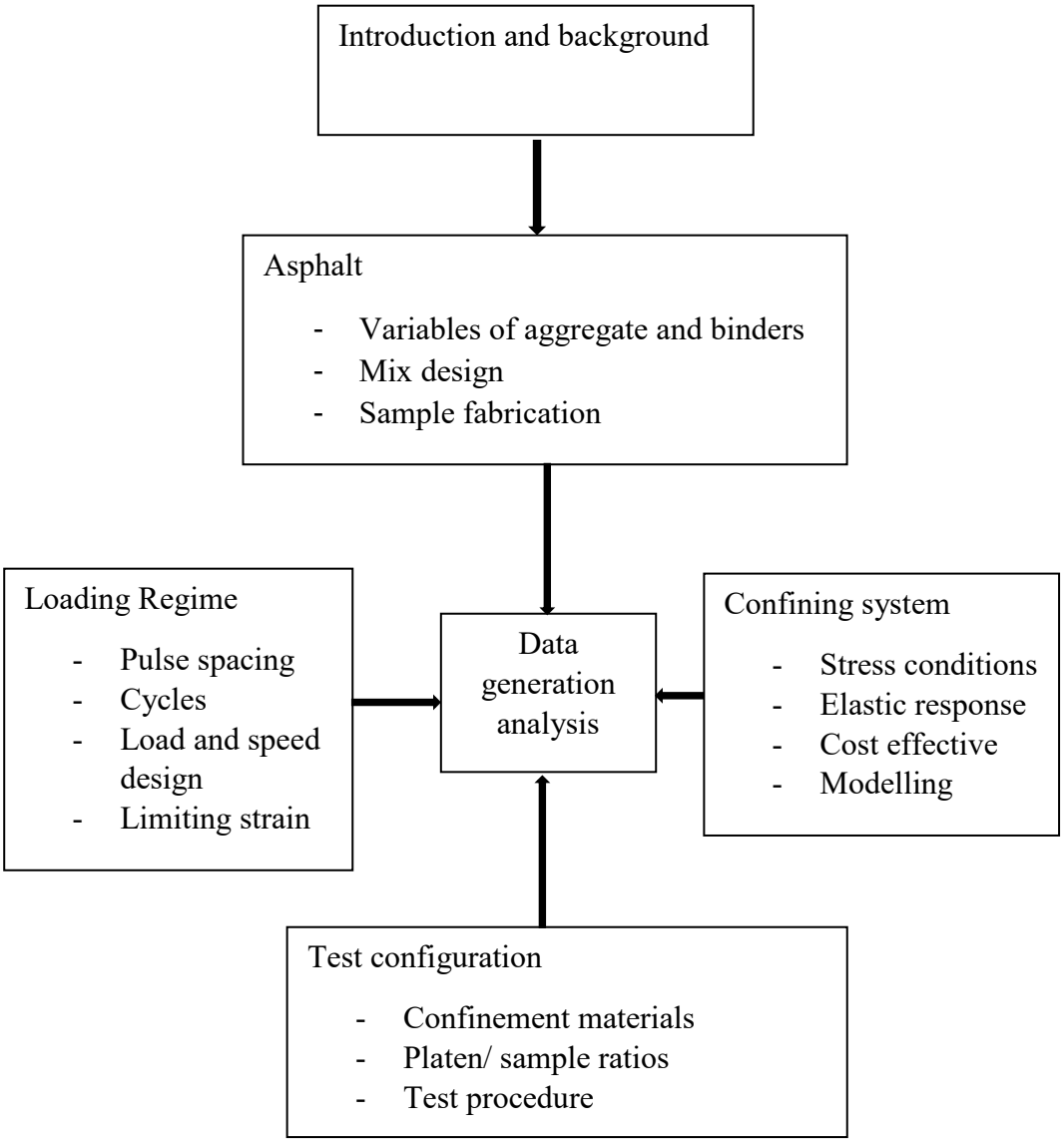

Figure: 4.1 Chart flow for the research methodology

4.2 Limitation of existing creep tests

The creep test is one of the most common techniques for evaluating asphalt susceptibility to plastic deformation and several standard test methods have been developed around the world. Specimens for the creep test are either cored from a road pavement or fabricated in a laboratory. In most tests an asphalt specimen is then exposed to axial, compressive, static or dynamic loads. The Australian dynamic creep test standard was published in November 1995 as the Australian Standard AS 2891.12.1995, and was reissued in 2008 in accordance with the asphalt mix design procedure of Austroads. However, many concerns have been reported (Oliver et al. 1995; Butcher & Lindsell 1996) concerning the ability of the current creep test to provide a precise prediction of plastic behaviour of asphaltic mixtures in the field. These concerns have been confirmed by comparing collected data from field studies with outcomes of laboratory creep tests (Oliver et al. 1995; Butcher & Lindsell 1996).

In Australia, a comprehensive study was undertaken by the ARRB Group to assess deformation resistance of various asphalt mixtures, and also to assess the relevancy of the creep test for predicting permanent deformation of asphalt. The experimental part was performed in conjunction with the Beerburrum Accelerated Loading Facilities (ALF) asphalt deformation trial (Oliver et al. 1995). By analysing field and experimental outcomes, it was found that the dynamic creep test had shortcomings for providing a precise prediction of asphalt rut-resistance. The study found that (Oliver et al. 1995):

1) The creep test ranked asphalt mixes with different aggregate gradations in a different order when compared to ALF rutting results.
2) The creep test indicated greater sensitivity to air voids content than was the case for field rutting.
3) The creep test indicated that by decreasing air void content to less than 3%, the rut-resistance of asphalt mixes continued to rise, which conflicted with field experience.

The Transport Research Laboratory (TRL) in the UK performed a comparison study (Smith 1996) on various techniques of analysing dynamic creep test outcomes. The

test was performed according to the "Draft for Development", published by the British Standards Institution named *"Method for determination of creep stiffness of bitumen aggregate mixtures subject to unconfined uniaxial loading"* (BS-DD-185 1990; Smith 1996)". In the study, specimens were cored from two motorways (M53 and M56). The study stated that a poor relationship was found between asphalt variables and creep test outcomes and it was concluded that it could be impractical for road agencies to use the creep test as a reliable test to indicate field performance (Smith 1996).

As mentioned previously, it has been hypothesised that the main reason of the creep test incapacity to duplicate field behaviour is a lack of an effective confinement around the laboratory specimens. As shown in figures 4.2, and 4.3 asphalt under a wheel load is surrounded by an asphalt mix that provides a confinement, while a (current) creep laboratory specimen does not have this condition. In many existing creep tests, specimens are unconfined. The stresses in a laboratory specimen are different to those in a field setting, leading to a failure to replicate in-situ asphalt behaviour (Oliver et al. 1995; Butcher & Lindsell 1996).

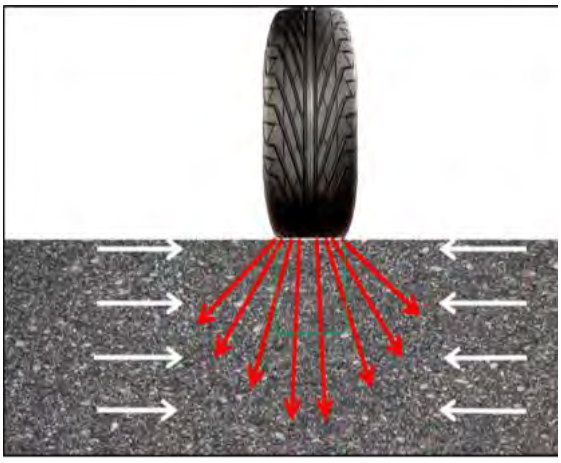

Figure 4.2 Pavement in the field surrounded by lateral asphalt

Figure 4.3 Existing Creep test without any confinement

The lack of an effective confining stress allows the aggregate skeleton to deform laterally. The "rut-resistance" of the asphalt in the current laboratory creep test is mainly attributed to flow resistance of the binder (or rheology of the binder). In the field, due to the confined state of the asphalt, the aggregate skeleton is constrained.

Hence, in addition to binder resistance to flow, plastic deformation of the asphalt is connected to internal frictional effects of aggregates (Oliver et al. 1995).

In summary, in an unconfined laboratory creep test, resistance to permanent deformation of the asphalt is mainly related to the binder properties, while in the field both binder and aggregate friction play significant roles.

4.3 Confining creep test

In response to the critical questions about the perceived inadequacy of the unconfined creep test to predict permanent deformation of asphalt, many researchers have been trying to develop new methods to improve laboratory test methods. It is expected that by providing a lateral pressure around the laboratory specimens, it will be possible to better simulate field conditions and obtain more relevant creep test outcomes. In this regard, different techniques such as repeat load triaxial cells have been developed.

4.3.1 Previous studies for developing confinement test

Liao Gong et al. (Liao et al. 2013) used an asphalt mix confinement for repeated load test as shown in the figure 4.4. In this process, an annulus of asphalt was provided as a confinement by using smaller top and bottom platens on a larger diameter specimen size. They used 75 mm diameter loading platens on a 150 mm diameter specimen size that provided a confinement annulus with 75 mm internal and 150 mm external diameters. The study reported that of four mix response factors, only one of them provided an acceptable relationship with rut depths of the asphalt pavement (R^2 greater than 0.7)

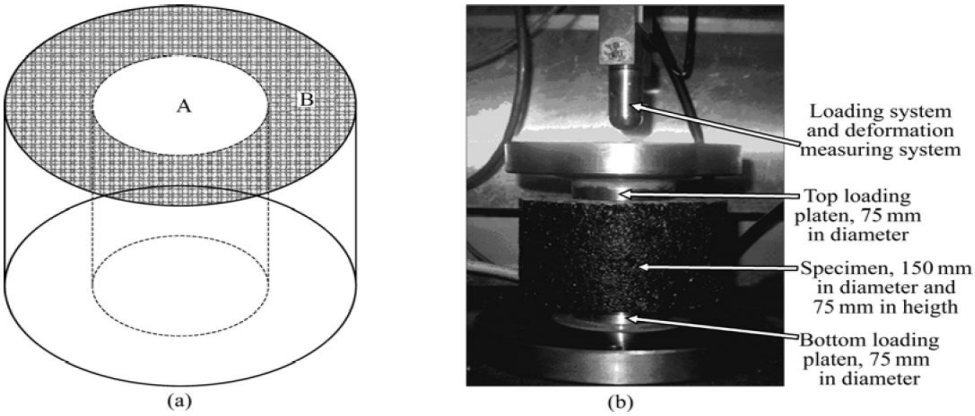

Figure: 4.4 Specimen confinement for the repeated load test: (a) section of a specimen: Core A, and confined ring B (schematic); (b) Test setup (Liao et al. 2013)

Young Doh et. al (Doh et al. 2007) developed a static strength test method for assessing permanent deformation of asphalt. The study stated that the asphalt underneath a tyre is surrounded by a portion of asphalt that acts as a barrier restricting shear deformation (Doh et al. 2007). In the test, a static load was applied through different loading head sizes. Specimen diameters were 100 and 150 mm, and the diameters of rounded heading loads were 30 mm (5 and 7.5 mm radius of round cut) and 40 mm (5 and 10 mm radius of round cut) (see figure 4.5). Failure modes of specimens under loading heads are shown in figure 4.6. In this test, deformation strength was measured and compared with other permanent deformation tests (wheel tracking and repeated –load creep). The authors concluded that the new test method would provide a good correlation with other rut parameters of asphalt.

Figure 4.5 Test equipment for 150 mm specimens (left) and 100 mm (right) with replaceable loading-head holders (Doh et al. 2007)

Figure 4.6 Failure mode of specimens by heading load (Doh et al. 2007)

Huang and Zhang (Huang & Zhang 2010) introduced a new confined creep test procedure named the Partial Triaxial Test (PTT), for assessing the rut resistance of asphalt. They used top and bottom smaller platen size (75 mm in diameter) on the bigger specimen size (150 mm in diameter) thereby providing a confinement for asphalt. Figure 4.7 show configurations of the PTT compared to other confined tests. The outcomes of the PTT test were compared with outcomes of the triaxial repeated load permanent deformation tests (TRTs). The study confirmed similar permanent deformation outcomes for PTT and TRT tests.

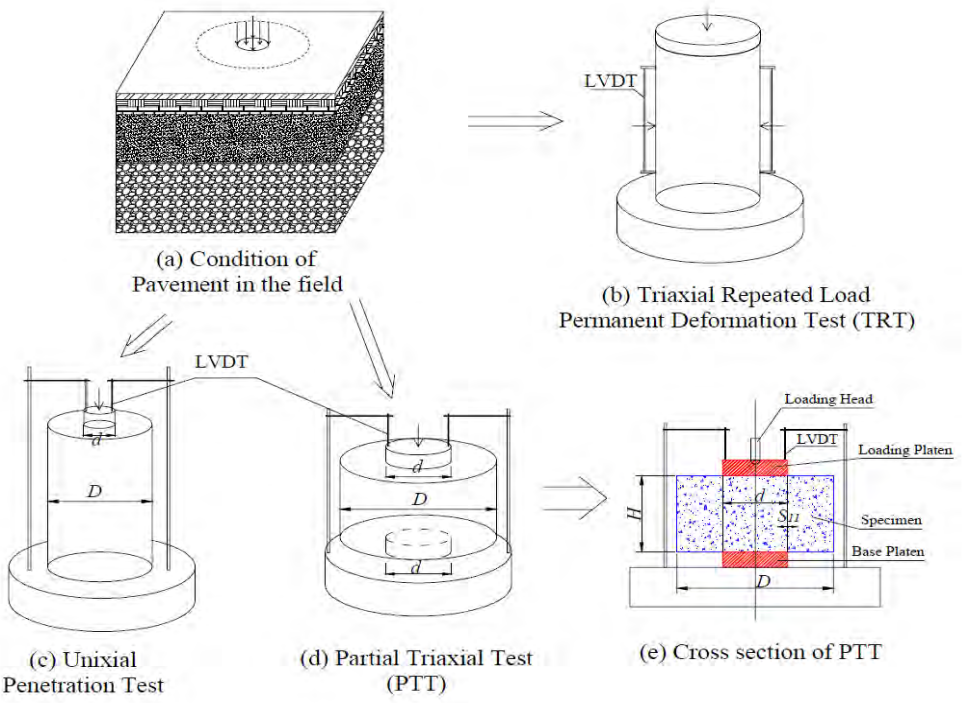

Figure: 4.7 Configuration of, a) In-situ condition of Pavement, b) TRT, c) Uniaxial Penetration Test, d) PTT, e) Cross Section of PTT (Huang & Zhang 2010).

4.3.2 Development of a new Confined Creep Test

To provide a suitable confinement and increase laboratory creep test relevancy, various methods have been evaluated from around the world. Triaxial cells and an asphalt annulus as confinement methods have been the most promising methods to date. However, these methods have their own specific disadvantages. Triaxial cells are able to produce either static or cyclic pulses as lateral pressure, nevertheless, they are complicated and time-consuming tests. Additionally, they are expensive techniques

and such equipment is not readily available in most asphalt production laboratories. Also some studies have describe test outcomes for triaxial testing that do not provide a good correlation with field assessments (Butcher & Lindsell 1996).

Providing a lateral restraint barrier with an asphalt annulus has been very popular as outlined earlier. The European standard uses the same technique for laboratory creep test and a 100mm diameter platen on a 150mm diameter specimen size for the European standard (BS-EN12697-25 2005). Although using an asphalt annulus for the creep test is simple to apply and provides a partial confinement for the specimen, it has its serious disadvantages in simulating in-situ rutting. Failure in the laboratory creep specimen and its condition post-test, indicate a different pattern to rutting mechanisms in the field pavement. Extensive cracking occurs in the specimens during the laboratory test (Figure 4.8). These cracks are mostly as result of tensile failure of the mix (bursting) and they do not replicate failure (rutting flow) in the field (Oliver et al. 1995).

Figure: 4.8 Crack development in the unconfined creep test

When a realistic stress is applied to simulate real traffic loads (around 750 kPa) in the laboratory, punching occurs in the specimen as shown in the figure 4.9. To resolve this problem and provide better confinement, a stress responsive elastic confinement is proposed (Oliver et al. 1995).

The research reported here developed a new method for providing confinement in a dynamic laboratory creep test. An annulus of asphalt was used with additional confinement provided by a PVC ring with a flowable epoxy resin infill. The rings were obtained by cutting a section from a PVC pipe, and the gap between ring and asphalt specimen was infilled with a flowable epoxy resin. The annulus of asphalt employed as part of the confinement was obtained by using 50 mm, 75 mm, and 100 mm diameter top platens on the 100 mm and 150 mm diameter asphalt specimens.

Figure: 4.9 Laboratory specimen punching when a simulated real traffic load was applied

It was anticipated that by providing such a stress-responsive confinement, it would be possible to change the failure pattern of the specimens to a more realistic deformation. It was expected that crack initiation and growth would be restricted and that some flow deformation would occur in the specimen, with the overall deformation in the laboratory specimen being closer to the flow deformation observed in the field.

In the new method, the magnitude and duration of lateral pressure (confinement) is generated as a function of applied load. It is possible to perform the new confined dynamic creep test with an existing Universal Testing Machine (UTS) and software without any changes allowing current users to easily employ the new method.

4.4 Material selection

The main goal of the mix material selections was to help to ensure realistic data from laboratory testing which would be able to more closely model in-situ asphalt performance. Asphalt mixes from an asphalt production plant correlate better with asphalt used in road pavements than laboratory produced mixes. Therefore, all materials, mixes, and asphalt samples were obtained from the Brisbane City Council (BCC) asphalt plant.

The properties and gradings of the aggregates, and details of the binders and fillers used in the production of the asphalt are provided below:

4.4.1 Aggregate

A crushed hornfels aggregate from the Mt Cootha Quarry in South-east Queensland, Australia was used as an aggregate and filler for fabricating asphalt specimens. Aggregate with maximum 13.2 mm particle size complying with a BCC as Type 2 aggregate gradation (dense graded mix) was chosen for all samples. Table 4.1 and figure 4.10 show the aggregate gradation.

Table: 4.1 BCC Type 2 aggregate gradation

Sieve	Grading	Upper Limit	Lower Limit
13.2	100	100	100
9.5	93	100	90
6.7	77	86	74
4.75	64	68	56
2.36	48	49	39
1.18	35	38	30
0.6	27	29	21
0.3	18	21	15
0.15	10.1	12	8
0.075	7.7	8	6

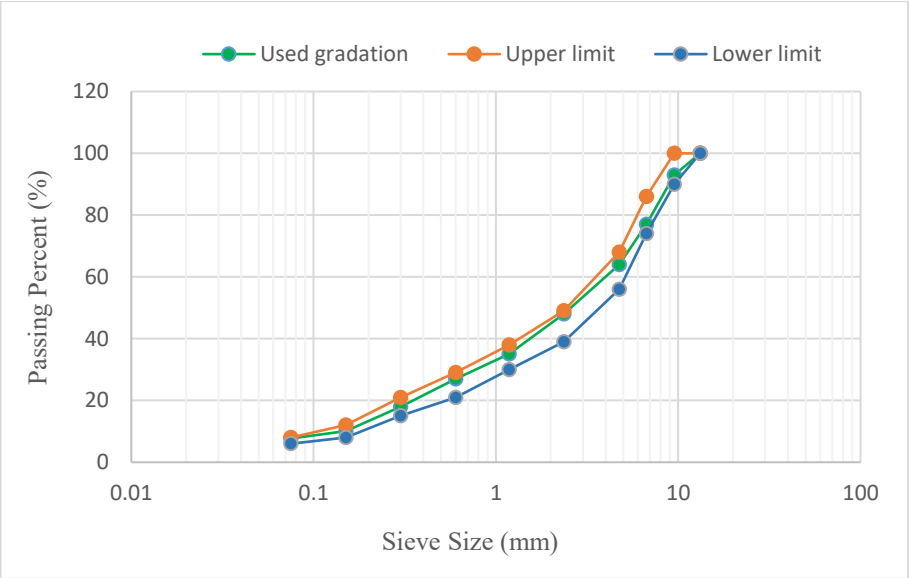

Figure: 4.10 BCC Type 2 aggregate gradation plot

Routine quality check were undertaken on the aggregates in line with relevant Australian standards (AS) and Queensland Department of Transport and Main Roads (Q) specifications as summarised in Table 4.2 and 4.3.

Table: 4.2 A ggregate characteristics

			7 mm	9 mm	14 mm
Test Method	Descriptio n	Limits	Test result	Test result	Test result
AS 1141.11	Grading	-	Conforming	Conforming	Conforming
AS 1141.15	Flakiness	<30%	9.5	13.3	7.8
Q 214 B	Water Absorption	Max 2%	0.61	0.49	0.24
Q 214 B	Particle density (Dry)	t/m3	2.671	2.654	2.673
Q 215	Crushed Particles	Min 80%	100	100	100
Q 217	Weak Particles	Max 1%	0.5	0.1	0.1
Q 205 B	10% Fines	Min 150 KN	296	272	239
	Product Conforms	(Yes/ No)	Yes	Yes	Yes

Note: Q refers to a Queensland Department of Transport and Main Roads test method

Table: 4.3 Filler characteristics

			Baghouse	Rockflour	Combined BH/RF
Test Method	Description	Limits	Test result	Test result	Test result
AS 1141.11	600 µm Grading (AS 2357 Limits)	100	100	100	100
AS 1141.11	300 µm Grading (AS 2357 Limits)	95-100	100	100	100
AS 1141.11	0.075 µm Grading (AS 2357 Limits)	75-100	92.8	97.1	97.1
AS 1141.17	Voids in Compacted Filler	Min 38%	48	49	46
AS 1141.7	Apparent Particle Density	TBR	2.706	2.756	2.729
	Products Conforms	(Yes/ No)	Yes	Yes	Yes

4.4.2 Bitumen

The minimum bitumen content of asphalt mixes in Australia is typically lower than that used in the USA and European countries. The main reason for this reduction in bitumen is the sub-tropical/temperate climates of most Australian states. This leads Australian pavement designers to use relatively lower bitumen contents to minimise surface flushing deterioration (Stephenson 2002). The bitumen content for this study was designed to be 5% for all mixes.

As previously mentioned, binder resistance to flow (or consistency of the binder) and the aggregate skeleton are two core contributors to the rut-resistance of pavements. As this study was investigating permanent deformation of asphalt, it was important to select binders with different rheologys. One rut-resistance bitumen i.e. Multigrade (1000/320) and one unmodified bitumen (C170) were used to fabricate specimens. The properties of the two bitumens were determined using standard Australian test procedures as shown in Tables 4.4 and 4.5.

Table: 4.4 Properties of bitumen class C170 (batch bitumen)

Property	Test Method	Limits	Test Result
Viscosity at 60° C (Pa.s)	AS 2341.2	140 - 200	189
Penetration at 25° C, 100g, 5s (pu)	AS 2341.12	Min 62	68
Viscosity at 135° C (Pa.s)	AS 2341.2	0.25 - 0.45	0.420
Density at 15° C (t/m^3)	AS 2341.7	1 min	1.058

Table: 4.5 Properties of Multigrade 1000/320 bitumen (batch bitumen)

Property	Test Method	Limits	Test result
Viscosity at 60° C (Pa.s)	AS 2341.2	Report value	910
Penetration at 25° C, 100g, 5s (pu)	AS 2341.12	Report value	43
Viscosity at 135° C (Pa.s)	AS 2341.4	1.5 max	0.78
Viscosity at 60° C after RTFOT (Pa.s)	AS 2341.2	3500 - 6500	5550
Penetration at 25° C, 100g, 5s after RTFOT	AS2341.12	26 min	26
Softening Point (C)	AS 2341.18	Report	58.5
Flash Point, °C	AS 2341.14	250 min	348
Density at 15° C (t/m^3)	AS 2341.7	Report	1.031

4.5 Sample preparation

4.5.1 Mix design

BCC type 2 mix with two different binders were selected, namely BCC Type 2 Multi-grade asphalt and BCC Type 2 C170 asphalt. The aggregate gradation, aggregate and binder properties of these were provided in the previous section. These mixes were chosen as both are popular in Queensland and many roads have been paved with these mixes. The rut-resistance of the two mixtures are very different, and they provide a good basis for this research. A wide range of mix air voids (from 2% to 9%) was investigated as part of the research.

4.5.2 Mix fabrication

All manufacturing of asphalt specimens was undertaken at the BCC Eagle Farm Asphalt Plant (figure 4.11). Materials were obtained during normal production runs. Bulk samples of 28 kg were placed in special containers and stored under controlled conditions at the asphalt plant. Around 800 kg asphalt in total was used to fabricate specimens for this research.

Figure: 4.11 The control room of the Eagle Farm Asphalt Plant

4.5.3 Compaction

Shear box compaction was used for all compacted mixes. The compaction process simulates in-situ pavement roller compaction by using a cyclic shear load, a constant compressive load, and a shear angle to the mix. Figure 4.12 shows the shear box compactor concept. The compactor is able to provide a thick slab (up to 190 mm), which can supply specimens for wheel-track, beam fatigue and cylindrical asphalt tests, with superior control of density and homogeneity of the final compacted product (Gabrawy 2000). Material was kept in an oven at 160° C for three hours prior to compaction. A total of 120 cylindrical asphalt samples were manufactured in two different sizes, i.e. 150mm diameter × 50mm height, and 100mm diameter × 50mm height by coring from 30 rectangular slabs of 440mm×170mm×150mm dimensions. The sample fabrication process is illustrated in Figure 4.13.

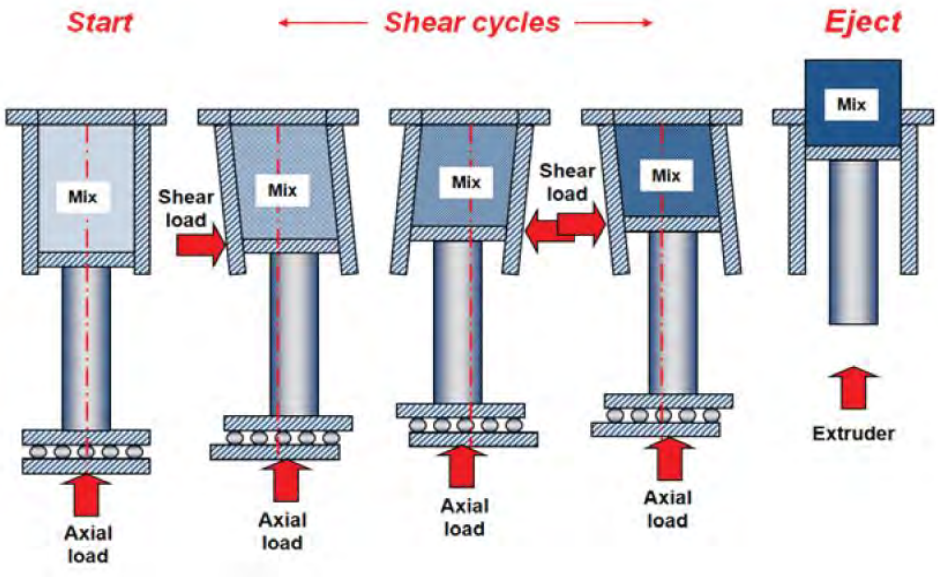

Figure: 4.12 Shear box compactor concept (Sullivan 2015)

Figure: 4.13 A) Placing asphalt mix in the shear box compactor. B) Coring specimens from slabs. C) Cutting specimen to the required sizes. D) Prepared specimens

4.6 Confinement arrangement

As described previously, the confining system consisted of a composite resin/ PVC ring. Two diameter sizes of PVC pipes of 100 mm and 150 mm were used. As the wall thickness of the pipes has a direct effect on the magnitude of confinement in addition to that provided by the infill epoxy, two different wall thicknesses of PVC of 4 mm and 2.5 mm were investigated.

In order to place rings around the asphalt specimens, it was necessary to have a small space between the PVC rings and samples and a 2.5 mm space was selected for all specimens. An epoxy resin was used as the gap filling material with the physical properties detailed in Table 4.6.

Table: 4.6 Physical properties of resin

Property	Description
Appearance	Part A: Dense and thick fluid Part B: Clear yellow colour liquid
Mix ratio	By weight: 10 to 1 for parts A and B respectively By volume: 4 to 1 for parts A and B respectively
Compressive strength	120 MPa after 7 days
Gel time	1 kg mix
Mixed density	2.12
Coverage	1×15 litre kit, yields 0.15 m^3
Proprietary name	HYCHEM PF-7

The process of providing the confining system is outlined below:

- Rings were cut from a section of 150mm diameter pipe for 150mm specimens and from 100mm diameter pipes for 100mm diameter specimens. As the height of the asphalt specimens was 50mm, the rings were cut to 50mm lengths.
- In order to obtain rings with 4 mm wall thickness and also to retain a 2.5mm space for resin, the insides of rings were machined. Rings with 2.5mm wall thickness and again preserving 2.5mm space for resin, both the inside and the outside of the rings were machined.
- As the resin was liquid after mixing (in the initial phase), it was necessary to seal the ring before filling with resin. Rings were placed on a plastic sheet and the bases sealed with a silicone sealant as shown in the figure 4.14. It required around 3 hours for the silicon sealant to be firm enough for in-filling the gap with resin.
- Resin was prepared by mixing its two parts. Mix ratios for the two parts were 10 to 1 by weight or 4 to 1 by volume for resin and hardener respectively.
- Finally, the space between rings and asphalt specimens was in-filled with resin. After 7 days resin reached its maximum compressive strength of 120 MPa.

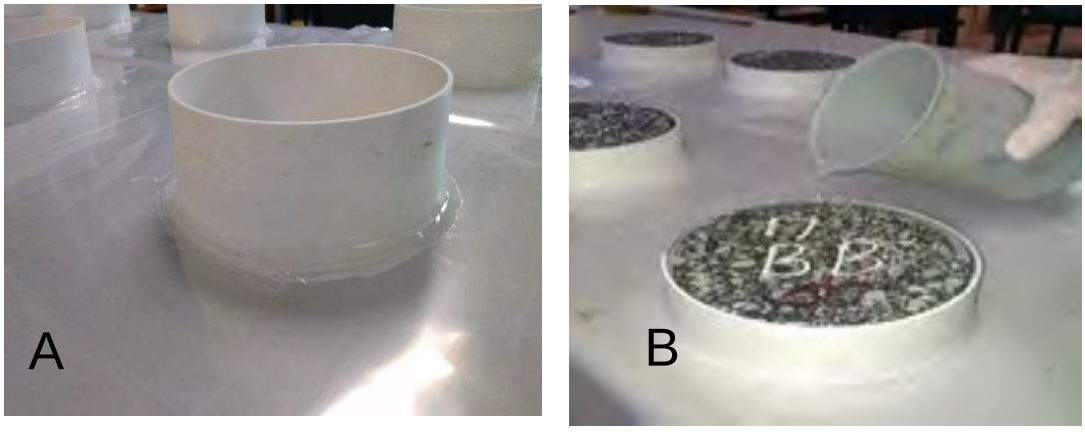

Figure: 4.14 A) Ring sealant, B) Filling gap with resin

4.7 Air voids content measurement

It is well established that air void content is correlated with creep deformation, fatigue, and resilient modulus. In this study a wide range of air voids were investigated, which would also cover the specification void range for the BCC asphalt. The percentage of air voids in the compacted mixes was determined according to Australian Standard method (AS-2891.8 2005) as follows:

$$AV = \frac{\rho_{max} - \rho_{bulk}}{\rho_{max}} \times 100 \qquad \text{Equation 4.1}$$

where

AV = is the air voids

ρ_{max} = maximum density of the mix (t/m^3)

ρ_{bulk} = bulk density of the compacted mix (t/m^3)

The bulk density of the compacted mixes was calculated in according with Australian standard number (AS-2891.9.2 2005) from following equation:

$$\rho_{bulk} = \frac{m_1 \rho_w}{m_3 - m_2} \qquad \text{Equation 4.2}$$

where

ρ_{bulk} = bulk density of the compacted mix (t/m^3)

m_1 = mass in air of the specimen (grams)

m_2 = mass in air of the saturated specimen (grams)

m_3 = mass in water of the specimen (grams)

ρ_w = water density at the test temperature.

The water displacement method was used for determining maximum density of the mixes. Australian standard test number (AS-2891.7.1 2004) was employed as a test method using the following equation:

$$\rho_{max} = \frac{(m_3 - m_1)\,\rho_w}{(m_3 - m_1) - (m_4 - m_2)} \qquad \text{Equation 4.3}$$

where

ρ_{max} = maximum density of the mix (t/m^3)

m_1 = the mass of the pycnometer and lid (grams)

m_2 = the calibrated mass of the pycnometer and lid, filled with water at 25°C (grams)

m_3 = the mass of the pycnometer, lid and test portion (grams)

m_4 = the mass of the pycnometer, lid, test portion and water (grams)

ρ_w = water density at 25°C (0.997 t/m^3).

4.8 The Marshall test results

The Marshall test is a common empirical test for preliminary checking of some properties of mixtures. The Marshall test has carried out as an initial quality control of slabs. Parameters such as Marshall Stability, Voids in the Mix (VIM), Marshall Flow, Density, Voids in Mineral Aggregate (VMA), and Voids Filled with Bitumen (VFB) were determined. Table 4.7 provides Marshall Test results.

Table: 4.7 Marshall Test results (C170 mix)

Description	Result	Limits
Air Voids (%)	4.4%	2% to 5%
VMA (%)	14.6	TBR
Voids Filled (%)	70	TBR
Density (t/m3)	2.37	TBR
Flow (mm)	3.9 mm	2mm to 4mm
Stability (kN)	11.3	Minimum 7.5 kN
Stiffness (kN)	2.9	TBR

TBR: To be report

4.9 Dynamic creep test

This study used the current Australian dynamic creep test method as a basis for the research. The Australian standard titled "Determination of the permanent compressive strain characteristics of asphalt - Dynamic creep test" known as (AS-2891.12.1 1995), and also a draft of Austroads titled "Testing Asphalt in Accordance with the Austroads Mix Design Procedures - Part 4- Dynamic Creep" (Alderson, Alan & Hubner, David 2008) were used as the base method to perform all dynamic creep testing. The most important variations to the standard dynamic creep test procedure were different platen sizes, magnitude of the cyclic load, and cycle numbers for test termination.

In the existing Australian standard, the magnitude of the compressive stress for the dynamic creep test is 200 kPa, while heavy vehicle axles and tyre pressures generate stresses on road pavements that are much higher. Many researchers have indicated that real tyre pressure is more than 500 kPa and for some special cases, it can be up to 1000 kPa, or even higher. Austroads has adopted 750 kPa tyre as a realistic pressure on asphalt pavements for its pavement design procedure (Youdale 1996; Gribble & Patrick 2008; Austroads 2012). The application of such a tyre pressure in the existing

dynamic creep test using a reduced platen size will ensure that bursting will occur in the specimen. The new confinement system provides an opportunity to apply real tyre pressure in the laboratory. In this study a 750 kPa compressive stress (constant stress) was used for all tests, with busting being mitigated through the generated hoop stress.

4.9.1 Strain gauging

As the magnitude of the stress generated within the confining PVC, is very important for evaluating the effectiveness of the new confinement, two strain gauges were attached on selected specimens (with and without confinement) to measure the load induced stresses. The measured strain in the laboratory was then compared with models in order to better investigate the impact of the confining system variables such as ring thickness. Table 4.8 provides details of the strain gauges used.

Table: 4.8 Strain gauge specifications

Property	Description
Gauge type	PFL-30-11
Gauge factor	2.13 ± 1%
Gauge resistance	119.6 ± 0.5Ω
Transverse Sensitivity	- 0.1 %
Gauge length	30 mm
Element	Single element

4.9.2 Platens and load cycles

As detailed in the figure 4.15, different platen sizes of 50 mm, 75 mm, 100 mm, and 150 mm diameter were used in testing. It is commonly understood that the diameter of the loading platen should be at least three times larger than maximum aggregate size. The 50 mm, 75 mm, 100 mm, and 150 mm platens, used in this study can be employed

for loading mixes with 16 mm, 25 mm, 33 mm, and 50 mm maximum aggregate sizes respectively.

The test standard for cycles recommends a maximum 30,000 microstrain accumulated strain, or a maximum 40,000 number of loading cycles as a test termination for the dynamic creep test. To have a more informative assessment of the new confined test, a maximum 100,000 microstrain accumulated strain, or 100,000 n loading cycles were used in the investigation.

Figure: 4.15 Different platen sizes

4.9.3 Test procedure

A Universal Testing System (UTS) machine developed by Industrial Process Controls (IPC Global) was used for performing dynamic creep tests. After applying confinement to specimens, the following steps accomplished the new confined creep test:

- The ends (top and base) of the specimen were polished using an 80 grit emery paper to remove any surface defects.
- The diameter and height of each specimen was recorded at four different locations around the specimen.
- Strain gauges were attached (for selected specimens).

- A silicon lubricant was applied on the relevant top and bottom parts of each specimen to reduce end friction.
- Specimens were placed in the control chamber at 50^{o}C for three hours to attain and preserve standard reference temperatures
- Specimen and platen were centrally aligned under the actuator.
- The required inputs were entered into the software of the creep machine. Table 4.9 records some inputs for the software.
- The machine was set to apply the selected number of loading cycles.

Figure 4.16 illustrates the new confined creep specimen under dynamic creep loading cycles.

Figure: 4.16 New confined creep specimen under dynamic creep loading cycles

Table 4.9 Inputs for dynamic creep test

Parameter	Description
Compressive stress	750 kPa
Seating stress	20 kPa
Loading period	500 milliseconds (ms)
Pulse repetition period	2000 milliseconds (ms)
Test temperature	50^{o} C
Termination strain	100,000 µs
Termination pulse count	100,000 cycles

As mentioned previously, Austroads has adopted 750 kPa as a realistic tyre pressure on asphalt pavements and thus a 750 kPa platen pressure was used for loading all asphalt samples. A 20 kPa pressure was used as a seating stress to seat the specimen into the jig (UTS-14.Manual 2011). The Australian temperature standard of 50°C was adopted for the dynamic creep tests.

A wide range of frequencies (from 0.1 to 12 Hertz) has been used for representing vehicle speed around the world (Sullivan 2015). Mollenhauer et al. (Mollenhauer et al. 2009) indicate that a 1.0 Hz loading frequency conformed to the frequency of asphalt strain induced by crossing a wheel at the speed of 7.6 km/h at the bottom of a 34 cm asphalt layer. NCHRP report 465 (Witzcak et al. 2002) has suggested to use 10 Hz and 0.1 Hz as the frequency for highway speed and creep-intersection traffic respectively. The Australian standard for dynamic creep test suggests 0.5 Hz frequency (500 milliseconds loading time) which is about a 3.2 km/h speed. Frequency concept of NCHRP 9-19 shown in the equation can be used to convert vehicle speed into designed frequency (Kumlai et al. 2014).

$$t = \frac{2(a+ h_{ac})}{17.6\ v}$$ Equation 4.4

where;

t: time of loading (second)

a: the radius of tyre pressure (4.886 inch)

h_{ac}: the thickness of the asphalt concrete layer (3.93 inch)

v: speed of vehicle (mph)

4.10 Modelling

In order to expand the application of the new confined test, elastic and viscoelastic modelling have also been undertaken. The models helped to obtain useful information on the distribution of stresses and strains in the pavement using the existing and new confined creep tests. Models also assist in the design of an adequate confining ring. According to model outcomes and laboratory dynamic creep test results, the optimum sample and platen size can be determined. Models helped to analyse different materials for fabricating the confining ring. The finite-element method was employed for elastic and visco-elastic models as detailed in the next chapter.

The finite-element approach is a popular technique widely used for investigating asphaltic pavements. It can model linear and nonlinear materials, two and three dimensional (2D, and 3D) geometries, elastic, plastic, viscoelastic material behaviours, and many complicated characteristics. Several finite-element based programs and software are available to model the structure of asphalt pavements such as Abaqus, Strand7, Adina, etc. Abaqus and Strand7 programs have been employed in this study.

Different elastic and visco-elastic models of single and multi-layer asphalt pavements under real tyres and pressures (750 kPa stress, with 200mm diameters tyre pressure) were set up to simulate field conditions. For laboratory modelling, various specimens with 150mm diameter and 50mm height (as laboratory samples), under varying platen sizes (50mm, 100mm), exposed to static and dynamic 750 kPa axial stress with

different confinement situations have been modelled. Figure 4.17 shows a schematic elastic model of a laboratory specimen.

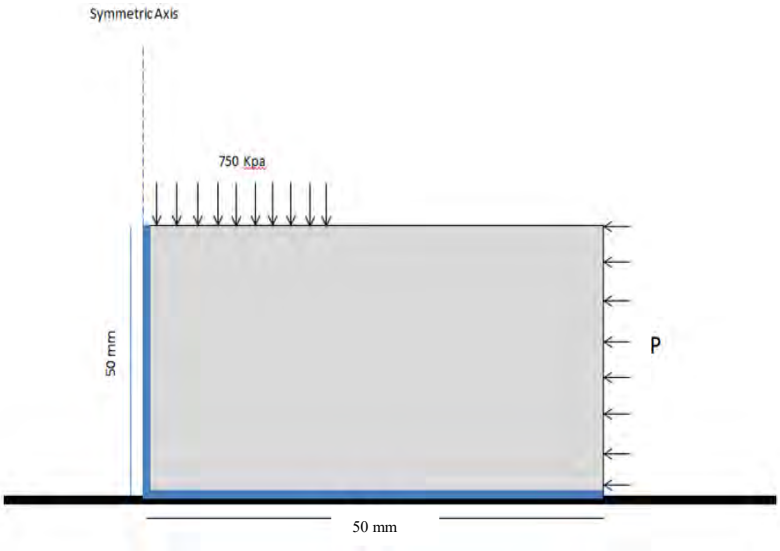

Figure: 4.17 Schematic of the creep test model

Some assumptions of the elastic model are as below;

a) Subdivide: 40 ×40 nodes.

b) Elements: 8 node quadrilateral elements.

c) Axisymmetric model: (Rx=Ry=Rz=0 and Z translation= 0).

d) Edge Restraints: (Y axial symmetric: Dy free, Dx=fixed, and, X axle: Dx free, Dy= fixed, where in all the other places: Dx= Dy= free).

e) Properties Input; [a) Material; Isotropic (other options: orthotropic- rubber-soil- fluid), b) Type; axisymmetric.

The following chapter (Chapter 5) will provide more details of the models.

4.11 Summary

The poor correlation of laboratory creep test outcomes with data collected from in-situ pavement assessment has raised many concerns about the adequacy of existing creep test methods employed to evaluate the rut-resistance of asphalt mixes. Many researchers believe the main reason for laboratory creep test shortcomings for duplicating field result is related to a lack of a realistic confinement for laboratory

specimens. As in-situ asphalt is confined by a surrounding mass, a measure of confinement is provided. Most existing creep tests are unconfined.

Several researchers have attempted to design better creep evaluation methodologies. It has been proposed that provision of confinement for the creep test might establish a better relationship between field and laboratory conditions. The European standard for creep test uses a smaller top platen size on a larger specimen size (100mm platen on 150mm specimen) to provide some limited measure of confinement. Although many researchers have tried to introduce a suitable method for improving the creep test, most developed methods have their own specific drawbacks.

In this chapter, a new confinement method for the creep test has been introduced. A composite arrangement of PVC pipe and resin was developed to provide a stress dependent effective confinement for specimens. Additionally, different platen/ specimen configurations using a smaller top platen were developed. The research reported here combines the elements of reduced platen sizes, effective confinement, and representation of realistic tyre pressures to provide a cost effective new dynamic creep test methodology.

CHAPTER 5

MODELLING

5.1 Introduction

Parametric modelling is widely seen as an integral part of research, allowing extrapolation of experimental work through validated models. Being representative of a system, they provide a basic reference for evaluation, and help to reduce cost and energy in research. Among the various types of available modelling techniques, finite element methods (FEM) are among the more popular in the pavement engineering field as they can efficiently model and predict asphalt behaviour under thermal and traffic loads. Abaqus is one of the most widely used computer software programs and is able to model a broad range of problems.

FEM modelling is employed in this study to provide a formative view about the study. It is used to develop a correlation between the new confined test and in-situ pavement conditions. Additionally, it helps to assess stress distributions in the new confined specimens, and provide a base reference for comparing outcomes of experimental work. A number of Abaqus FEM models have been created including, a new confined test model, an existing unconfined test, and for an in-situ pavement. Outcomes of the models are compared to each other and to the outcomes of experimental tests. As outlined in Chapter 1 the modelling outcomes provides both industry and researchers with better confidence in the laboratory outcomes generated from the revised testing methodology.

5.2 Modelling

Various techniques are available to model and analyse rigid and flexible pavements. Some of the most common techniques for modelling flexible pavements include analytical methods, multilayer elastic theory (MLET), finite element methods (FEM), finite difference methods, discrete element method (DEM), boundary element methods (BEASY), and hybrid methods (Uzarowski et al. 2007). These techniques each have

their own advantages and disadvantages and the FEM is considered as the most popular technique for modelling flexible pavements worldwide.

5.3 Finite Element Methods (FEM)

FEM is widely recognised as a capable method for evaluating structures and materials behaviour. The first application of FEM was in 1965 (Williamson 2015). In the pavement engineering field, complex visco-elasto-plastic behaviour of asphalt under thermal and traffic loads has boosted application of FEM as a powerful technique for evaluating mechanistic behaviour of flexible pavements (Williamson 2015). It is able to analyse linear and non-linear elastic material, viscoelastic and visco-plastic materials, static and dynamic analysis, fracturing, reflection cracking, thermal cracking, hardening, large strains/deformations, and other sophisticated pavement phenomena (Uzarowski et al. 2007; Ebrahimi 2015).

In the FEM method, the physical geometry of the structure to be analysed is divided into numerous finite elements. The body of a structure is represented by a collection of finite elements that are connected at their shared nodal points. The stiffness matrix for any specified finite element can be determined and the total body stiffness is determined by integrating the discrete stiffness matrix of elements. The outcome is a collection of equations that indicate nodal displacements and the loading force. Solving these equations can determine nodal displacements, and consequently, allow the calculation of stresses and strains in any individual elements (Uzarowski et al. 2007). The stresses and strains in the body of the structure are calculated by a displacement function in each finite element (Uzarowski et al. 2007; Abaqus-6.13 2013).

Several FEM software programs have been successfully used to model flexible pavements. Some of the commercially available FEM programs for pavement modelling include Abaqus, ADINA (Automatic Dynamic Incremental Nonlinear Analysis), Strand7, ILLI-PAVE, Plaxis, MICHPAVE (Uzarowski et al. 2007; Bohagr 2013). This study has adopted Abaqus as the main FEM program, although Strand7 was used for some initial investigative work.

5.4 Abaqus

Abaqus is a capable general purpose program able to model a broad class of structures and materials from comparatively plain linear analyses and linear elastic to the most complicated non-linear problems. Abaqus has a large library of material properties and also a wide-range of finite element types such as continuum, rigid, shell, beam, and truss elements (Uzarowski et al. 2007; Ebrahimi 2015).

Abaqus program includes three analysing programs namely; Abaqus/Standard, Abaqus/Explicit, and Abaqus/CFD. The function of each program is as follows (Abaqus-6.13 2013):

- Abaqus/Standard is a multipurpose product which is able to solve an extensive range of linear and non-linear issues.
- Abaqus/Explicit is a special-purpose product which applies an explicit dynamic finite element formulation.
- Abaqus/CFD is a powerful Computational Fluid Dynamics (CFD) product.

5.5 Modelling the laboratory test and in-situ pavement

Modelling was employed to develop a theoretical analysis of the existing unconfined laboratory test, the new confined test, and an in-situ asphalt pavement. In this regard, various FEM simulations by Abaqus and Strand7 software were created. The primary purposes of the modelling for this study were as follows;

- To obtain a broad informed view about the study through parametric analysis
- To compare the new confined test with the existing unconfined test and in- situ asphalt pavement stresses.
- To analyse developing stresses in various specimens under a 750 kPa tyre pressure.
- To assess different materials for the optimal confinement.
- To evaluate and develop a relationship between laboratory and field conditions.
- To compare the outcomes of the experimental research with FEM modelling.

In order to fulfil the research needs, several models with various load and boundary conditions were developed. The new confined specimens (with 100 mm diameter and a 50mm height) were modelled subjected to 750 kPa pressure, applied via a 50mm platen. For the confined model, two concentric layers of materials encompassed the wall of the specimen as confinement. The first layer was a resin with 2.5 mm thickness, and the second layer was the PVC ring with either 2.5 mm or 4mm thickness. The two different thicknesses were selected for the PVC to provide different confining conditions.

Since a wide range of resins with different engineering properties exist, several resins with various elastic properties were selected and used in the models. Selecting different resins and PVCs enabled the design of appropriate confinement. A full depth asphalt pavement and a multilayer pavement were both modelled to represent real in-situ asphalt pavements.

An elastic model was used for assessment in the study. In this model fundamental engineering parameters of asphalt, resin and PVC such as Poisson ration, elastic modulus, and density were introduced as material properties. It should be mentioned that a viscoelastic model was trialled for simulation in the study through Prony series of the generalized Maxwell model. The unavailability of laboratory equipment for measuring asphalt relaxation modulus for a viscoelastic model meant that some data viscoelasticity parameters had to be accessed from the literature. However, modelling outcomes proved spurious and consequently they are not included in this study.

5.6 Model creation

Abaqus includes several modules for creating a model. These modules are as follows: 1) geometry creation, 2) material selection, 3) specifying outputs, 4) assembling the Instance, 5) specifying steps in analysis, 6) introducing boundary and load conditions, 7) defining finite element types, 8) meshing the model and 9) data submitting for analysing (Uzarowski et al. 2007).

Abaqus does not have any built-in system of units and before starting the creation of a model it is necessary to choose a system of units for consistency. In this study SI-mm

was selected as the unit system. The following are the required steps for creating models in Abaqus.

5.6.1 Axisymmetric model

In the geometry of some structures, each element and also the loading position are symmetric around a specific line. It is known as an axisymmetric element and the line is named the axisymmetric axis. Cylindrical geometries are mainly considered as axisymmetric problems in simulations (Logan 2007; Monographs 2013). In this type of model only one cross-section represents all properties of a structure thus saving analysis time. As the specimen geometry of this study can be categorized in the axisymmetric group, an axisymmetric finite element model is used. Figure 5.1 provides a schematic of the axisymmetric model used for the confined laboratory test.

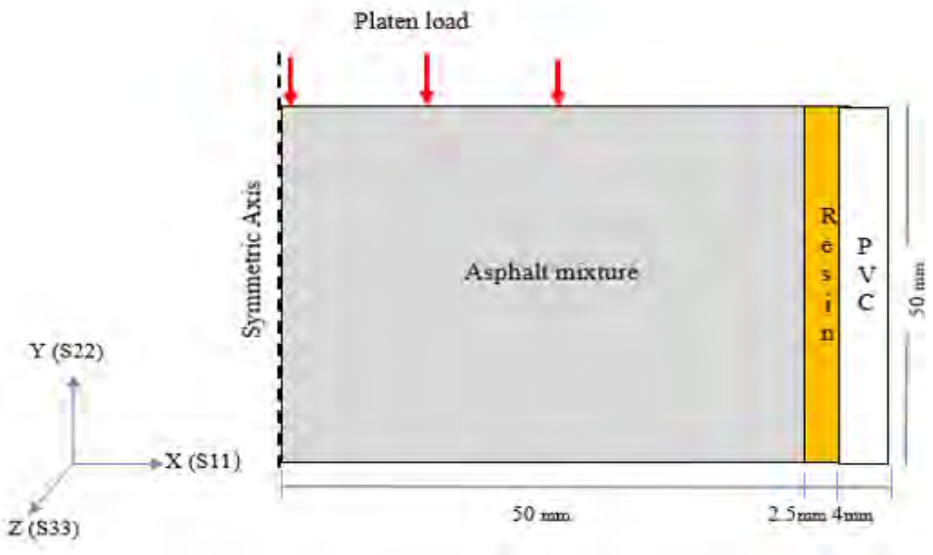

Figure: 5.1 Schematic of FEM axisymmetric model of the confined specimen

5.6.2 Geometric configuration

Geometry configuration is the first step for creating a model in Abaqus. Physical geometry of a model is defined by a part which is the building block of a model. Several configurations have been used to model different conditions (laboratory and in-situ position). As outlined below, a 100mm diameter specimen under 50mm diameter platen size, confined with 2.5mm resin and 4mm (or 2.5mm) PVC wall thicknesses is the basic model employed.

A 100mm diameter platen on a 100mm diameter unconfined specimen (existing test configuration) was also created. In-situ pavement was also modelled with different configurations such as a 2000mm to 1000 mm asphalt under 200 mm tyre size, and a multi-layer pavement with 2000mm to 500mm subgrade, 300mm base and 200 mm asphalt. These two created geometries in Abaqus are depicted in Figures 5.2 and 5.3.

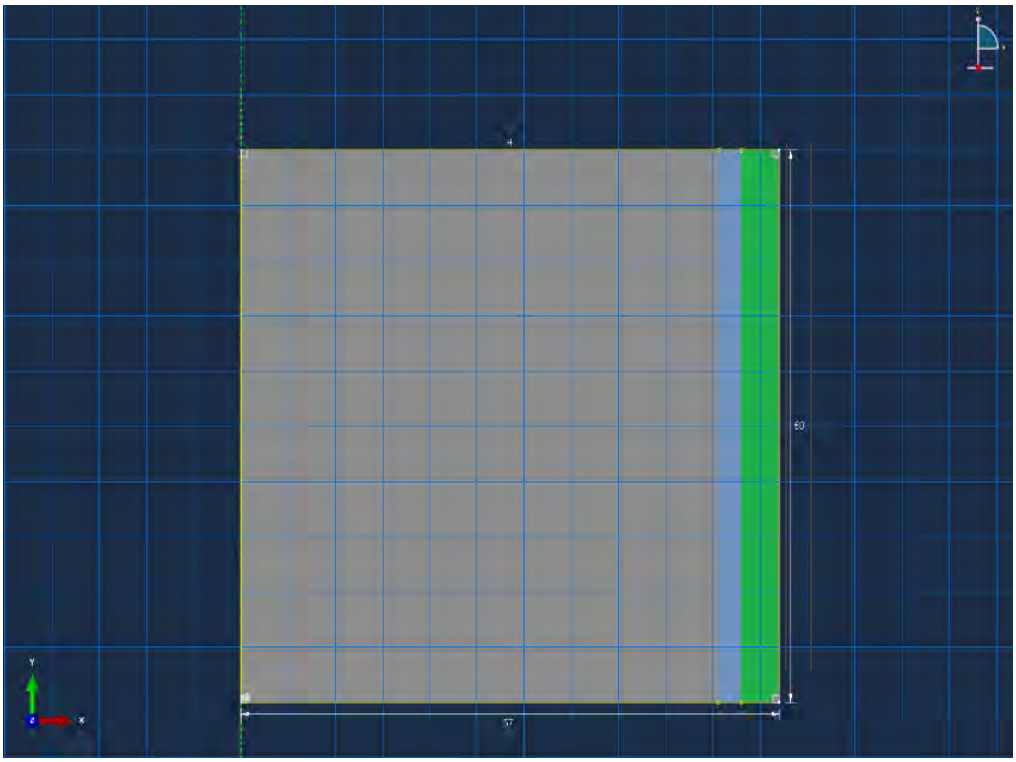

Figure: 5.2 Sketched geometry of the confined specimen

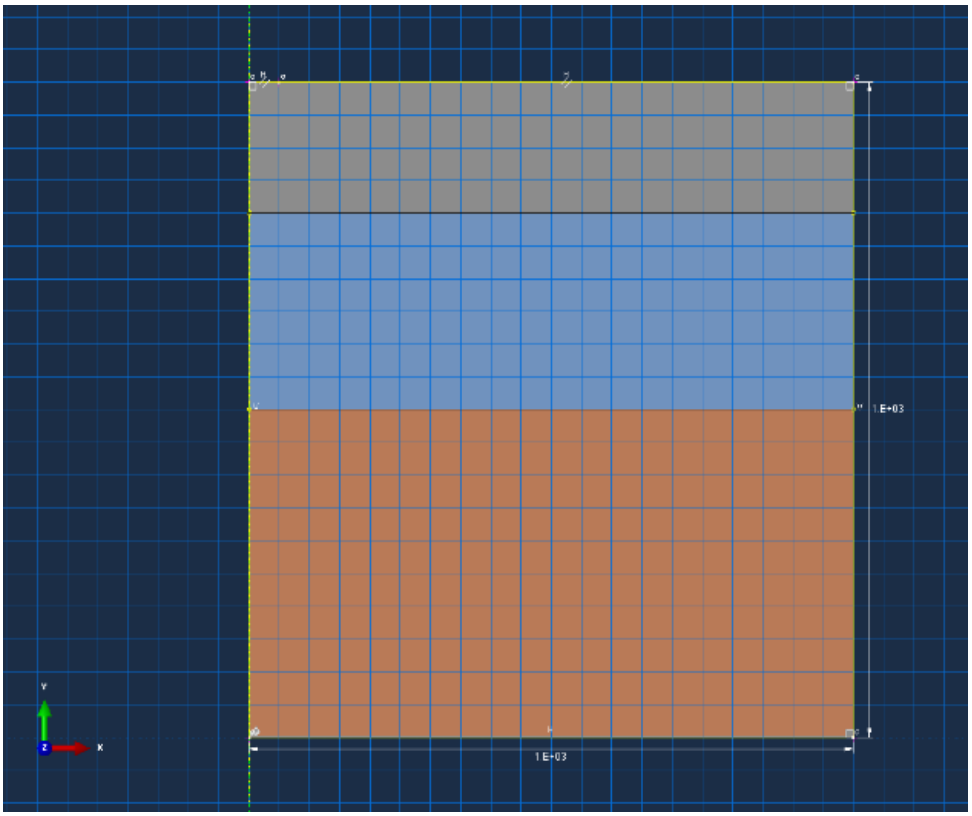

Figure: 5.3 Sketched geometry of a multilayered pavement

5.6.3 Entering material properties

Entering material properties is the next step after drawing the model geometry. Properties of asphalt, resin and PVC are introduced in this module. For elastic-static models, Young modulus and Poisson's ratio, and for elastic-dynamic models, Young modulus, Poisson's ratio and density of materials are used to characterise the materials. As the laboratory tests are performed at 50°C, properties of materials at 50°C are introduced in the models. To check the effects on asphalt of confinement conditions, a wide range of resins and PVCs with different modulus of elasticity were examined as documented in the table 5.1.

For viscoelastic models, in addition to Young modulus, Poisson's ratio and density, asphalt relaxation modulus parameters for Prony series needed to be included in the materials creation part. Prony series (or Prony's method) is widely used to adequately represent and describe viscoelastic materials' behaviour. It represents for storage and loss moduli corresponding to a generalized viscoelastic Maxwell model containing multiple Maxwell elements (spring and dashpot) (Gibson et al. 2003; Liao 2007).

Equations 5.1 and 5.2 detail the equations used for the Prony series of a generalized Maxwell model. Table 5.2 illustrates the asphalt relaxation modulus parameters (Al-Qadi et al. 2010). Parameters for viscoelasticity modelling were obtained from the literature. As indicated earlier the outcomes produced by the viscoelastic modelling were of little use and this line of investigation was discontinued.

Table: 5.1 Properties for resin and PVC in models (at 50°C)

Materials	Young Modulus (Mpa)	Poisson's ratio	Density (Tonne/mm^3)
Asphalt	1200	0.48	2.37×10^{-9}
Resin	5273	0.3	2.12×10^{-9}
	527	0.3	2.12×10^{-9}
	150	0.3	2.12×10^{-9}
	250	0.3	2.12×10^{-9}
	850	0.3	2.12×10^{-9}
PVC	2900	0.4	1.4×10^{-9}
	1500	0.4	1.4×10^{-9}

$$G(t) = G_0\left[1 - \sum_{i=1}^{n} G_i\,(1 - e^{-t/\tau_i})\right] \qquad \text{Equations 5.1}$$

$$K(t) = K_0\left[1 - \sum_{i=1}^{n} K_i\,(1 - e^{-t/\tau_i})\right] \qquad \text{Equations 5.2}$$

where,

G = shear modulus,
K = bulk modulus,
t = reduced relaxation time,
G_0 and K_0 = instantaneous shear and volumetric modulus, respectively
Gi, Ki, and τ_i= Prony series parameters.

Table: 5.2 Asphalt Prony series parameters for viscoelasticity (obtained from literature (Al-Qadi et al. 2010))

i	g_i Prony	k_i Prony	tau_i Prony
1	0.631	0.631	0.0206
2	0.251	0.251	0.173
3	0.0847	0.0847	1.29
4	0.0267	0.0267	5.35
5	0.0066	0.0066	106

5.6.4 Creating and assigning Sections

This module is used to define specific properties of each part, such as elastic properties. According to the types of material in each model, several material sections were created i.e. asphalt section, resin section, PVC section, base section, and a subbase section. By creating sections it is possible to assign the relevant properties of each material to the related piece of the geometry i.e. the properties for the resin are assigned to that section in the confined laboratory model.

5.6.5 Assembly and configuring analysis

The geometry of the assembly is defined by creating parts, locating them and connecting to each other in a global coordinate system. The model analysis configuration is created by generating analysis steps as follows; an elementary step in which boundary conditions will be applied, and an analysis step where a 750 kPa pressure is applied. A Dynamic/Explicit step is created for dynamic models. The models were designed to provide stresses, strains, displacements, and forces/reactions as output.

5.6.6 Boundary conditions and load creations

Boundary conditions were applied to specific regions of the geometry to restrict displacements and rotations. Bases have been constrained in the vertical direction

while free to move in the horizontal direction. As the axisymmetric model is used in this study, boundary conditions also have been applied for the symmetry axis where movement is in the horizontal direction, and rotation about 2-direction and 3-direction have been fixed (XSYMM boundary condition).

The *Load* term in Abaqus is used to apply pressure loads, temperature loads, concentrated forces, and nonzero boundary conditions. In the models, a uniform 750 kPa load (pressure type) has been applied to the top surface. As a 50mm platen on 100mm specimen was used for laboratory models, pressure was applied on the corresponding distance in the axisymmetric models (pressure on 25mm distance of top of a 50mm specimen as half of a body is modelled in an axisymmetric simulation). A 200mm tyre size was selected (as a loading area) for the in-situ pavement and likewise where it is applied at the corresponding location in the axisymmetric models.

5.6.7 Meshing module

Abaqus includes a broad range of elements for meshing structures. Each element is classified with several factors namely; Family, Formulation, Degree of Freedom, Number of Nodes, and Integration. According to these five aspects, every element has its specific name. For example, in the CAX4R element, the initial letter designates its family (C indicates Continuum family), or last letter that indicates Integration (R indicate it is a Reduced-integration element). Some of the most common element Families in Abaqus are documented in Figure 5.4.

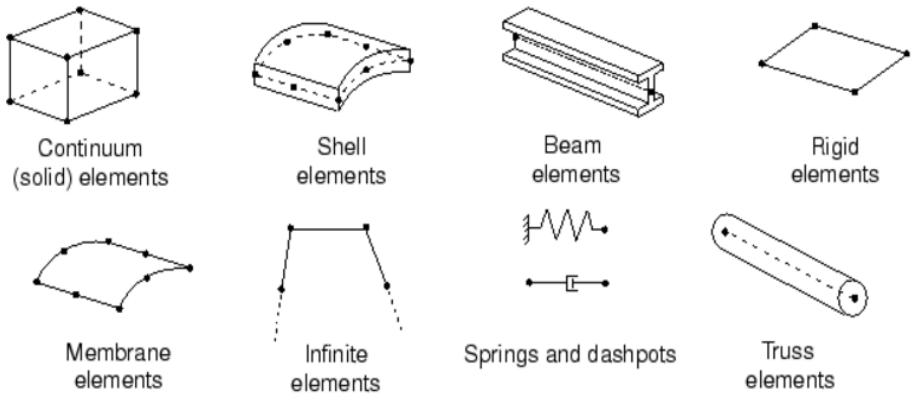

Figure: 5.4 Some of the most common element families in Abaqus (Abaqus-6.13 2013)

In this study, an axisymmetric stress family is used with Reduced-integration elements. Quadrilateral element shape is employed with the linear geometric order. Meshing size (or approximate global size) for laboratory models is specified to be 1mm to 1mm, while 10mm to 10mm is used for in-situ pavement models (because of its large body size (2000mm to 2000mm)). CAX4R element is used for meshing models which refers to; 4-node, bilinear axisymmetric quadrilateral, reduced-integration element. Figure 5.5 depicts a laboratory model after meshing.

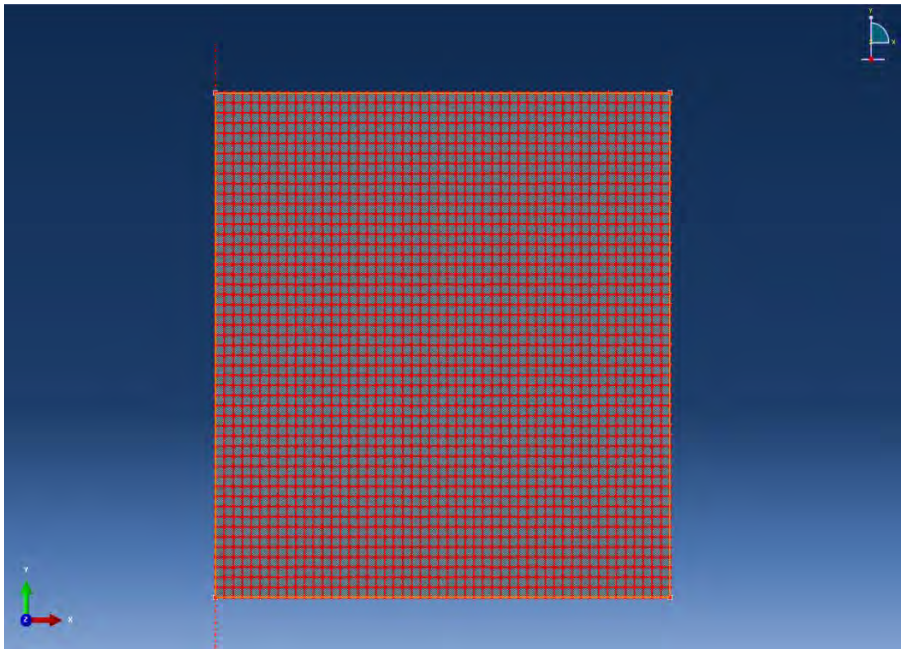

Figure: 5.5 Schematic of FEM mesh for confined specimen model

5.7 Modelling outcomes

Modelling outcomes are presented in this section. A wide range of outputs have been obtained from each model and include Mises stresses, stress Max in-plane principal, stress max in-plane principal (Abs), stress Min in-plane principal, Tresca stress, stresses and deformations in X, Y and Z directions. All these outputs are available in the Appendix. Stress distribution in the main axes of the coordinate system (X, Y and Z axis as identified in Figure 5.1) have been selected and analysed in this study. Stress distributions in the X and Y axes are discussed in this chapter, and data for the Z axis will be discussed and compared with laboratory outputs in chapter 7.

Figures 5.6 to 5.8 show schematic models of existing unconfined test, new confined test, and asphalt pavement. Figures 5.9 to 5.22 shows stress conditions in the X and Y directions for the following models;

1) Existing unconfined test (with 200 kPa load)
2) Existing unconfined test (with 750 kPa load)
3) New confined test (with 4mm PVC ring)
4) New confined test (with 2.5mm PVC ring)
5) Full depth asphalt pavement
6) Multi-layer pavement
7) Single-layer asphalt pavement.

As the applied stress for the existing Australian creep test is 200 kPa, the existing test has been modelled with a 200 kPa pressure load. Since the real surface pressure in the road pavement and also for the new confined test will be in the order of 750 kPa that value is applied in the relevant models.

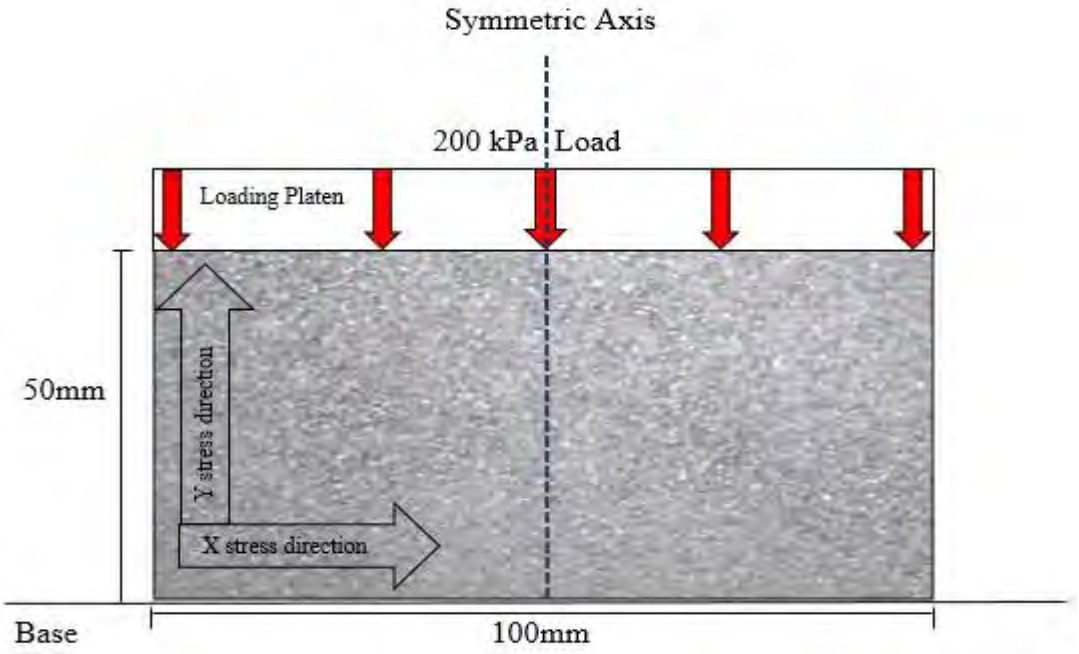

Figure 5.6 Schematic model of Existing unconfined test

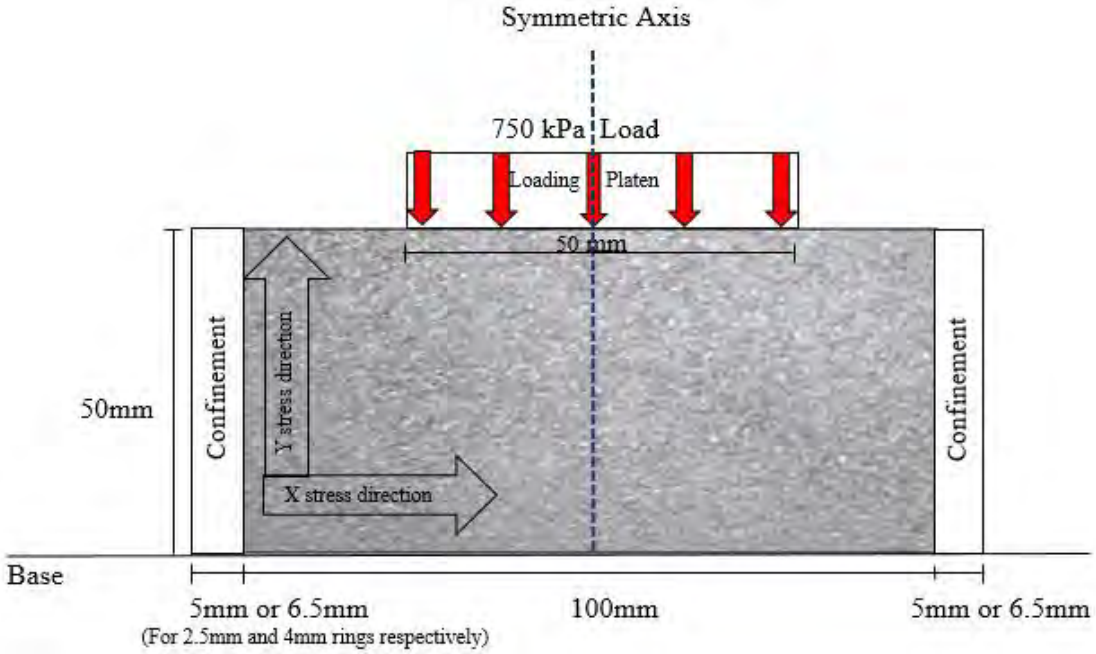

Figure 5.7 Schematic model of New confined test

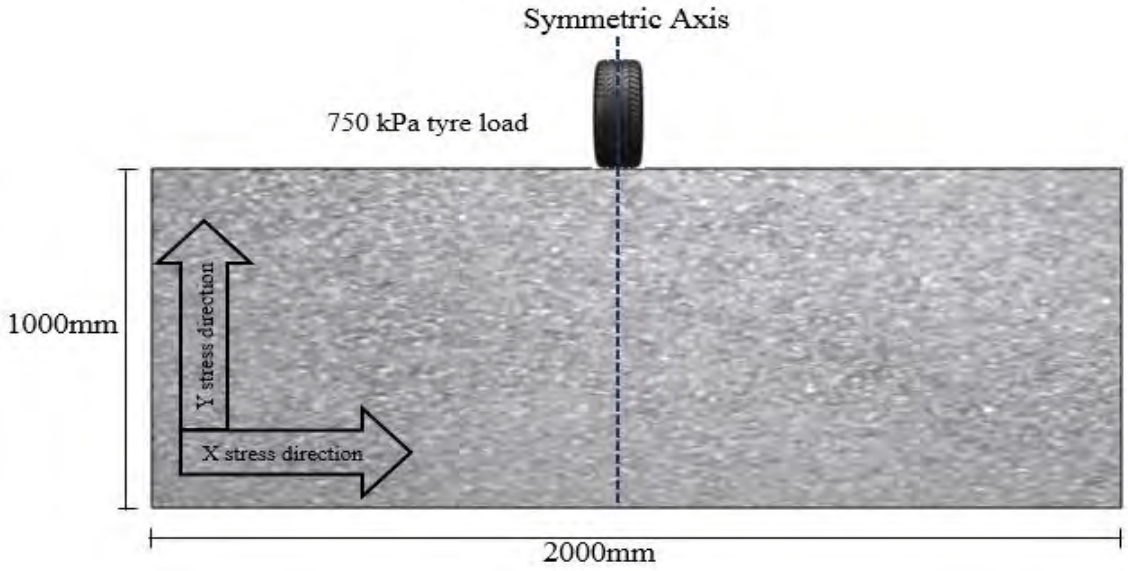

Figure 5.8 Schematic model of asphalt pavement

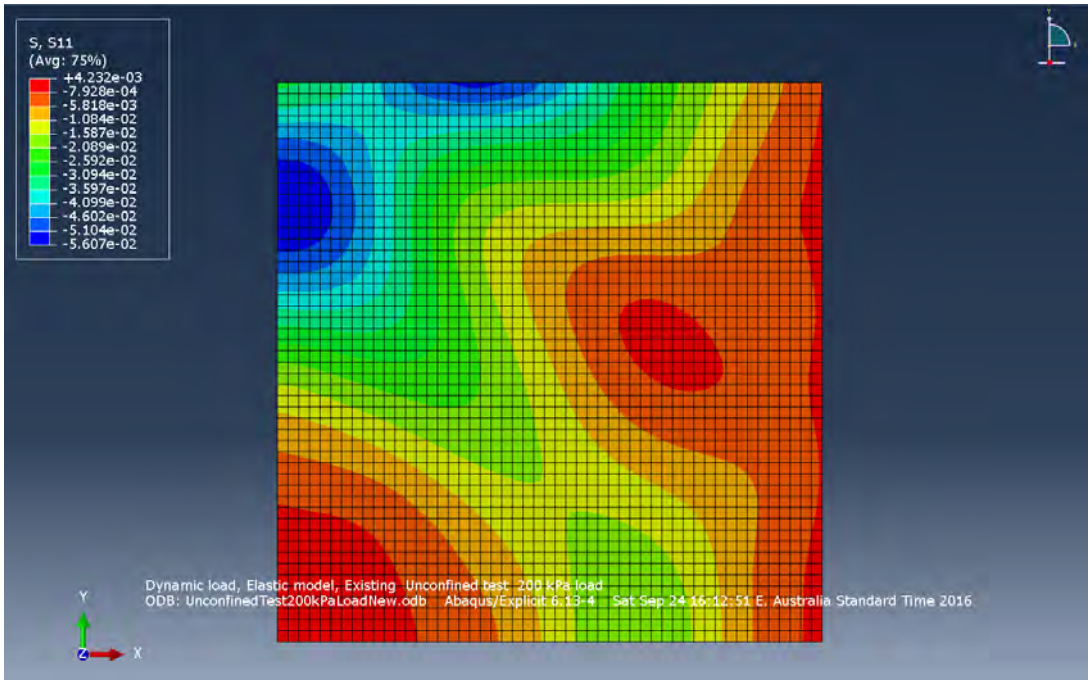

Figure: 5.9 Existing unconfined test for a 100/ 100mm section (200 kPa load) in the X axis direction

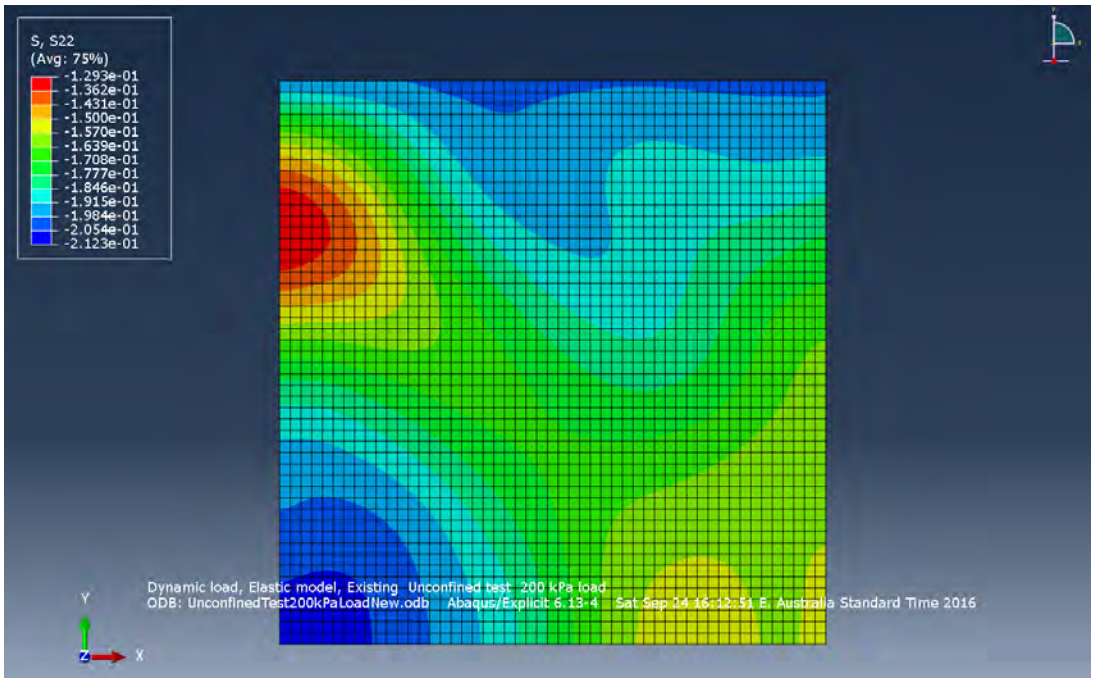

Figure: 5.10 Existing unconfined test for a 100/ 100mm section (200 kPa load) in the Y axis direction

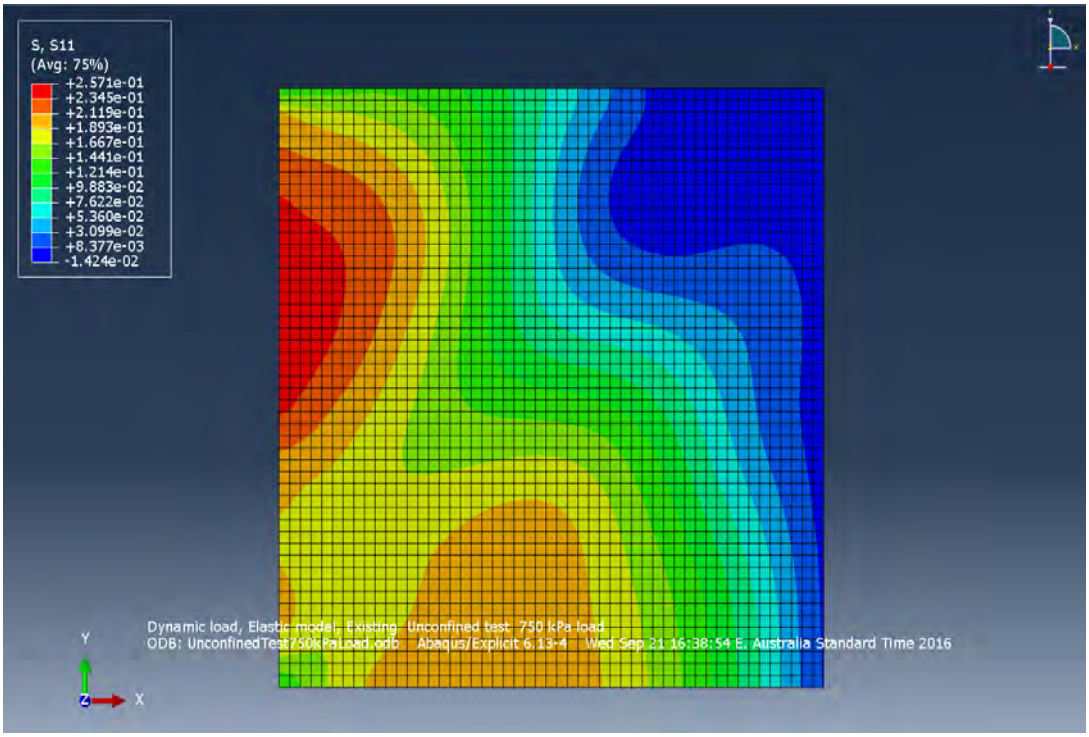

Figure: 5.11 Existing unconfined test for a 100/ 100mm section (750 kPa load) in the X axis direction

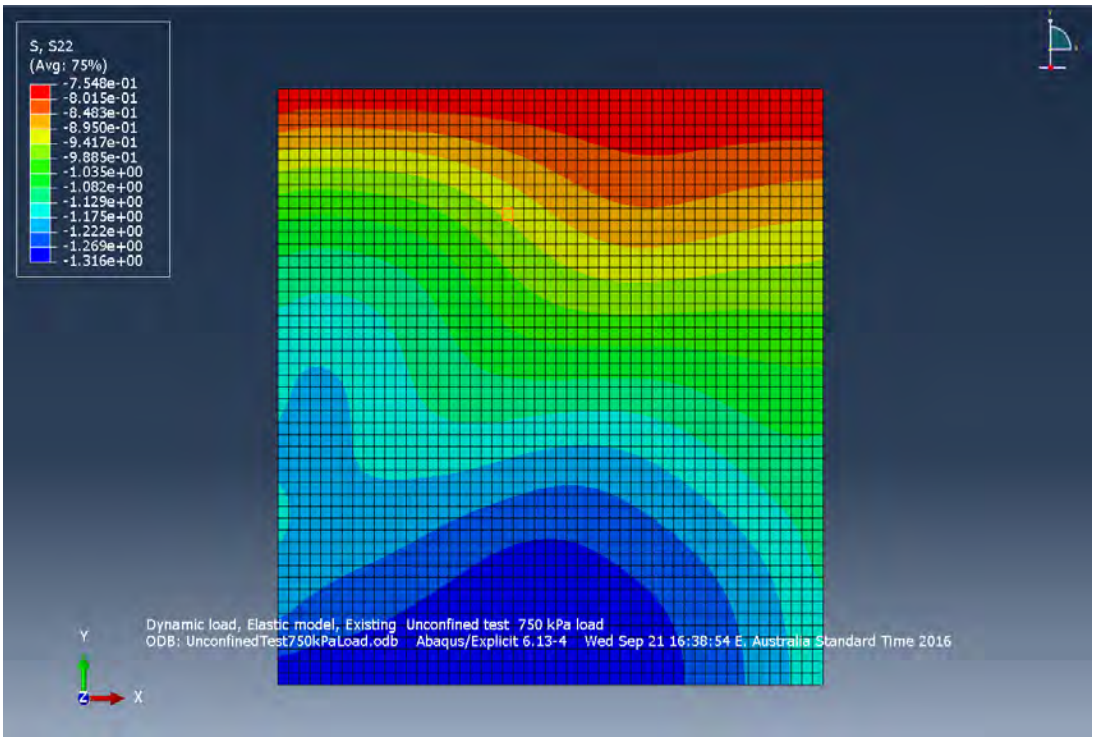

Figure: 5.12 Existing unconfined test for a 100/ 100mm section (750 kPa load) in the Y axis direction

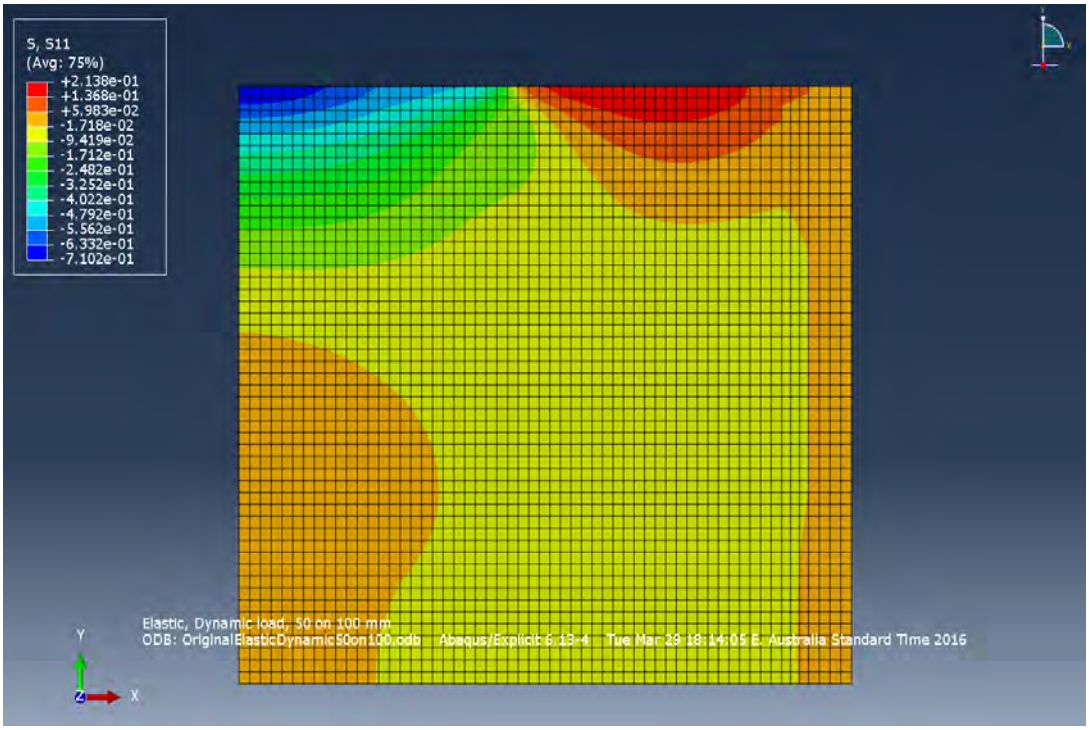

Figure: 5.13 New confined (4mm ring) test for a 50/100 mm section in the X axis direction

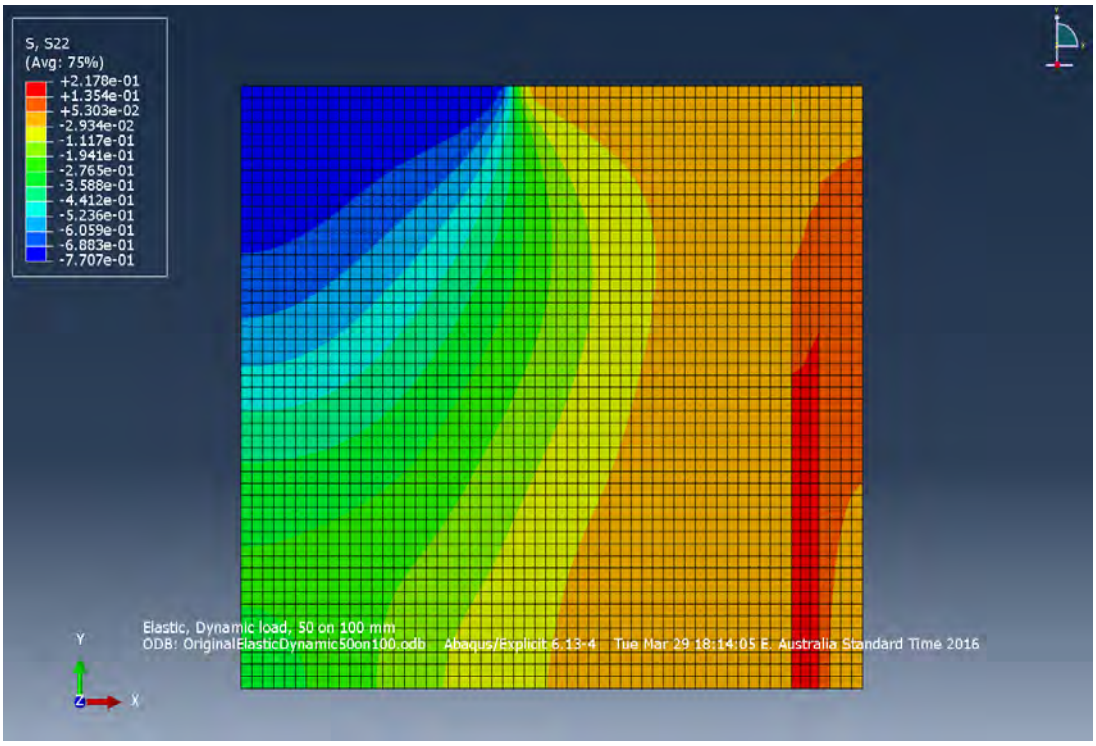

Figure: 5.14 New confined (4mm ring) test for a 50/100 mm section in the Y axis direction

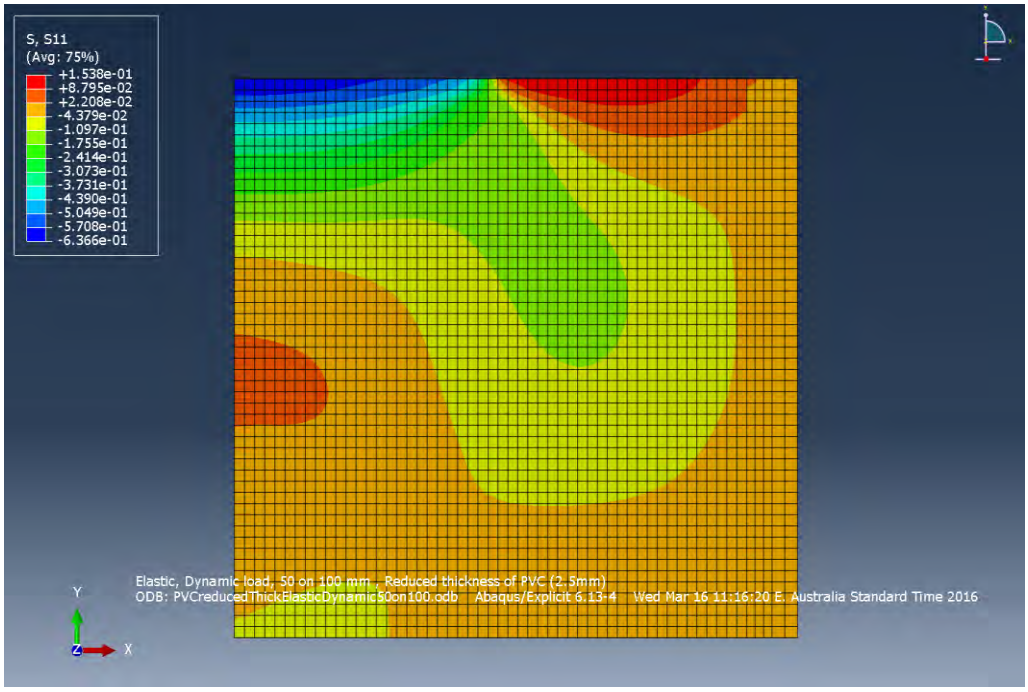

Figure: 5.15 New confined (2.5mm ring) test for a 50/100 mm section in the X axis direction

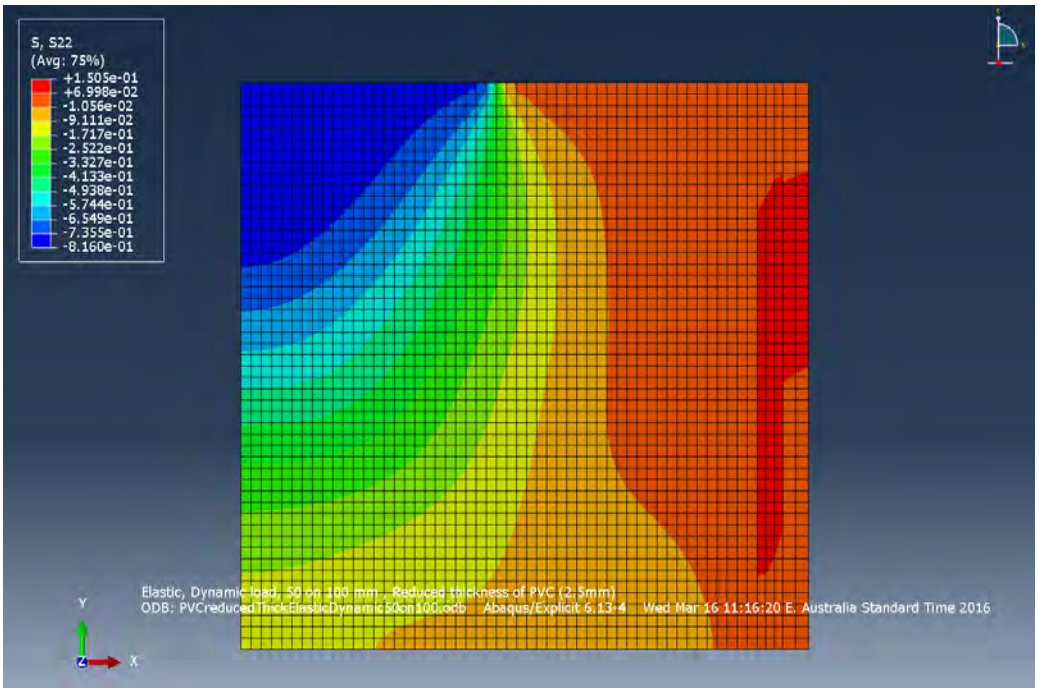

Figure: 5.16 New confined (2.5mm ring) test for a 50/100 mm section in the Y axis direction

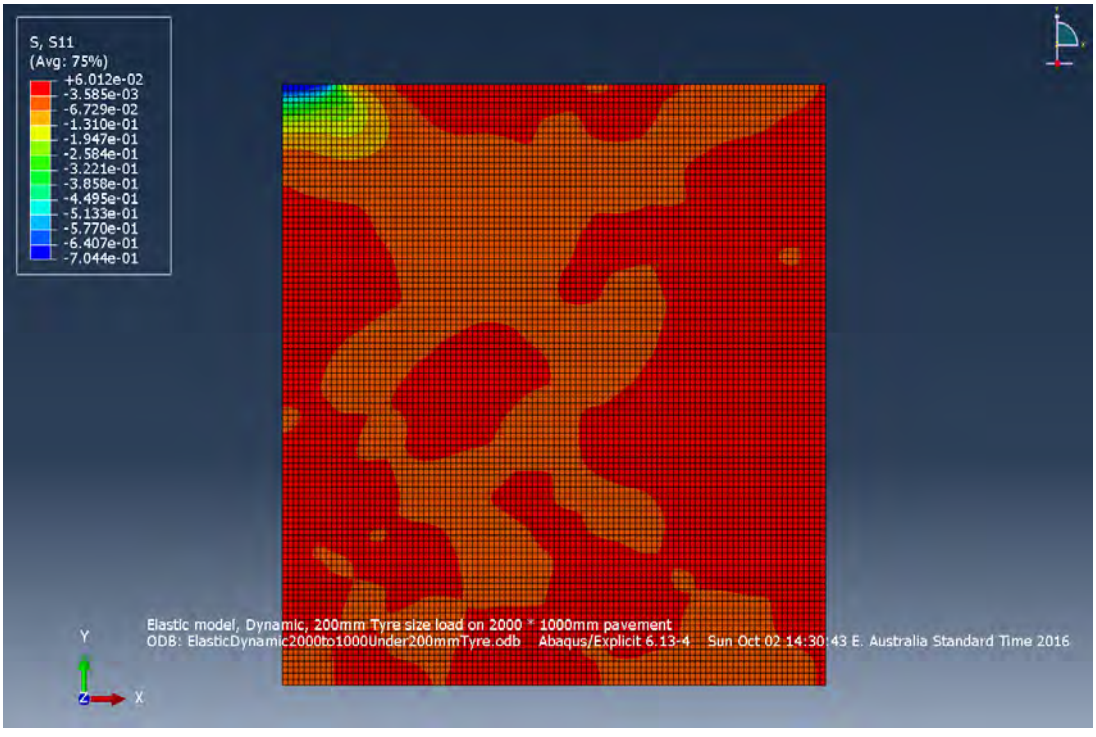

Figure: 5.17 Full depth asphalt pavement, 2000×1000mm section under a 200mm tyre in the X direction

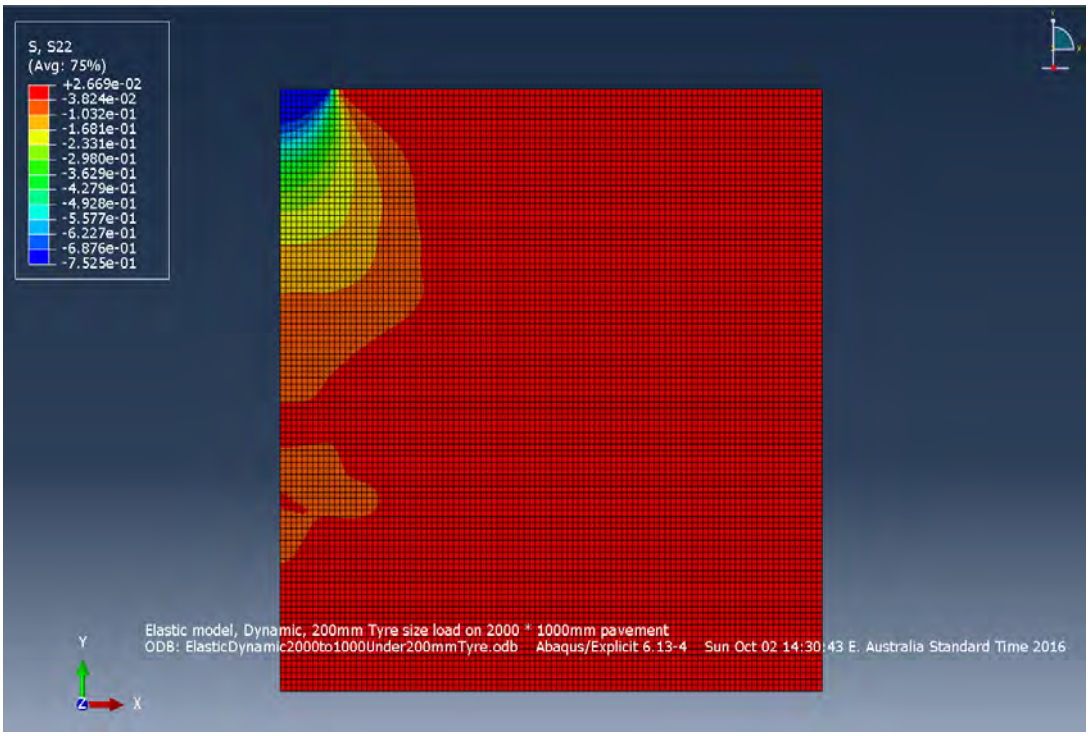

Figure: 5.18 Full depth asphalt pavement, 2000×1000mm section under a 200mm tyre in the Y direction

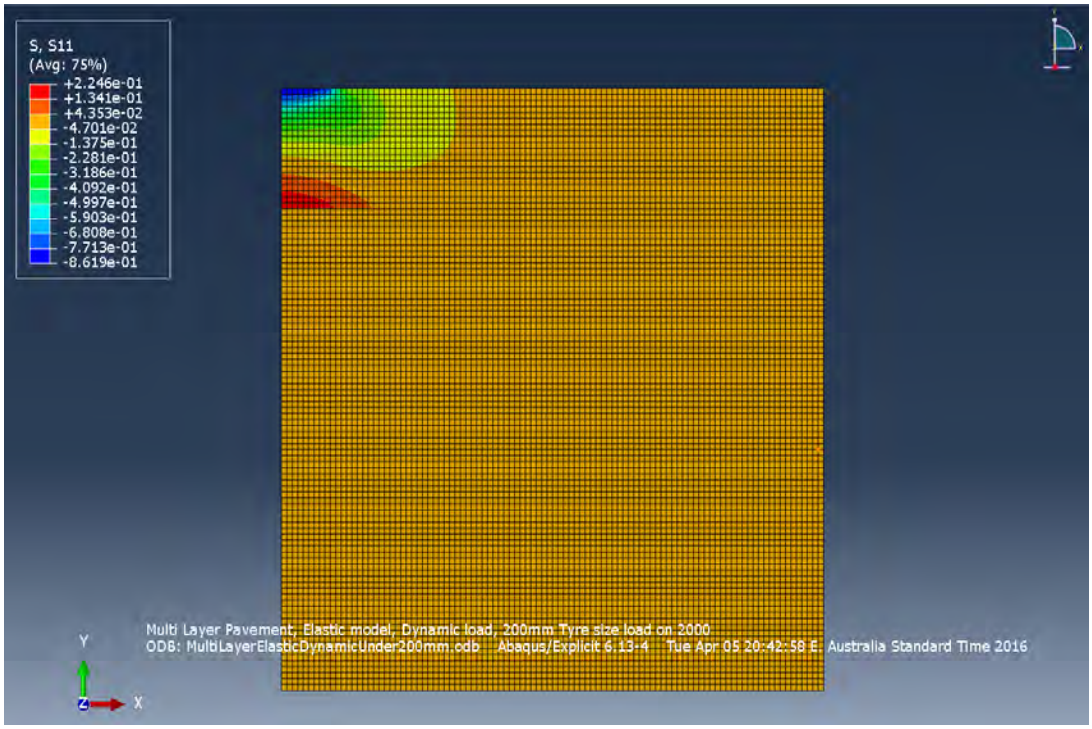

Figure: 5.19 Multi-layer pavement 2000×1000mm section under a 200mm tyre in the X direction

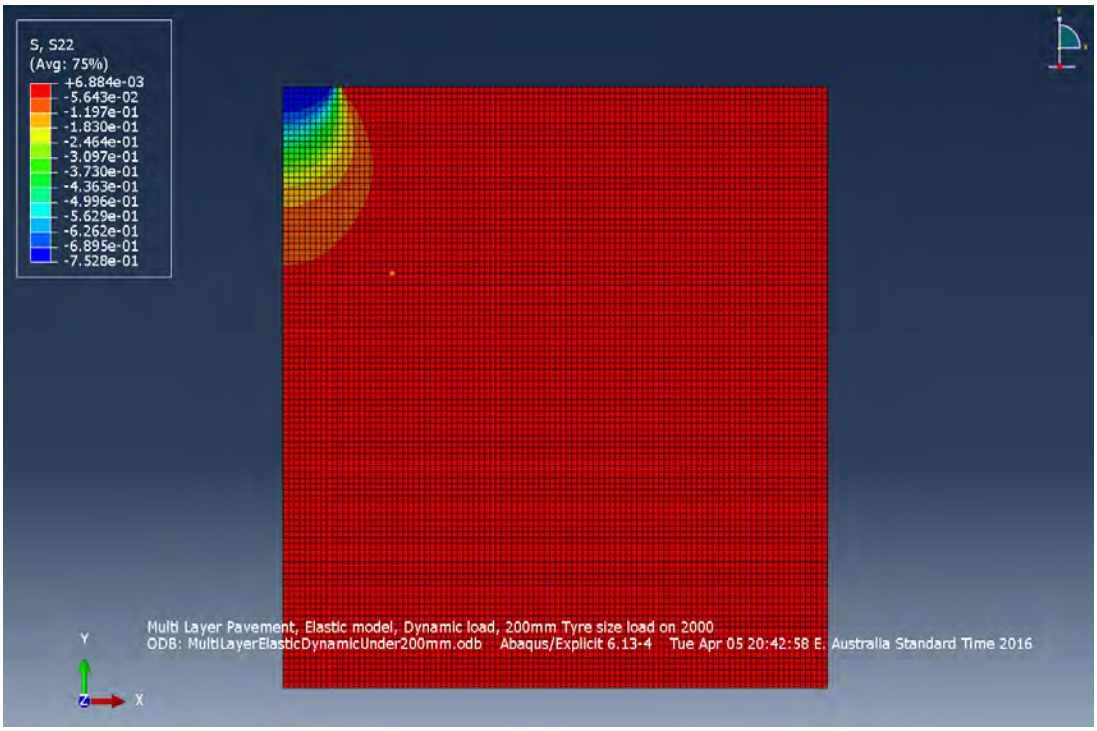

Figure: 5.20 Multi-layer pavement 2000×1000mm section under under 200mm tyre in the Y direction

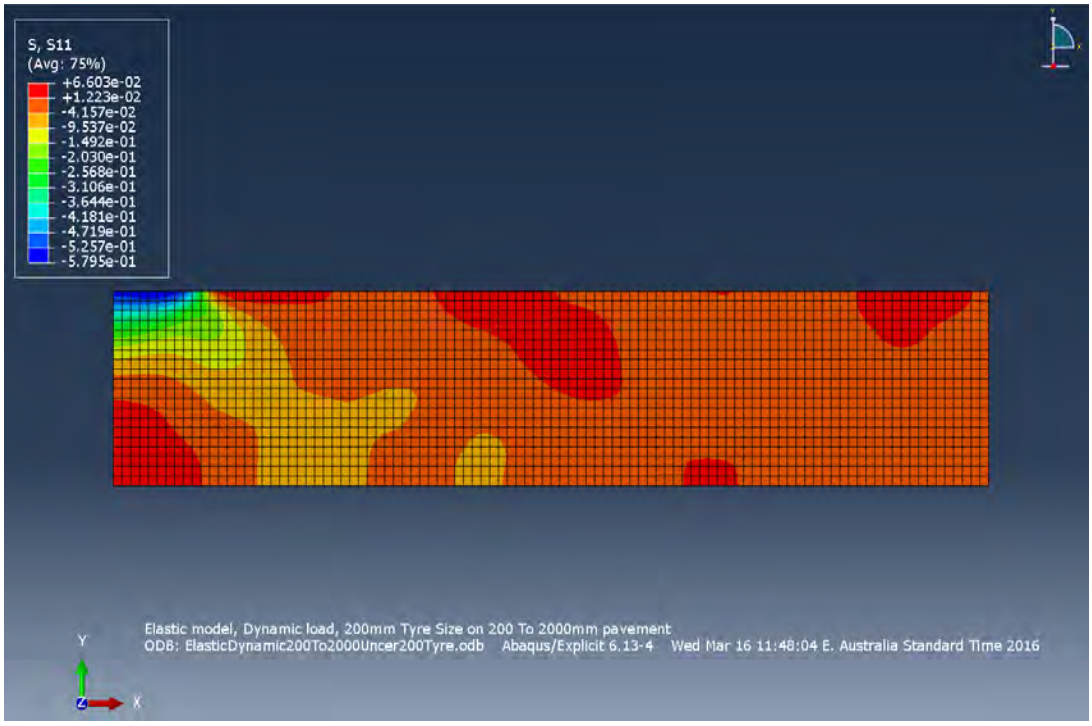

Figure: 5.21 Single asphalt layer 200×2000mm section under a 200mm tyre in the X direction

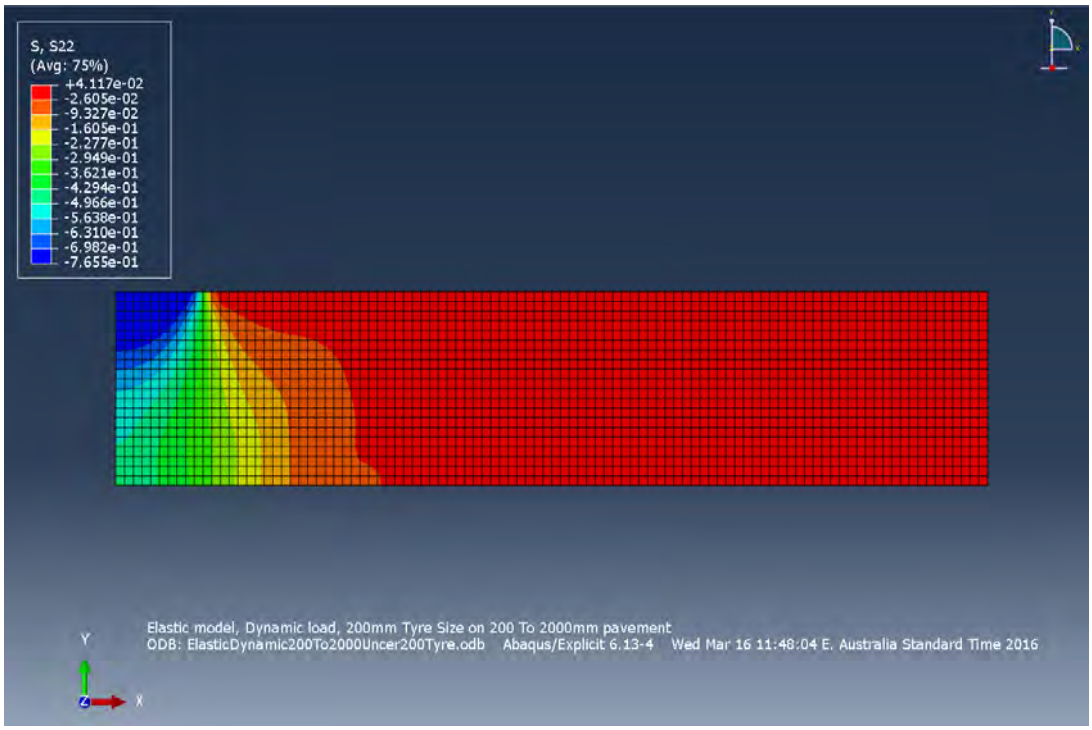

Figure: 5.22 Single asphalt layer 200×2000mm section under a 200mm tyre in the Y direction

Stresses at different points in the models have been extracted to enable a better comparison across the models. The grid points of the selected axes (A, B and C in vertical, and 1, 2, and 3 in the horizontal directions) have been used for obtaining stress in each model. The geometrically corresponding points are determined using a 200mm diameter tyre size for in-situ models when comparing with the 50mm platen. This means that a 4:1 scale is used for finding equivalent points within the in-situ pavement models. Figure 5.23 shows the selected axes.

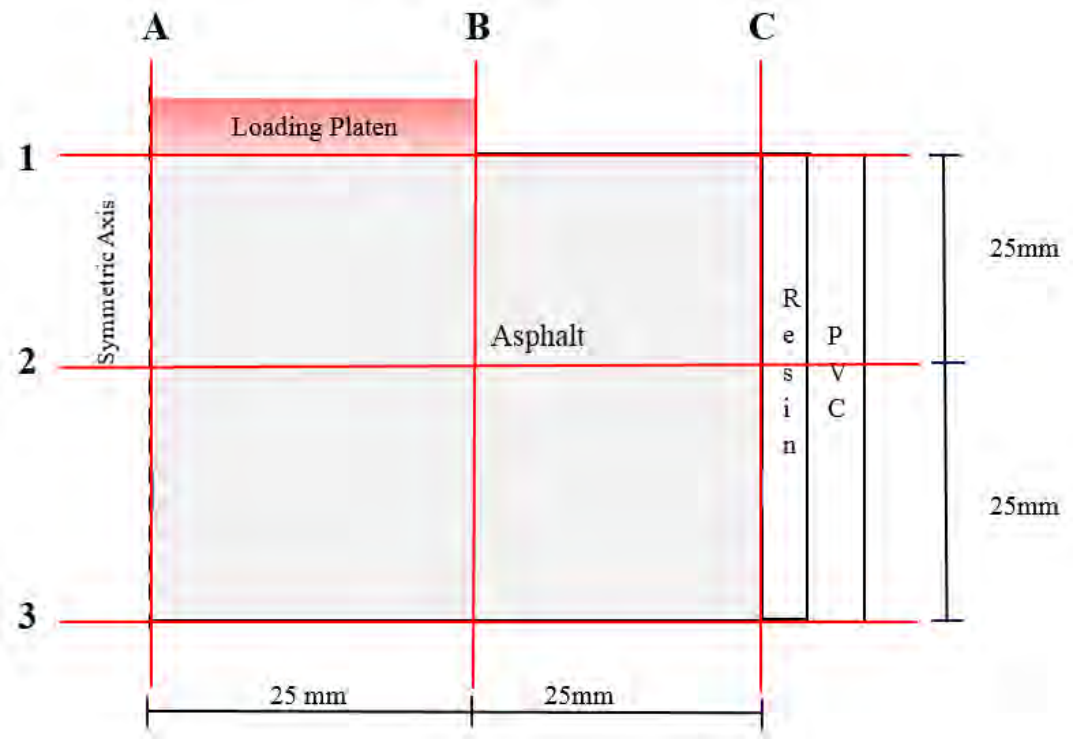

Figure: 5.23 Selected axes for checking stress distribution in the models

Stress magnitudes at the selected points have been inserted in the figures 5.24 to 5.27. As shown in the figures, stress distribution in the existing unconfined specimens (for both 200 kPa and 750 kPa models) have a very different trend to those for the field asphalt pavement models (all single asphalt layer, full depth asphalt and multi-layer pavements). The stresses at the geometrically similar points for the confined creep tests and in-situ models are similar. The modelling results demonstrate that stress conditions within the existing unconfined test do not replicate those for in-situ conditions.

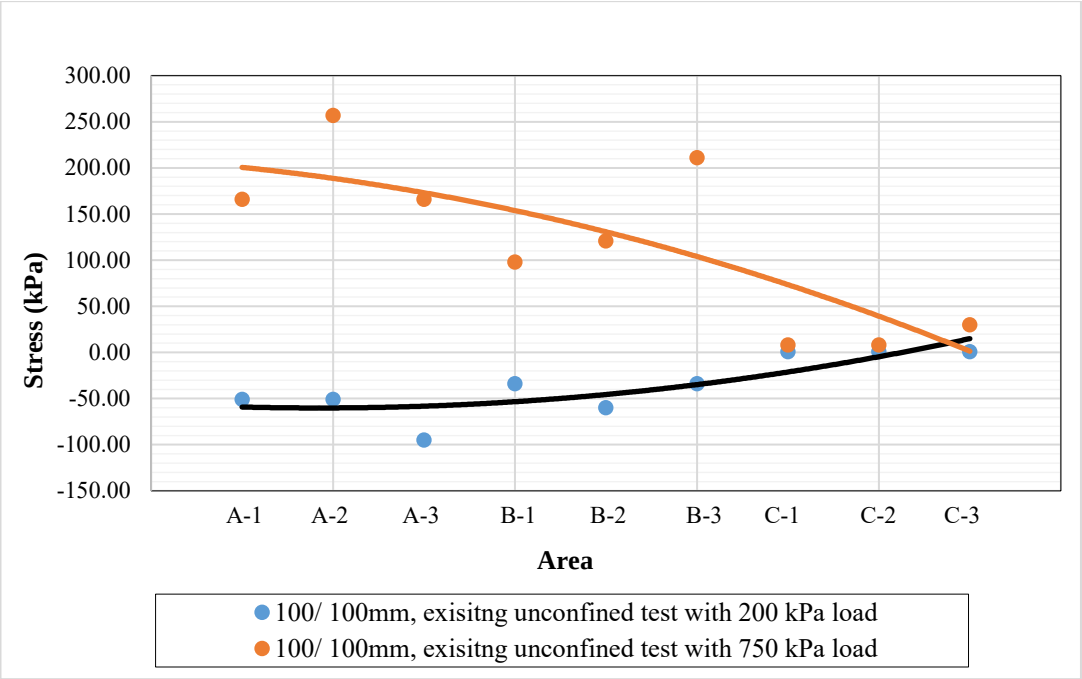

Figure: 5.24 Stress distribution in the models of existing unconfined tests – X direction

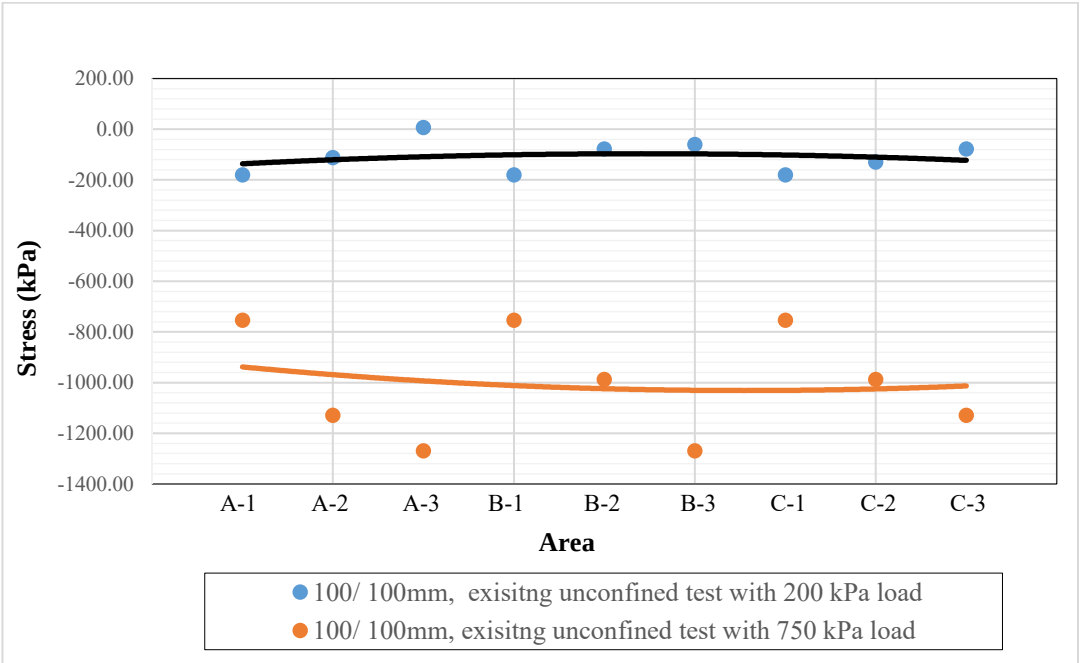

Figure: 5.25 Stress distribution in the models of existing unconfined tests – Y direction

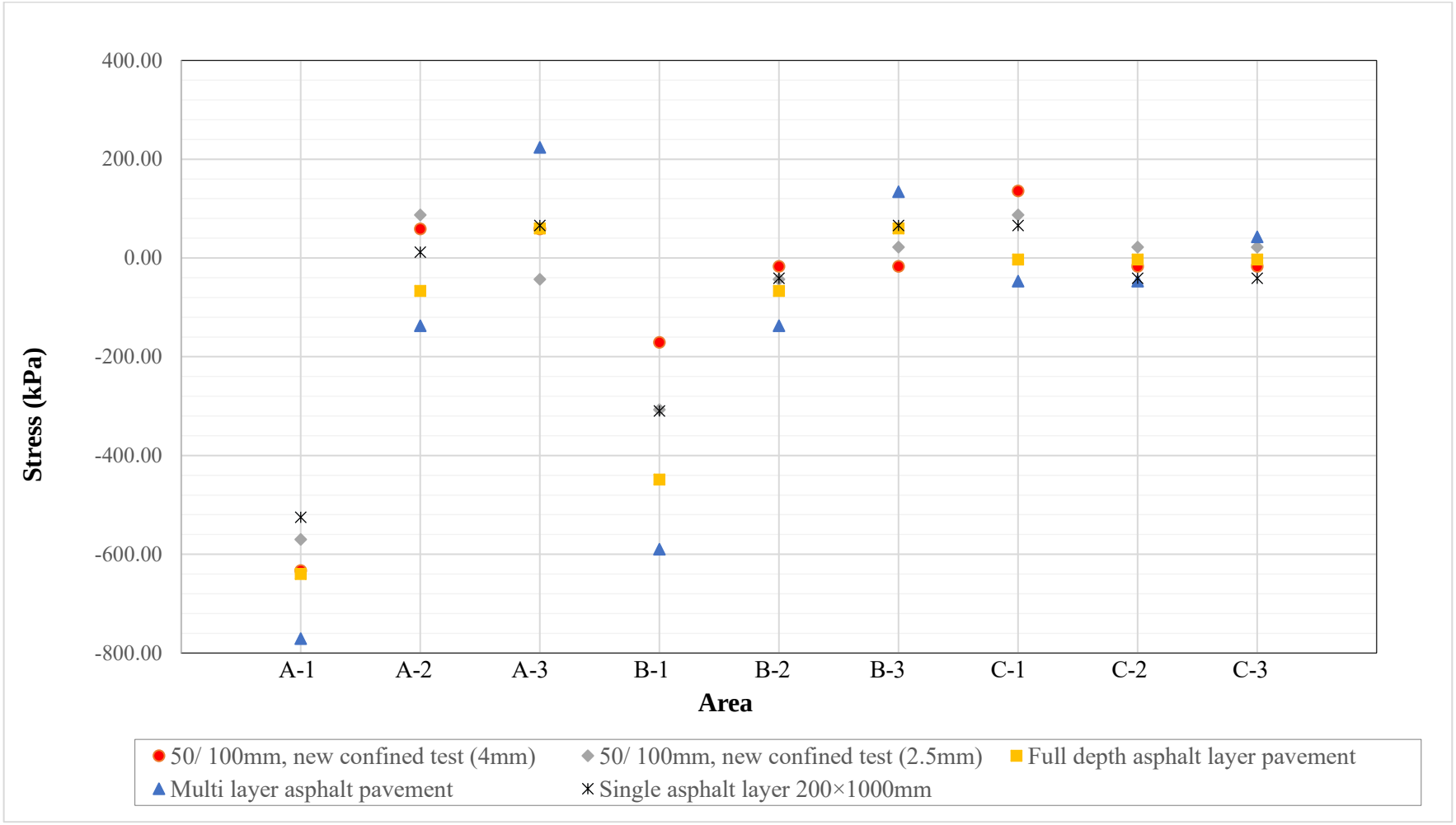

Figure: 5.26 Stress distribution in the different models – X direction

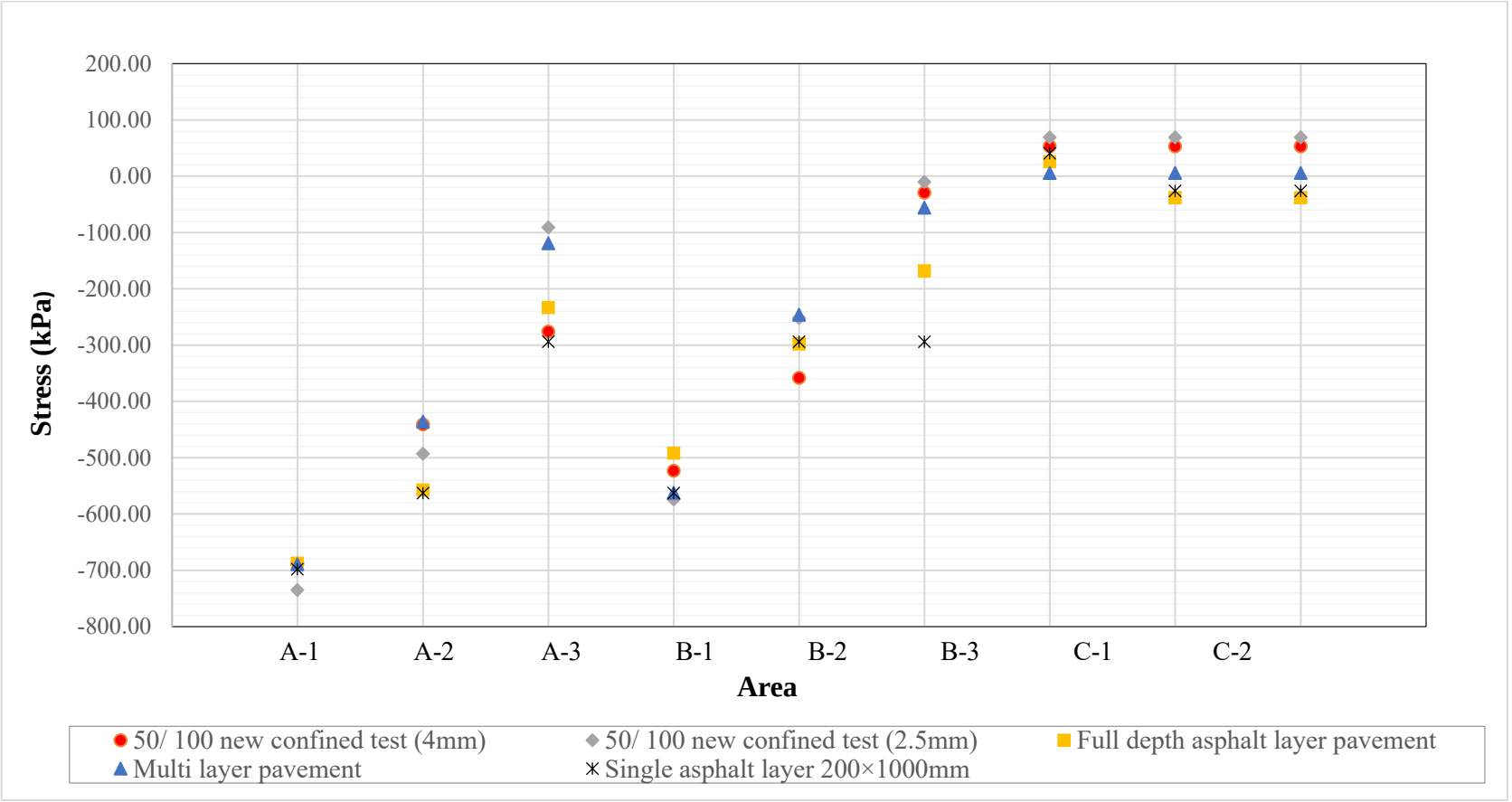

Figure: 5.27 Stress distribution in the different models – Y direction

There is a good correlation in stress condition between the new creep test and the field asphalt pavement models as portrayed in figures 5.26 and 5.27. Similar and close trends were found together with stress magnitudes for the new confined creep test and field pavement models. The stress fields in the loading zone (the area between A and B axes) and asphalt annulus (the area between B and C axes) of the new confined test and the field pavement models have good agreement. As depicted in the figure 5.28, and 5.29 such stress action exists in the road pavement.

Stress distribution in the Y direction of the models displays compressive stress under the loading zone (the area between A and B axes), which gradually changes to tension stress towards the C axis (especially in the C-3 area). The compressive stress under the platen (or tyre) tends to compress material underneath the loading zone (the area between A and B axes), and elevates the asphalt on both sides of the platen. Densification and shear deformation in the field (as shown in the figure 3.1) are the rutting mechanisms which are replicated in the new confined test models.

The modelling shows the newly-designed lateral confinement of the specimen (filler + PVC) is more able to provide representative conditions for the laboratory specimen that better approximate in-situ stress conditions.

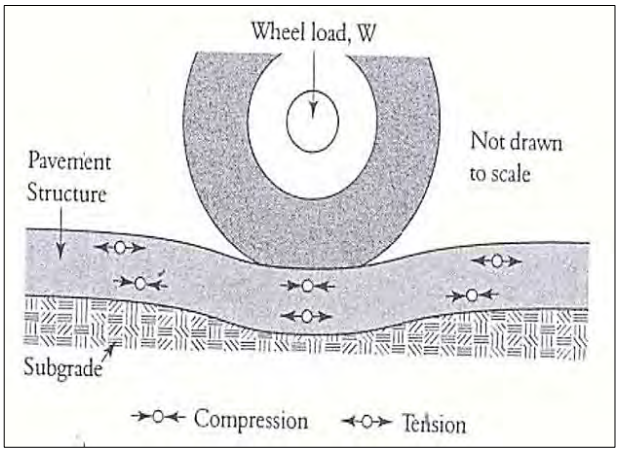

Figure: 5.28 Compressive and tensile stresses in the asphalt pavement structure (Al-Rousan 2016)

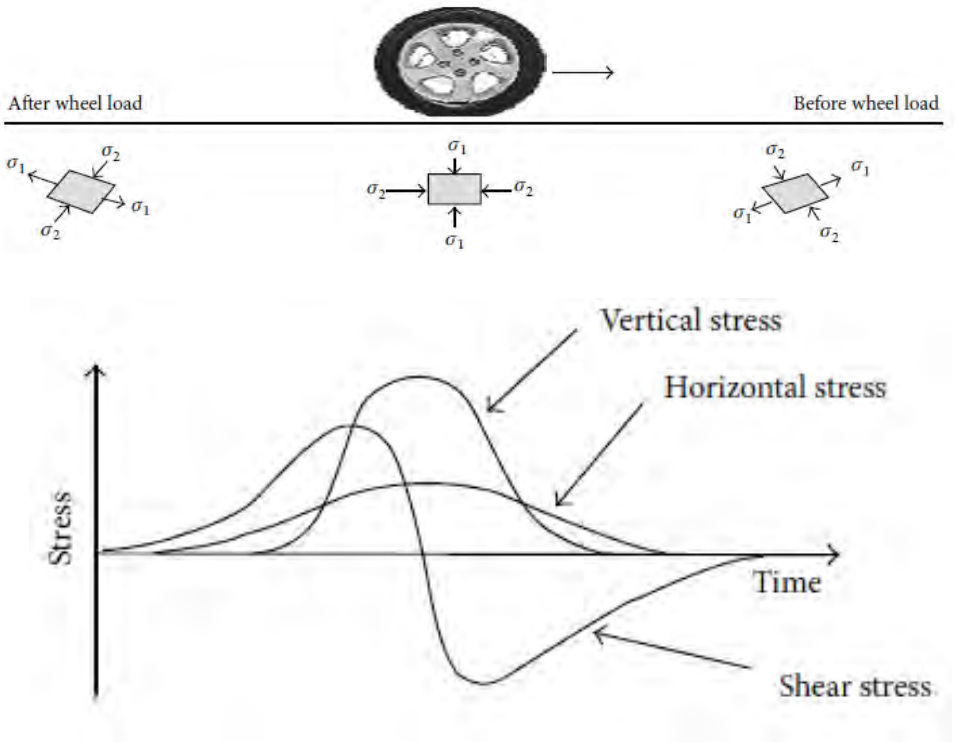

Figure: 5.29 Stress distribution under tyre load (Mashaan et al. 2014)

5.7.1 Models with various resin and PVC properties

When designing confinement of specimens, several types of resins and PVCs have been modelled using different elastic properties (modulus of elasticity and poison ratio). Figures 5.30, and 5.31 present the stress distribution on the asphalt specimens as result of using different resins and PVC thickness. As the figures demonstrate, the different types of resin and PVC create the same basic effect with only the magnitude of the stress differing. This behaviour (same trend, different stress level), is indicative of the combination of materials.

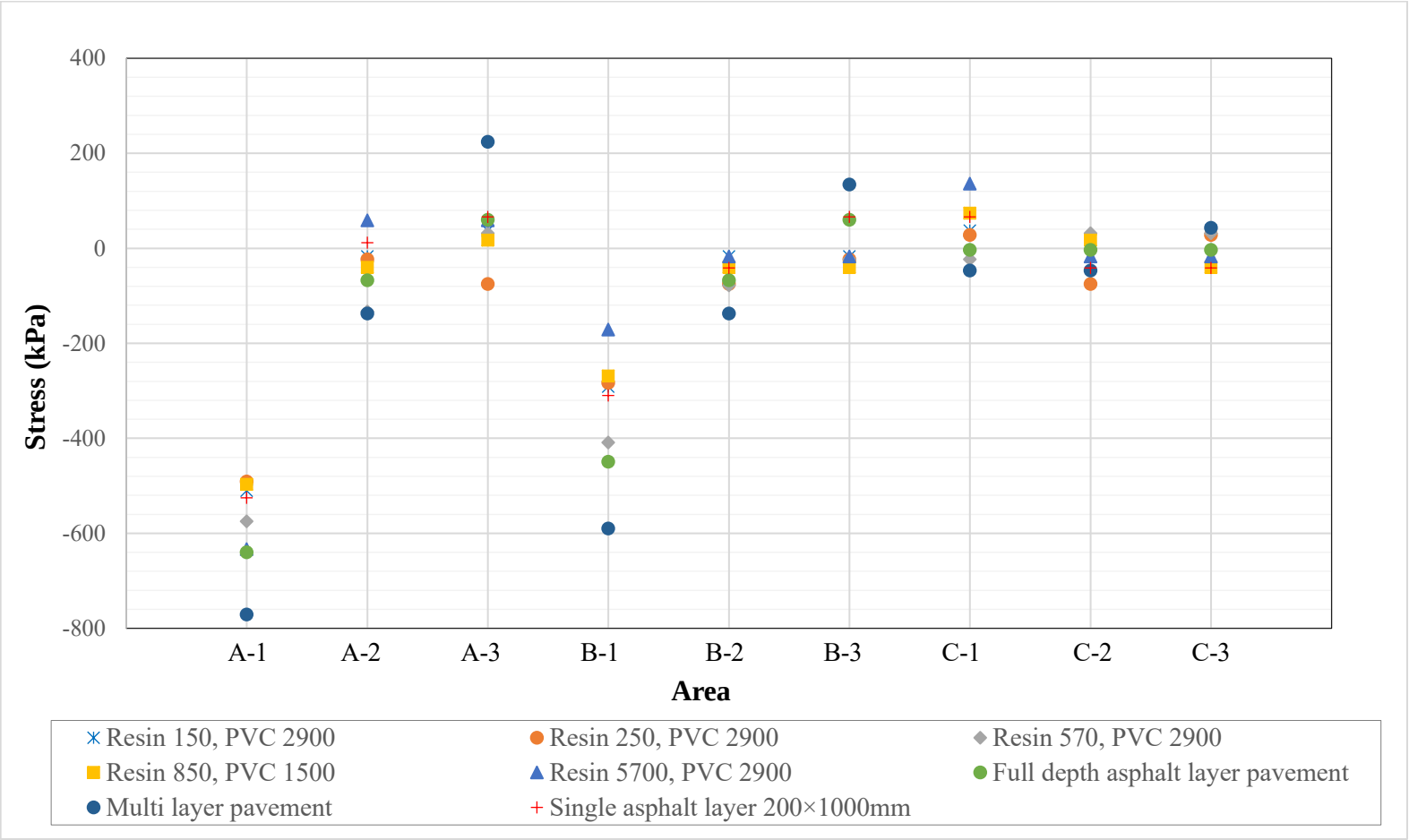

Figure: 5.30 Stress distribution in the different models as result of using various resin and PVC properties – X direction

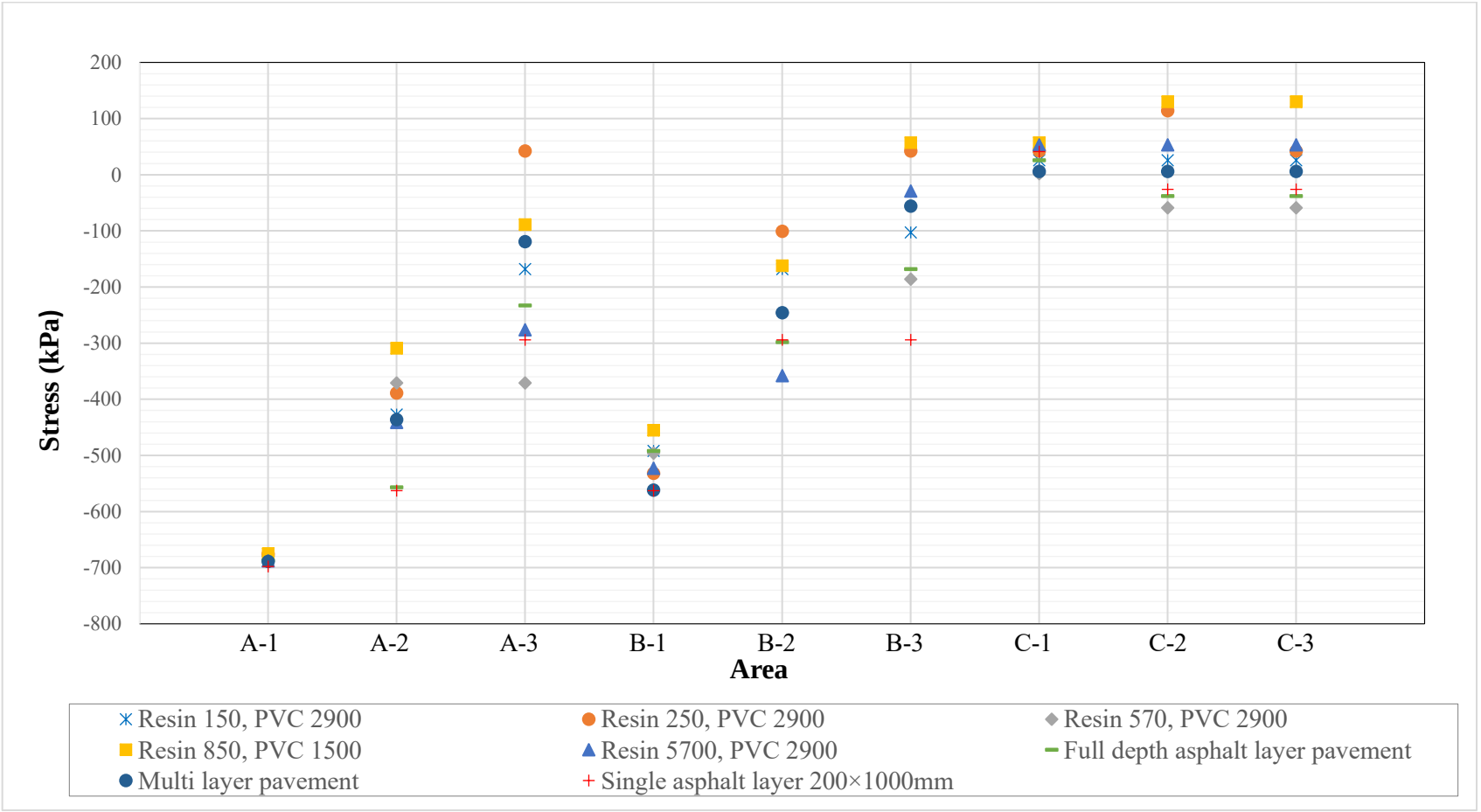

Figure: 5.31 Stress distribution in the different models as result of using various resin and PVC properties – Y direction

5.8 Data analyses to peruse confined laboratory and in-situ models relationships and determine the best ring size

As indicated by FEM models, both confined creep tests with 4mm and 2.5mm PVC rings appeared to have a good level of agreement with the in-situ pavement models. To study the relationship between confined creep tests and in-situ models, and also to determine the best ring size, a simple data analysis has been undertaken by using Standard Deviation and Regression. Stress distribution in the Y axis (as defined in figure 5.1) of the grid points (A, B and C in vertical, and 1, and 2 in the horizontal directions, as defined in figure 5.23) of the laboratory, and the geometrically corresponding points for in-situ model (single asphalt layer 200×1000mm model) was used for the analyses.

The formula for calculating Standard Deviation is provided in the equations 5.3, and outcomes show in Table 5.3 together with Absolute Values of stresses used for calculating Standard Deviation. Table 5.3 shows that for the 2.5 mm ring compared to the 4 mm ring the average Absolute Difference is slightly less, and the Standard Deviation is much better (i.e. lower value). It confirms that the comparison between laboratory and in-situ models is reasonable. Additionally, it confirms that the 2.5mm ring provides a more consistent comparison between the laboratory and in-situ models than the 4mm ring.

$$SD = \sqrt{\frac{\sum(x-\bar{x})^2}{N}} \qquad \text{Equation 5.3}$$

where;

SD = standard deviation

x = each values in the population

$\bar{x}$ = the mean of values

N = the number of values

Table: 5.3 Data analysis using Standard Deviation

Area	*50/ 100 Confined Dynamic Creep test with 4mm Ring*	*50/ 100 Confined Dynamic Creep test with 2.5mm Ring*	*Single asphalt layer 200×1000mm*	*Mean (of 4mm and in-situ model)*	*Absolute difference (of 4mm and in-situ model)*	*Mean (of 2.5mm and in-situ model)*	*Absolute difference (of 2.5mm and in-situ model)*
A-1	688	735	698	693	10	717	37
A-2	441	493	563	502	122	528	70
B-1	523	574	563	543	40	569	11
B-2	358	252	294	326	64	273	42
C-1	53	69	41	47	12	55	28
C-2	53	69	26	40	27	48	43
				Average	46	***Average***	39
				Standard Deviation	42	***Standard Deviation***	19

Table: 5.4 Regression analysis

	Models	
Parameters	2.5mm Ring in comparing with in-situ pavement	4mm Ring in compare with in-situ model
Multiple R	0.947	0.958
R Square	0.896	0.919
Adjusted R Square	0.881	0.907
Standard Error	92.682	74.338
P-value	0.00011	0.00005

In the regression analysis, in-situ pavement model was assigned as the reference models (independent variables) and laboratory models (confined test with 4mm and 2.5mm PVC rings) were assessed with them (dependent variable). Table 5.4 provides a summary of the regression analysis. Very low P-values (or Probability value) obtained for both cases that indicate a significant relationship between stress distribution in the laboratory and the in-situ models (more than 99% level of confidence).

The correlation coefficient between laboratory and in-situ models is determined by Multiple R. The obtained Multiple R for all situations was higher than 0.94 indicating a strong correlation between both 4mm and 2.5mm confined tests and the in-situ models. R square for all the models were higher than 89% showing that it is possible to explain more than 89% of variables in the laboratory models by in-situ model. Standard Error represents the typical deviation between the actual results (what was obtained in the laboratory model) and what the mathematical model predicted. As shown in the Table 5.4, the Standard Errors of 2.5mm ring is lower than for 4mm. It confirms that 2.5mm ring has a better performance than 4mm ring.

By considering both Coefficient of Variation and Regression analyses, it can be concluded that 2.5mm ring is a better option for confining specimens, however, the 4mm ring also demonstrated good correlation.

5.9 Summary

A FEM model using Abaqus has been developed for evaluating the new confined test. Various conditions for the new confined test, the existing unconfined test, and in-situ field asphalt pavement have been assessed. The modelling outcomes were compared to identify any correlation between outcomes.

The existing test method modelling provides very different stress distributions to that which occurs in a test sample compared to the stress distribution in an in-situ field asphalt pavement. As expected, the model using the same sized platen as the size of

specimen used in the existing test method, produced almost a constant level of stress throughout the specimen. The modelling outcomes indicated that the existing test method is not representative of an in-situ asphalt pavement.

The new confined test provided very promising outcomes. A strong correlation was observed for stress levels between the new test and in-situ asphalt models at geometrically similar positions. Similar stress distributions and stress magnitudes were found for the new confined specimens to those for field asphalt pavement models. The modelling shows the new test method is able to better represent the pavement rutting mechanism in the laboratory test specimens. Data analyses confirm good correlations between the new confined test models and in-situ pavement models, with the best outcome being for a 2.5mm ring.

In summary, the modelling indicates that the new confined creep test method has excellent potential for the laboratory evaluation of the creep deformation of asphalt. The modelling validates the use of a confining annulus of asphalt to provide lateral stress distribution that better replicates field conditions. The modelling also indicates that the hoop stresses generated within the confinement system prevent the lateral stresses bursting the asphalt samples. The modelling shows that the combination of the asphalt annulus and stress responsive confining system is better able to represent field conditions than any existing methodologies.

The outcomes of the FEM studies undertaken underpins the methodology adopted for the extensive laboratory investigation undertaken described in Chapter 6.

CHAPTER 6

LABORATORY RESULTS

6.1 Introduction

As outlined in earlier chapters, deformation development in asphalt is a complex process that depends on a broad spectrum of parameters including mix characteristics, loading and temperature conditions. To predict and analyse in-situ asphalt performance, it is important to have valid laboratory tests correlated to field conditions. To refine and improve the current Australian creep test, new confinement conditions (as described in Chapter 4) that better replicate field conditions have been designed for laboratory creep evaluation including the use of a more realistic 750 kPa cyclic stress. The finite element modelling undertaken in Chapter 5 outlined the relevance and authenticity of the new test methodology.

This chapter reviews the laboratory test outcomes incorporating the variables of confining ring wall thicknesses, platen/ specimen configurations and asphalt mix types.

6.2 Experimental work

Although a range of laboratory creep tests are widely used around the world for predicting permanent deformation of asphalt, further improvement can be achieved by use of more realistic conditions. As shown in the figure 6.1, in-situ asphalt pavement is confined when wheel loads are applied. In this research confinement for laboratory specimens has been designed to better simulate field conditions.

The focus of the study is on designing confined dynamic creep test, consequently laboratory testing is largely dedicated to developing the Confined Dynamic Creep Test method (CDCT). Generally, the experimental creep tests used in this work can be

categorised into three groups namely; the Existing Australian Dynamic Creep Test method (EDCT), Confined, and Semi-Confined tests (SCDCT). In the SCDCT various platen/ specimen configurations were used such as 50mm diameter platen on 100mm diameter specimen (50/ 100mm), and 50mm on 150mm (50/ 150mm). Here a measure of confinement was provided by the unloaded asphalt annulus.

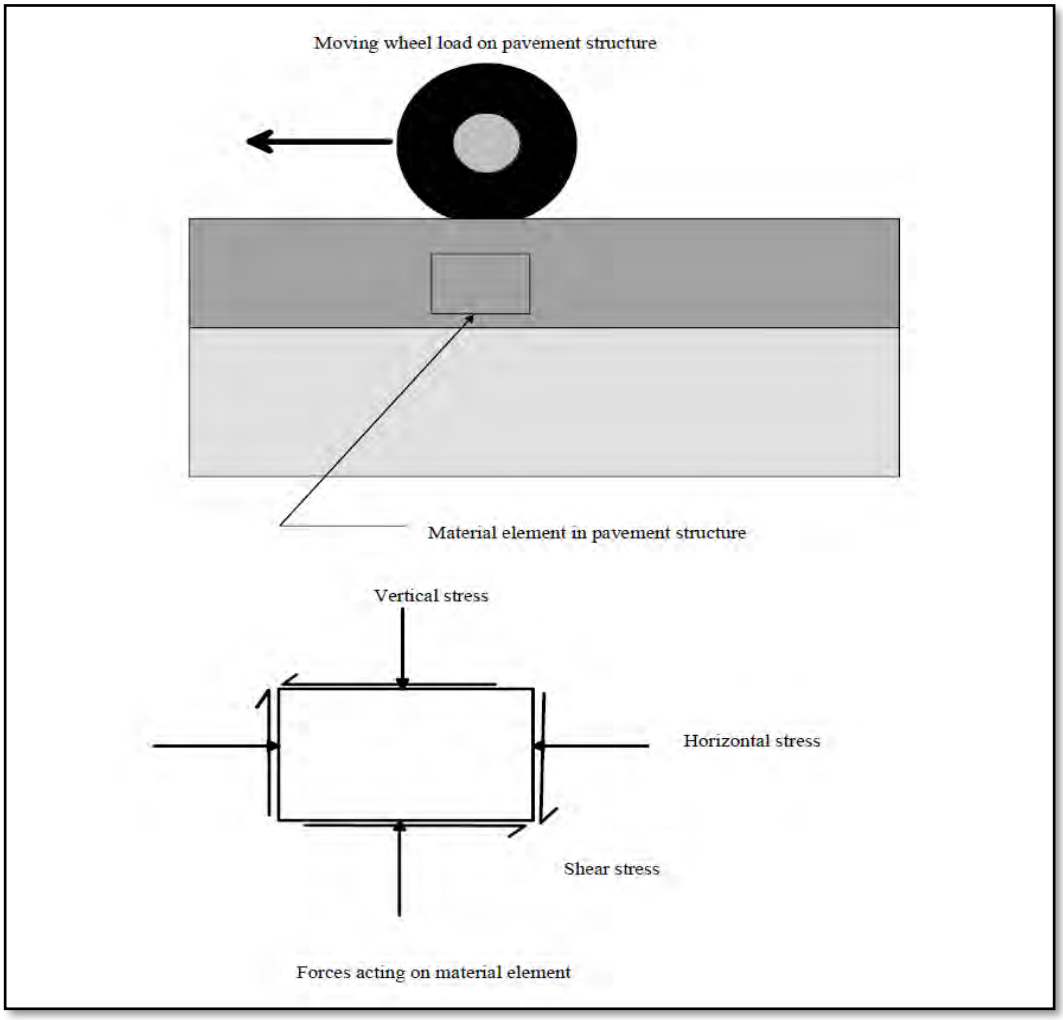

Figure: 6.1 Stress action on the asphalt pavement (Garba 2002)

In the CDCT designed in this research, a confining arrangement of a PVC ring with a resin infill provides lateral confinement. A smaller top platen size is used on a larger diameter specimen size to provide an asphalt annulus around the specimen to ensure lateral stress distribution through the depth of the sample. A number of CDCT test samples were strain gauged at the PVC confining ring to measure hoop strain, as

described in Chapter 4. That data is not provided in this section and is discussed in detail in Chapter 7 to further validate the new test methodology.

The Australian standard dynamic creep test procedure (AS 2891.12.1-1995), and Austroads dynamic creep test procedure named "Testing Asphalt in Accordance with the Austroads Mix Design Procedures - Part 4- Dynamic Creep" (Alderson, Alan & Hubner, David 2008) were used as the base techniques. The following modifications were made as part of the research experimental design. A750 kPa compressive stress was used instead of 200 kPa, and a smaller top platen size on a larger diameter specimen employed instead of same platen/ specimen diameter. A maximum 100,000 loading cycles was adopted to obtain a more representative creep curve.

A number of specimens were tested in full accordance with the current Australian dynamic test procedure (EDCT) to produce a reference against which the new test method could be evaluated.

For each individual dynamic creep test, the total permanent strain versus cycles was plotted. The test data for SCDCT and EDCT specimens is provided as power trend line to enable some correlation to be obtained. The test data for CDCT specimens is provided as linear plots, which are more appropriate for both representation and interpretation. The minimum creep slope, creep life and plastic deformation were determined as following:

Minimum creep slope: Minimum creep slope referenced in this section is the slope of the linear secondary creep phase.

Creep life: creep life is defined as the number of cycles between the end of stage 1 and the start of stage 3.

Plastic deformation; Plastic deformation referenced in this section is the total accumulated deformation (average of LVDTs) that has occurred at the end of the primary creep phase (for plastic deformation of stage 1), and that has occurred at the end of secondary creep phase (for plastic deformation of stage 2). Figure 6.2 provides a typical dynamic creep curve for determining aforementioned parameters.

The minimum creep slope, which occurs in Stage 2 of the creep curve, is specified as the main parameter for evaluating creep potential in the current Australian dynamic creep test (Alderson, Allan & Hubner, David 2008). As recognised within the international literature, the minimum creep slope obtained from as unconfined creep test is inadequate for fully evaluating the creep potential of an asphalt mix. It was proposed that the plastic deformation that occurs in Stage 1 of the creep test could provide good useful supplementary data for evaluating creep potential, and may be used when analysing laboratory creep data. Review of the test data will show that few of the confined samples achieved the end of Stage 2 creep, and then only at very long large test cycles. The minimum creep slope was recorded as the deformation rate (µs/cycle).

The ratio of creep occurring within Stage 1 and at 100,000 cycles for confined testing should provide an indication of potential in-situ performance. For example, it will later be seen that in the case of confined creep at 5.54% air voids, the end of Stage 1 creep occurred in the range of 40,000 to 45,000 cycles at 1.24 mm deformation. The total creep at 100,000 cycles was 1.35mm, indicating that Stage 1 creep may significantly contribute to in-situ rutting.

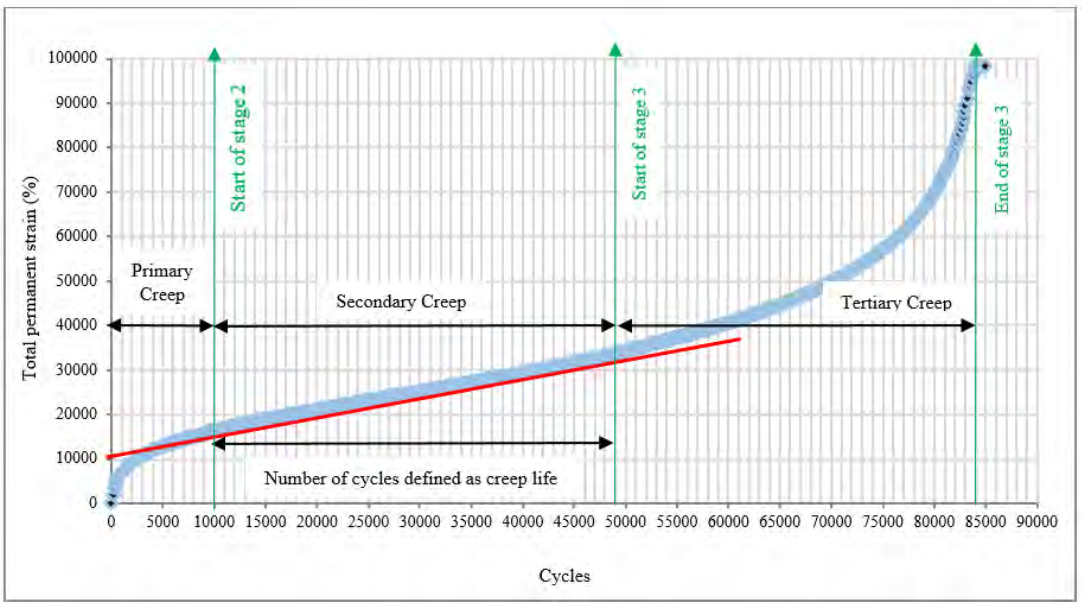

Figure: 6.2 Dynamic creep curve for 50/ 150mm, Multi-grade mix

6.2.1 Semi-confined Dynamic Creep Test method (SCDCT)

Although the main focus of the study is on the CDCT tests, a group of semi-confined tests has been undertaken without confining rings. For those specimens an annulus of asphalt provided confinement by using a smaller top platen size.

For the SCDCT tests, two platen/ specimen configurations, and two types of mix (Multigrade, and C170) were investigated. A 50mm diameter platen was used on 100mm diameter specimens for both multigrade and C170 mixes. A 50 mm diameter platen was used for 150mm diameter multigrade specimens.

The UTS machine was adjusted to apply 750 kPa compressive pressure (as outlined in chapter 4), with 500 milliseconds loading and 1500 milliseconds rest time. Tests were undertaken at 50°C, and the test termination was adjusted to occur at an accumulated strain of 100,000 microstrain, or at 100,000 cycles.

6.2.1.1 SCDCT Multigrade mix, 50/ 100mm

Table 6.1, and Figures 6.3, 6.4, and 6.5 provide a summary of outcomes of SCDCT tests for 50/100mm multigrade specimens. The minimum creep slope, creep life and plastic deformation have been derived for each test. Each specimen was assigned a unique code that enables tracking. These details are available in the Appendix.

In figure 6.3, the minimum creep slope is plotted versus air void content. The data shows a good correlation between increasing air void contents, and minimum creep slope. This indicates decreasing rut resistance of a mix as a function of increasing air voids.

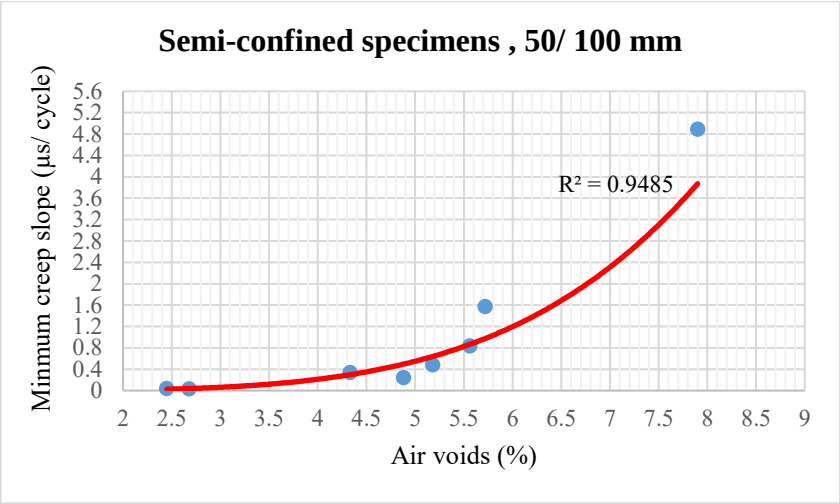

Figure: 6.3 Minimum creep slope for the semi-confined 50/100mm multigrade SCDCT tests

Table: 6.1 SCDCT outcomes for the 50/ 100mm multigrade specimens

(NA= result not achieved)

Air Voids	*Creep Life*	*Minimum Creep Slope*	*Plastic Deformation at the End of*		*Specimen No.*
			Stage 1	*Stage 2*	
(%)	*Cycles*	*(µs/cycle)*	*mm*	*mm*	
2.45	NA	0.038	0.75	NA	109
2.68	NA	0.032	0.798	NA	112
4.33	46400	0.339	0.68	1.81	11
4.88	NA	0.24	0.392	NA	3
5.18	30000	0.484	0.88	1.75	8
5.56	17000	0.833	1.379	2.109	105
5.72	15200	1.57	0.692	1.93	2
7.9	2200	4.89	0.69	1.28	34

Figure 6.4 provides details of plastic deformation of specimens at the end of stages 1 and 2 of the creep deformation. Overall, results display a very poor correlation. Although, there is some correlation for creep at the end of stage 2 that (illogically)

suggests plastic deformation is decreased by increasing air void contents from 4% to 8% there is no relationship between primary and secondary creep deformation. It appears that the test arrangement (50/ 100 mm, SCDCT) does not describe the plastic behaviour of the mix.

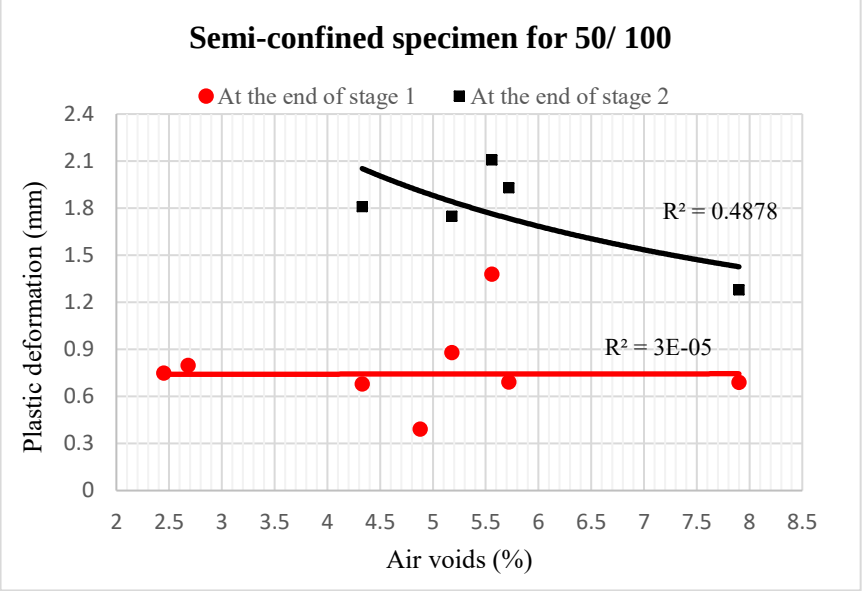

Figure: 6.4 Plastic deformation for the semi-confined 50/ 100mm multigrade SCDCT tests

There is good correlation between creep life of specimens and their air void contents displayed in Figure 6.5. Furthermore, creep life decreases with increasing air void contents (see Figure 6.5).

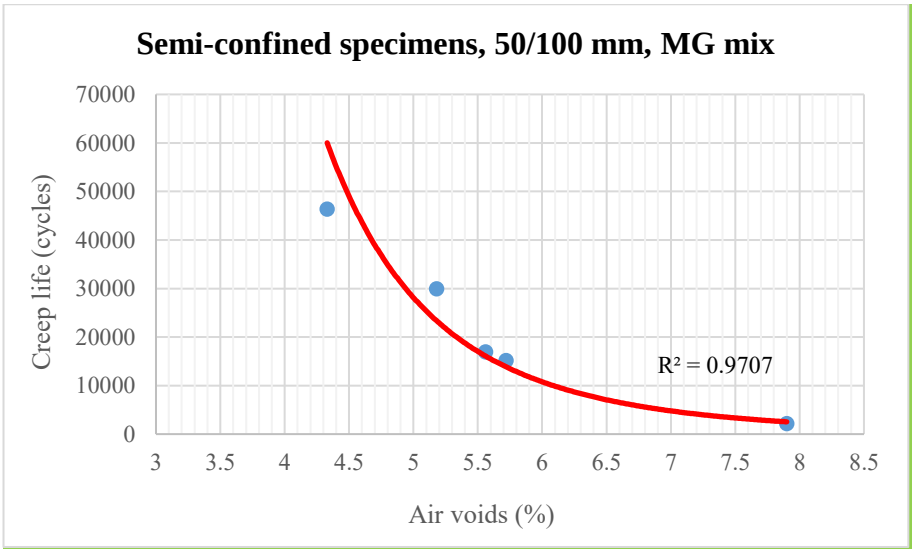

Figure: 6.5 Creep life for the semi-confined 50/ 100 mm multigrade SCDCT tests

As indicated in Table 6.1 most samples displayed all three stages of creep and entered stage 3 over a wide range from 2000 to 100,000 plus cycles. Failure was not through accumulation of plastic strain, but rather sample bursting due to a lack of effective confinement via the asphalt annulus.

Figure 6.6 graphically illustrates a Semi-confined laboratory specimen (50/ 100mm, MG) after testing. During the test, cracks were developed gradually in the specimens and continued until sample collapse. This pattern is not related to rutting deformation mechanism in the road pavements. It was therefore necessary to investigate the confining mechanism in more detail.

Figure: 6.6 Failure pattern for the Semi-confined 50/ 100 mm multigrade SCDCT tests

6.2.1.2 SCDCT Multigrade mix, 50/150 mm

The next level of confinement was via a wider asphalt annulus of 50mm. Table: 6.2, and Figures 6.7, 6.8 and 6.9 illustrate the test results for the 50/150mm multigrade specimens. As is evident in Figure 6.7, the minimum slope is increased by raising air void contents with a reasonable correlation but with much data scatter.

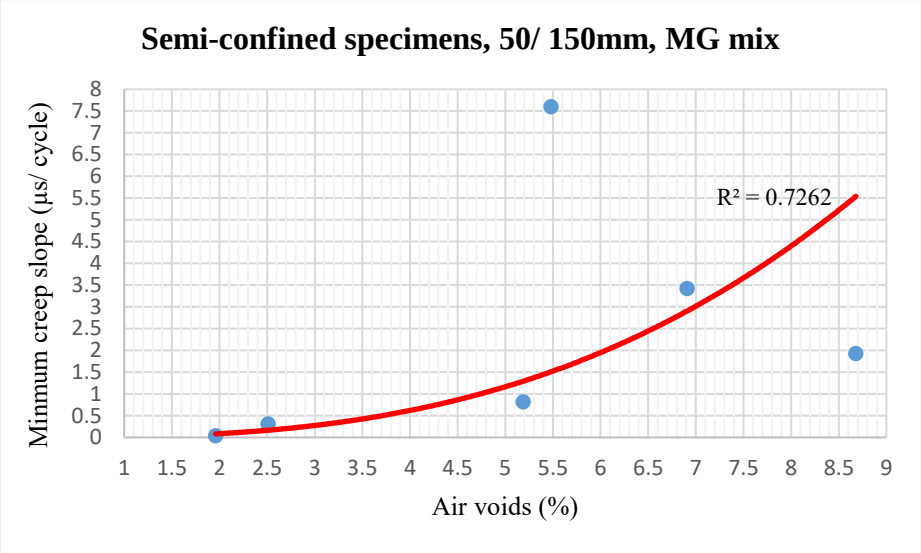

Figure: 6.7 Minimum creep slope for the Semi-confined 50/ 150mm multigrade SCDCT tests

Table: 6.2 SCDCT outcomes for the 50/ 150mm multigrade specimens

(NA= result not achieved)

Air Voids	*Creep Life*	*Minimum Creep Slope*	*Plastic Deformation at the End of*		*Specimen No*
			Stage 1	*Stage 2*	
(%)	*Cycles*	*(µs/cycle)*	*mm*	*mm*	
1.96	NA	0.034	0.807	NA	48
2.51	27,000	0.31	1.671	2.135	58
5.19	36000	0.813	0.89	2.56	20
5.48	3400	7.6	0.83	2.25	24
6.91	8000	3.42	1.1	2.6	31
8.68	15,000	1.93	1.571	3.119	69

Plastic deformation at the end of primary and secondary creep stages is displayed in Figure 6.8. A better correlation was achieved for 50/150mm configuration compared to 50/100mm correlation for stage 2 plastic deformation.

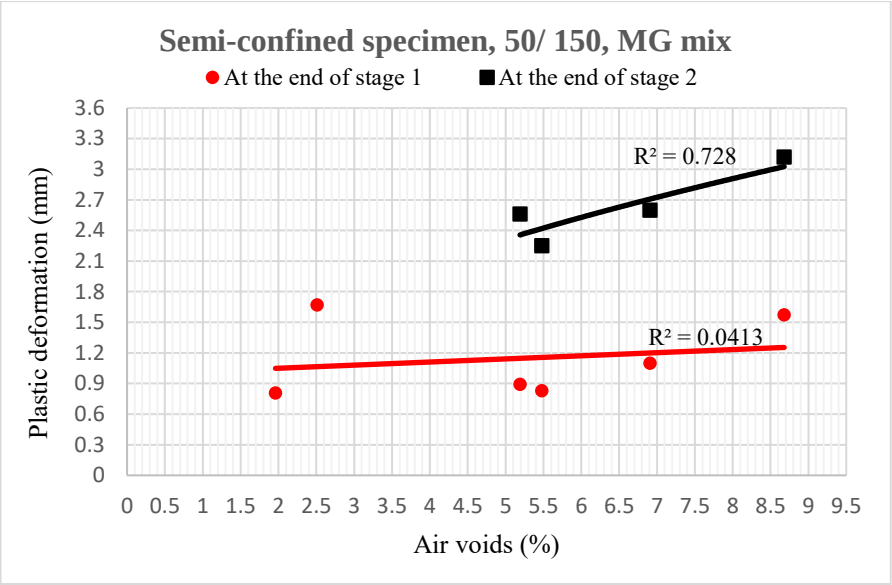

Figure: 6.8 Plastic deformation for the Semi-confined 50/ 150mm multigrade SCDCT tests

An absence of perceptible trends for evaluating creep life in Figure 6.9 is associated, with a poor correlation for results. As discussed previously, the lack of an effective confinement appeared to be the main cause of the short creep life.

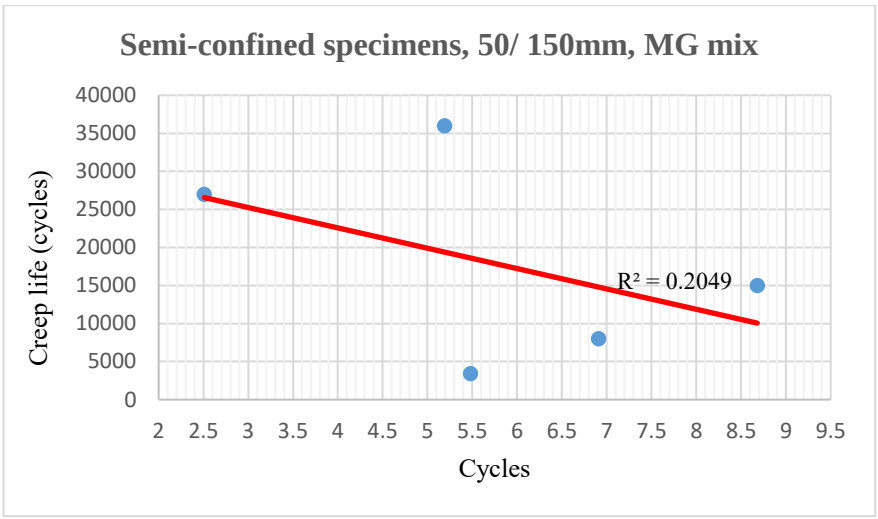

Figure: 6.9 Creep life for the Semi-confined 50/ 150mm multigrade SCDCT tests

Failure of samples with a 50/150mm arrangement displayed the same failure trend as for the 50/100mm arrangement. As shown in the figure 6.10, specimens punched and burst under simulated tyre pressure, and this is a different failure mechanism to in-situ rutting. Although the 50/150mm arrangement provides a wider asphalt annulus for

specimens (in comparison with 50/ 100mm arrangement), the same failure mechanism (cracks and punching of specimens) occurred. Test results indicate that providing a 50mm asphalt annulus (50/150mm) does not provide a realistic confining medium.

Figure: 6.10 Failure pattern for the Semi-confined 50/ 150 mm multigrade SCDCT tests

6.2.1.3 SCDCT C170 mix, 50/ 100mm

For this part a different mix type was used to evaluate the SCDCT method. Table 6.3, figures 6.11, 6.12, and 6.13 document outcomes of the tests for C170 mix when a 100 mm specimen was loaded by a 50mm platen. As a limited spectrum of air void contents was available for C170 mix, only limited testing was undertaken to further validate the previous SCDCT multigrade 50/100mm testing outcomes. Generally the plots followed the same trend as for the multigrade 50/100mm testing.

Table: 6.3 SCDCT outcomes for the 50/ 100mm C170 specimens

Air Voids	*Creep Life*	*Minimum Creep Slope*	*Plastic Deformation at the End of*		*Specimen No.*
			Stage 1	*Stage 2*	
(%)	*Cycles*	*(µs/cycle)*	*mm*	*mm*	
4.76	190	102.04	0.929	1.881	137
4.88	200	95.52	1.025	2.043	130
5.01	110	163.6	1.048	2	127
5.42	110	157.4	1.167	2.083	132

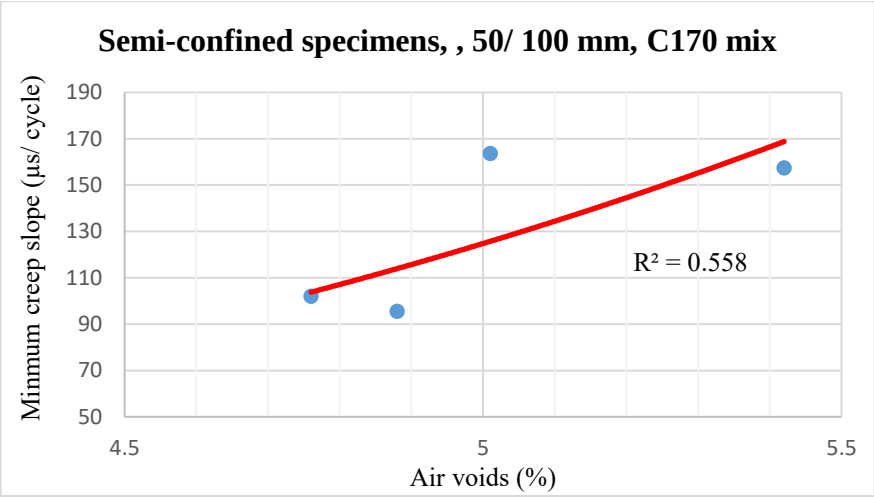

Figure: 6.11 Minimum creep slope for the Semi-confined 50/ 100mm C170, SCDCT tests

Figure 6.11 illustrates minimum creep slope versus air void contents. By raising the air void content, the minimum creep slope increased (similar to figure 6.3). Comparison of Figures 6.3 and 6.11 (as shown in Figure 6.52) indicates that the minimum creep slope of C170 mix was much higher than that for the multigrade mix. Primary and secondary creep deformations have the same trend. As shown in figure 6.12, plastic deformation increased with increasing air voids.

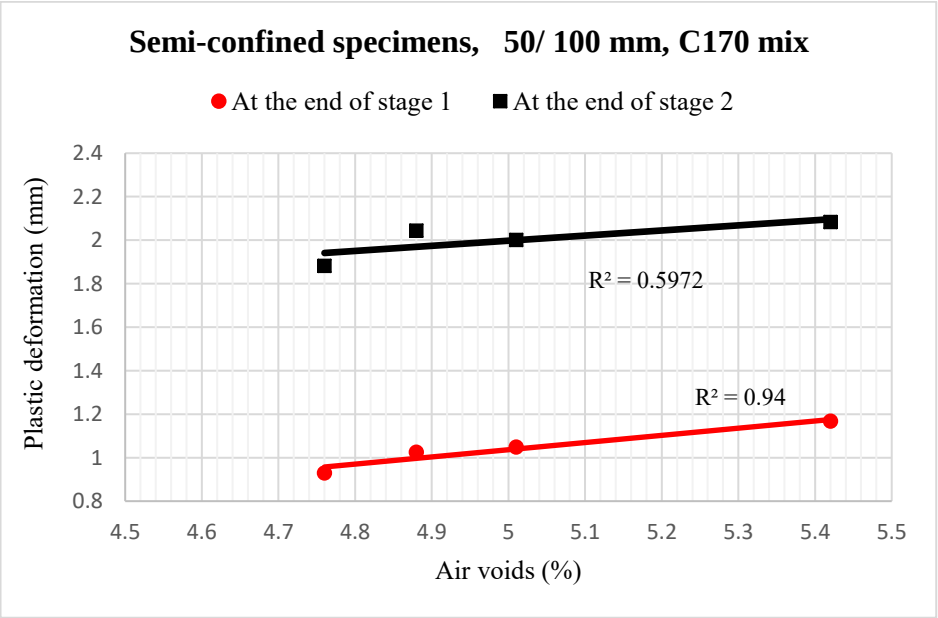

Figure: 6.12 Plastic deformation for the Semi-confined 50/ 100mm C170, SCDCT test

The creep life graph (figure 6.13) confirms a very short service life for all specimens (only 100 to 200 cycles). The tests were completed in a few minutes, although they were expected to have a much longer lifetimes in the field.

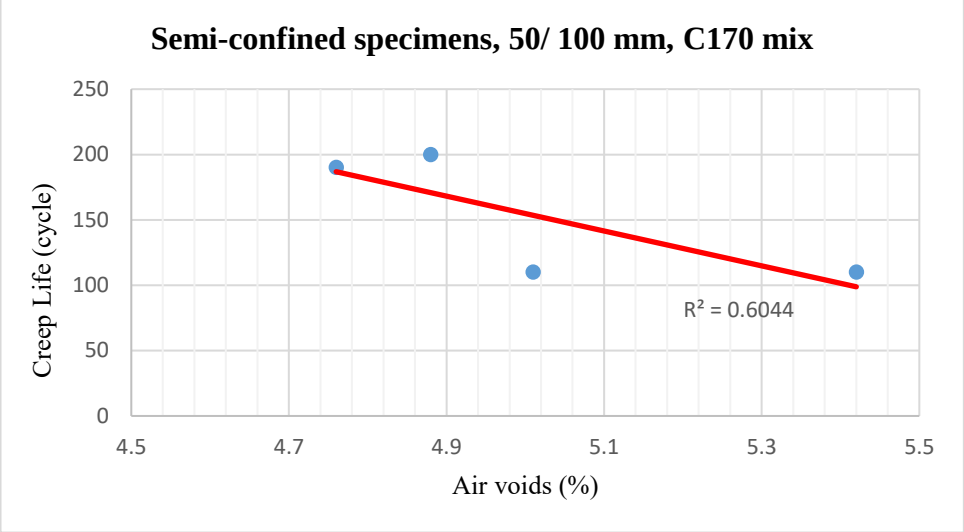

Figure: 6.13 Creep life for the Semi-confined 50/ 100 mm C170, SCDCT tests

The failure patterns of the C170 specimens had the same problem as multigrade specimens. Cracks were developed and the platen continued to punch into specimens under load. Figure 6.14 shows a C170 specimen after testing. Results confirmed that regardless of mix type (typical or rut resistance mix), semi-confined specimens did not exhibit the same rut mechanism as road pavements. It is evident that a single asphalt annulus cannot provide sufficient confinement for the specimens. Therefore, it was necessary to further explore more effective methods of applying a realistic confining medium for laboratory evaluation.

Figure: 6.14 Rapid collapse failure pattern for the Semi-confined 50/ 100 mm C170 test

6.2.2 Confined dynamic creep test method (CDCT) results

Here the test outcomes of specimens confined with the flow able resin and a PVC ring are discussed. Various platen/specimen diameter configurations were used for loading i.e. 50/ 100mm, 50/ 150mm, and 75/ 150mm. Two types of asphalt mixes (multigrade, and C170) were used for fabricating specimens. Two different PVC wall thicknesses have also been used for confining asphalt samples that divided CDCT tests into two groups namely, 4mm thick ring, and 2mm thick ring confinement.

A 750 kPa pressure was applied to simulate real commercial vehicle tyre pressure, with 500 milliseconds loading and 1500 milliseconds rest time. Test termination was adjusted to be attained at accumulated strains of 100,000 μs, or 100,000 cycles.

6.2.2.1 CDCT tests with Multigrade mix, 4 mm PVC ring, 50/ 150mm

Table 6.4, figures 6.15, and 6.16 summarise the outcomes of the tests. The minimum creep slope increased with increasing air void contents as documented in the Figure 6.15. If compared with semi-confined specimens (figure 6.7 and 6.15), the minimum creep slope dropped significantly, and occurred over much greater cycle ranges.

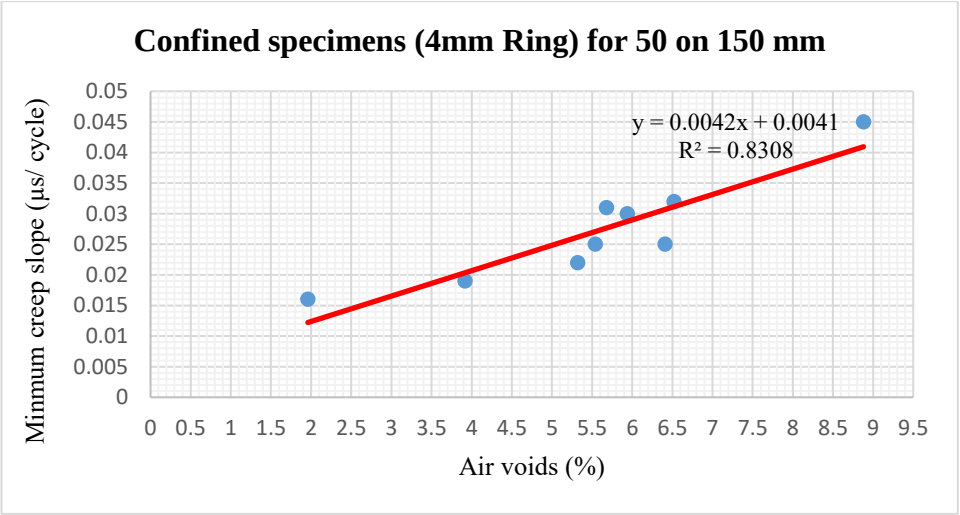

Figure: 6.15 Minimum creep slope for the Confined 50/ 150mm multigrade, CDCT test

Table: 6.4 CDCT outcomes for the 50/ 150mm Multigrade specimens with 4 mm PVC ring

Air Voids	*Minimum Creep Slope*	*Plastic Deformation at the End of Stage 1*	*Specimen No.*
(%)	*(µs/cycle)*	*mm*	
1.96	0.016	0.674	47
3.92	0.019	0.94	53
5.32	0.022	1.145	26
5.54	0.025	1.238	28
5.68	0.031	1.08	25
5.94	0.03	1.381	18
6.41	0.025	1.331	27
6.52	0.032	1.678	32
8.88	0.045	1.666	70

Stage 1 plastic deformation increased with increasing air voids content in the specimens as is evident from Figure 6.16. Although plastic deformation had a reasonable trend for middle to high air void contents, its trend for specimens with low air voids (less than 3%) appeared to be contrary to that indicated in the literature.

Although 100,000 cycles with 750 kPa tyre pressure were applied in laboratory tests, third stage creep was not reached in any of the specimens.

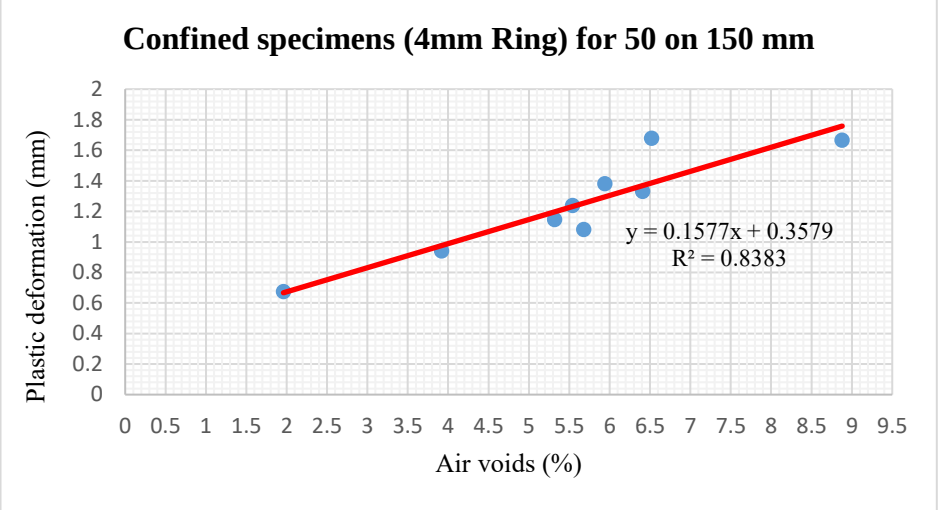

Figure: 6.16 Stage 1 plastic deformation for the Confined 50/ 150mm multigrade, CDCT tests

A promising outcome occurred in the failure patterns of specimens. Figure 6.17 depicts the failure pattern of a confined specimen after testing. The confinement was able to produce a more realistic failure pattern compared to that achieved in the SCDCT testing. Confinement eliminated radial cracking in the specimens and bursting and punching did not occur for any specimens with 750 kPa pressure being applied. The asphalt was pushed down under the platen, displaced sidewards and slightly raised up around the platen. The duplication of in-situ pavement rutting deformation in the laboratory is an encouraging aspect of the new confined test.

A) specimens after testing

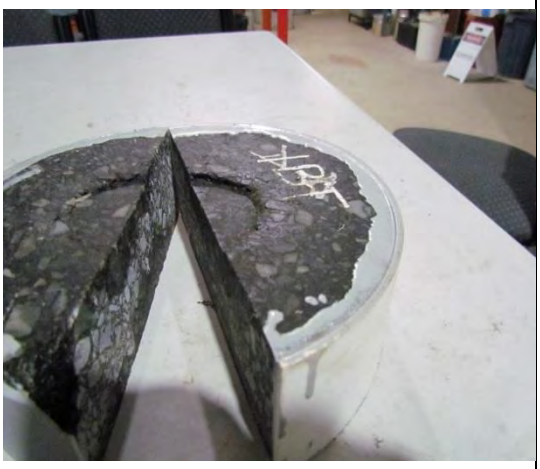

B) cut specimen from the centre

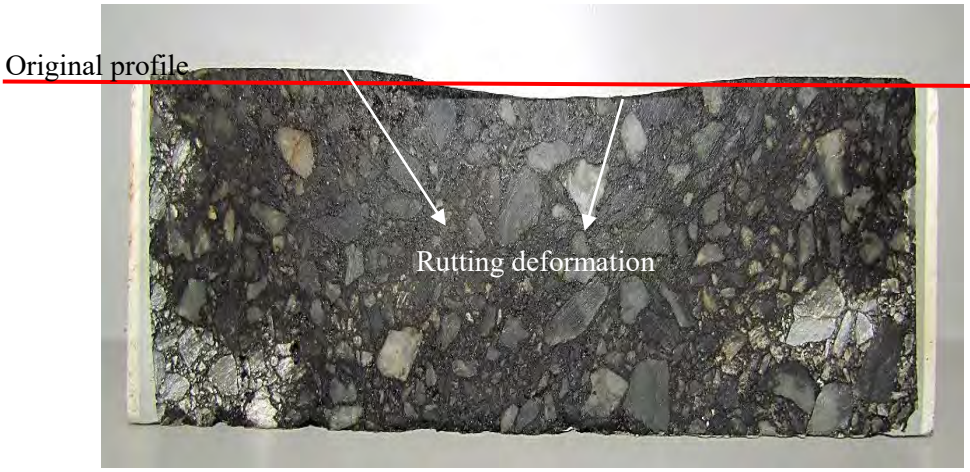

C) a cross section of the cut specimen

Figure: 6.17 Specimen's failure pattern of the CDCT tests. 50/ 150 mm

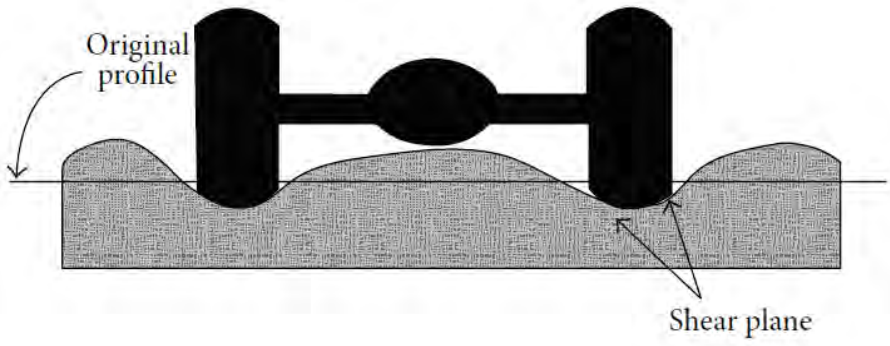

Figure: 6.18 A schematic of in field asphalt rutting deformation (Mashaan et al. 2014)

6.2.2.2 CDCT tests with Multigrade mix, 4 mm PVC ring, 50/ 100mm

The outcomes of laboratory tests for 100mm diameter multigrade mix specimens, confined with a 4mm wall thickness PVC ring and loaded with 50 mm platen, are illustrated in Table 6.5, figures 6.19 and 6.120. A wide range of air voids (from around 2% to 10% air void contents) have been investigated.

Figure 6.19 records that the minimum creep slope increased at a gradual rate when the air void content increased. The rate of minimum slope increase was less than in the 50/ 150mm CDCT configuration. This can be explained by a lesser amount of asphalt around the loading area to provide the same amount of deformation as seen in the 50/150mm specimens.

Table: 6.5 CDCT outcomes for the 50/ 100mm Multigrade specimens with 4 mm PVC ring

Air Voids	*Minimum Creep Slope*	*Plastic Deformation at the End of*	*Specimen No.*
		Stage 1	
(%)	*(μs/cycle)*	*mm*	
2.3	0.006	0.276	111
3.32	0.013	0.358	95
4.18	0.013	0.711	85
5.42	0.012	0.428	5
7.39	0.013	0.99	33
8.04	0.018	0.864	35
8.78	0.013	1.033	39
9.55	0.016	0.841	43
9.93	0.013	0.874	44
10.14	0.019	1.137	42

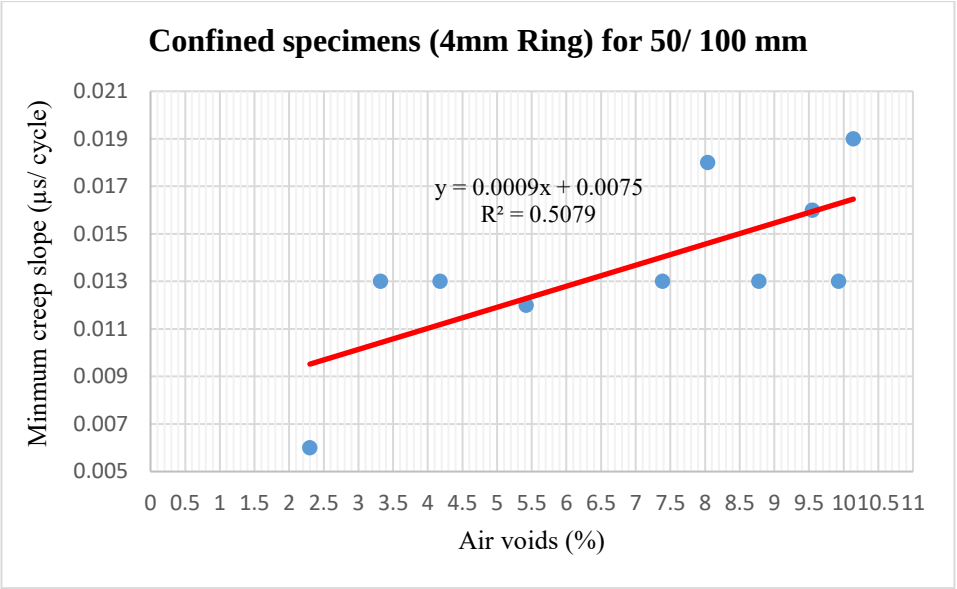

Figure: 6.19 Minimum creep slope for the Confined 50/ 100mm multigrade, CDCT tests

Plastic deformation increased with increasing air voids in the specimens as documented in the Figure 6.20., Third creep stage was not attained in any of the specimens.

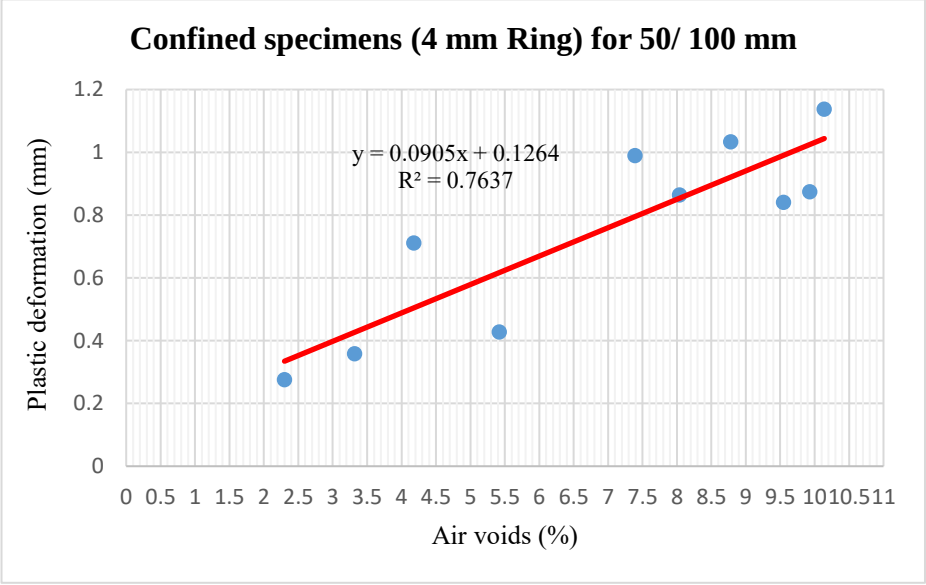

Figure: 6.20 Plastic deformation for the Confined 50/ 100mm multigrade, CDCT test

The failure patterns of specimens were similar to that for 50/ 150mm specimens (as displayed in the figure 6.21). The deformation happened in the specimens without cracking, busting or punching.

Figure: 6.21 Failure pattern for the CDCT confined 50/ 100 mm multigrade

6.2.2.3 CDCT tests with multigrade mix, 4 mm PVC ring, 75/ 150mm

A 75mm diameter platen was used to load 150mm specimens. Outcomes of tests are provided in Table 6.6, and Figures 6.22, and 6.23. The minimum creep slope increased with increasing air voids content. The level of the minimum slope for 75/150mm specimens was higher than that for 50/100mm, and lower than 50/150mm configurations, suggesting that the rate of minimum slope was a function of the asphalt annulus thickness.

Table: 6.6 CDCT outcomes for the 75/ 150mm Multigrade specimens with 4 mm PVC ring

Air Voids	*Minimum Creep Slope*	*Plastic Deformation at the End of*	*Specimen No*
		Stage 1	
(%)	*(µs/cycle)*	*mm*	
2.05	0.013	0.979	45
3.33	0.015	0.781	62
5.09	0.019	1.313	83
6.02	0.025	1.598	65
8.65	0.031	1.7	72

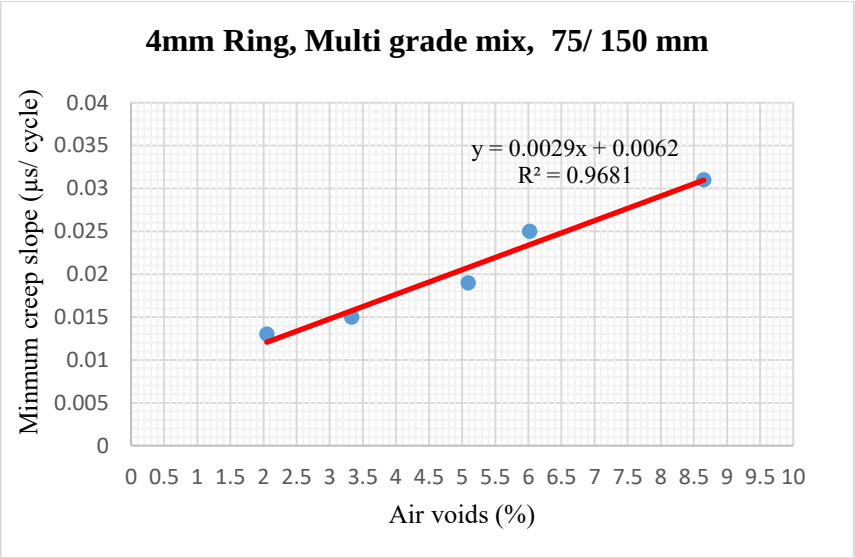

Figure: 6.22 Minimum creep slope for the Confined 75/ 150mm multigrade, CDCT tests

Plastic deformation increased with increasing air void content in the specimens. Third stage creep did not occur for any of the specimens and no cracking or punching was observed in any of the specimens.

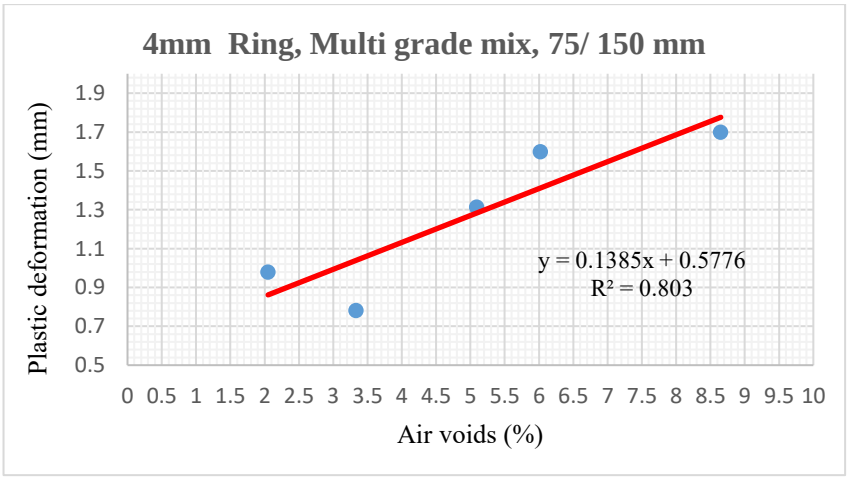

Figure: 6.23 Plastic deformation for the Confined 75/ 150mm multigrade, CDCT test

6.2.2.4 CDCT test with multigrade mix, 2.5 mm PVC ring, 50/ 150mm

To better quantify the effects of reduced confining stress, a PVC ring (2.5mm) was used for generating the confinement. The results for confined 150mm specimens when loaded with 50mm platen are presented in Table 6.7, and Figures 6.24, and 6.25. The

test results for 2.5mm PVC ring produce a similar trend to that for the 4mm ring. The minimum creep slope and plastic deformation increased with increasing air voids (see Figures 6.24 and 6.25). Stage 3 creep deformation again did not occur for any of the specimens, and there was no evidence of cracking, busting or punching.

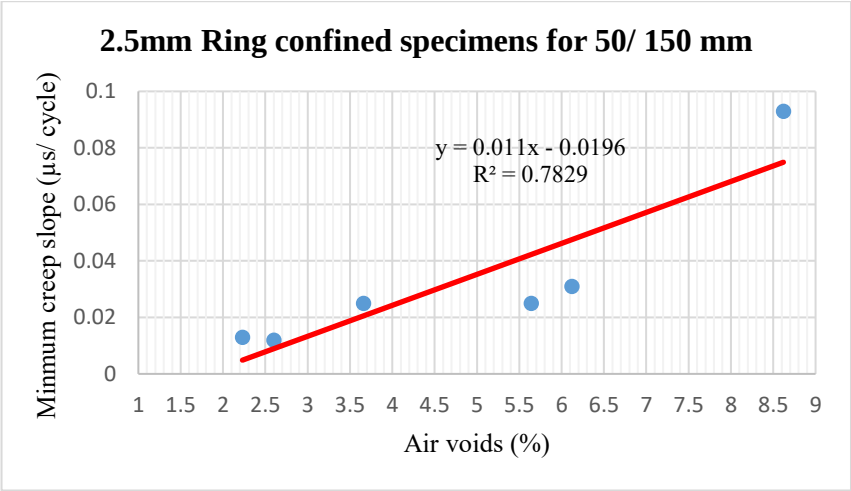

Figure: 6.24 Minimum creep slope for the confined (2.5 mm) 50/ 150mm multigrade, CDCT tests

Table: 6.7 CDCT outcomes for the 50/ 150mm Multigrade specimens with 2.5 mm PVC ring

Air Voids	*Minimum Creep Slope*	*Plastic Deformation at the End of*	*Specimen No*
		Stage 1	
(%)	*(µs/cycle)*	*mm*	
2.23	0.013	0.338	49
2.6	0.012	1.092	60
3.66	0.025	0.723	61
5.64	0.025	1.355	78
6.12	0.031	1.157	82
8.62	0.093	1.756	71

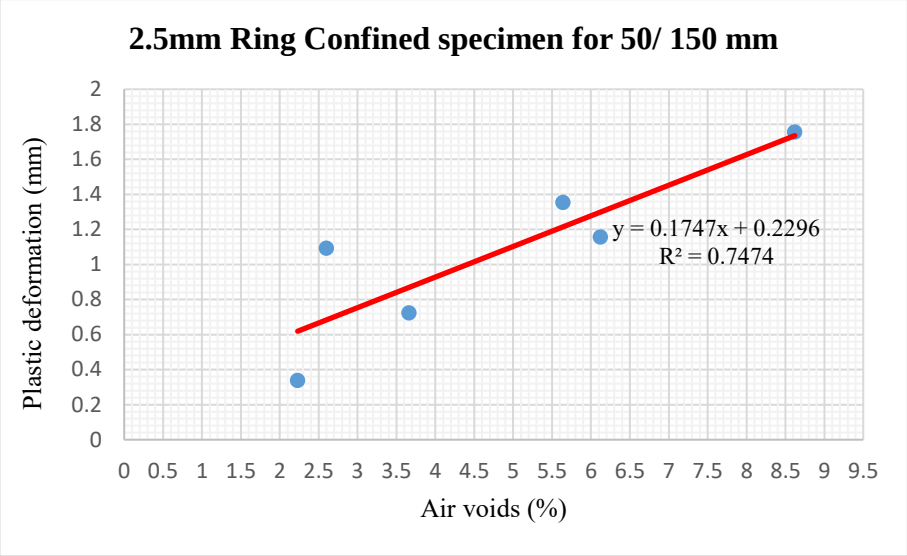

Figure: 6.25 Plastic deformation for the confined (2.5 mm) 50/ 150mm multigrade, CDCT test

6.2.2.5 CDCT tests with C170 mix, 2.5 mm PVC ring, 50/ 150mm

This part is related to 2.5mm PVC ring confinement for the C170 mix tests. Test results are presented in the following Figures 6.26, 6.27 and Table 6.8.

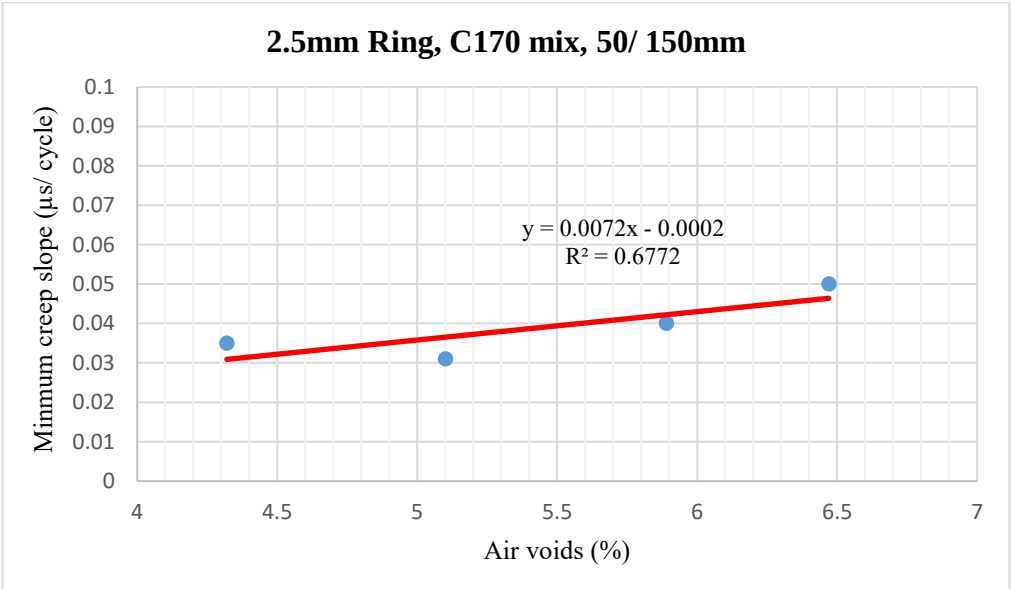

Figure: 6.26 Minimum creep slope for the Confined (2.5 mm) 50/ 150mm C170, CDCT

Table: 6.8 CDCT outcomes for the 50/ 150mm C170 specimens with 2.5 mm PVC ring

Air Voids	*Minimum Creep Slope*	*Plastic Deformation at the End of*	*Specimen No*
		Stage 1	
(%)	*(µs/cycle)*	*mm*	
4.32	0.035	2.442	121
5.1	0.031	2.383	118
5.89	0.04	2.64	122
6.47	0.05	2.948	117

As shown in the figure 6.26, Yet again, the minimum creep slope increased with increasing air voids in the specimens (refer to Figure 6.26). The creep third stage did not occur in any specimens. Creep deformation occurred without presenting cracks or punching.

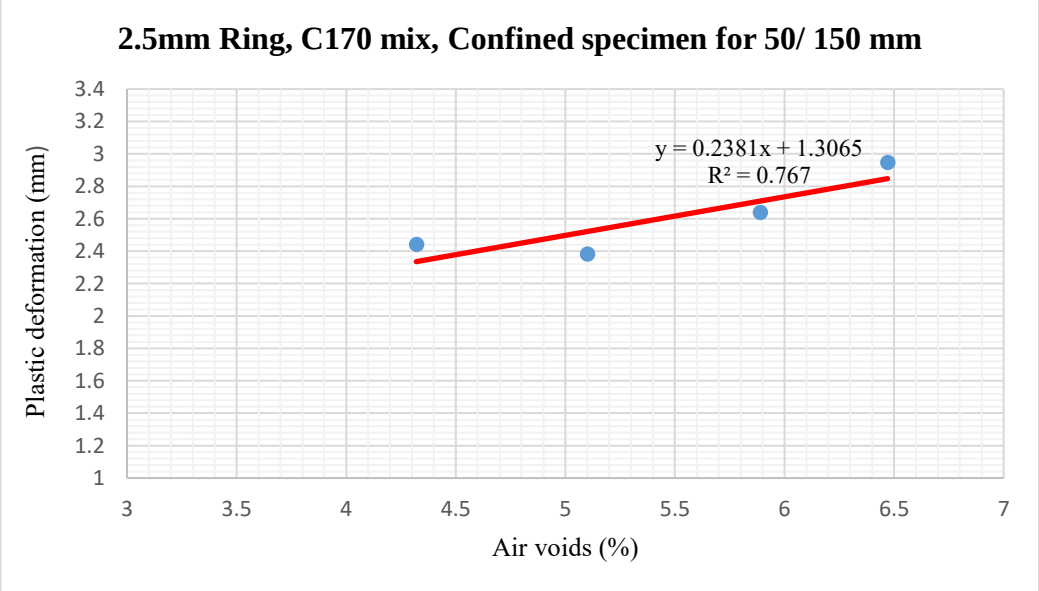

Figure: 6.27 Plastic deformation for the Confined (2.5 mm) 50/ 150mm C170, CDCT

6.2.2.6 CDCT tests with C170 mix, 2.5 mm PVC ring, 50/ 100mm

As a limited range of air voids was available for this type of mix, only limited testing was undertaken. Outcomes of the tests are provided in Table 6.9, and Figures 6.28, and 6.29.

Both minimum creep slope and plastic deformation increased with increasing air voids with the third creep phase not reached for any specimens.

Table: 6.9 CDCT outcomes for the 50/ 100mm C170 specimens with 2.5 mm PVC ring

Air Voids	*Minimum Creep Slope*	*Plastic Deformation at the End of Stage 1*	*Specimen No*
(%)	*(µs/cycle)*	*mm*	
4.59	0.016	1.093	136
4.97	0.016	1.452	138
5.03	0.016	1.087	129
5.12	0.016	1.023	134
5.36	0.018	1.452	135

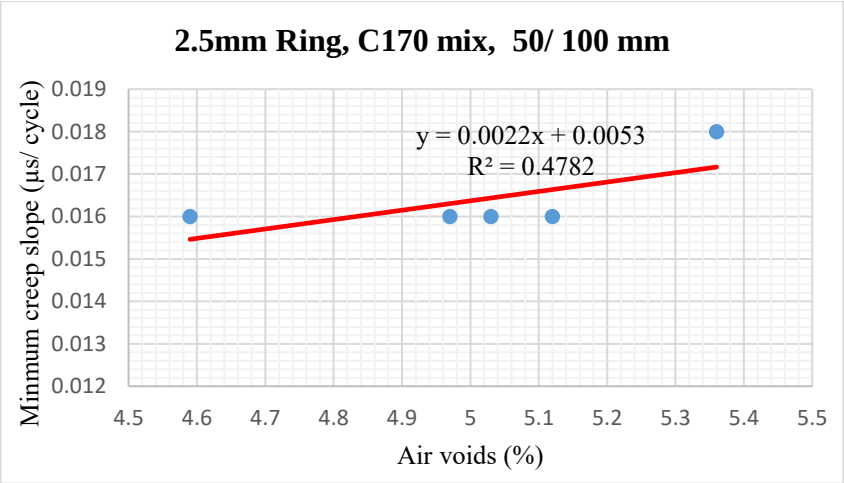

Figure: 6.28 Minimum creep slope for the Confined (2.5 mm) 50/ 100mm C170, CDCT

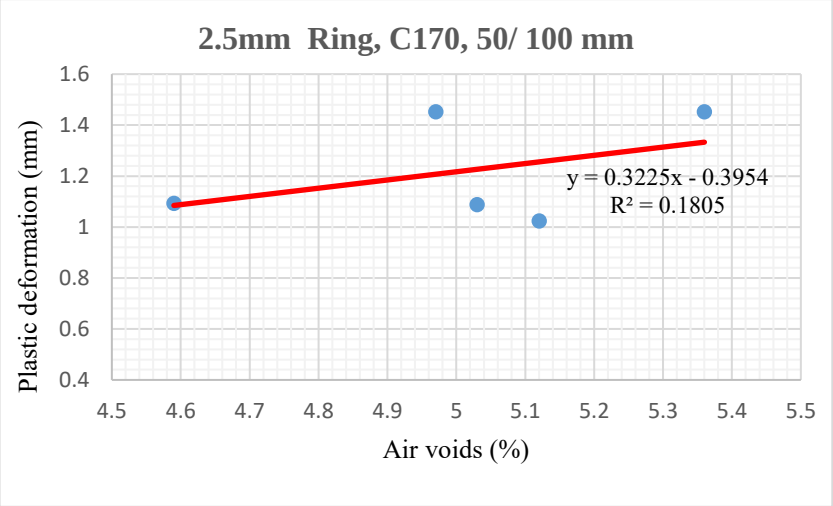

Figure: 6.29 Plastic deformation for the Confined (2.5 mm) 50/ 150mm C170, CDCT

Figure: 6.30 Failure pattern for the CDCT confined (2.5 mm) 50/ 100 mm C170

6.2.2.7 CDCT tests with C170 mix, 2.5 mm PVC ring, 75/ 150mm

Table 6.10, and Figures 6.31 and 6.32 demonstrate test outcomes. As seen in the results, the minimum creep slope and plastic deformation increased with increasing air voids in the specimens, while the third creep stage did not occur in any of the specimens.

Table: 6.10 CDCT outcomes for the 75/ 100mm C170 specimens with 2.5 mm PVC ring

Air Voids	*Minimum Creep Slope*	*Plastic Deformation at the End of*	*Specimen No*
		Stage 1	
(%)	*(µs/cycle)*	*mm*	
4.51	0.022	1.632	126
4.81	0.022	1.79	124
5.04	0.025	1.86	120
5.66	0.025	1.911	123

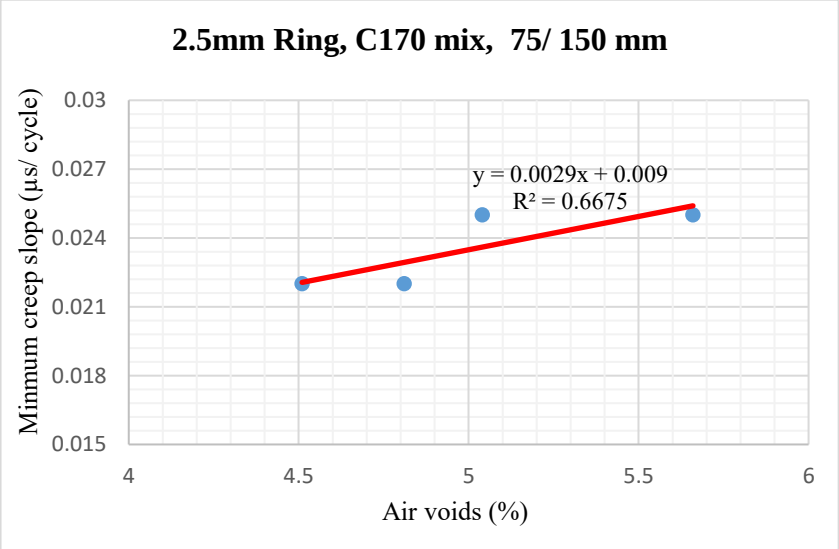

Figure: 6.31 Minimum creep slope for the Confined (2.5 mm) 75/ 150mm C170, CDCT

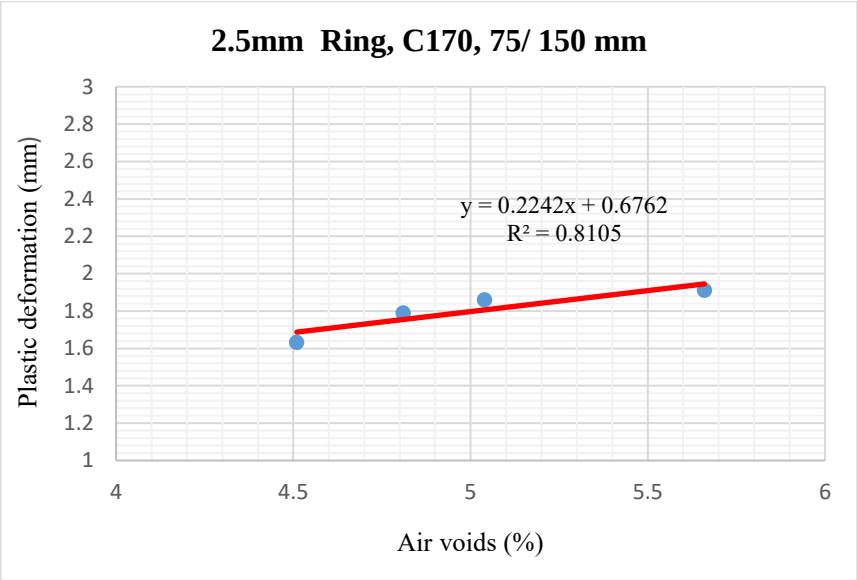

Figure: 6.32 Plastic deformation for the Confined (2.5 mm) 75/ 150mm C170, CDCT

6.2.3 Existing Dynamic Creep Test method (EDCT)

This data set provided the baseline data by undertaking testing in accordance with Australian standard for dynamic creep test (AS 2891.12.1-1995). A 200 kPa cyclic pressure was applied through 100 mm and 150 mm platen sizes for 100 mm and 150 mm specimens, respectively. Tables 6.11, and Figures 6.33, and 6.34 present the test results and demonstrate poor correlations.

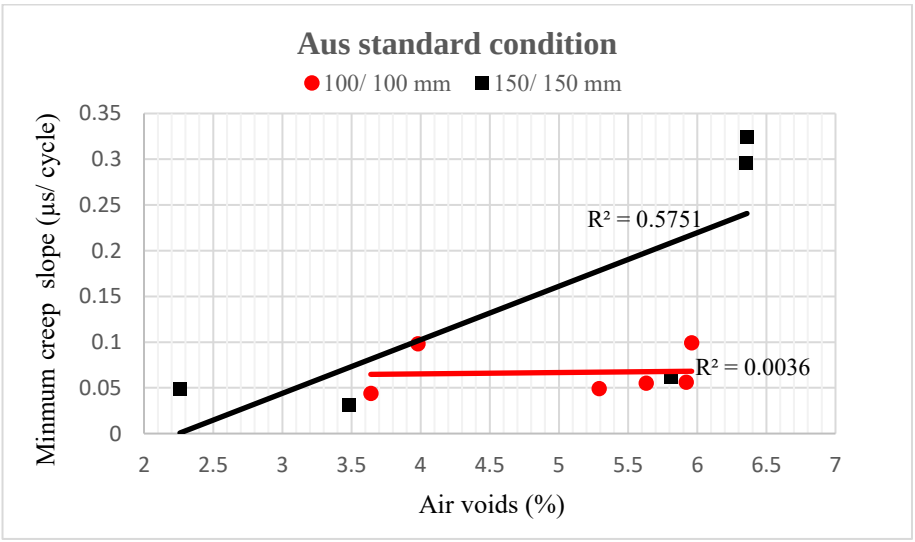

Figure: 6.33 Minimum creep slope for multigrade mix, EDCT

Table: 6.11 EDCT outcomes for the 100/ 100mm and 150/150mm specimens

Platen/ specimen size	*Air Voids*	*Minimum Creep Slope*	*Plastic Deformation at the End of Stage 1*	*Specimen No*
mm	*(%)*	*(µs/cycle)*	*mm*	
100/ 100	3.64	0.044	0.352	88
100/ 100	3.98	0.098	1.171	91
100/ 100	5.29	0.049	0.24	107
100/ 100	5.63	0.055	0.788	103
100/ 100	5.92	0.056	0.851	102
100/ 100	5.96	0.099	0.495	101
150/ 150	2.26	0.049	0.489	59
150/ 150	3.48	0.031	0.701	63
150/ 150	3.96	0.098	1.157	54
150/ 150	5.81	0.062	0.81	74
150/ 150	6.35	0.296	1.11	67
150/ 150	6.36	0.324	1.22	66

As is evident from the figures, the minimum creep slope increased with increasing air voids, however, no trend was observed for plastic deformation. The 150/150mm tests had a higher level of creep slope and plastic deformation. The third creep phase did not occur. Data for a tested sample is portrayed in figure 6.35.

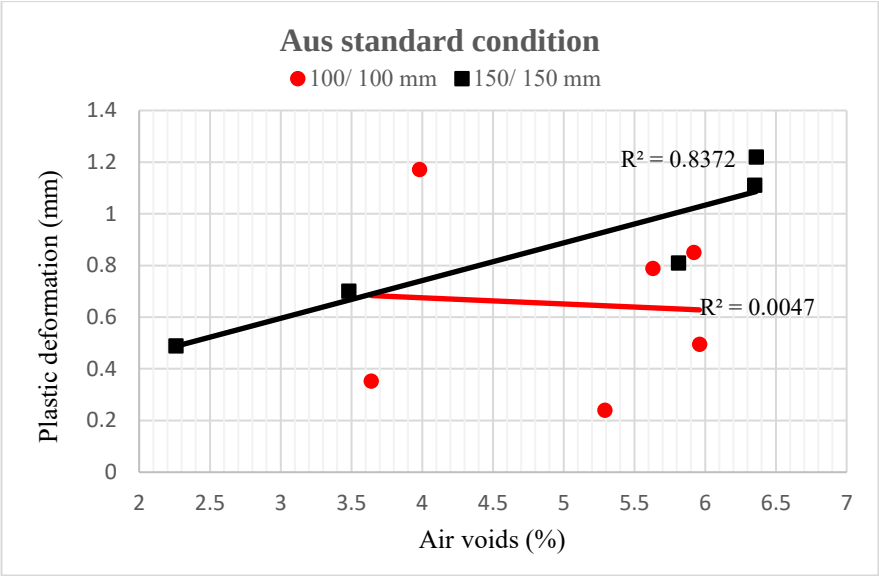

Figure: 6.34 Plastic deformation for multigrade mix, EDCT

Figure: 6.35 Failure pattern for the EDCT, 150/ 150mm

6.3 Experimental data comparison

Laboratory outcomes of the EDCT, CDCT and SCDCT tests have been compared to investigate the capability of the new test methods. Effects of platen sizes, ring thicknesses, and confinements have been evaluated. To study the effects of platen sizes, various sizes of platen were used while mix type, confinement condition, and test method were fixed.

6.3.1 Comparison between the CDCT and EDCT test methods

Figures 6.36 to 6.39 provide outcomes of the dynamic creep test in accordance with the Australian standard versus the new test method. Both standard specimen sizes (100mm and 150mm) were compared with the same sizes of the new confined specimen with reduced platen sizes.

The outcomes confirm that the standard method had a much higher minimum creep slope when compared to the new method for a same mix but with a much lower correlation. The plastic deformation in the new test method was higher than in the standard test and also exhibited enhanced correlation with air voids.

The data presented in the this section indicates that the new proposed test methodology utilising realistic tyre pressure and confining medium provided much better correlation with air voids than the current Australian standard.

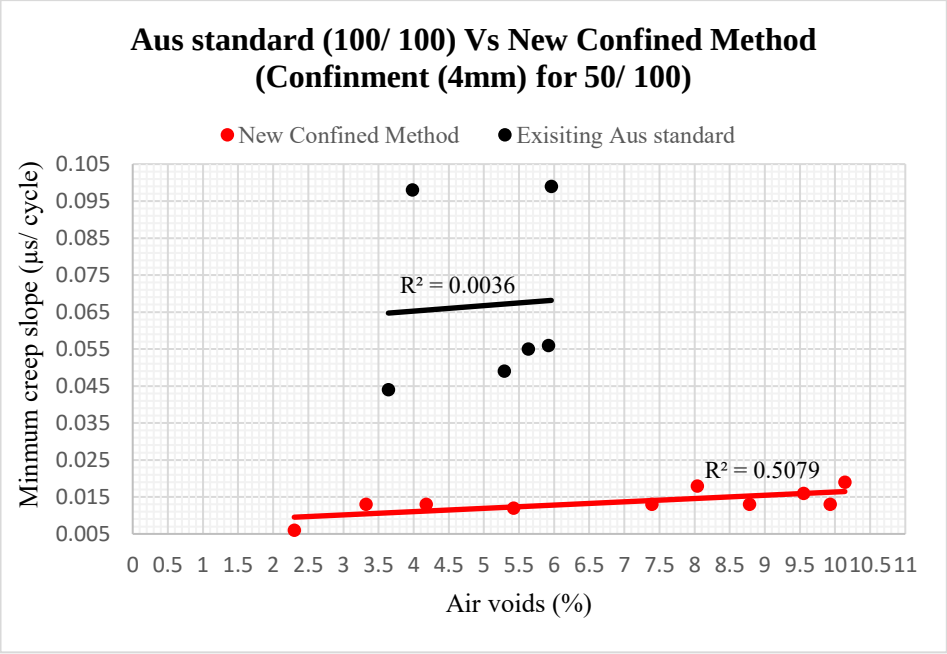

Figure: 6.36 Minimum creep slope comparison between EDCT and CDCT test methods for 100mm specimen

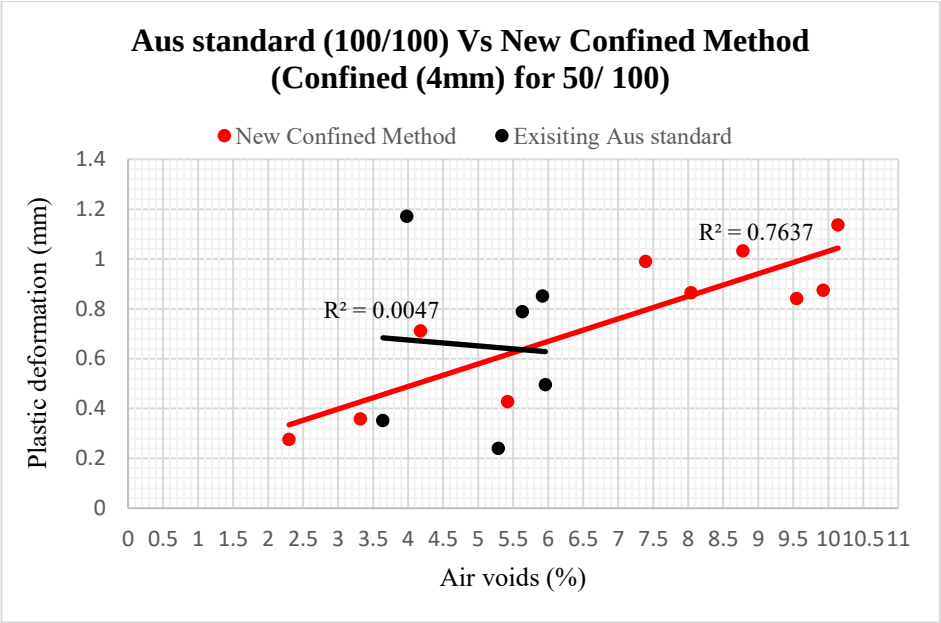

Figure: 6.37 Plastic deformation comparison between EDCT and CDCT test methods for 100mm specimen

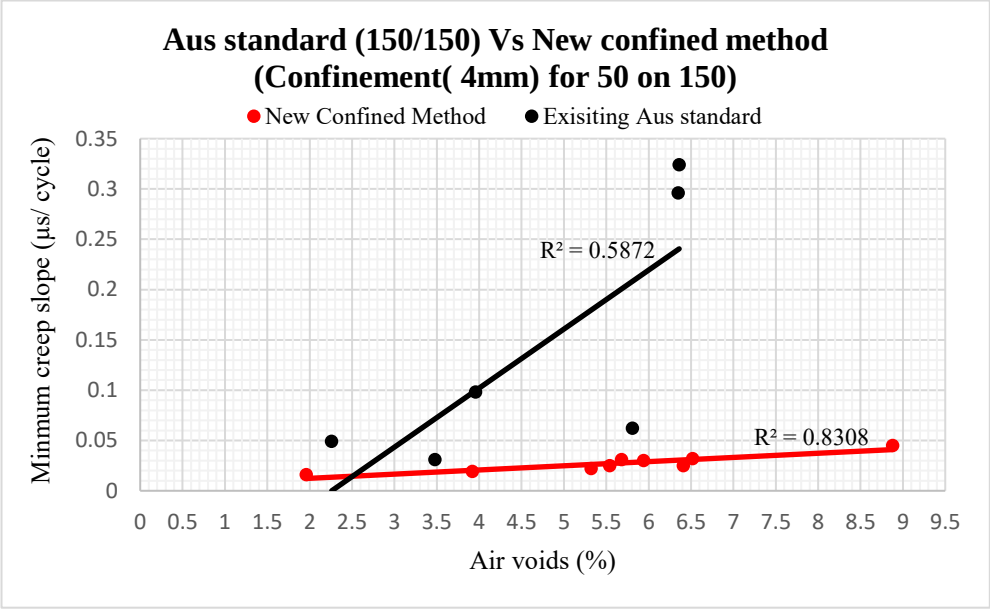

Figure: 6.38 Minimum creep slope comparison between EDCT and CDCT test methods for 150mm specimen

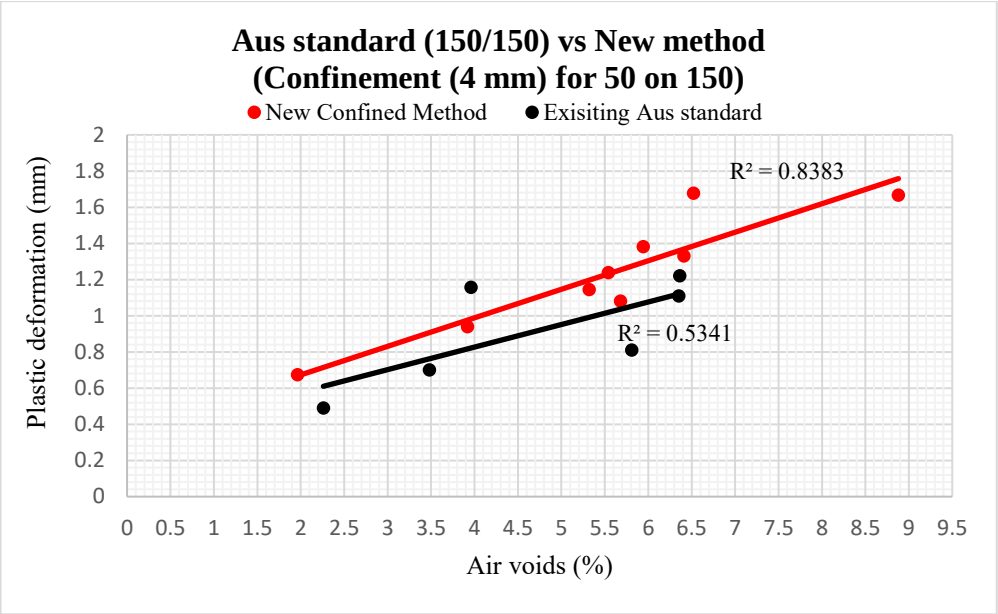

Figure: 6.39 Plastic deformation comparison between EDCT and CDCT test methods for 150mm specimen

6.3.2 CDCT and SCDCT tests comparison

Test results for the SCDCT and CDCT specimens are presented in Figures 6.40 to 6.43. The minimum slope of the semi-confined specimens was significantly higher than that for the confined specimens (Figures 6.40 and 6.41). It is possible that the high second creep rates are partially related to crack nucleation and do not solely represent creep. The data provided in figure 6.42 and 6.43 indicate comparable levels of stage 1 deformation to those for the CDCT data indicating good correlation with air voids, while a very poor correlation is found for SCDCT.

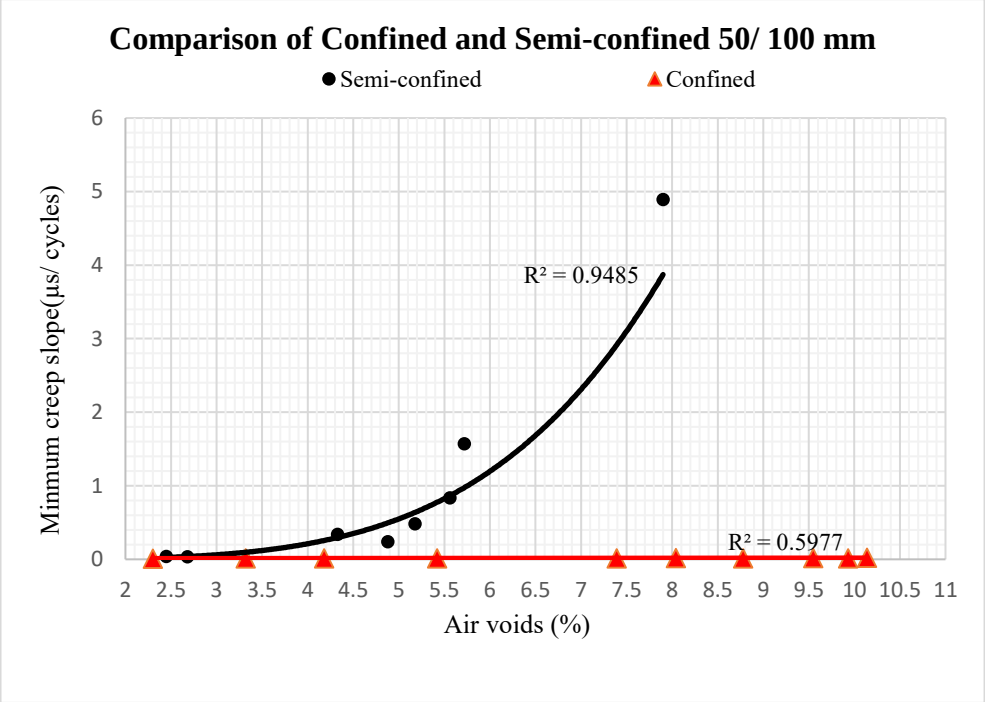

Figure: 6.40 Minimum creep slope comparison between SCDCT and CDCT test methods for 100mm specimen

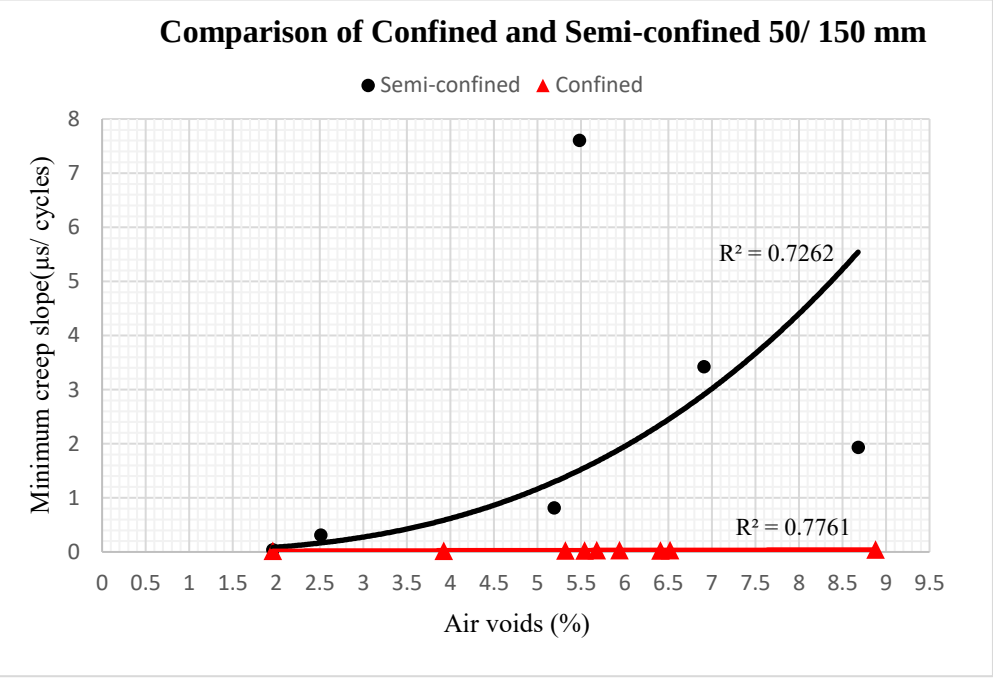

Figure: 6.41 Minimum creep slope comparison between SCDCT and CDCT test methods for 150mm specimen

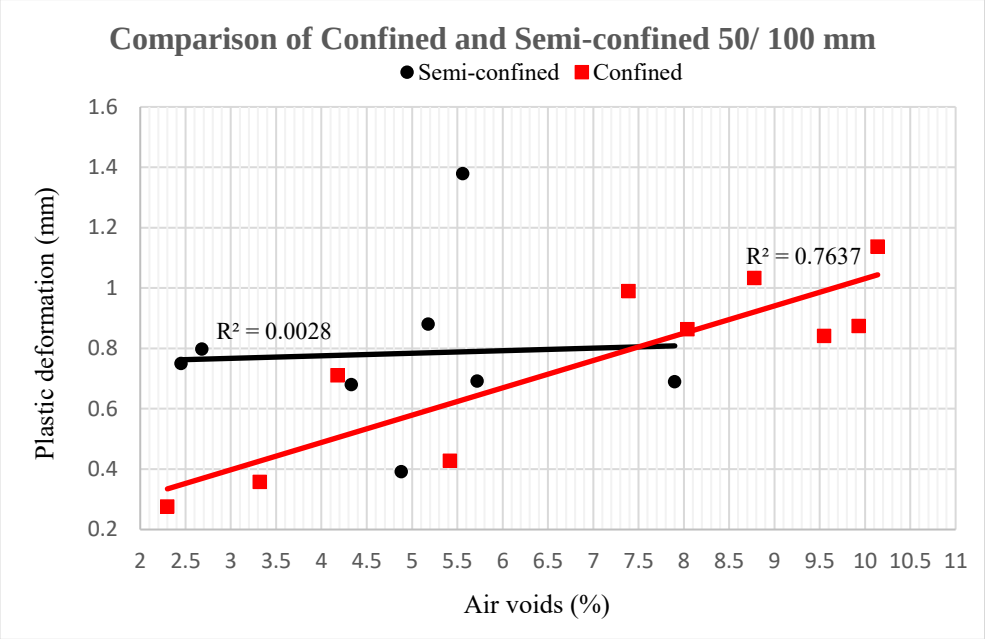

Figure: 6.42 Plastic deformation comparison between SCDCT and CDCT test methods for 100mm specimen

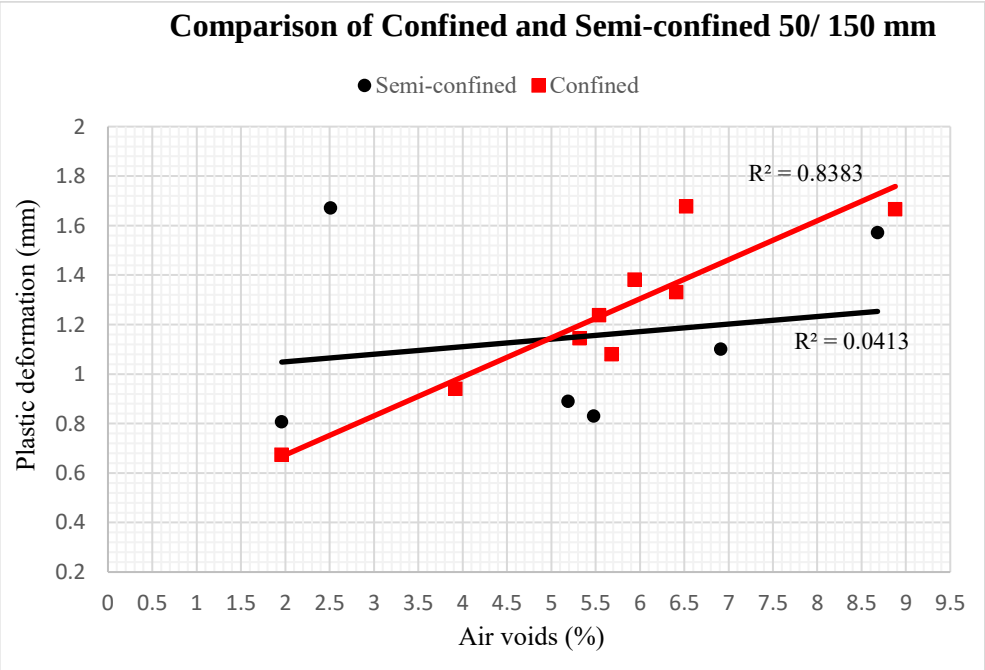

Figure: 6.43 Plastic deformation comparison between SCDCT and CDCT test methods for 150mm specimen

As discussed previously, the most important point concerning confined and semi-confined specimens was related to their failure patterns. In the semi-confined tests, cracks developed in the specimens during stage 2 creep, and continued until punching occurred. The confined specimens had a failure pattern more representative of observed field behaviour due to the realistic test procedure.

6.3.3 Effects of platen size

Various platen/ specimen configurations have been compared in this chapter to establish the effects of platen size and to permit selection of the most appropriate sample/ platen combination. Experimental results of three configurations namely; 50/ 100mm, 50/ 150mm, and 75/ 150mm have been compared in Figures 6.44 to 6.49.

Figures 6.44 and 6.45 compare 50/ 100mm and 50/ 150mm configurations when SCDCT multigrade specimens were tested. Minimum slope and plastic deformation for 50/ 150mm configuration was higher due to the thicker asphalt annulus around the specimen.

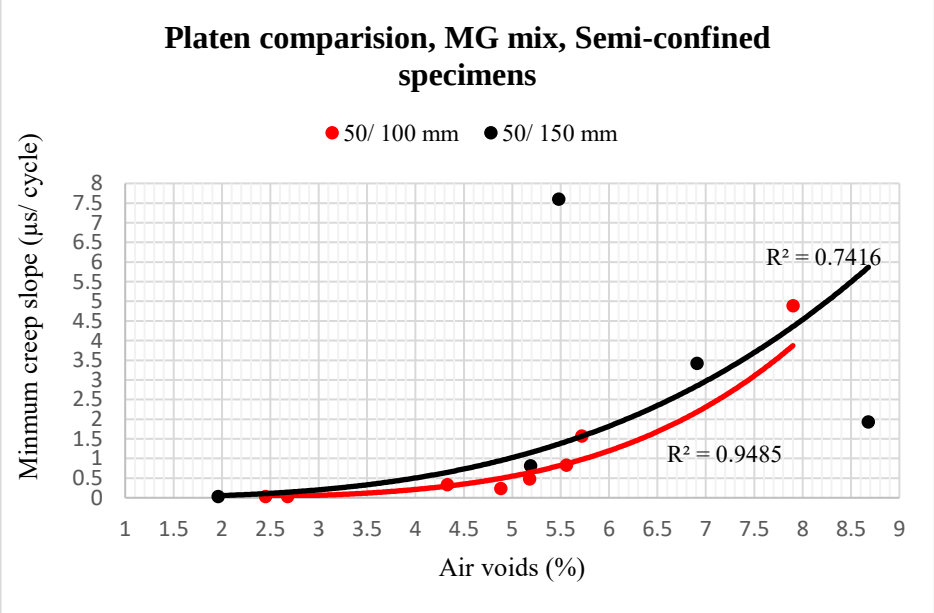

Figure: 6.44 Platen size comparison, SCDCT multigrade specimen

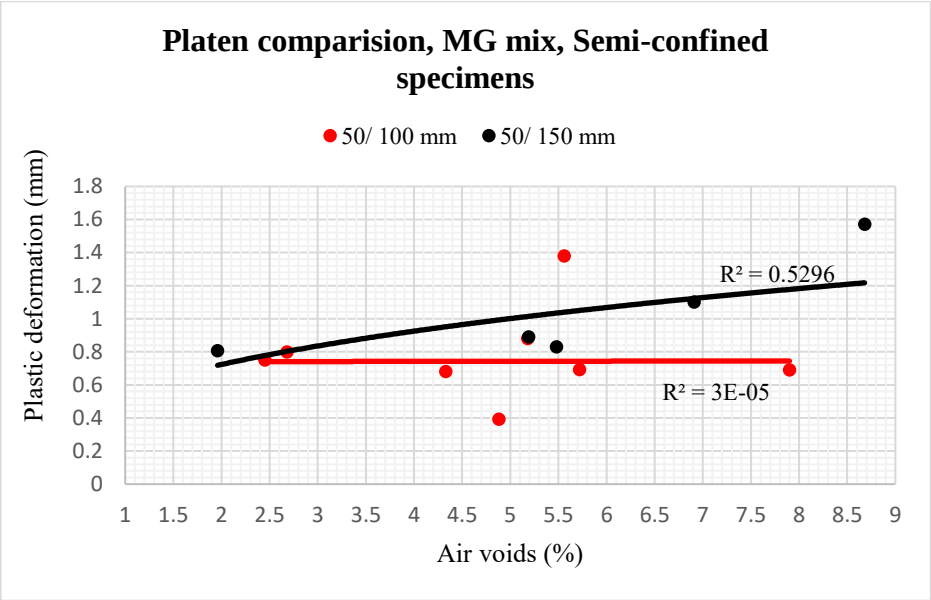

Figure: 6.45 Platen size comparison, SCDCT multigrade specimen

Comparison of 50/ 100mm, 50/ 150mm and 75/ 150mm platen/specimen configurations for confined multigrade specimen (with the 4 mm ring thickness) are provided in Figures 6.46 and 6.47. All configurations exhibited similar trends. The minimum slope increased when the thickness of the asphalt annulus around the specimens was increased (Figure 6.46). In each instance, plastic deformation shows an ascending trend for all configurations, however, Figure 6.47, has a lower plastic deformation for the, 50/ 100 mm configuration, while 75/ 150mm has a higher deformation than 50/150mm.

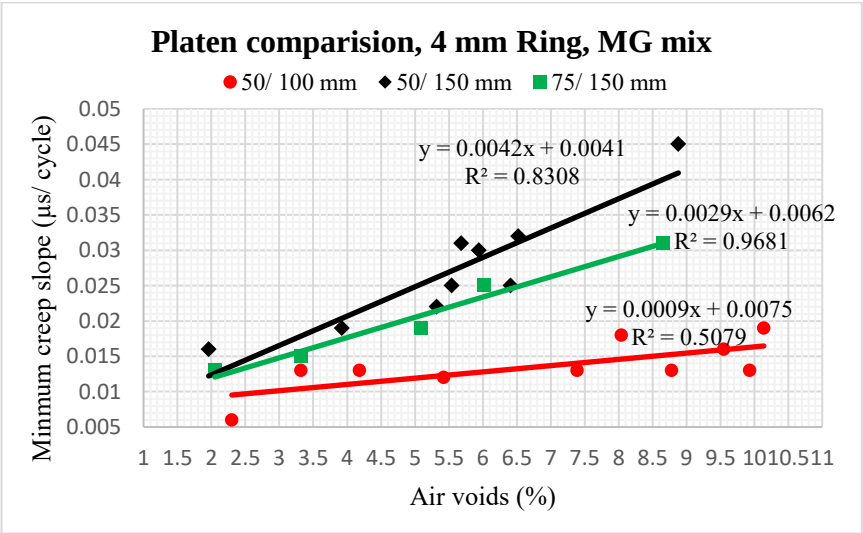

Figure: 6.46 Platen size comparison - CDCT (4mm) multigrade specimen

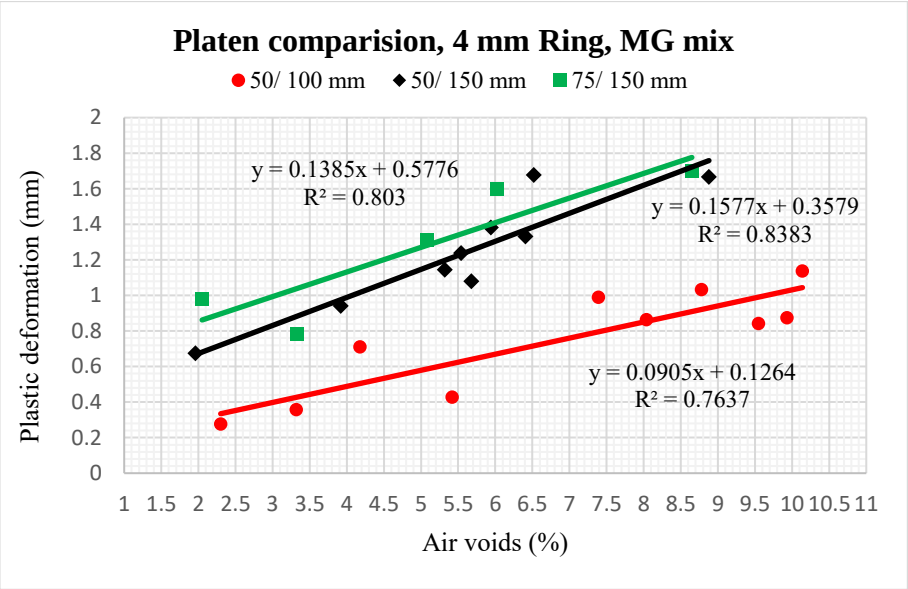

Figure: 6.47 Platen size comparison - CDCT (4mm) multigrade specimen

Various platen/ specimens configurations have been compared for the confined C170 mix (with a 2.5mm ring) as displayed in Figures 6.48 and 6.49. Both creep slope and plastic deformation exhibited similar trends. Creep slope and plastic deformation also increased by increasing the proportion of asphalt surrounding the specimens, as 50/ 150mm had the highest rate and 50/ 100 mm had the lowest level.

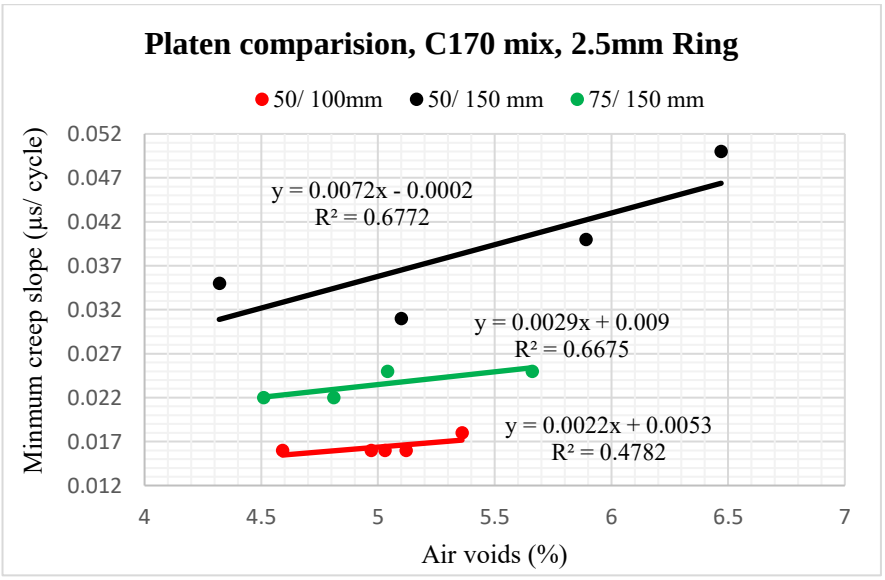

Figure: 6.48 Platen size comparison - CDCT (2.5mm) C170 specimen

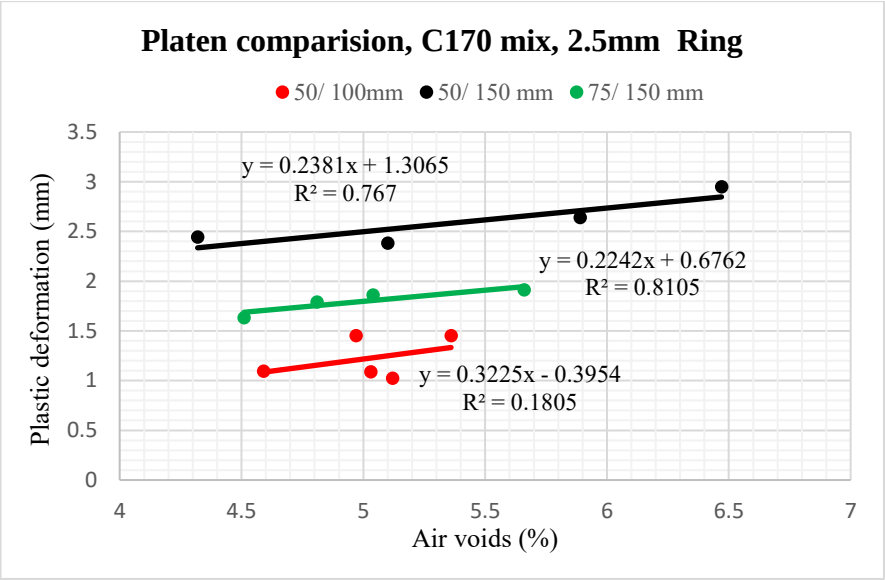

Figure: 6.49 Platen size comparison - CDCT (2.5mm) C170 specimen

It can be seen that data for all configurations have a similar trends. It is worth noting that the confinement conditions (thicknesses of asphalt annulus and PVC) and mix type did not appear to make any substantial differences to the performance of various platen/ specimens sizes. However, as the 75 mm platen can cover a greater range of asphalts (in regard to maximum aggregate size), the 75/150 mm configuration is the preferred option for the new test method.

6.3.4 Effects of the ring thickness

Laboratory test results of the CDCT test with 4mm and 2.5mm rings are presented in the Figures 6.50 and 6.51. As shown in the figures, both rings produced identical trends for minimum creep slope and plastic deformation. However, the graph for the 2.5mm ring possesses a higher slope probably attributed to it being a thinner ring, which in turn makes it more sensitive to deformation. It is worth noting that both rings have a similar slope up to 6% air voids content.

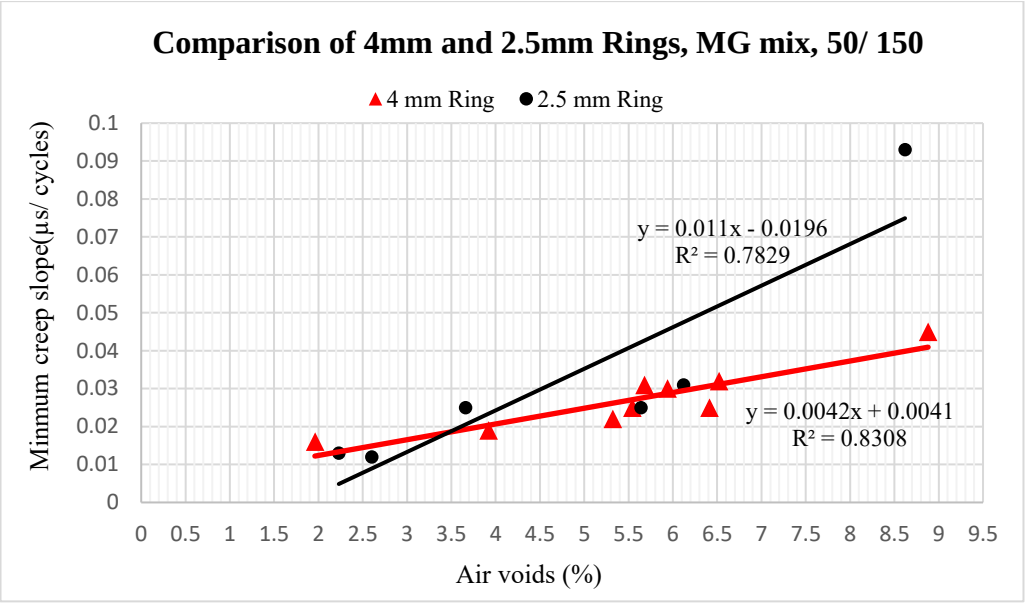

Figure: 6.50 Ring comparison of CDCT – minimum slope

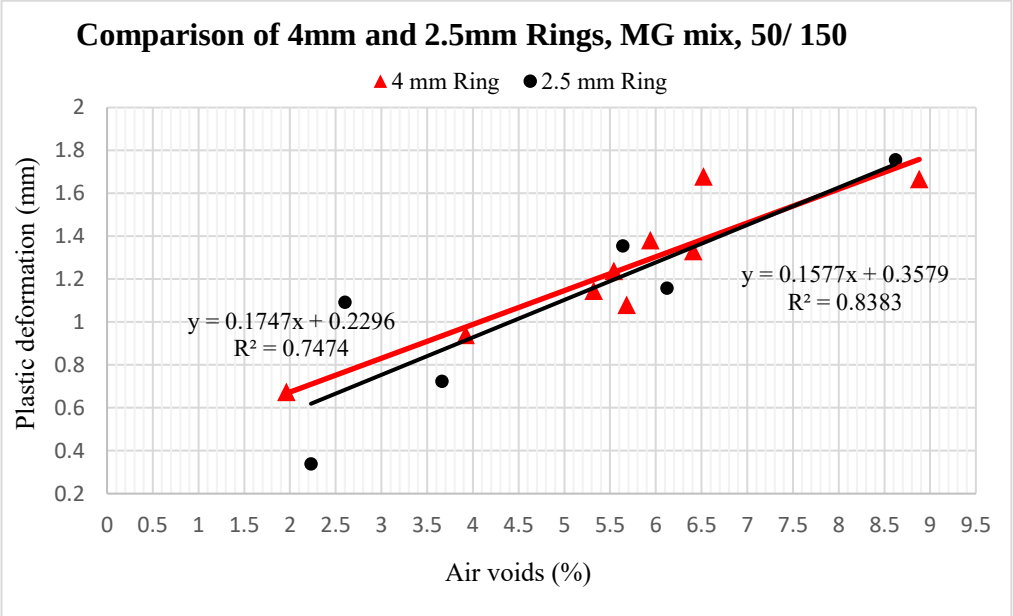

Figure: 6.51 Ring comparison of CDCT – plastic deformation

6.3.5 Mix classifying comparison by using different methods

Two mix types were evaluated using both the SCDCT and the CDCT to ascertain the ability of the refined test method to discriminate between asphalt mix types. The test outcomes are presented in the Figures 6.52, to 6.54. Figure 6.52, confirms that the obtained minimum creep slope for C170 was very much higher than the slope for the

multigrade mix, when the SCDCT method was used. The SCDCT method was not able to produce consistent plastic deformation results for the multigrade mix, but the results exhibited a reasonable correlation for the C170 mix. The results show the inability of the SCDCT method to produce acceptable results for classifying mixes.

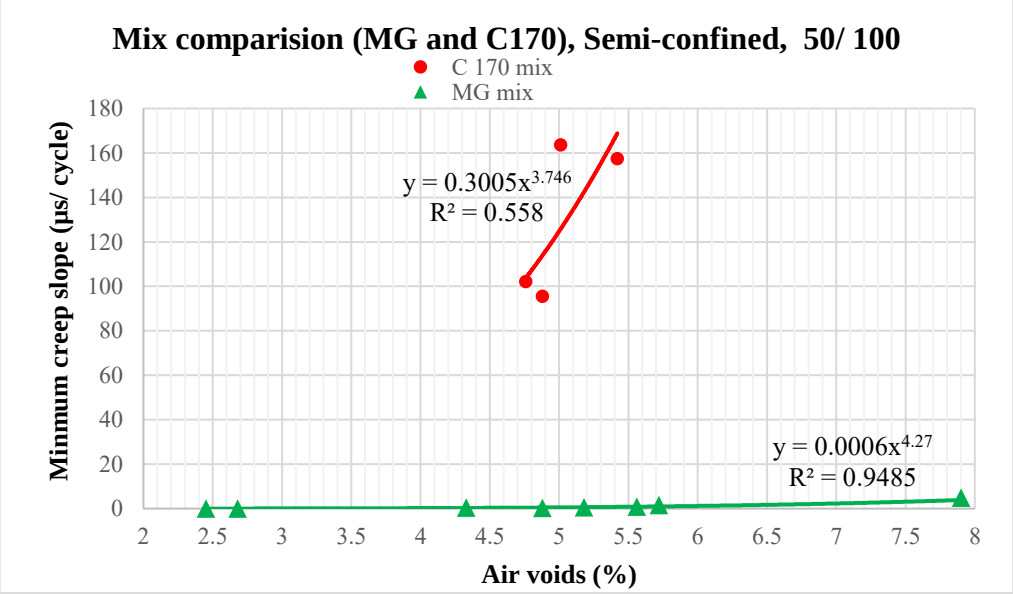

Figure: 6.52 Mix classifying by using SCDCT method – Minimum creep slop

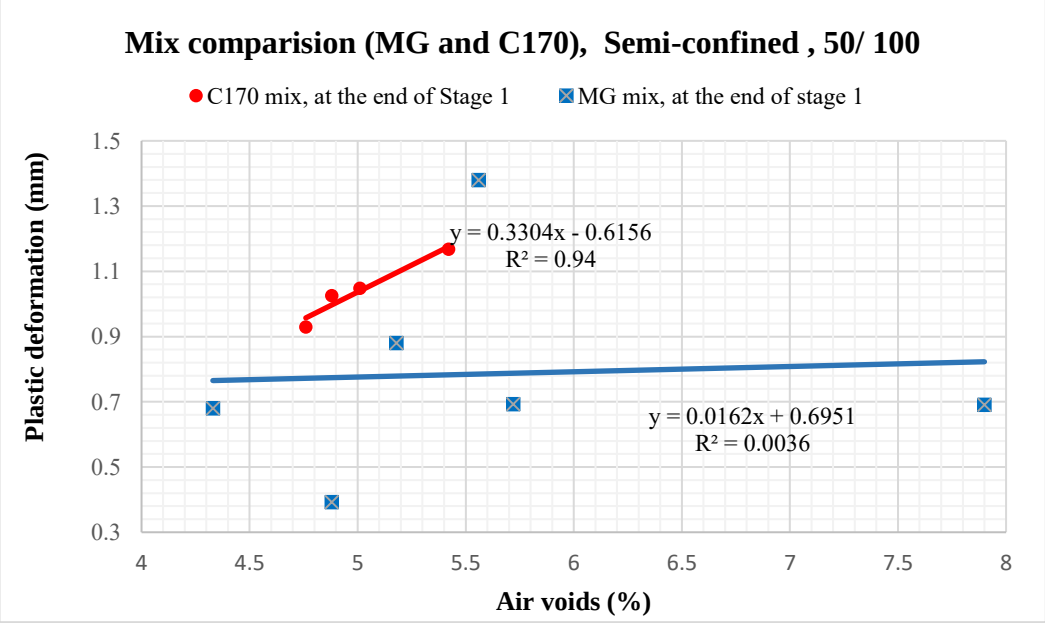

Figure: 6.53 Mix classifying by using SCDCT method – Plastic deformation

With reference to Figure 6.54, the confined testing method, yields trends and magnitudes for the minimum creep slopes for C170 and multigrade mixes that are almost the same when evaluated using the CDCT. The plastic deformation obtained for C170 was higher than for the Multigrade mix, and both exhibited good correlation with air voids. This demonstrates that using plastic deformation results from the CDCT provides a reasonable method for classifying mixes.

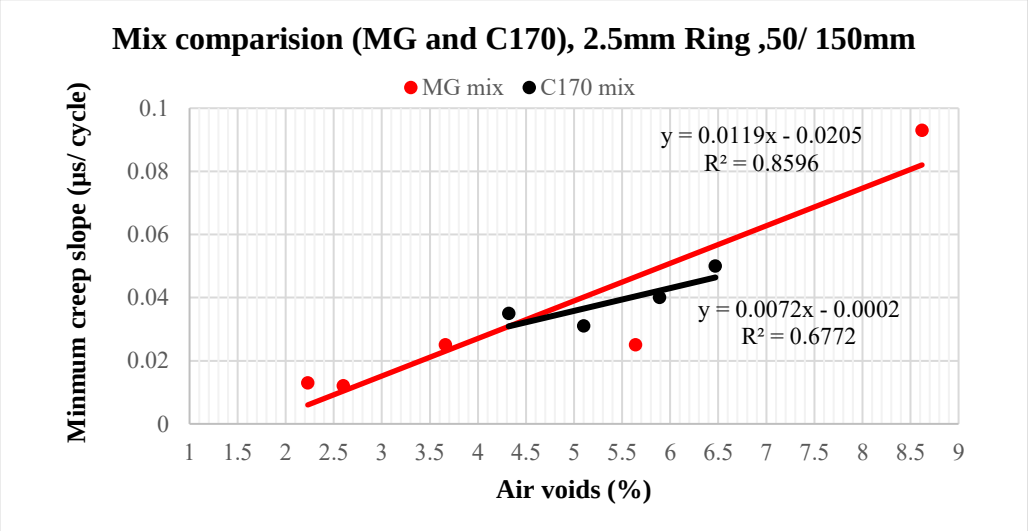

Figure: 6.54 Mix classifying by using CDCT method – Minimum creep slope

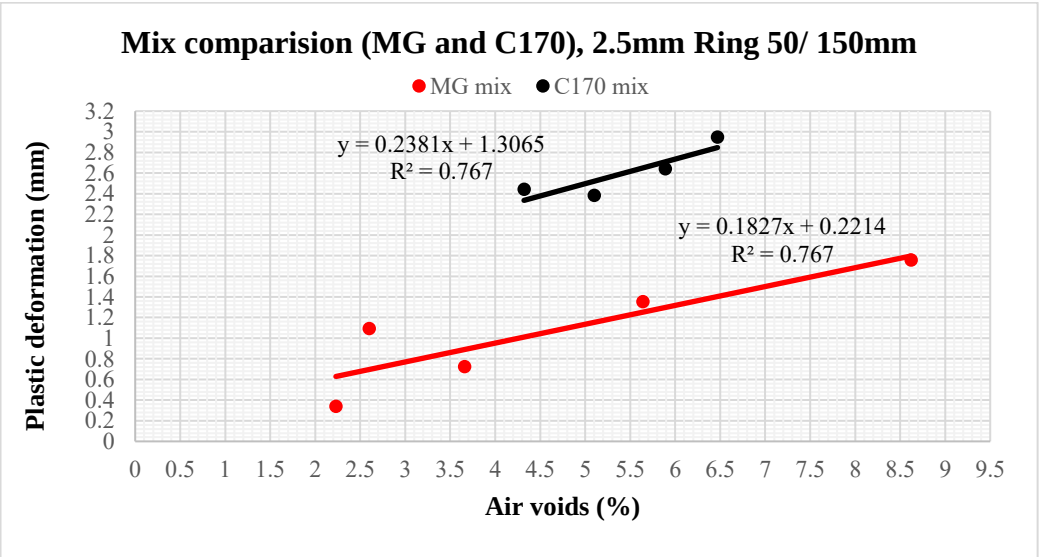

Figure: 6.55 Mix classifying by using CDCT method – Plastic deformation

6.3.6 Coefficient of determination (R^2) comparison for various test conditions

The results provided in this chapter summarise the broad range of comparative laboratory evaluations undertaken across variations in loading and confinement conditions. The data is summarised in the form of test criteria and regression coefficients (R^2) with varying air voids for creep slope (Table 6.12) and stage 1 plastic deformation (Table 6.13).

Table: 6.12 R^2 of the minimum creep slope curves

Test condition	Configuration	PVC thickness	Mix Type	R^2
SCDCT	50/ 100mm	-	multigrade	0.949
SCDCT	50/ 150mm	-	multigrade	0.726
SCDCT	50/ 100mm	-	C170	0.558
CDCT	50/ 150mm	4mm	multigrade	0.831
CDCT	50/ 100mm	4mm	multigrade	0.508
CDCT	75/ 150mm	4mm	multigrade	0.968
CDCT	50/ 150mm	2.5 mm	multigrade	0.783
CDCT	50/ 150mm	2.5 mm	C170	0.677
CDCT	50/ 100mm	2.5 mm	C170	0.478
CDCT	75/ 150mm	2.5 mm	C170	0.668
EDCT	100/ 100mm	-	multigrade	0.013
EDCT	150/ 150mm	-	multigrade	0.534

Table: 6.13 R^2 of the plastic deformation curves

Test condition	Configuration	PVC thickness	Mix Type	R^2
SCDCT	50/ 100mm	-	multigrade	3.00E-05
SCDCT	50/ 150mm	-	multigrade	0.041
SCDCT	50/ 100mm	-	C170	0.929
CDCT	50/ 150mm	4mm	multigrade	0.838
CDCT	50/ 100mm	4mm	multigrade	0.764
CDCT	75/ 150mm	4mm	multigrade	0.803
CDCT	50/ 150mm	2.5 mm	multigrade	0.747
CDCT	50/ 150mm	2.5 mm	C170	0.767
CDCT	50/ 100mm	2.5 mm	C170	0.181
CDCT	75/ 150mm	2.5 mm	C170	0.811
EDCT	100/ 100mm	-	multigrade	0.001
EDCT	150/ 150mm	-	multigrade	0.882

6.4 Summary

Three separate test methods for assessing dynamic creep were investigated to ensure development of an optimum test methodology. They were the existing Australian dynamic creep test (EDCT), semi-confined dynamic creep test (SCDCT), and confined dynamic creep test (CDCT). For each of these test methods various conditions such as different platen/ specimen sizes, different ring thickness, were investigated.

The test results for the EDCT were found to be inconclusive. As the specimens of the existing test method are unconfined, deformation of the specimen largely depended on the binder properties while the aggregate's role was minimised. Failure of test samples

was via bursting with no indication of tertiary creep. The characteristics of the EDCT suggest that it is not suitable for evaluating the creep potential of asphalt in the laboratory.

For the SCDCT, an annulus of asphalt was provided by using a platen size smaller than the sample diameter. The annulus provided some capacity for lateral stress transfer. However, as with the EDCT, the data obtained was inconclusive. The test results show the provided asphalt annulus was unable to provide adequate confinement to allow proper development of secondary creep. The main problems with SCDCT were related to specimen failure patterns. During tests cracking developed in the specimens followed by punching failure, which differs to the rutting mechanism of in-situ pavements. The results indicate that a single thin asphalt annulus does not significantly improve the current approach (i.e. EDCT), and provide a more realistic test.

Outcomes of the CDCT display potential to overcome the failings of other tests This test method provides much more consistent data in comparison with the other methods. Additionally, the designed confinement can appropriately control crack development and specimen punching. The CDCT can better duplicate real traffic loads, having a proper lateral pressure around the specimens, and providing a more realistic rutting mechanism in the laboratory. The 75mm platen on the 150mm specimen with 4mm PVC ring may be the best option for the CDCT.

As indicated at the start of the chapter, strain gauge data was obtained from a number of CDCT tests to evaluate hoop strain in the PVC confining ring. The success of the CDCT methodology as shown in this chapter now enables use of the strain gauge data in Chapter 7 to further validate the proposed approach.

CHAPTER 7

CORRELATIONS BETWEEN PAVEMENT SAMPLE MODELLING AND LABORATORY TEST

7.1 Introduction

The modelling outcomes provided in Chapter 5 have demonstrated a very good correlation between the redesigned confined creep test and in-situ asphalt pavement performance. The laboratory tests described in Chapter 6 also confirmed that the redesigned new creep test appears to be an appropriate method for evaluating permanent deformation of asphalt mixes. To obtain correlation between pavement models and laboratory test data it was necessary to initially model laboratory conditions and correlate the model generated stresses with measured laboratory stress/strain data. Stress conditions within the laboratory model were then correlated with a pavement model to provide a link between the laboratory data and modelled pavement performance. This chapter considers the modelling and laboratory relationships.

7.2 Stresses in the laboratory specimens and models

As described in Chapter 5 and Chapter 6, the ring stresses around the laboratory confined specimens were calculated using the hoop stain measured using strain gauges. As illustrated in the figure 7.1, two strain gauges were attached to the exterior of the PVC ring wall, at the middle height of the specimens (25 mm). Strain gauges were connected to a data logger that was set to record strain every 0.2 seconds (or 10 readings for each cycle). Stresses were measured for 50/100mm, and 50/150mm platen/specimen test configurations. The average stresses from the strain gauges were calculated. Figure 7.2 shows a record of strain for one of the new confined dynamic creep tests during the initial cycles.

Figure: 7.1 Confined dynamic creep sample with attached strain gauges

The measured stresses on the laboratory specimens aligned with the Z axis of the models. Therefore, the Z axis data has been used for studying modelling and laboratory test relationships. The locations of the strain gauges for the specimens are almost at the C-2 area of the models. Figure 7.3 represents a model of the new test designed for a 50/100mm (with 4mm ring) configuration, with Z axis stresses used for comparison.

7.3 Relationships of the laboratory and modelling outcomes

It was important to ascertain if the ring stresses generated in the confining PVC were of similar magnitude to those within an asphalt mass. The ring stresses for 50/100 mm and 50/150 mm test configurations were measured and compared to the stresses within the asphalt pavement model.

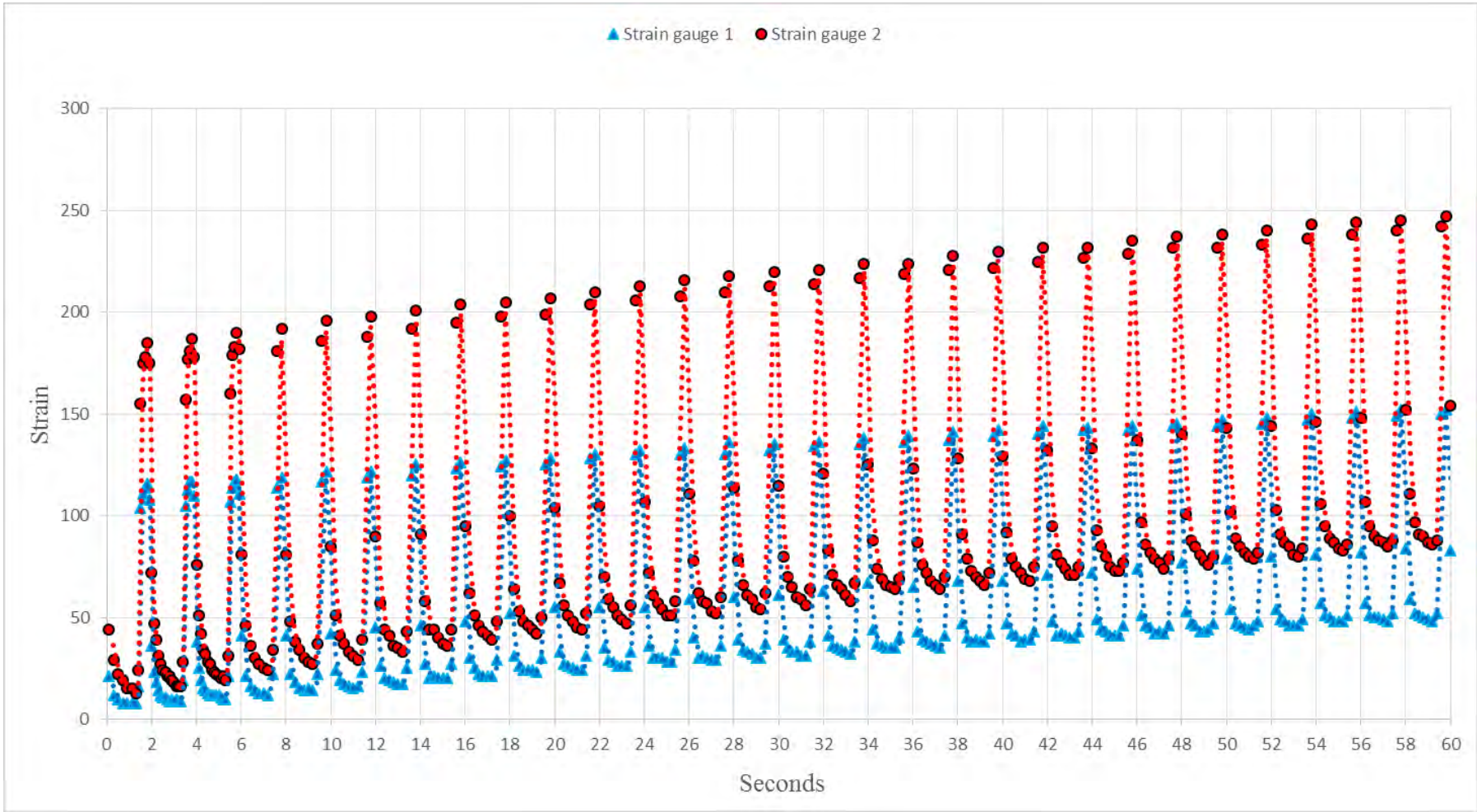

Figure: 7.2 Strain on the confined laboratory specimen measure by strain gauges

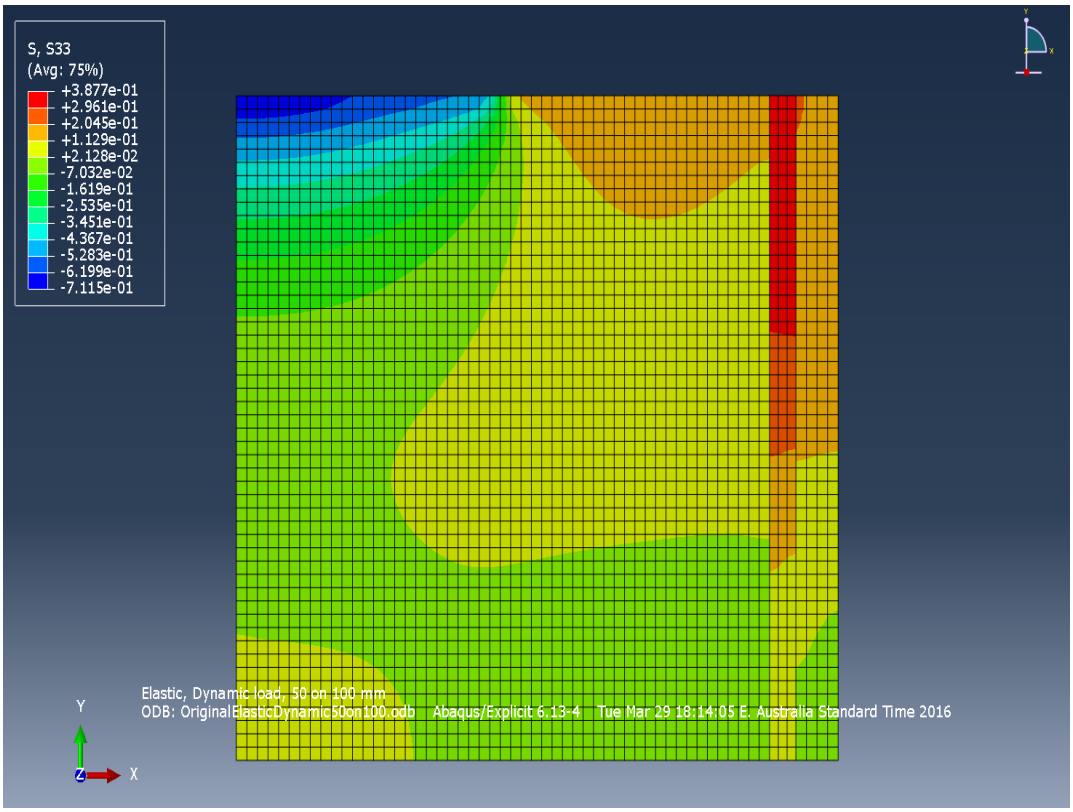

Figure: 7.3 New confined (4mm ring) test for 50/100 mm in the Z axis direction

The stress laboratory measurement utilising strain gauges showed a stress existed on the outer part of the PVC wall. The related model for the new designed creep test (50/100 mm configuration, with 4mm ring) confirmed that a 250 kPa stress existed on the outer part of the PVC ring. Table 7.1 records a summary of stresses for laboratory specimens and models. In the table, the measured stress is reasonably close to the model stresses. A lower stress was obtained for the 50/150mm configuration (with 4 mm ring) that reflects the different levels of stress generated by the different configuration.

A comparison was made between the stress provided by a theoretical stress analysis on the exterior part of the designed confined dynamic creep sample, and the ring stress for the laboratory confined dynamic creep test. This result shows acceptable agreement between the confined laboratory test and the FEM modelling. Similar good agreement was found between the confined laboratory dynamic creep test model results and in-situ pavement models (that were previously discussed in detail in chapter 5). It can

therefore be concluded that the new designed confined dynamic creep test has good potential for simulating in-situ pavement conditions. The existing unconfined creep test model did provide a closer match with the in-situ models, and it can be concluded that the new designed confined test provides a better approximation to in-situ pavement conditions than the existing unconfined test.

Table: 7.1 Calculated stress for model and laboratory specimens

Item	Stress (kPa)
Elastic dynamic model for 50/100mm new designed test	250
Laboratory test 50/100mm, 4mm ring	285
Laboratory test 50/150mm, 4mm ring	163

7.4 Summary

A comparison of stress levels produced in modelling and laboratory tests has been undertaken. Strain gauge data for calculating confining (hoop) stresses for CDCT samples was obtained as part of the laboratory tests described in Chapter 6. This allowed correlation with stress data at the corresponding locations for the model of the laboratory set up. In Chapter 5 the model of the CDCT test was shown to be correlated with models for an asphalt mass with similar stress distribution and magnitude existing.

This chapter provides further validation of the use of the CDCT as a tool for improved evaluation of creep potential of asphalt mixes under laboratory condition.

CHAPTER 8

DISCUSSION

8.1 Introduction

The previous chapters have reported the outcomes of the extensive laboratory experimental tests (Chapter 6) and finite element modelling (Chapters 5 and 7). In this chapter, an overarching discussion is provided on the outcomes. Some of the more significant modelling and laboratory outcomes have been reproduced in this chapter to enable effective contextual discussion. Testing and modelling outcomes have indicated that the new confined dynamic creep test is better able to address problems associated with the existing unconfined test method.

The chapter considers how data generated for the proposed CDCT methodology could be utilised to better rank asphalt mixes in the laboratory. This further assist in the confirmation of the research hypothesis outlined in Chapter 1. The chapter also considers the potential development of creep master curves, similar to those recently developed for estimating asphalt resilient modulus.

8.2 Modelling

Stress conditions in FEM models for the 100/100mm existing dynamic creep tests (EDCT), 50/100mm confined dynamic creep test (CDCT), and in-situ pavement models in the horizontal and vertical directions at geometrically similar locations, as shown in the figure 8.1, have been reproduced in figures 8.2 and 8.3. (Note that the grid points of the selected axes (A, B and C in vertical, and 1, 2, and 3 in the horizontal directions) have been used for comparing stresses in each model.)

The stresses produced in the models of the CDCT test show a good trend agreement with the stresses calculated for the in-situ pavement models. Similar stress levels and

trends were found for the in-situ and CDCT models. The asphalt annulus provides enough space for effective stress distribution, and the PVC ring provides an effective hoop stress for confining the asphalt specimens. The stress distribution in the EDCT specimen is very different to the field asphalt pavement models.

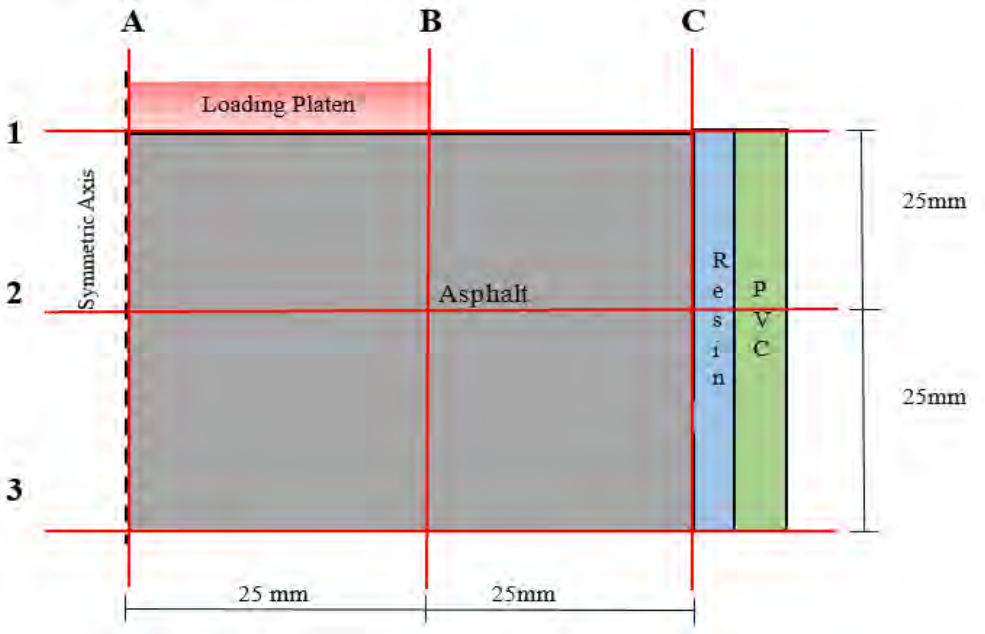

Figure: 8.1 Selected axes for checking stress distribution in the models

FEM deformation for the CDCT and EDCT models is presented in Figure 8.4 and 8.5. Models clearly indicate a rutting type mechanism for the CDCT test. Arrows show mix deformation directions. In the confined specimen (figure 8.5), the arrows' direction are downward under the platen and then gradually reversing and becoming upward in the asphalt annulus region. Modelling indicated the CDCT test is better able to duplicate the rutting mechanism of the asphalt pavement in the laboratory. A schematic of CDCT and EDCT deformation behaviours under platen loads is provided in the Figure 8.6.

In general, modelling indicates that the CDCT is more able than EDCT to duplicate in-situ asphalt conditions in the laboratory.

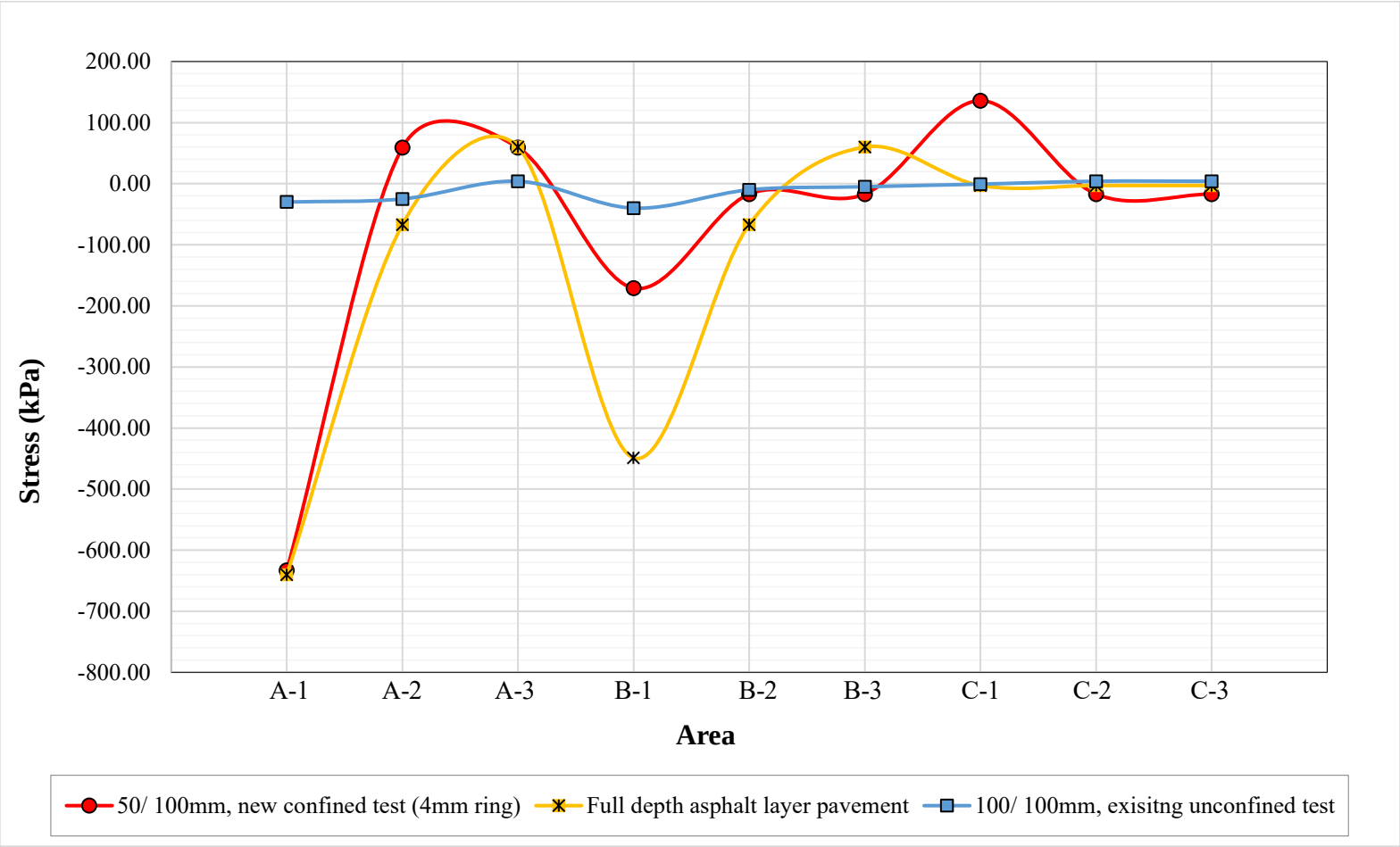

Figure: 8.2 Stress distribution in the various models – X (horizontal) direction

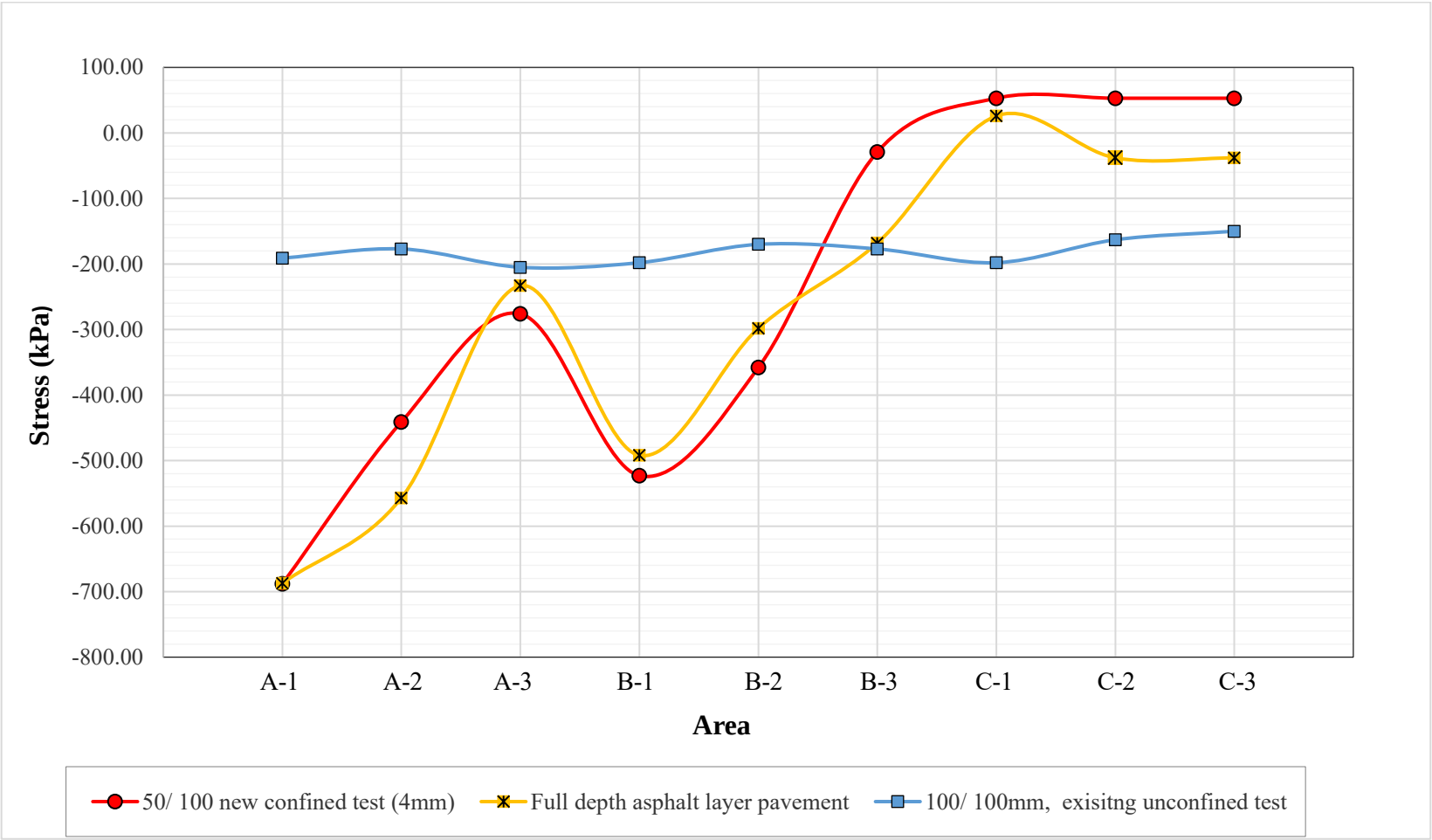

Figure: 8.3 Stress distribution in the various models – Y (vertical) direction

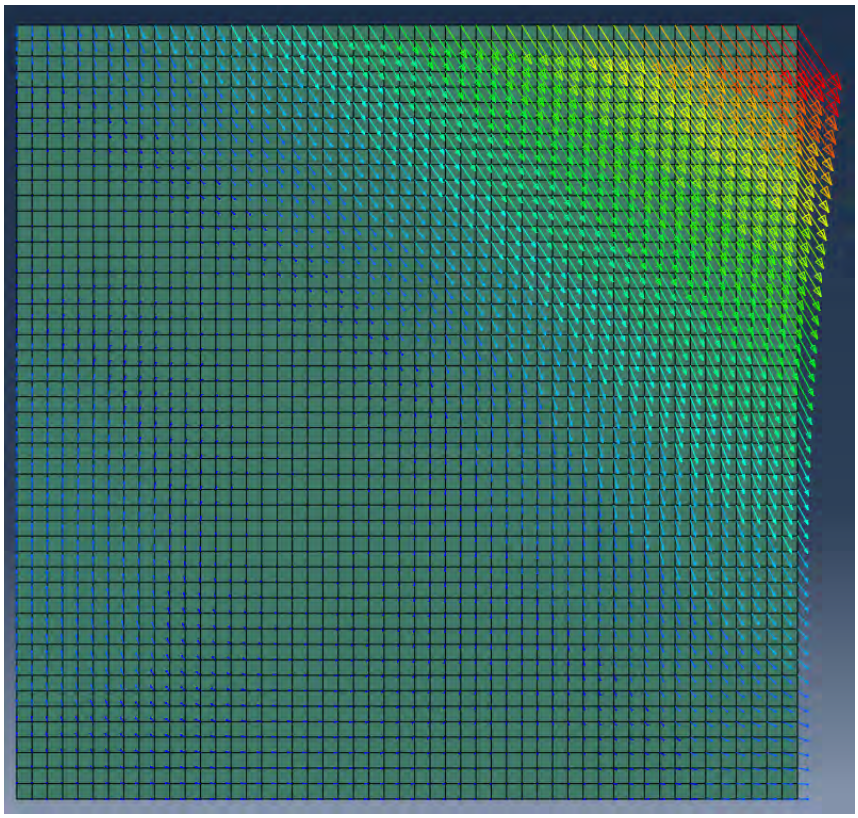

Figure: 8.4 FEM model of specimen deformation in the EDCT test (100/ 100mm)

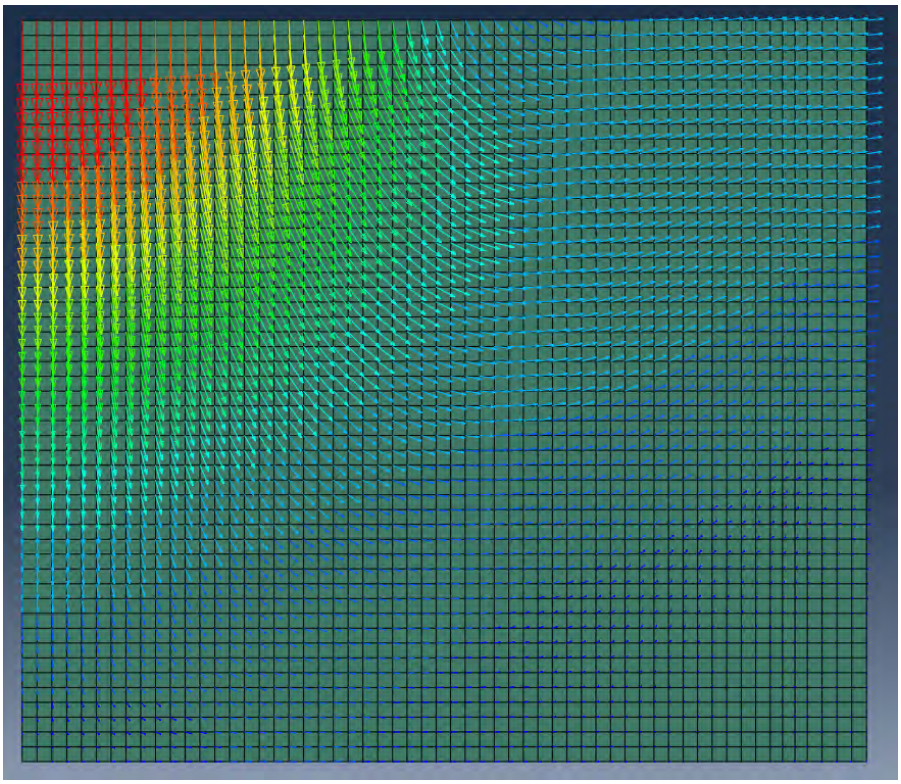

Figure: 8.5 FEM model of specimen deformation in the CDCT test (50/ 100mm)

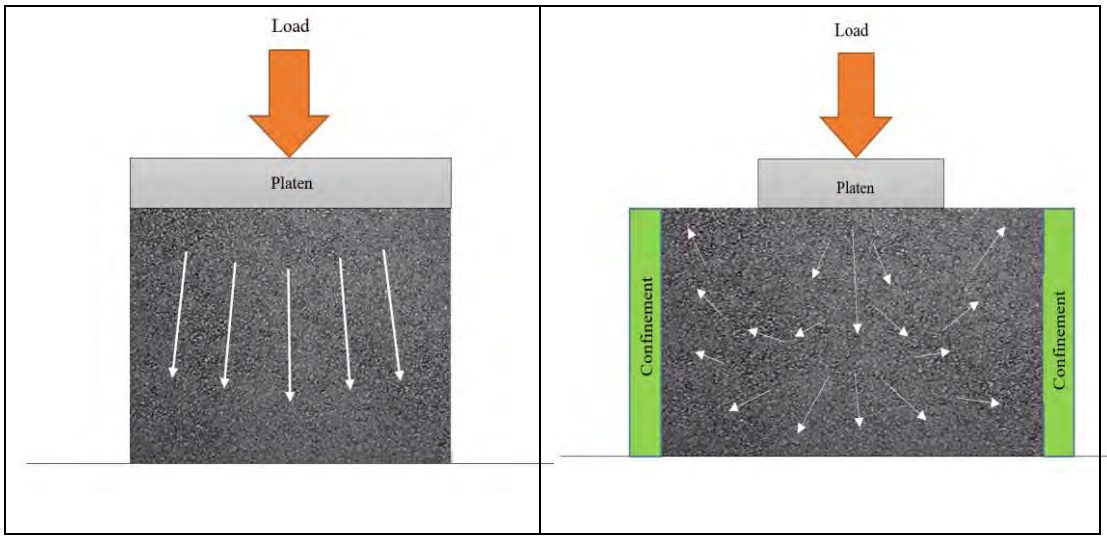

Figure: 8.6 Schematic of CDCT and EDCT specimen deformation behaviours under applied loads

8.3 Experimental

Figures 8.7 to 8.9 reproduce the minimum creep slope and plastic deformation curves for EDCT, CDCT, and semi-confined dynamic creep test (SCDCT) methods. As previously discussed in the chapter 6, the two significant parameters selected as indicators of creep potential were minimum stage 2 creep slope, and stage 1 plastic deformation.

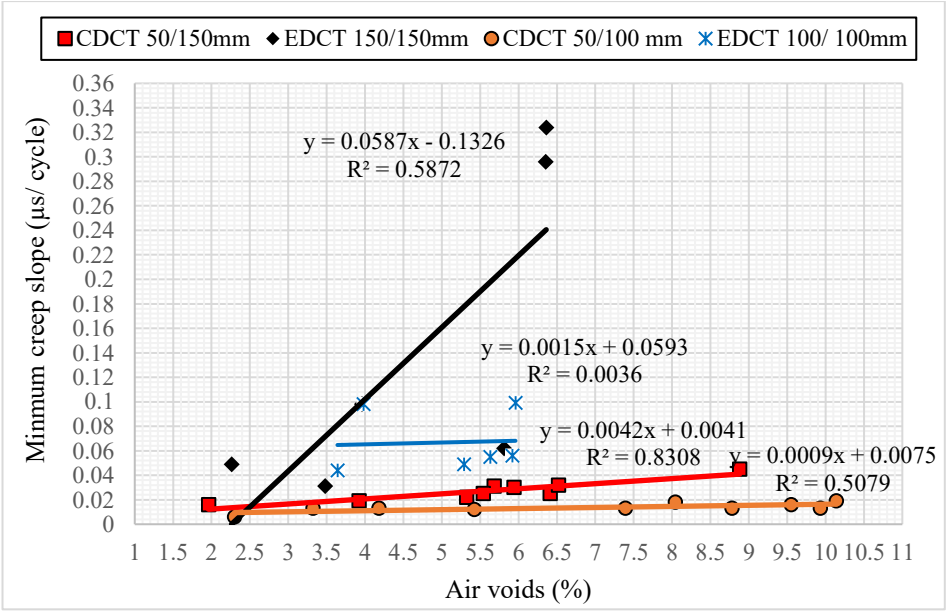

Figure: 8.7 Minimum creep slope for EDCT and CDCT test methods. (Note: 200 kPa pressure applied for EDCT, and 750 kPa for CDCT)

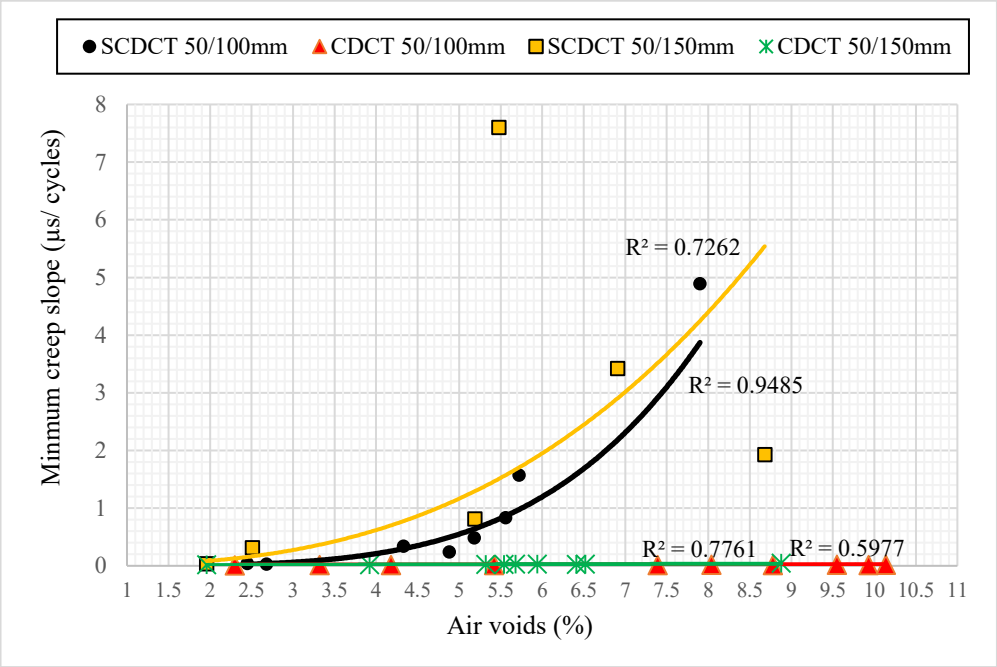

Figure: 8.8 Minimum creep slope for SCDCT and CDCT test methods

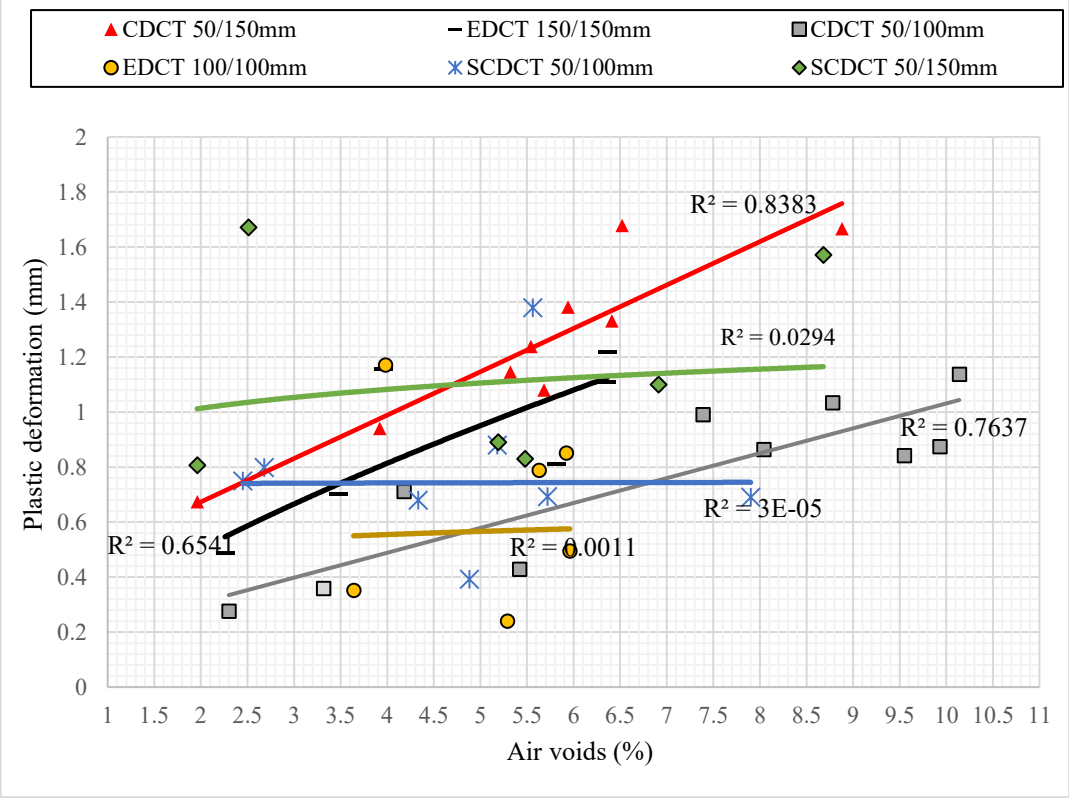

Figure: 8.9 Plastic deformation (stage 1) for EDCT, SCDCT and CDCT test methods

Table 8.1 reproduces regression data (R^2) of minimum creep slope and plastic deformation by EDCT, CDCT, and SCDCT methods. R^2 of the EDCT tests for 100/100mm are low with the test not demonstrating any reasonable trend of correlation between creep and air voids.

For the SCDCT tests, an annulus of asphalt was used to provide semi confinement and the specimens subjected to a 750 kPa pressure load. Test results indicated a short creep life for samples, even for multigrade mix specimens. As with EDCT, and SCDCT results for both multigrade and C170 mixes, both had very high minimum creep slopes (as provided in the figures 8.7 and 8.8). Such a short creep life and high creep slope are a product of the asphalt annulus providing an adequate lateral pressure thus supporting asphalt under real tyre pressures. During testing, numerous cracks developed in SCDCT specimens until punching failure occurred under the loading platen. Figure 8.10 is a representative sample of specimen failure patterns for various test methods. The failure mode of the SCDCT specimens did not reflect accumulation of plastic strain, and the failure mechanism differed to that with occurs with in -situ rutting. Such crack development and specimen punching were a result of tensile failure of the binder.

Both 50/100mm and 50/150mm SCDCT configurations showed similar trends. Minimum creep slope was significantly affected by changing mix types. C170 mix had a much higher (more than 100 times) minimum creep slope compared to that for the multigrade mix. However, plastic deformation existed over a similar range of deformation for different mixes. Overall, the SCDCT tests failed to yield reasonable correlation between creep performance and air voids.

Table: 8.1 R^2 of the minimum creep slope and plastic deformation curves of various test methods

Test method	Configuration	PVC thickness	Mix Type	R^2 of minimum creep slope curves	$R^2$of plastic deformation curves
EDCT	100/ 100mm	-	multigrade	0.013	0.001
EDCT	150/ 150mm	-	multigrade	0.534	0.882
SCDCT	50/ 100mm	-	multigrade	0.949	3.00E-05
SCDCT	50/ 150mm	-	multigrade	0.726	0.041
SCDCT	50/ 100mm	-	C170	0.558	0.929
CDCT	50/ 150mm	4mm	multigrade	0.803	0.838
CDCT	50/ 100mm	4mm	multigrade	0.508	0.764
CDCT	75/ 150mm	4mm	multigrade	0.968	0.803
CDCT	50/ 150mm	2.5mm	multigrade	0.783	0.747
CDCT	50/ 150mm	2.5mm	C170	0.677	0.767
CDCT	75/ 150mm	2.5mm	C170	0.668	0.811

The CDCT data demonstrated good correlation between both minimum creep slope and stage 1 plastic deformation, and air voids. The slight change in the confinement condition (from 4mm ring thickness to 2.5mm) did not produce any significant difference in the trends. A noteworthy comment about the CDCT method is related to its deformation mechanism. Analysing specimen failure patterns indicated the CDCT could change laboratory specimen deformation to a more realistic outcome. The arranged confinement for the specimens stops crack development, and also it prevents specimens bursting and punching, when high pressures were applied on specimens. The portion of the asphalt under the platen was pressed downward, and abutting asphalt responded with a sliding movement which created upheavals that are typical of densification and shear deformation mechanisms which occur in rutting.

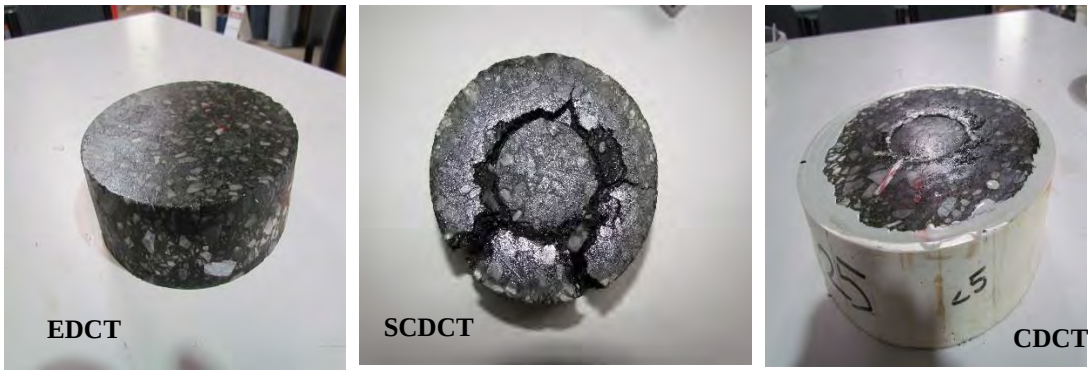

Figure: 8.10 Specimens' failure pattern for various test methods

8.4 Experimental and modelling connection

Experimental tests and modelling outcomes confirmed the potential of the new confined creep test. Both confirm that the CDCT method had a more realistic failure pattern that duplicates the rutting mechanism of in-situ asphalt pavement in the laboratory. A connection was established between modelling and laboratory work by measuring stress distribution on the exterior part of the confined specimens and comparing this with the models. The outcomes demonstrated that the stress on the external part of the confined specimens was similar to the level of stress in the corresponding laboratory FEM models. As there was a good agreement between stress distributions of the experimental tests and models of the CDCT on the one hand, and as established there is good agreement between CDCT and in-situ asphalt models

stress distributions on the other hand, it can be concluded that the new laboratory CDCT test delivers good agreement with in-situ asphalt behaviour with regard to stress distribution patterns.

8.5 The CDCT and reported issues with the EDCT

Numerous studies have been undertaken around the world to assess the efficiency of creep tests. The literature indicates some issues about the tests' ability to properly evaluate permanent deformation of asphalt.

Studies in Australia have indicated that the creep test data could not be matched with the field data (Butcher & Lindsell 1996). It has been found that the creep test could not consistently and properly rank mix performance (deformation performance) against mix composition (e.g. different aggregate gradation). Additionally, it has been shown that the creep test is more sensitive to air void variations (and consequently degree of compaction) than is the case for in-situ asphalt rutting. It was reported that the deformation resistance of the mixes on the creep test were mostly related to binder properties while frictional effects of aggregate became minimised (Oliver et al. 1995).

Researchers in other countries have reported further difficulties for other creep tests. For example, unconfined creep tests performed at low loads and temperatures cannot duplicate the field condition (real traffic load and temperature) due to specimen bursting (Brown & Foo 1994; Brown et al. 2001; Oscarsson 2007). Additionally, little relationship was found between unconfined creep test data with sample air voids, with the in-situ asphalt air voids, and with pavement rutting (Brown & Foo 1994). Furthermore, minimizing the aggregate interlock role for evaluating creep deformation has been reported as one of the main disadvantages of the unconfined test (Dołżycki & Judycki 2008; Taherkhania 2011). Some studies have reported that the creep test should not be considered as it was unable to simulate in-situ conditions and that test outcomes provided a low R^2 for test parameters (Brown et al. 2001).

Other studies of the creep test indicated that by providing an effective confinement it is possible to provide test conditions that better replicate the field (Brown et al. 2001; Brown et al. 2004; Oscarsson 2007; Dołżycki & Judycki 2008; Taherkhania 2011). Many attempts have been made to provide effective confining conditions for the creep test. Using a triaxial cell (figure 8.11) for the creep test is one of the most promising approaches for enhancing dynamic creep accuracy. However, as indicated by some studies (Huang & Zhang 2010), applying a constant confining pressure in the triaxial cell does not match reality as the in-situ asphalt confinement changes with traffic load, ambient temperature and asphalt mixture type. Additionally, suitable triaxial cell equipment installations are expensive, complex to operate and unavailable in most asphalt laboratories.

Figure: 8.11 Triaxial cell for creep test (Molenaar 2004)

The research reported here has demonstrated that a modified CDCT method can address most of the serious problems facing existing creep tests. It provides a test condition that duplicates in-situ conditions (applying both realistic traffic loads and high temperatures to the creep specimen). It avoids the issues mentioned by Brown et al (Oscarsson 2007) and other studies where sample bursting occurs with existing unconfined and semi-confined creep tests. By providing an effective confinement the modified CDCT method, provides a condition that allows recognition of internal

friction of aggregates (in addition to binder resistance to flow) for assessing plastic deformation of mixes. As previously mentioned, minimising the role of the aggregate skeleton contributes to the failure of existing creep tests to represent field situations. Additionally, the new confined test overcomes some problems encountered with the triaxial cell. In contrast to triaxial cell testing, the confinement provided by the asphalt annulus of the CDCT test varies with the applied load, temperature and mix condition thereby allowing better simulation of in-situ pavement conditions. The modified test provides effective confinement for samples with a simple operating and low-cost method while eliminating problems with using a complex triaxial cell. The new confined test can also model the rutting mechanism of the in-situ asphalt in the laboratory- a significant advantage of the modified test.

8.6 A new parameter for analysing permanent deformation

As outlined previously the current Australian dynamic creep test method uses minimum creep slope as the main parameter for the evaluation of creep test data. While the minimum creep slope of the secondary creep phase can be obtained in most cases under the current test criteria, this is not possible with a confined creep test unless load cycles exceeding 10^5 are employed. Analysis of the data generated in this research has shown that Stage 1 plastic deformation is a reliable parameter for interpreting creep test data.

The CDCT test data confirms that Stage 1 plastic deformation (which Stage1 creep moved to Stage2 creep) largely occurs in the range of 40,000 cycles for many cases of the tests as indicated in figure 8.12. It is interesting that the 40,000 cycles aligns with the current Australian dynamic creep test recommendation of using a maximum of 40,000 cycles for dynamic creep test. The data in figure 8.12 confirms the use of 40,000 cycles by comparing data from for the 75/150 mm CDCT test with a 4mm PVC ring for air voids between 2% and 8%. The data is for both plastic deformation at the end of Stage 1 and that at 40,000 cycles. It thus appears that plastic deformation at 40,000 cycles could be employed as a measure of asphalt creep potential using confined creep testing.

Table 8.2 Plastic deformation for multigrade 75/150 mm CDCT test with 4mm ring

		Plastic deformation at 40,000 cycles (mm)	Plastic deformation at 100,000 cycles (mm)	Extrapolation ratio 100,000/40,000	Plastic deformation at 1,000,000 cycles (mm)
Air voids (%)	2.05	0.96	1.02	1.063	1.69
	3.33	0.75	0.83	1.107	1.64
	5.09	1.29	1.39	1.078	2.28
	6.02	1.57	1.70	1.083	2.56
	8.65	1.65	1.83	1.109	3.64

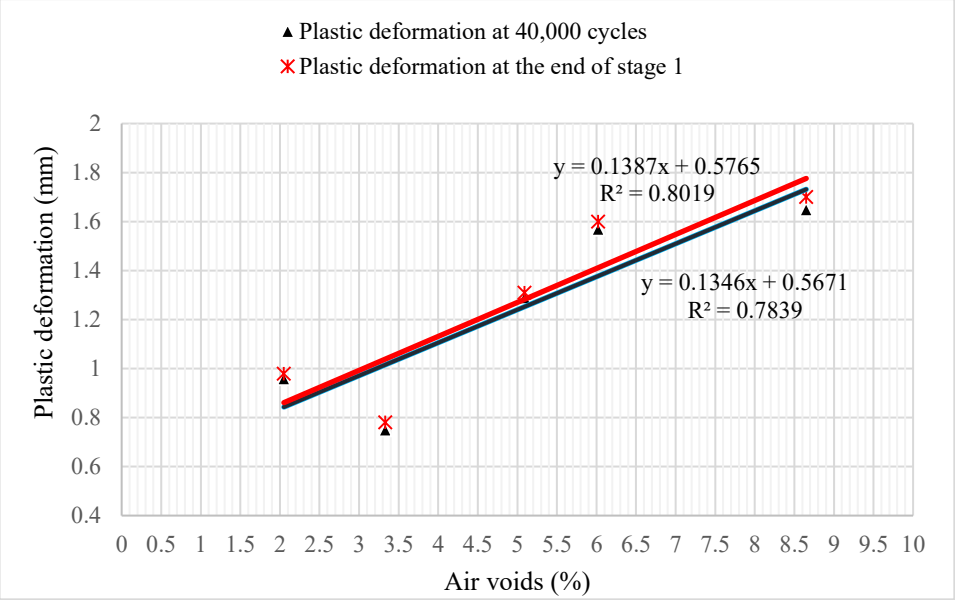

Figure 8.12 Plastic deformation at 40,000 cycles versus plastic deformation at the end of Stage 1

Test data for this research was obtained for samples up to 10^5 cycles, which allows the extrapolation of data to 10^6 as seen in table 8.2 and figure 8.13.

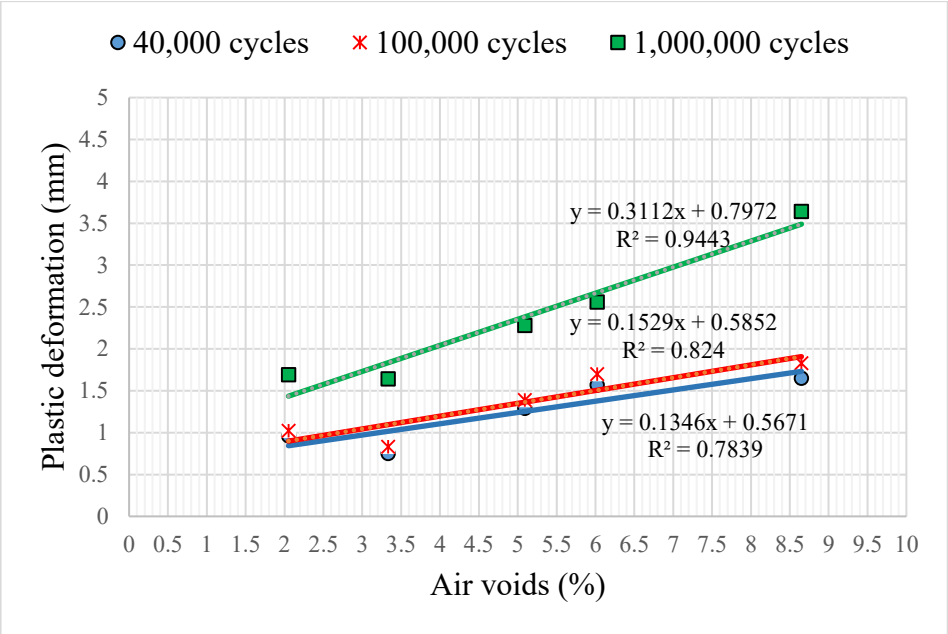

Figure 8.13 Plastic deformation for multigrade 75/150 mm CDCT test with 4mm ring, at various loading cycles

It is possible to hypothesis some new criteria for ranking mixes based on plastic deformation at 40,000 cycles as outlined in Table 8.3. The table assumes that C170 mixes are overall regarding as providing poor rutting resistance and is assigned the lowest, a Level 3 ranking. Similarly it is widely accepted that Multigrade provides a moderate level of rutting resistance and is assigned a Level 2 ranking. At 40,000 cycles and a midpoint value of 5% voids C170 has a plastic deformation of 1.85 mm and Multigrade a value of 1.29 mm.

Table 8.3 A criteria for ranking mixes according to their plastic deformation at 40,000 cycles and 5% voids for CDCT

Ranks	Mix deformation index	Rut depth at 40,000 cycles
Level 1	Rut-resistance mix	≤ 0.8 mm
Level 2	Medium rut-resistance mix	0.8mm < to > 1.6 mm
Level 3	Low rut-resistance mix	≥ 1.6 mm

It is also worth considering the use of a secant modulus for evaluating creep rate. It was noted that the secant modulus between 20,000 and 40,000 cycles approached the secant modulus from 40,000 to 10^5 cycles. The data in figure 8.14 for the secant creep slope between 20,000 and 40,000 cycles for the CDCT test data (75/150 mm with 4mm ring) suggest that the parameter is well able to discriminate between creep rates as a function of the different air voids. Thus applying a maximum value for strain rate/cycle may be useful means of augmenting the data in Table 8.3. For example a range from 0.06 to 0.12% maybe able to be applied for a Level 2 mix.

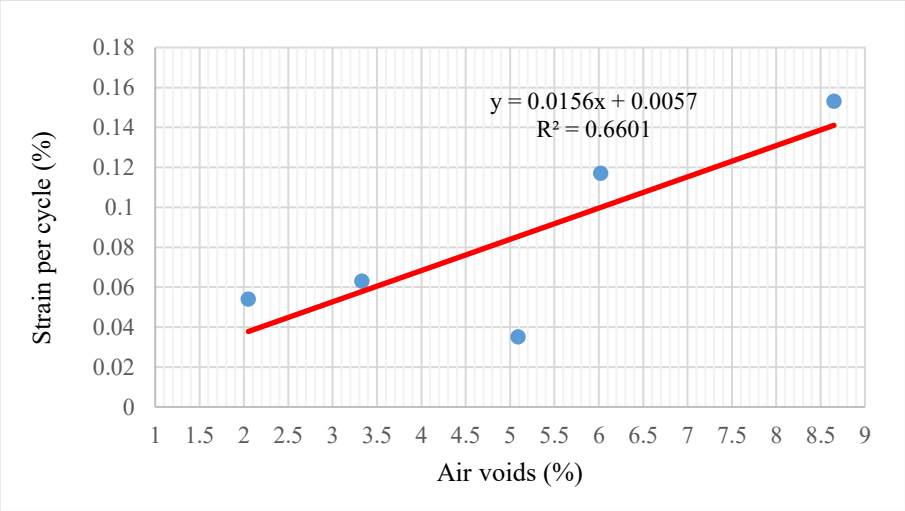

Figure 8.14 Creep slope (secant value) between 20,000 and 40,000 cycles

8.7 Recommended test procedure for the CDCT test

The criteria outlined in Table 8.4 is proposed as the basis for a new Australian dynamic creep test. The methodology addresses confinement arrangements, revised loading conditions and a platen/specimen configuration.

Table 8.4 Inputs for dynamic creep test

Parameter	Description
Compressive stress	750 kPa
Loading period	500 milliseconds (ms)
Pulse repetition period	2000 milliseconds (ms)
Test temperature	50^{o} C
Termination pulse count	40,000 cycles
Platen/ Specimen configuration	75mm/ 150mm
Ring	2.5mm thickness with 2.5 mm space between the PVC rings and samples
Gap filling material	Flowable Epoxy resin

8.8 Possibility of developing CDCT master curve

Recently, an extensive study was undertaken in Australia to develop master curves allowing the estimation of the modulus of asphalt at various vehicle speeds and ambient temperatures based on the dynamic modulus test (Sullivan 2015). This work was based on current international research. These master curves could improve the existing Australian asphalt design method. The master curve development process (see Figure 8.15) presents dynamic modulus outcomes of an ordinary mix as a function of frequency for four different test temperatures. It is believed that it is possible to provide some master curves based on the new confined creep test towards improving the evaluation of asphalt permanent deformation. Providing such master curves could help in enhancing permanent deformation design for asphaltic pavements. As an example, the existing mix design specification of BCC (Queensland) (BCC 2001, 2014) states a 2% to 5% air voids limit in the compacted mix for BCC Type 2 mix. However, use of the CDCT indicates that there is around 40% difference in plastic deformation of BCC Type 2 mix with a change from 2% to 5% air voids. A similar concern would occur for air voids of a compacted mix (or in field compaction) for all other BCC mix types, and also binder contents of mixes. Therefore, it is worthwhile developing effective master curves based on the creep test to make improvements in existing mix design specifications such as tightening the void content of compacted asphalt.

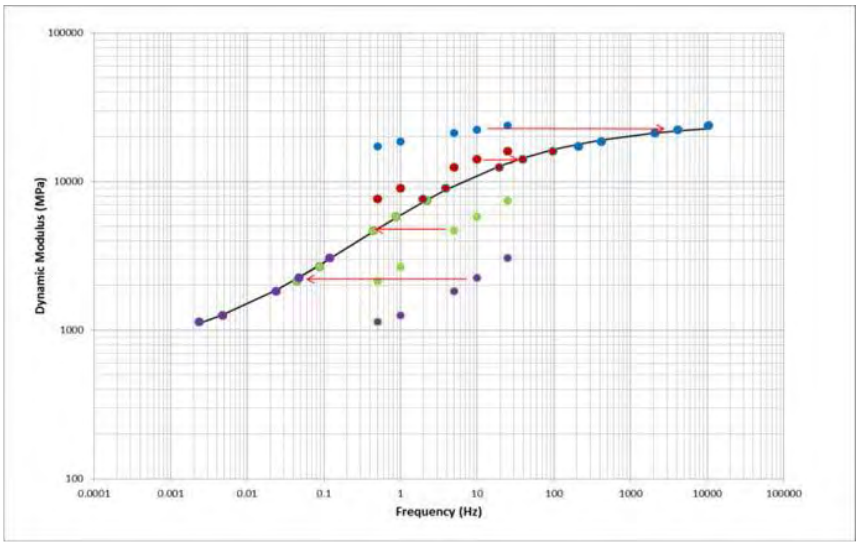

Figure: 8.15 Construction of Dynamic Modulus Master curve and Temperature Shift Factor Function (Sullivan 2015)

Generally, the CDCT test can potentially decrease problems with the existing dynamic creep test to the extent that creep testing would provide a good indication of likely permanent deformation of in-situ asphalt mixes. Existing UTS machines, (which are available in the most asphalt laboratories) or any other similar equipment without any changes or requiring additional attachments, can be used for performing such effective pulsed confinement for the new CDCT. The capacity to apply realistic truck tyre pressures and high temperatures on laboratory specimens, duplicating field rutting conditions, and providing effective confinement for the mix, are the significant outcomes from the research undertaken here to develop a new test methodology. It is concluded that the new creep test provides a superior approximation to field conditions and can significantly improve the existing dynamic creep test. The test is more practical for initial evaluation of the creep potential of asphalt mixes.

8.9 Summary

As outlined in Chapters 5 and 7, and discussed above the finite element modelling undertaken has indicated that the CDCT approach correlates well with modelled field conditions.

The extensive laboratory investigations outlined in Chapter 6 demonstrated that the CDCT approach could replicate realistic tyre pressure while providing a similar stress

distribution to that which exists within the field. The hoop stresses generated within the confining system were seen to be stress dependent as occurs within an asphalt mix in actual road pavement.

A new parameter (Plastic deformation at 40,000 cycles) is established for analysing creep deformation, which may possibly also be augmented by a secant creep slop from 20,000 to 40,000 cycles. A 2.5mm PVC confining ring and 75/150mm platen/sample configuration may be the overall most practical option for the CDCT test.

Outcomes of this study indicate that the CDCT will significantly improve laboratory evaluation of creep by reducing the current problems associated with the existing creep test. It is concluded that CDCT is a much-improved test method that is more representative of in-situ conditions and is capable of being a new test for the evaluation of permanent deformation potentials of asphaltic pavements.

CHAPTER 9

CONCLUSIONS AND RECOMMENDATIONS

The research undertaken has confirmed the hypothesis that; *"The existing Australian dynamic creep test can be redesigned to more accurately predict in-situ permanent deformation of asphalt".* This has occurred via an international literature review, extensive laboratory testing and relevant finite element modelling. The international literature review undertaken provided evidence that a better and cost-effective test methodology was essential if the creep potential of asphalt was to be evaluated in time-constrained laboratories.

Key outcomes of the research are a new Confined Dynamic Creep Test and the formulation of new test parameters for the ranking of asphalt mixes with respect to creep potential. The new parameters are plastic deformation at 40,000 cycles and the secant creep slope between 20,000 to 40,000 cycles. These key outcomes are discussed in more detail below.

9.1 The Confined Dynamic Creep Test (CDCT)

Previous research around various confinement systems was extrapolated to develop a new and innovative approach where a combination of an asphalt annulus, PVC ring and epoxy infill provided a stress responsive confinement. The new test methodology, which has been denoted as the CDCT removes the need for complex and expensive repeat load triaxial apparatus, is cost effective and provides a stress responsive test environment.

Stress conditions within the CDCT can be varied are required via modification of ring thickness to ensure that the confining system is able to duplicate the stress distributions with the asphalt material being evaluated.

9.2 Finite element modelling

Finite element modelling (FEM) undertaken was able to validate that the stress conditions within the CDCT were similar to those within models of asphalt pavement structures that are commonly used by pavement designers.

The FEM was also able to demonstrate that the stresses obtained in the models were similar with those stresses measured in the laboratory at geometrically similar positions. The modelling was able to provide a link between the CDCT stress conditions and those within an asphalt road pavement.

9.3 Air voids and creep potential

CDCT results demonstrated that creep potential increased as a function of voids in a compacted asphalt mix. This has significant application to asphalt mix compaction specification that are formulated by road owners. The research has shown for example that an increase in compacted air voids from 2% to 5% can result in a 40% increase in plastic deformation.

A consequence of the research outcomes could be that road owners may consider tighter specifications around compacted void limits. This would reduce the both the level of stage 1 plastic deformation and longer term stage 2 creep.

9.4 Plastic deformation and secant modulus

The interrogation of CDCT test results revealed that creep potential could be better estimated by applying a realistic tyre pressure of 750 kPa and the use of two new test parameters. This would replace the current 200 kPa and significantly improve on the current “secondary creep slope” approach for ranking asphalt mixes with respect to creep potential.

The first parameter is the level of plastic strain at 40,000 cycles. This ranks asphalt mixes with regard to stage 1 plastic deformation, which occurs during the early life of the road pavement as the aggregate skeleton realigns and voids are reduced. The second parameter is the secant modulus between 20,000 and 40,000 cycles that ranks the asphalt mixes with regard to stage 2 creep. This parameter is similar to the current Australian Standards test that uses the minimum slope of the secondary creep curve, but further develops that approach for use with confined asphalt sample

9.5 Extrapolating test data

The research shows that the secant modulus creep slope between 20,000 and 40,000 cycles approached that of steady state creep at 100,000 cycles. Extrapolation of the secant modulus creep slope to design equivalent standard axels has the potential to estimate long life creep performance of asphalt mixes.

While this approach was explored in the research and seen to have good potential it was not intimately linked to the original research hypothesis and will be further discussed as a recommendation for future research.

9.6 A revised Australian standard

The research has concluded that the current Australian Standard would benefit from the following modifications:

- An increase in cyclic stress from 200 kPa to 750 kPa to better replicate current tyre pressure that are typically in the range of 500 to 1000 kPa.
- The use of a stress responsive confining system that enables the development of stress distributions within laboratory samples similar to those expected in the field. The PVC-epoxy system developed within the research satisfies those requirements.
- The use of a reduced size top test platen that enables a surrounding asphalt annulus to exist and allow lateral stress transfer within the asphalt. The research

outcomes recommends a 75mm platen on a 150mm sample to fulfil this requirement.

- The use of two new test parameters to rank asphalt mixes in the laboratory. These are plastic deformation at 40,000 cycles and the secant modulus of the creep curve between 20,000 and 40,000 cycles. The use of the current test parameter of "secondary creep slope" may be retained but is considered non-essential.

9.7 Recommendations for future research

This study has developed a new methodology for evaluating asphalt creep deformation based on the modification of the current Australian test method. The research has uncovered more areas for future exploration and some recommendations for future research are outlined below:

- The current research maintained a constant mix aggregate grading with material compacted to specific voids. The effects of variation in grading might be investigated.

- The FEM models developed in the current research were correlated to laboratory test through indirect modelling and strain gauging. Future data acquisition from stress monitoring in actual pavements would enable enhanced correlations to be obtained.

- The use of extrapolation of creep data at early stages within the secondary creep life should be further explored. While the research undertaken here was able to show that the secant modulus between 20,000 and 40,000 cycles could approximate longer term secondary creep the use of mathematical models to better predict creep life should be explored. The models could be based on the shape of the creep curve as it transforms from stage 1 creep into the more extensive stage 2.

REFERENCES CITED

AASHTO 2003, 'T321-03', Determining the fatigue life of compacted Hot-Mix Asphalt (HMA) subjected to repeated flexural bending.

Abaqus-6.13 2013, Getting Started with Abaqus: Interactive Edition, Manual.

Abbas, AR 2004, Simulation of the micromechanical behavior of asphalt mixtures using the discrete element method, Washington State University.

Abdelaziz, M 2008, 'Properties and performance of stone mastic asphalt reinforced with glass fibers', University of malaya (UM), Malaysia.

Abdulshafi, AA 1983, 'Viscoelastic/plastic characterization, rutting and fatigue of flexible pavements', Ohio State University, USA.

Ahmadinia, E 2012, 'Using waste plastic bottles as additive for stone mastic asphalt', University of Malaya (UM) Malaysia.

Aksoy, A & Iskender, E 2008, 'Creep in conventional and modified asphalt mixtures', Proceedings of the Institution of Civil Engineers: Transport, vol. 161, no. 4, pp. 185-95.

Al-Qadi, I, Wang, H & Tutumluer, E 2010, 'Dynamic analysis of thin asphalt pavements by using cross-anisotropic stress-dependent properties for granular layer', Transportation Research Record: Journal of the Transportation Research Board, no. 2154, pp. 156-63.

Al-Rousan, TM 2016, 'Flexible pavement thickness design / Asphalt Institute Method', viewed 2016,<http://www.docfoc.com/flexible-pavement-thickness-design-asphalt-institute-method-source-chapter>.

Alderson, A & Hubner, D 2008, Testing asphalt in accordance with the Austroads mix design procedures, Austroads, Sydney.

Alderson, A & Hubner, D 2008, Testing asphalt in accordance with the Austroads mix design procedures, Austroads technical report, TT 1353, AP-T100/08, Austroads, Australia.

AS-1348.1 1986, Road and traffic engineering—Glossary of terms. Part 1: Road design and construction, Australian Standard, Australia.

AS-2891.7.1 2004, Methods of sampling and testing asphalt - Determination of maximum density of asphalt - Water displacement method, Australian Standard, Australia.

AS-2891.8 2005 Methods of sampling and testing asphalt - Voids and density relationships for compacted asphalt mixes, Australian Standard, Australia.

AS-2891.9.2 2005, Methods of sampling and testing asphalt - Determination of bulk density of compacted asphalt - Presaturation method, Australian Standard, Australia.

AS-2891.12.1 1995, Methods of sampling and testing asphalt - Determination of the permanent compressive strain characteristics of asphalt - Dynamic creep test, Australian Standard, Australia.

Asphalt-Institute 2015, The Bitumen Industary-A global perspective Third edn, USA.

Austroads 2012, Guide to Pavement Technology. Part 2: Pavement Structural Design, Sydney.

Austroads 2013, Air voids in asphalt, Pavement work tips, Austroads in conjunction with AAPA, Australia.

Bai, F, Yang, X, Yin, A & Zeng, G 2014, 'Modified Cross model for predicting long-term creep behavior of sand asphalt', Construction and Building Materials, vol. 65, pp. 43-50.

BCC 2001, Urban Management Division Reference Specifications for Civil Engineering Work S310 Supply of Dense Graded Asphalt, Brisbane City Council, Australia.

BCC 2014, Brisbane City Council Reference Specifications for Civil Engineering Work S310 Supply of Dense Graded Asphalt, Brisbane City Council, Australia.

Behiry, AEAE-M 2012, 'Fatigue and rutting lives in flexible pavement', Ain Shams Engineering Journal, vol. 3, no. 4, pp. 367-74.

Bohagr, AA 2013, 'Finite element modeling of geosynthetic reinforced pavement subgrades', Washington state university, USA.

Brown, ER & Foo, Y, K. 1994, 'Comparison of unconfined and confined creep tests for hot mix asphalt', Journal of materials in civil engineering, vol. 6, no. 2, p. 20.

Brown, ER, Kandhal, PS & Zhang, J 2001, Performance testing for hot mix asphalt, NCAT Report 01-05, National Center for Asphalt Technology Alabama, USA.

Brown, ER, Hainin, MR, Cooley, A & Hurley, G 2004, Relationship of Air Voids,Lift Thickness, and Permeability in Hot Mix Asphalt Pavements, Report 531, NCHRP, Washington, D.C.

BS-DD-185 1990, 'Method for determination of creep stiffness of bitumen aggregate mixtures subject to unconfined uniaxial loading'.

BS-EN12697-25 2005, Bituminous mixtures. Test methods for hot mix asphalt. Cyclic compression test.

Building-Science 2016, 'Asphalt pavement evaluation', viewed 2016,<http://www.torontoinspection.ca/building-science/>.

Bullen, F & Preston, N 1992, 'Extending the use of the Nottingham Asphalt Tester', in ISAP 7th International Conference on Asphalt Pavements : Design, Construction and Performance: Proceedings of the ISAP 7th International Conference on Asphalt Pavements : Design, Construction and Performance pp. 35-44.

Butcher, M & Lindsell, J 1996, Creep properties of asphalt, MTRD report No. 33-1, Department of Transport , Materials technology section, Walkley Heights, Australia.

Cai, W 2013, 'Discrete element modelling of constant strain rate and creep tests on a graded asphalt mixture', University of Nottingham, UK.

Carpenter, SH & Jansen, M 1997, 'Fatigue behavior under new aircraft loading conditions', in Aircraft/Pavement Technology In The Midst Of Change, pp. 259-71, <http://worldcat.org/isbn/0784402868>.

Carvalho, RL 2012, 'Prediction of permanent deformation in asphalt concrete', University of Maryland, Maryland, USA.

Chatti, K, Salama, H & El Mohtar, C 2004, 'Effect of heavy trucks with large axle groups on asphalt pavement damage', in Proc., 8th Int. Symp. on Heavy Vehicle Weights and Dimensions.

Chiangmai, CN 2010, 'Fatigue-fracture relation on asphalt concrete mixtures', University of Illinois at Urbana-Champaign.

Choi, Y-T 2013, 'Development of a mechanistic prediction model and test protocol for the permanent deformation of asphalt concrete', North Carolina State University.

Doh, YS, Yun, KK, Amirkhanian, SN & Kim, KW 2007, 'Framework for developing a static strength test for measuring deformation resistance of asphalt concrete mixtures', Construction and Building Materials, vol. 21, no. 12, pp. 2047-58.

Dołżycki, B & Judycki, J 2008, 'Behaviour of asphalt concrete in cyclic and static compression creep test with and without lateral confinement', Road Materials and Pavement Design, vol. 9, no. 2, pp. 207-25.

Ebrahimi, MG 2015, 'Investigation of viscoelastic behaviour and permanent deformation modelling for New Zealand hot mix asphalts', University of Canterbury, New Zealand.

EN12697-24 2004, Bituminous mixtures–test methods for hot mix asphalt–Part 24–Resistance to fatigue, Comité Européen de Normalisation.

Gabrawy, T 2000, 'Towards laboratory replication of field compaction: the Asphalt Shear Box Compactor', in World of Asphalt Pavements, International Conference Sydney, New South Wales, Australia.

Garba, R 2002, 'Permanent deformation properties of asphalt concrete mixtures', Norwegian university of science and technology, Norway.

Garber, NJ & Hoel, LA 1997, Traffic and highway engineering, PWS Pub. Co, Boston.

Geber, R, Apkaryan, A, Kulkov', S & Gomez, LA 2014, 'Linear viscoelastic properties of asphalt mastics using creep-recovery technique', Materials Science and Engineering, vol. 39, no. 2, pp. 5-11.

Gibb, JM 1996, 'Evaluation of resistance to permanent deformation in the design of bituminous paving mixtures', The University of Nottingham, UK.

Gibson, N, Schwartz, C, Schapery, R & Witczak, M 2003, 'Viscoelastic, viscoplastic, and damage modeling of asphalt concrete in unconfined compression', Transportation Research Record: Journal of the Transportation Research Board, no. 1860, pp. 3-15.

Gribble, M & Patrick, J 2008, Adaptation of the Austroads pavement design guide for New Zealand conditions, Land Transport New Zealand.

Huang, X & Zhang, Y 2010, 'A new creep test method for asphalt mixtures', Road Materials and Pavement Design, vol. 11, no. 4, pp. 969-91.

Huang, YH 2004, Pavement analysis and design, Pearson Prentice Hall, Upper Saddle River.

Khanzada, S 2000, 'Permanent deformation in bituminous mixtures', University of Nottingham.

Kumlai, S, Jitsangiam, P & Nikraz, H 2014, 'Comparison between resilient modulus and dynamic modulus of Western Australian hot mix asphalt based on flexible pavement design perspectives', in 26th ARRB Conference, Sydney, New South Wales, Australia.

Lai, JS & Hufferd, WL 1976, 'Predicting permanent deformation of asphalt concrete from creep tests', Transportation Research Record, vol. 616, p. 13.

Liao, GY, Yang, YW, Huang, XM & Xiang, JY 2013, 'Permanent deformation response parameters of asphalt mixtures for a new mix-confined repeated load test', Journal of Central South University, vol. 20, no. 5, pp. 1434-42.

Liao, Y 2007, Viscoelastic FE modeling of asphalt pavements and its application to US 30 perpetual pavement, ProQuest.

Logan, DL 2007, A first course in the finite element method, Fourth Edition edn, Chris Carson.

Ma, HY, Feng, DC & Jing, RX 2012, 'Site Monitoring on Temperature Field Distribution of Asphalt Pavement in Seasonal Frozen Soil Region', in Advanced Engineering Forum, Trans Tech Publ, pp. 265-70.

Mahan, HM 2013, 'Influence of mineral filler- asphalt ratio on asphalt mixture performance', Journal of Babylon University, vol. 21.

Mashaan, NS, Ali, AH, Karim, MR & Abdelaziz, M 2014, 'A review on using crumb rubber in reinforcement of asphalt pavement', The Scientific World Journal, vol. 2014.
Mathew, TV & Rao, KVK 2007, Introduction to Transportation Engineering, NPTEL.

Matić, B, Matić, D, Ćosić, Đ, Sremac, S, Tepić, G & Ranitović, P 2013, 'A model for the pavement temperature prediction at specified depth', Metalurgija, vol. 52, no. 4, pp. 505-8.

McCrum, NG, Buckley, CP & Bucknall, CB 1997, Principles of Polymer Engineering, Second edn.

Merbouh, Mh 2012, 'Effect of thermal cycling on the creep-recovery behaviour of road bitumen', Energy Procedia, vol. 18, pp. 1106-14.

Molenaar, JMM 2004, 'Performance related characterisation of the mechanical behaviour of asphalt mixtures', TU Delft, Delft University of Technology.

Mollenhauer, K, Wistuba, M & Rabe, R 2009, 'Loading frequency and fatigue: In situ conditions & impact on test results', in 2nd Workshop on four point bending, University of Minho.

Monographs, I 2013, Bitumen and bitumen emissions, vol. 103, lyon, France.

NCHRP 2004, Guide for Mechanistic-Empirical design of new and rehabilitatd pavement structures, National Cooperative Highway Research Program, Illinois.

NCHRP 2011, A manual for design of hot mix asphalt with commentary, Report 673, National Cooperative Highway Research Program, Washington, D.C.

Nunn, ME, Brown, AJ & Guise, SJ 1998, Assessment of Simple Tests to Measure Deformation Resistance of Asphalt, Report PR/CE/92/98.

Oliver, JWH, Alderson, AJ, Tredrea, PF & Karim, MR 1995, Results of the laboratory program associated with the ALF asphalt deformation trial, APRG report No. 12- ARR 272, Austroads Pavement Research Group, Australia.

Ongel, A & Harvey, J 2004, Analysis of 30 years of pavement temperatures using the enhanced integrated climate model (EICM), Pavement Research Centre, University of California Davis, CDo Transportation, Pavement research center, Institute of transportation studies Berkeley, USA.

Oscarsson, E 2007, 'Prediction of permanent deformations in asphalt concrete using the mechanistic-empirical pavement design guide', Institutionen för teknik och samhälle, Lunds tekniska högskola.

Oscarsson, E 2011, 'Mechanistic-empirical modeling of permanent deformation in asphalt doncrete layers', Bulletin – Lunds Universitet, Sweden.

Öztürk, HI 2007, 'Parametric study on selected mathematical models for dynamic creep behavior of asphalt concrete', Middle east technical university, Turkey.

Pavement-Interactive 2011, ' Moisture Susceptibility', viewed 2016,<http://www.pavementinteractive.org/article/moisture-susceptibility/>.

Pearson, RA & Foley, GD 2001, Emerging issues in the Australian transport industry (2000-2015), ARRB 350, Australia.

Perl, M, Uzan, J & Sides, A 1983, 'A visco-elasto-plastic constitutive law for a bituminous mixture under repeated loading', Transportation Research Record, no. 911, p. 8.

Rebbechi, J 2014, Guide to pavement technology: part 4B: asphalt, Second edn, Austroads Ltd., Sydney NSW 2000 Australia.

Rebbechi, J & Liddle, G 2006, Introduction to asphalt mix design, Austroads technical report, AP–T62/06, Austroads, Sydney, Australia.

Roque, R, Birgisson, B, Drakos, C & Sholar, G 2005, Guidelines for use of modified binders, 4910-4504-964-12, Florida Department of Transportation, Florida, USA.

Scholz, TV & Rajendran, S 2009, Investigating premature pavement failure due to moisture, SPR 632, ODo Transportation, Kiewit Center for Infrastructure and Transportation, Oregon, USA.

Sharp, K 2009, Guide to pavement technology: part 1: introduction to pavement technology, Second edn, Austroads Ltd, Sydney NSW 2000 Australia.

Shrapnel, B 2011, Road Maintenance in Australia 2001-2026, BIS Shrapnel Pty Ltd.

Shuiyou, X 2003, 'Effect of the Tire/Pavement Contact Pressure on Asphalt Pavement', Chanan University.

Smith, T 1996, 'A comparison of different methods of analysing dynamic creep test results', TRL report, no. 159.

Smith, T, Tighe, S & Fung, R 2001, 'Concrete pavement in Canada: A review of their usage and performance', in The pavement technology advancements session of the 2001 annual conference of the transportation association of Canada, Halifax, Nova Scotia.

Sohm, J, Gabet, T, Hornych, P, Piau, J-M & Di Benedetto, H 2012, 'Creep tests on bituminous mixtures and modelling', Road Materials and Pavement Design, vol. 13, no. 4, pp. 832-49.

Sousa, JB, Craus, J & Monismith, CL 1991, Summary report on permanent deformation in asphalt concrete, SHRP-A/IR-91-104, Contract A-003A, Institute of Transportation Studies, University of California, Berkeley, California, Washington, D.C.

Stephenson, G 2002, 'Use of stone mastic asphalt mixtures in road pavement maintenance and construction', Queensland University of Technology, Brisbane, Australia.

Sullivan, BW 2015, 'Development of a long life design procedure for Australian asphalt pavements', Curtin University, Australia.

Taherkhania, H 2011, 'Compressive creep behaviour of asphalt mixtures', Procedia Engineering, vol. 10, pp. 583-8.

Tarakji, G 1992, 'A rationale for the development of an end-result design method for bituminous concrete', Construction and Building Materials, vol. 6, no. 4, pp. 213-4.

Transport engineering, 2013, University of Southern Queensland, Toowoomba, Australia UTS-14.Manual 2011, Universal Testing software, UTS test no 14.

Uzarowski, L, Tighe, S & Rothenburg, L 2007, 'Development of Asphalt Mix Creep Parameters and Finite element Modeling of Asphalt Rutting', in Proceedings of the fifty-second annual conference of the Canadian technical asphalt association (CTAA) Niagara Falls, Ontario.

Vavrik, WR 2000, 'Asphalt mixture design concepts to develop aggregate interlock', University of Illinois at Urbana-Champaign.

Vazquez, CG, Aguiar-Moya, JP, Smit, AdF & Prozzi, JA 2010, Laboratory evaluation of influence of operational tolerance (acceptance criterion) on performance of hot-mix asphalt concrete.

Vliet, KJV & Ortiz, C 2006, Mechanical Behavior of Materials.

White, TD, Haddock, JE, Hand, AJT & Fang, H 2002, Contributions of pavement structural layers to rutting of hot mix asphalt pavements, 0309067219, Transportation Research Board.

Williamson, MJ 2015, 'Finite element analysis of hot-mix asphalt layer interface bonding', Kansas State University.

Witzcak, MW, Kaloush, K, T.Pellinen & Basyouny, ME 2002, Simple performance test for superpave mix design, vol. 465, Transportation Research Board.

Xu, Q & Solaimanian, M 2010, 'Modeling temperature distribution and thermal property of asphalt concrete for laboratory testing applications', Construction and Building Materials, vol. 24, no. 4, pp. 487-97.

Xu, T & Huang, X 2012, 'Investigation into causes of in-place rutting in asphalt pavement', Construction and Building Materials, vol. 28, no. 1, pp. 525-30.

Yang, J, Zhao, H, Chen, J, Qian, G, Pan, W & Yang, Y 2005, 'Study of the rutting resistance of asphalt surfacing mixtures', in 24th Southern African Transport

Conference (SATC 2005), Pretoria, South Africa, pp. 943-50, <http://usq.summon.serialssolutions.com/2.0.0/link/0/eLvHCXMwY2BQSAI2MowsDY1SzJONTJJTLRLTDFMME9OAtU2KoVEaeBrGJ9AsJMLMx8nEA6k0dxNiYErNE2WQd3MNcfbQhdUN8aD9GaXF8cCmg6khsEA1FGPgTQQt_84rAW8TSwEA-nUdHw>.

Youdale, G 1996, Australian pavement research-the last twenty years, Austroads, Australia.

Zhou, F, Fernand, E & Scullion, T 2008, A review of performance models and test procedures with recommendations for use in the Texam M-E design program, Report 0-5798-1, Texas Transportation Institute, The Texas A&M University System College Station, USA, Texas.

Zulkati, A, Diew, WY & Delai, DS 2012, 'Effects of fillers on properties of asphalt-concrete mixture', Journal of transportation engineering, vol. 138, no. 7, pp. 902-10.

APPENDIX

Part 1: (Experimental and literature)

Table 1: A comparison of test methods for evaluation permanent deformation of asphalt mixtures (Sousa et al. 1991; Gibb 1996; Brown et al. 2001; Zhou et al. 2008)

		Sample Shape and dimension	Advantage	Disadvantage
Empirical tests	Marshall Test	Cylindrical, 4 inch diameter × 2.5 inch height or 6 inch diameter × 3.75 inch height	* Easy to implement * Equipment generally available in labs * Standardized for mix design - short test time	* Not able to correctly predict and rank asphalt mixture for rutting
	Hveem Test	Cylindrical, 4 inch diameter × 2.5 inch height	* Short test time * Triaxial load applied	* Special compacter is needed for test (California kneading compacter) * Not able to correctly predict and rank asphalt mixture for rutting
	Gyratory Testing Machine	Loose sample	* Simulate the action of rollers during construction * Criteria available * Parameters are generated during compaction	* Equipment not widely available - not able to correctly predict and rank asphalt mixture for rutting
Fundamental Tests	Uniaxial Creep	Cylindrical, 4 inch diameter × 8 inch height & others	* Wide spread, well known * Easy to implement * Test equipment generally available in labs * More technical information	* Ability to predict permanent deformation in questionable * Restricted test temperature and load levels dose not simulate field situations * Does not simulate field dynamic phenomena
	Uniaxial repeated Load		* Better expresses traffic conditions	* Equipment is more complex * Restricted test temperature and load levels does not simulate field situations
	Uniaxial Dynamic Modulus		* Capability of determining the damping as a function of frequency for different temperatures * Non-destructive tests	* Equipment is more complex * Difficult to obtain 2:1 ratio specimens in lab

	Triaxial Creep	Cylindrical, 4 inch diameter × 8 inch height & others	* Relatively simple test and equipment * Test temperature and load levels better simulate field conditions than unconfined * Potentially inexpensive	* Requires a triaxial chamber * Confinement increases complexity of the test
	Triaxial repeated Load		* Test temperature and load levels better simulate field conditions than unconfined * Better expresses traffic conditions * Can accommodate varied specimen sizes * Criteria available	* Equipment is more complex and expensive * Requires a triaxial chamber
	Triaxial Dynamic Modulus		* Ability of determining the damping as a function of frequency for different temperatures * Non-destructive tests * Provides necessary input for structural analysis	* At high temperature it is a complex test system (small deformation measurement sensitivity is needed at high temperature) * Some possible minor problem due to stud, LVDT arrangement. * Equipment is more complex and expensive * Requires a triaxial chamber
	Diametral Creep	Cylindrical, 4 inch diameter × 2.5 inch height	* Easy to implement Equipment is relatively simple and generally available in most labs * Specimen is easy to fabricate	* State of stress is non uniform and strongly dependent on the shape of the specimen * Maybe inappropriate for estimating permanent deformation * High temperature (load) changes in the specimen shape affect the state of stress and the test measurement significantly * Found to overestimate rutting * For the dynamic test, the equipment is complex
	Diametral Repeated Load		* Easy to implement * Specimen is easy to fabricate	
	Diametral Dynamic Modulus		* Specimen is easy to fabricate * Non-destructive test	

	ST Frequency Sweep Test – Shear Dynamic	Cylindrical, 6 inch diameter × 2 inch height	* The applied shear strain simulate the effect of road traffic *AASHTO standardized procedure available * Master curve could be drawn from different temperatures and frequencies * Non-destructive test	* Equipment is extremely expensive and rarely available * Test is complex and difficult to run, usually need special training
	SST Repeated Shear at Constant Height		* The applied shear strains simulate the effect of road traffic * AASHTO procedure available	* Equipment is extremely expensive and rarely available * Test is complex and difficult to run, usually need special training * More than three replicate are needed
	Triaxial Shear Strength Test		* Short test time	* Much less used * Confined specimen requirements add complexity
	Hollow Cylindrical	1 inch wall thickness 18 inch high 9 inch external diameter	*Almost all states of stress can be duplicated. * Capability of determining damping as a function of frequency for different temperatures for shear as well as axial	* Sample preparation is tedious. * Expensive equipment * Cores cannot be obtained from pavement.
Simulative tests	Asphalt Pavement Analyser	Cylindrical, 6 inch × 3.5 or 4.5 inch or beam	* Simulates field traffic and temperature conditions * Simple to perform * 3-6 samples can be tested at the same time * Most widely used LWT in the US * Guidelines (criteria) are available	* Relatively expensive except new table top version
	Hamburg Wheel-Tracking Device	Slab, 10.2 inch × 12.6 inch × 1.6 inch	* Widely used in Germany * Capable of evaluating moisture-induced damage * Two samples tested at same time	* Less potential to be accepted widely in the word
	French Rutting Tester	Slab 7.1 inch × 19.7 inch × 0.8 to 3.9 inch	* Successfully used in France * Two HMA slabs can be tested at one time	* Not widely available

Table 2: Summary of the dynamic creep test outcomes and samples' properties

Specimen No.	Specimen place in the slab	Test method	Platen/Sample size	Tyre Pressure	P Bulk	P max	Air voids	Creep curve		Minimum creep slope	Plastic Deformation		Cycle number at minimum strain rate
								Stage 1	Stage 2		Stage 1	Stage 2	
			(mm)	kPa	tonnes/ m3	tonnes/ m3	(%)	Cycles	Cycles	(µs/cyc)	mm	mm	
11	-	SCDCT	50 mm/ 100 mm	750	2.389	2.497	4.33	5600	52000	0.339	0.68	1.81	29,953
20	-	SCDCT	50 mm/ 150 mm	750	2.367	2.497	5.19	6000	42000	0.813	0.89	2.56	28,865
4	-	-	100 mm/100 mm	750	2.351	2.497	5.84	800	5600	7.96	1.51	3.48	10,817
8	-	SCDCT	50 mm/ 100 mm	750	2.368	2.497	5.18	6000	36000	0.484	0.88	1.75	23745
9	-	-	100 mm/ 100 mm	750	2.374	2.497	4.94	1400	-	3.73	1.17	-	2.893
17	-	-	100 mm / 100 mm	750	2.368	2.497	5.18	600	-	6.98	1.27	-	1,165
6	-	-	100 mm/ 100 mm	750	2.38	2.497	4.7	1800	-	3.67	1.18	-	3,277
2	-	SCDCT	50 mm/ 100 mm	750	2.354	2.497	5.72	3800	19000	1.57	0.692	1.93	32,769
3		SCDCT	50 mm/ 100 mm	750	2.375	2.497	4.88	5500	-	0.24	0.392	-	51,201
24	6 BB	SCDCT	50 mm/ 150 mm	750	2.36	2.497	5.48	800	4200	7.6	0.83	2.25	2,769
31	8 BT	SCDCT	50 mm/ 150 mm	750	2.32	2.497	6.91	2000	10,000	3.42	1.1	2.6	7,777

Specimen No.	Specimen place in the slab	Test method	Platen/Sample size	Tyre Pressure	P Bulk	P max	Air voids	Creep curve		Minimum creep slope	Plastic Deformation		Cycle number at minimum strain rate
								Stage 1	Stage 2		Stage 1	Stage 2	
			(mm)	kPa	tonnes/ m3	tonnes/ m3	(%)	Cycles	Cycles	(µs/cyc)	mm	mm	
22	6 AB	-	75 mm/ 150 mm	750	2.359	2.497	5.53	1500	6800	6.54	1.46	3.3	3,537
23	6 BT	-	75 mm/ 150 mm	750	2.33	2.497	6.59	600	3100	14.77	1.29	3.27	1,825
29	8 AT	-	75 mm/ 150 mm	750	2.326	2.497	6.86	4000	13500	2.56	0.96	2.24	8,737
30	8 AB	-	75 mm/ 150 mm	750	2.337	2.497	6.41	1500	7000	5.79	1.37	3.07	4,097
34	9 AB	SCDCT	50 mm/ 100 mm	750	2.299	2.497	7.9	1800	4000	4.89	0.69	1.28	2.033
5	-	CDCT	50 mm/ 100 mm	750	2.362	2.497	5.42	43,000	-	0.012	0.428	-	89,437
18	-	CDCT	50 mm/ 150 mm	750	2.349	2.497	5.94	49,000	-	0.03	1.381	-	96,129
35	9 BT	CDCT	50 mm/ 100 mm	750	2.296	2.497	8.04	55,000	Plus 100,000 (Did not reach)	0.018	0.864	Did not happen	81,281
39	10 AT	CDCT	50 mm/ 100 mm	750	2.278	2.497	8.78	43,000	Plus 100,000 (Did not reach)	0.013	1.033	Did not happen	94,977
42	10 BB	CDCT	50 mm/ 100 mm	750	2.244	2.497	10.1	43,000	Plus 100,000 (Did not reach)	0.019	1.137	Did not happen	91,265
44	10 CB	CDCT	50 mm/ 100 mm	750	2.249	2.497	9.93	38,000	Plus 100,000 (Did not reach)	0.013	0.874	Did not happen	93,953
33	9 AT	CDCT	50 mm/ 100 mm	750	2.313	2.497	7.39	45,000	Plus 100,000 (Did not reach)	0.013	0.99	Did not happen	97,793
26	7 AB	CDCT	50 mm/ 150 mm	750	2.364	2.497	5.32	40,000	-	0.022	1.145	-	78,721

Specimen No.	Specimen place in the slab	Test method	Platen/Sample size	Tyre Pressure	P Bulk	P max	Air voids	Creep curve		Minimum creep slope	Plastic Deformation		Cycle number at minimum strain rate
								Stage 1	Stage 2		Stage 1	Stage 2	
			(mm)	kPa	tonnes/ m3	tonnes/ m3	(%)	Cycles	Cycles	(µs/cyc)	mm	mm	
27	7 BT	CDCT	50 mm/ 150 mm	750	2.337	2.497	6.41	45,000	Plus 100,000 (Did not reach)	0.025	1.331	Did not happen	94,209
28	7 BB	CDCT	50 mm/ 150 mm	750	2.359	2.497	5.54	40,000	Plus 100,000 (Did not reach)	0.025	1.238	Did not happen	91,777
32	8 BB	CDCT	50 mm/ 150 mm	750	2.334	2.497	6.52	40,000	-	0.032	1.678	-	78,977
25	7 AT	CDCT	50 mm/ 150 mm	750	2.355	2.497	5.68	50,000	Plus 100,000 (Did not reach)	0.031	1.08	Did not happen	97,537
47	14 BT	CDCT	50 mm/ 150 mm	750	2.448	2.497	1.96	45,000	Plus 100,000 (Did not reach)	0.016	0.674	Did not happen	92,289
53	16 AB	CDCT	50 mm/ 150 mm	750	2.399	2.497	3.92	43,000	Plus 100,000 (Did not reach)	0.019	0.94	Did not happen	97,793
70	22 AB	CDCT	50 mm/ 150 mm	750	2.275	2.497	8.88	45,000	Plus 100,000 (Did not reach)	0.045	1.666	Did not happen	97,409
48	14 BB	SCDCT	50 mm/ 150 mm	750	2.448	2.497	1.96	55,000	Plus 100,000 (Did not reach)	0.034	0.807	Did not happen	94,849
69	22 AT	SCDCT	50 mm/ 150 mm	750	2.28	2.497	8.68	5,000	20,000	1.93	1.571	3.119	13,697
111	26 BT	CDCT	50 mm/ 100 mm	750	2.44	2.497	2.3	45,000	Plus 100,000 (Did not reach)	0.006	0.276	Did not happen	65,537
43	10 CT	CDCT	50 mm/ 100 mm	750	2.259	2.497	9.55	45,000	Plus 100,000 (Did not reach)	0.016	0.841	Did not happen	97,025

Specimen No.	Specimen place in the slab		Platen/Sample size	Tyre Pressure	P Bulk	P max	Air voids	Creep curve		Stage 2	Plastic Deformation		Cycle number at minimum strain rate
								Stage 1	Stage 2	Creep slope	Stage 1	Stage 2	
			(mm)	kPa	tonnes/ m3	tonnes/ m3	(%)	Cycles	Cycles	(µs/cyc)	mm	mm	
85	11 AB	CDCT	50 mm/ 100 mm	750	2.393	2.497	4.18	45,000	Plus 100,000 (Did not reach)	0.013	0.711	Did not happen	96,257
95	12 CT	CDCT	50 mm/ 100 mm	750	2.414	2.497	3.32	50,000	Plus 100,000 (Did not reach)	0.013	0.358	Did not happen	90,753
109	26 AT	SCDCT	50 mm/ 100 mm	750	2.436	2.497	2.45	50,000	Plus 100,000 (Did not reach)	0.038	0.75	Did not happen	98,433
112	26 BB	SCDCT	50 mm/ 100 mm	750	2.43	2.497	2.68	48,000	Plus 100,000 (Did not reach)	0.032	0.798	Did not happen	70,273
105	20 BT	SCDCT	50 mm/ 100 mm	750	2.358	2.497	5.56	13,000	30,000	0.833	1.379	2.109	18,497
36	9 BB	CDCT	50 mm/ 100 mm	750	2.284	2.497	8.53	40,000	Plus 100,000 (Did not reach)	0.022	1.55	Did not happen	98.433
41	10 BT	CDCT	50 mm/ 100 mm	750	2.239	2.497	10.3	45,000	Plus 100,000 (Did not reach)	0.013	1.49	Did not happen	73,729
21	6 AT	CDCT	50 mm/ 150 mm	750	2.34	2.497	6.27	45,000	Plus 100,000 (Did not reach)	0.045	2.59	Did not happen	97,025
66	21 AB	EDCT	150mm/ 150mm	200	2.338	2.497	6.36	21,000	Plus 40,000 (Did not reach)	0.324	1.22	Did not happen	35,329
67	21 BT	EDCT	150mm/ 150mm	200	2.338	2.497	6.35	14,000	Plus 40,000 (Did not reach)	0.296	1.11	Did not happen	19,297
74	23 AT	EDCT	150mm/ 150mm	200	2.352	2.497	5.81	23,000	Plus 40,000 (Did not reach)	0.062	0.81	Did not happen	37,825

Specimen No.	Specimen place in the slab	Test method	Platen/Sample size	Tyre Pressure	P Bulk	P max	Air voids	Creep curve		Stage 2	Plastic Deformation		Cycle number at minimum strain rate
								Stage 1	Stage 2	Creep slope	Stage 1	Stage 2	
			(mm)	kPa	tonnes/ m3	tonnes/ m3	(%)	Cycles	Cycles	(µs/cyc)	mm	mm	
88	11 BB	EDCT	100mm/ 100mm	200	2.406	2.497	3.64	25,000	Plus 40,000 (Did not reach)	0.044	0.352	Did not happen	38,081
101	19 CB	EDCT	100mm/ 100mm	200	2.348	2.497	5.96	27,000	Plus 40,000 (Did not reach)	0.099	0.495	Did not happen	35,201
102	19 CT	EDCT	100mm/ 100mm	200	2.349	2.497	5.92	23,000	Plus 40,000 (Did not reach)	0.056	0.851	Did not happen	35,969
103	20 AB	EDCT	100mm/ 100mm	200	2.356	2.497	5.63	24,000	Plus 40,000 (Did not reach)	0.055	0.788	Did not happen	35,073
107	20 CT	EDCT	100mm/ 100mm	200	2.365	2.497	5.29	26,000	Plus 40,000 (Did not reach)	0.049	0.24	Did not happen	38,465
115	1 AT	EDCT	150mm/ 150mm	200	2.339	2.477	5.55	300	Plus 40,000 (Did not reach)	23.28	1.054	Did not happen	521
131	5 CT	EDCT	100mm/ 100mm	200	2.341	2.477	5.48	2100	Plus 40,000 (Did not reach)	5.83	1.26	Did not happen	561
49	15 AT	CDCT	50 mm/ 150 mm	750	2.441	2.497	2.23	52,000	Plus 100,000 (Did not reach)	0.013	0.338	Did not happen	80129
71	22 BT	CDCT	50 mm/ 150 mm	750	2.282	2.497	8.62	37,000	-	0.093	1.756	Did not happen	58113
78	24 AT	CDCT	50 mm/ 150 mm	750	2.356	2.497	5.64	45,000	Plus 100,000 (Did not reach)	0.025	1.355	Did not happen	95233

Specimen No.	Specimen place in the slab	Test method	Platen/Sample size	Tyre Pressure	P Bulk	P max	Air voids	Creep curve		Stage 2	Plastic Deformation		Cycle number at minimum strain rate
								Stage 1	Stage 2	Creep slope	Stage 1	Stage 2	
			(mm)	kPa	tonnes/ m3	tonnes/ m3	(%)	Cycles	Cycles	(μs/cyc)	mm	mm	
60	17 BB	CDCT	50 mm/ 150 mm	750	2.432	2.497	2.6	48,000	Plus 100,000 (Did not reach)	0.012	1.092	Did not happen	83329
61	18 AB	CDCT	50 mm/ 150 mm	750	2.405	2.497	3.66	35,000	-	0.025	0.723	Did not happen	59841
117	1 BT	CDCT	50 mm/ 150 mm	750	2.317	2.477	6.47	45,000	Plus 100,000 (Did not reach)	0.05	2.948	Did not happen	93,569
118	1 BB	CDCT	50 mm/ 150 mm	750	2.351	2.477	5.1	40,000	Plus 100,000 (Did not reach)	0.031	2.383	Did not happen	96,769
121	3 BB	CDCT	50 mm/ 150 mm	750	2.37	2.477	4.32	40,000	Plus 100,000 (Did not reach)	0.035	2.442	Did not happen	98,433
122	3 BT	CDCT	50 mm/ 150 mm	750	2.331	2.477	5.89	40,000	Plus 100,000 (Did not reach)	0.04	2.64	Did not happen	93,441
134	6 AB	CDCT	50 mm/ 100 mm	750	2.35	2.477	5.12	55,000	Plus 100,000 (Did not reach)	0.016	1.023	Did not happen	97,409
135	6 BT	CDCT	50 mm/ 100 mm	750	2.344	2.477	5.36	48,000	Plus 100,000 (Did not reach)	0.018	1.452	Did not happen	84,737
136	6 BB	CDCT	50 mm/ 100 mm	750	2.363	2.477	4.59	52,000	Plus 100,000 (Did not reach)	0.016	1.093	Did not happen	86,273
127	5 AT	SCDCT	50 mm/ 100 mm	750	2.353	2.477	5.01	40	150	163.6	1.048	2	95
130	5 BB	SCDCT	50 mm/ 100 mm	750	2.356	2.477	4.88	60	260	95.52	1.025	2.043	189
132	5 CB	SCDCT	50 mm/ 100 mm	750	2.343	2.477	5.42	50	160	157.4	1.167	2.083	94
137	6 CT	SCDCT	50 mm/ 100 mm	750	2.359	2.477	4.76	50	240	102.04	0.929	1.881	124
120	2 AB	CDCT	75 mm/ 150 mm	750	2.352	2.477	5.04	45,000	-	0.025	1.86	Did not happen	95,873
123	4 AT	CDCT	75 mm/ 150 mm	750	2.337	2.477	5.66	45,000	-	0.025	1.911	Did not happen	92,801

Specimen No.	Specimen place in the slab	Test method	Platen/Sample size	Tyre Pressure	P Bulk	P max	Air voids	Creep curve		Stage 2	Plastic Deformation		Cycle number at minimum strain rate
								Stage 1	Stage 2	Creep slope	Stage 1	Stage 2	
			(mm)	kPa	tonnes/ m3	tonnes/ m3	(%)	Cycles	Cycles	(µs/cyc)	mm	mm	
124	4 AB	CDCT	75 mm/ 150 mm	750	2.358	2.477	4.81	50,000	-	0.022	1.79	Did not happen	93,825
126	4 BB	CDCT	75 mm/ 150 mm	750	2.365	2.477	4.51	48,000	-	0.022	1.632	Did not happen	74,753
45	14 AB	CDCT	75 mm/ 150 mm	750	2.446	2.497	2.05	55,000	-	0.013	0.979	Did not happen	81,793
62	18 AT	CDCT	75 mm/ 150 mm	750	2.414	2.497	3.33	55,000	-	0.015	0.781	Did not happen	93,185
65	21 AT	CDCT	75 mm/ 150 mm	750	2.347	2.497	6.02	48,000	-	0.025	1.598	Did not happen	93,057
72	22 BB	CDCT	75 mm/ 150 mm	750	2.281	2.497	8.65	50,000	-	0.031	1.7	Did not happen	93,825
83	25 BT	CDCT	75 mm/ 150 mm	750	2.37	2.497	5.09	50,000	-	0.019	1.313	Did not happen	92.033
58	17 AT	SCDCT	50 mm/ 150 mm	750	2.434	2.497	2.51	15,000	42,000	0.31	1.671	2.135	33,281
54	16 AT	EDCT	150mm/ 150mm	750	2.398	2.497	3.96	25,000	-	0.098	1.157	Did not happen	39,169
91	12 AT	EDCT	100mm/ 100mm	750	2.398	2.497	3.98	25,000	-	0.098	1.171	Did not happen	37,249
82	25 AT	CDCT	50mm/ 150mm	750	2.344	2.497	6.12	60,000	-	0.031	1.793	Did not happen	37,595
129	5 BT	CDCT	50mm/ 100mm	750	2.352	2.477	5.03	55,000	-	0.016	1.087	Did not happen	83,585
138	6 CB	CDCT	50mm/ 100mm	750	2.354	2.477	4.97	55,000	-	0.016	1.452	Did not happen	89,601

Table 3: Brisbane City Council mix design and material properties

Brisbane Field Services Group
Eagle Farm Laboratory
260 Curtin Ave West
Eagle Farm,Qld.4009
Ph. 34031003
Fax : 34031000

BCC Asphalt Mix Design

Asphalt Mix Type:	BCC Type 2: 10mm Dense Graded Asphalt
Mix Name/Code:	[redacted]
Mixing Plant/Type:	Eaglefarm Asphalt Plant(Continuous)
Source Quarry Aggregate:	Mt Cootha Quarry (Hornfels)

Mix Design Components

Material	Source
C1000/320 Bitumen	SAMI
REC DUST	BCC EagleFarm
SAND	SPS Ningi
FINE RAP	BCC Pine Mountain
18mm	Mt Cootha Quarry
14mm	Mt Cootha Quarry
9mm	Mt Cootha Quarry
7mm	Mt Cootha Quarry
DUST	Mt Cootha Quarry

Raw Aggregate Properties

			7mm		9mm		14mm		18mm	
Test Method	Description	Limits	Test Result	Test Report	Test Result	Test Report	Test Result	Test Report	Test Result	Test Report
AS1141.11	Grading		Conforming	E120797.3	Conforming	E120764.4	Conforming	E1207156.4	Conforming	E1205160.2
AS1141.15	Flakiness	<30%	9.5	E120797.3	13.3	E120764.4	7.8	E1207156.4	17.6	E1205160.2
Q214B	Water Absorption	Max. 2%	0.61	E120797.3	0.49	E120764.4	0.24	E1207156.4	0.31	E1205160.2
Q214B	Particle density (Dry)	t/m3	2.671	E120797.3	2.654	E120764.4	2.673	E1207156.4	2.671	E1205160.2
Q215	Crushed Particles	Min. 80%	100	E120797.3	100	E120764.4	100	E1207156.4	100	E1205160.2
Q217	Weak Particles	Max. 1%	0.5	E120797.3	0.1	E120764.4	0.1	E1207156.4	0	E1205160.2
Q205B	10% Fines	Min.150kN	296	E1112131.1	272	E1112131.2	239	E1112131.3	215	E1112131.4
Q205C	Wet/Dry Variation	Max.30%	-	-	-	-	-	-	14	E1112131.4
Q208B	Degradation	Min.40%	-	-	-	-	-	-	-	-
Q203	PAFV	Min.>65%	-	-	50	E1112131.2	-	-	-	-
	Product Conforms	(Yes / No)	Yes	-	Yes	-	Yes	-	Yes	-
	Non-Conformances									

Filler Properties

			Baghouse		Rockflour		Combined BH/RF	
Test Method	Description	Limits	Test Result	Test Report	Test Result	Test Report	Test Result	Test Report
AS1141.11	600um Grading (AS2357 Limits)	100	100	E111208.1	100	E111208.2	100	E111208.3
AS1141.11	300um Grading (AS2357 Limits)	95-100	100	E111208.1	100	E111208.2	100	E111208.3
AS1141.11	0.075um Grading (AS2357 Limits)	70-100	92.8	E111208.1	97.1	E111208.2	97.1	E111208.3
AS1141.17	Voids in Compacted Filler	Min. 38%	48	E120514.2	49	E120514.1	46	E120514.3
AS1141.7	Apparent Particle Density	TBR	2.706	E120514.2	2.756	E120514.1	2.729	E120514.3
Q129	Clay Index	Max.2.2%	-	-	-	-	1.8	E120514.3
	Product Conforms	(Yes / No)	Yes		Yes		Yes	
	Non-Conformances							

Combined Aggregates Q208B

Test Method	Description	Limits	Test Result	Test Report
Q208B	Degradation	Min.40%	45	E111212

Plasicity Index - Crusher Dust

Test Method	Description	Limits	Test Result	Test Report
Q104A	Liquid Limit		20.4	E101236
Q105	Plastic Limit		-	-
Q106	LinearShrinkage		2.6	E101236
	Plasticity Index	Max.4	3.6	E101236

Plasicity Index

Test Method	Description	Limits	Test Result	Test Report
Q104A	Liquid Limit		18.4	E120825.3
Q105	Plastic Limit		16.4	E120825.3
Q106	LinearShrinkage		1.4	E120825.3
	Plasticity Index	Max. 4	2.0	E120825.3

Binder Properties

			C170			
Date	Lower Limits	Higher Limits	Test Result	Test Report	Test Result	Test Report
Viscosity (60 oC)	-	-	189	23220	183	23096
Penetration (25 oC)	60	-	68	23220	66	21698
Viscosity (135 oC)	0.25	0.45	0.420	23220	0.410	21698
Viscosity (RTFO 60 oC)	-	-	-	-	-	-
Penetration (RFTO 25 oC)	-	-	-	-	-	-
Matter insoluble in Toluene	-	-	-	-	-	-
Flash Point	-	-	-	-	-	-
Density at 15 oC	-	-	1.058	23220	1.058	21698
Ductility (RFTO 15 oC)	-	-	-	-	-	-
Loss on Heating	-	-	-	-	-	-

Asphalt Gradings

AS Sieve Size	Lower Limits	Upper Limits	Test Result	Test Report	Test Result	Test Report
26.5 mm	100	100	100	E130374A	100	E130335A
19.0 mm	100	100	100	E130374A	100	E130335A
13.2 mm	100	100	100	E130374A	100	E130335A
9.5 mm	90	100	95	E130374A	95	E130335A
6.7 mm	74	80	78	E130374A	78	E130335A
4.75 mm	60	72	62	E130374A	63	E130335A
2.36 mm	39	48	42	E130374A	42	E130335A
1.18 mm	30	36	31	E130374A	31	E130335A
600 um	22	28	23	E130374A	24	E130335A
300 um	16	21	16	E130374A	16	E130335A
150 um	8.0	12.0	9.0	E130374A	9.0	E130335A
75 um	6.0	8.0	6.9	E130374A	6.7	E130335A

Marshall Properties

			Test Result	Test Report
Air Voids	2.0	5.0	4.4	E130335A
VMA	TBR	TBR	14.6	E130335A
Voids Filled	TBR	TBR	70.0	E130335A
Pat Density(t/m3)	TBR	TBR	2.37	E130335A
Flow (mm)	2mm	4mm	3.9	E130335A
Stability (kN)	Min 7.5kN	-	11.3	E130335A
Stiffness (kN)	TBR	TBR	2.9	E130335A

Page 1 of 1

Table 4: Brisbane City Council Type 2 Mix (Aggregate gradation)

ASPHALT MIX DESIGN

Eagle Farm Asphalt Plant

Asphalt Operations
Eagle Farm Asphalt Plant
260 Curtin Ave. West
Eagle Farm 4009
Telephone 340 21001

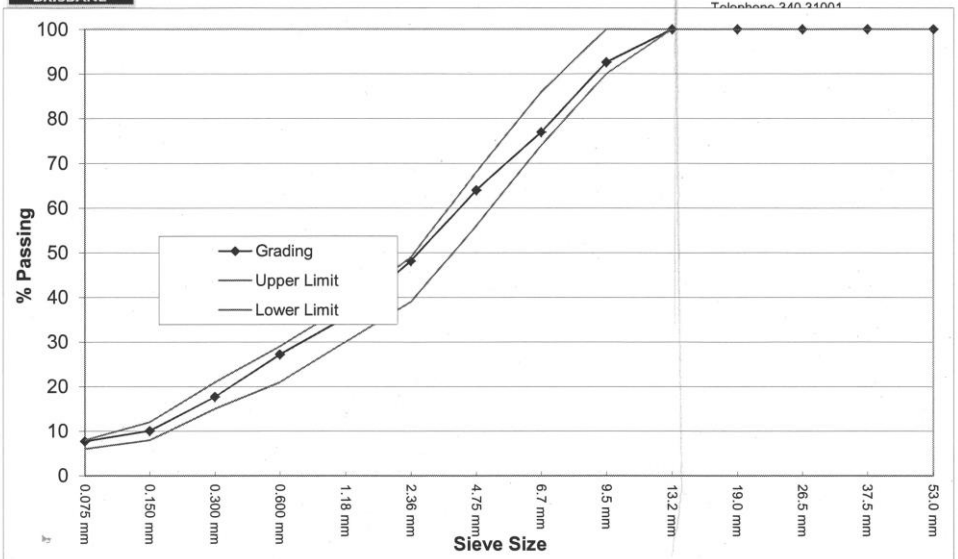

Material	Source	Plant %	Min %	Max %	Design %
C170 Bitumen	SAMI				
C320 Bitumen	SAMI				
C600 Bitumen	SAMI				
C1000/320 Bitumen	SAMI	**5.00**	4.70	5.30	5.00
A5S Bitumen	SAMI				
A5S Bitumen	SAMI				
A0.6S Bitumen	SAMI				
A0.6S Bitumen	SAMI				
Fricseal Bitumen	SAMI				
HYD LIME	DML Gympie				
REC DUST	BCC EagleFarm	**2.0**	**1.9**	**2.9**	2.5
ROCK FLOUR	Mt Cootha Quarry				
FLY ASH	CA Swanbank				
SAND	SPS Ningi	**9.0**	**7.6**	**11.4**	10
FINE RAP	BCC Pine Mountain				
35mm	Mt Cootha Quarry				
25mm	Mt Cootha Quarry				
18mm	Mt Cootha Quarry				
14mm	Mt Cootha Quarry				
9mm	Mt Cootha Quarry	**23.0**	**13.7**	**20.5**	18
7mm	Mt Cootha Quarry	**15.0**	**19.0**	**28.5**	25
DUST	Mt Cootha Quarry	**46.0**	**32.5**	**42.5**	39.5
BQ 35mm	Bracalba Quarry				
BQ 20mm	Bracalba Quarry				
DUST	Bracalba Quarry				
BQ 7mm	Bracalba Quarry				
Glass	Visy				
AG LIME	Unimin Lime				
Diesel	BP				
FIBRE	Topcel				
	Total Material %	**100**			100
	Total Binder Content		**5.00**		

Sieve	Grading	Upper Limit	Lower Limit
53.0 mm	**100**	100	100
37.5 mm	**100**	100	100
26.5 mm	**100**	100	100
19.0 mm	**100**	100	100
13.2 mm	**100**	100	100
9.5 mm	**93**	100	90
6.7 mm	**77**	86	74
4.75 mm	**64**	68	56
2.36 mm	**48**	49	39
1.18 mm	**35**	38	30
0.600 mm	**27**	29	21
0.300 mm	**18**	21	15
0.150 mm	**10.1**	12.0	8.0
0.075 mm	**7.7**	8.0	6.0

Specification Bitumen Tolerance: 0.3

Mix Design Name: **BCC Type 2 MG**

Mix Design No: 003

Designed By: T.B.Akers

Date: 25-Mar-14

Authorised by: _____

Date: _____

Plant Baghouse Draw Down (%): **1.5**

Mix Design Abbreviation: M770

Comments: New batch card system.

Design Inputted By : _____ Date Inputted : _____

Mix Design Last Used: 002 Design Last Used: Current

Table 5: Properties of the used bitumen

NATA Accredited for compliance with ISO/IEC 17025 Accreditation Number 5598

SAMI BITUMEN

PRODUCT TEST REPORT

SAMI Bitumen Technologies

12 Grand Ave, Camellia
NSW 2142 Or PO Box 163
Granville, NSW 2142

Ph: 02 9638 0150
Fax: 02 9638 4983
Fax: 02 8209 4873

Test Report No.: 25908
Product: SAMIfalt Multigrade Plus
Batch Number: PB14055
SAMI Sample No.: PB140551
Date of Sampling: 10-02-2014
Sample Details: T12 SBT QLD
Date Tested: 12-02-2014
Specification: AS 2008 – 2013 for M1000

Method	Property	Result	Specification
AS 2341.2	Viscosity at 60C, Pas	910	Report
AS 2341.12	Penetration at 25C, 100g, 5s, 0.1mm	43	Report
AS 2341.4	Viscosity at 135C, Pas	0.78	1.5 max.
AS 2341.2 AS/NZS 2341.10	Viscosity at 60C after RTFOT, Pas	5550	3500 - 6500
AS 2341.12 AS/NZS 2341.10	Penetration at 25C, 100g, 5s after RTFOT, 0.1mm	26	26 min.
AS 2341.18	Softening Point, C	58.5	Report
Frequency Tests (Batch number: PB14034)			
AS 2341.20	Matter insoluble in toluene, % mass	<0.1	1.0 max
AS 2341.14	Flash Point, °C	348	250 min
AS 2341.7	Density at 15C, t/m³ (partial filling)	1.0310	Report
AS/NZS 2341.10	Mass Change before and after exposure, % mass	-0.07	-0.6 to +0.6

Sampling Method: Test as received
Testing Operator: G. Y.
Certificate Issued Date: 12-02-2014

Authorised Officer of the Company
B. Chik, Lab Manager (national)

Part 2: *FEM modelling outputs for various laboratory and in situ conditions.*

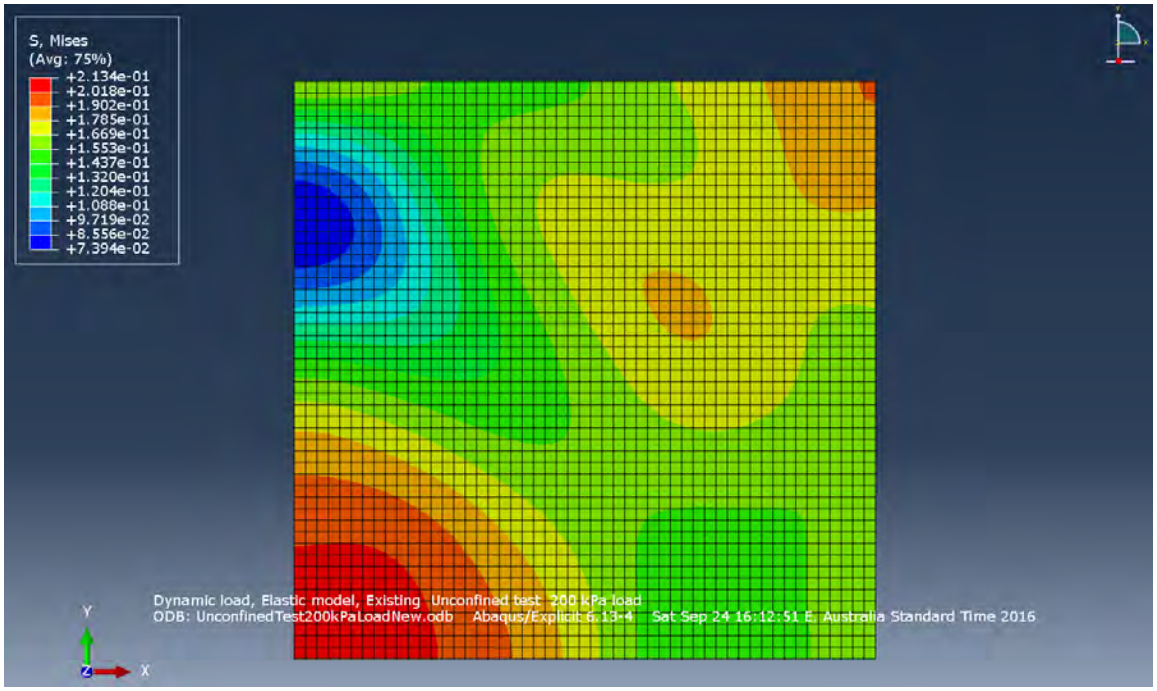

Figure 1: Existing unconfined test for a 100/ 100mm section (200 kPa load) – Mises stress.

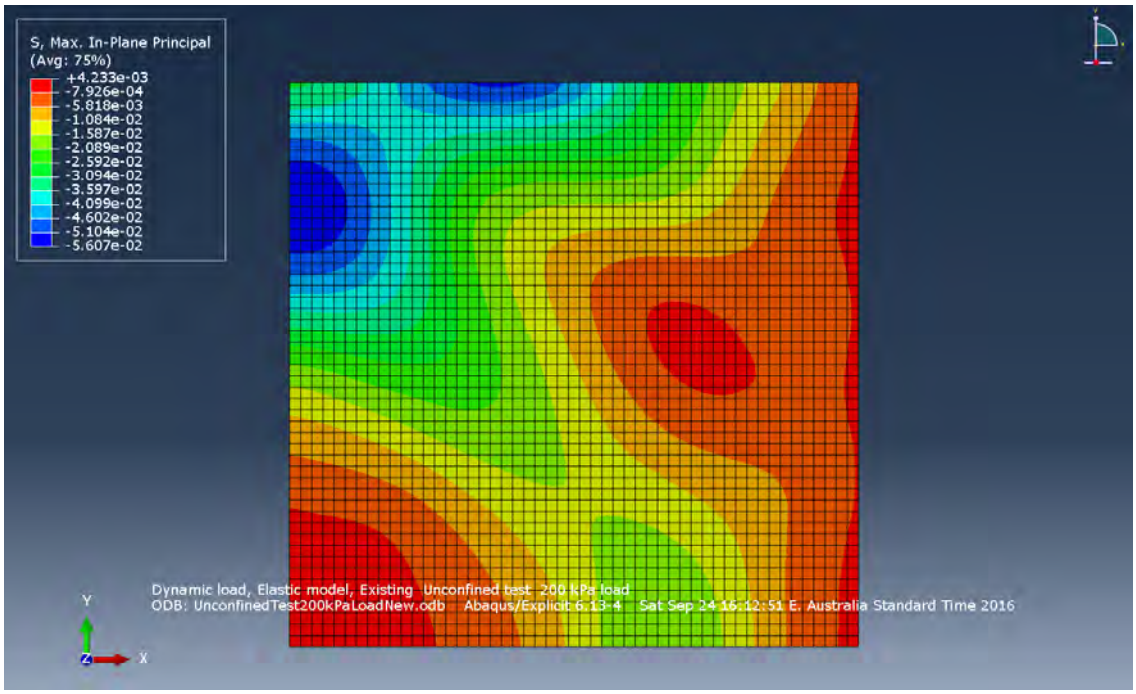

Figure 2: Existing unconfined test for a 100/ 100mm section (200 kPa load) – Max, In-Plane Principal stress.

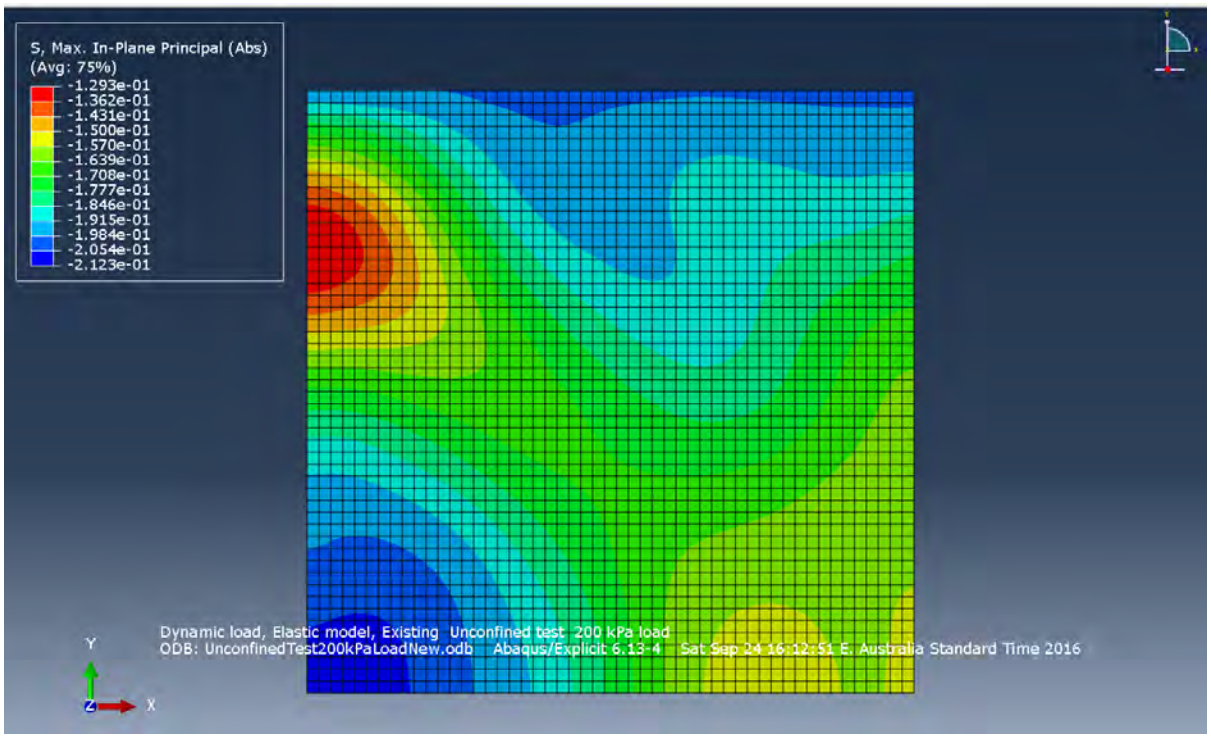

Figure 3: Existing unconfined test for a 100/ 100mm section (200 kPa load) – Max, In-Plane Principal (Abs) stress.

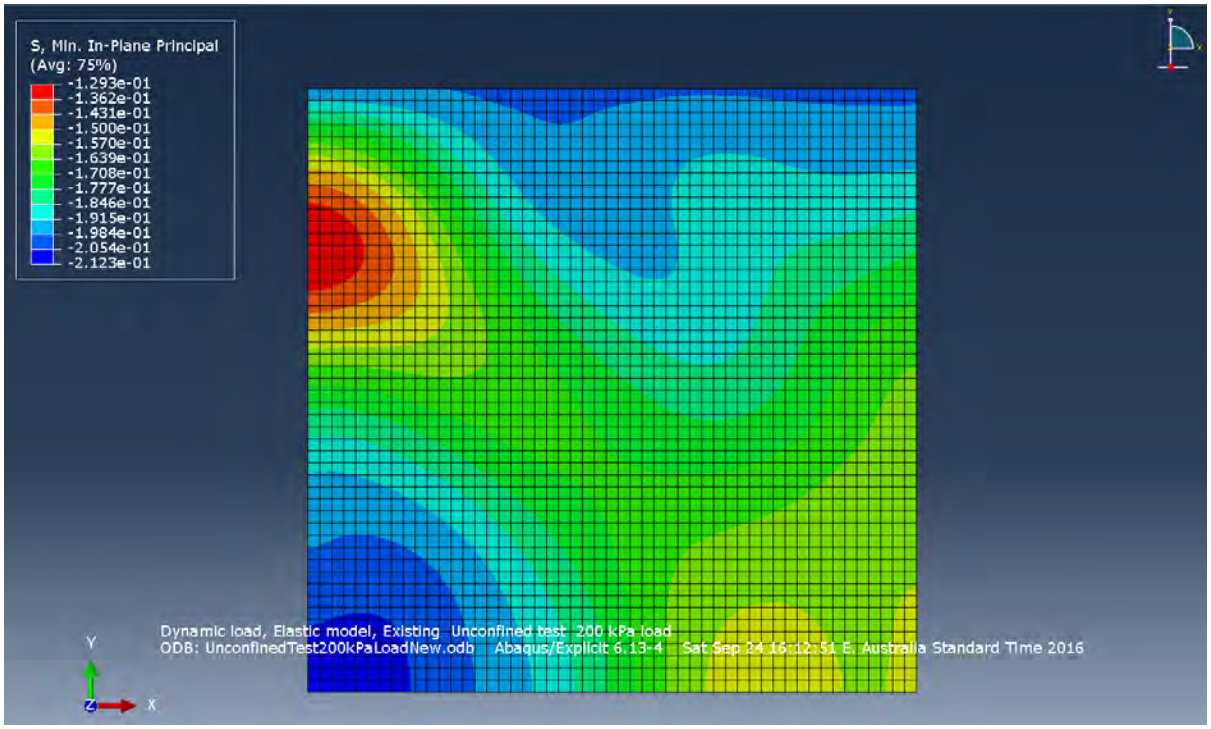

Figure 4: Existing unconfined test for a 100/ 100mm section (200 kPa load) – Min, In-Plane Principal stress.

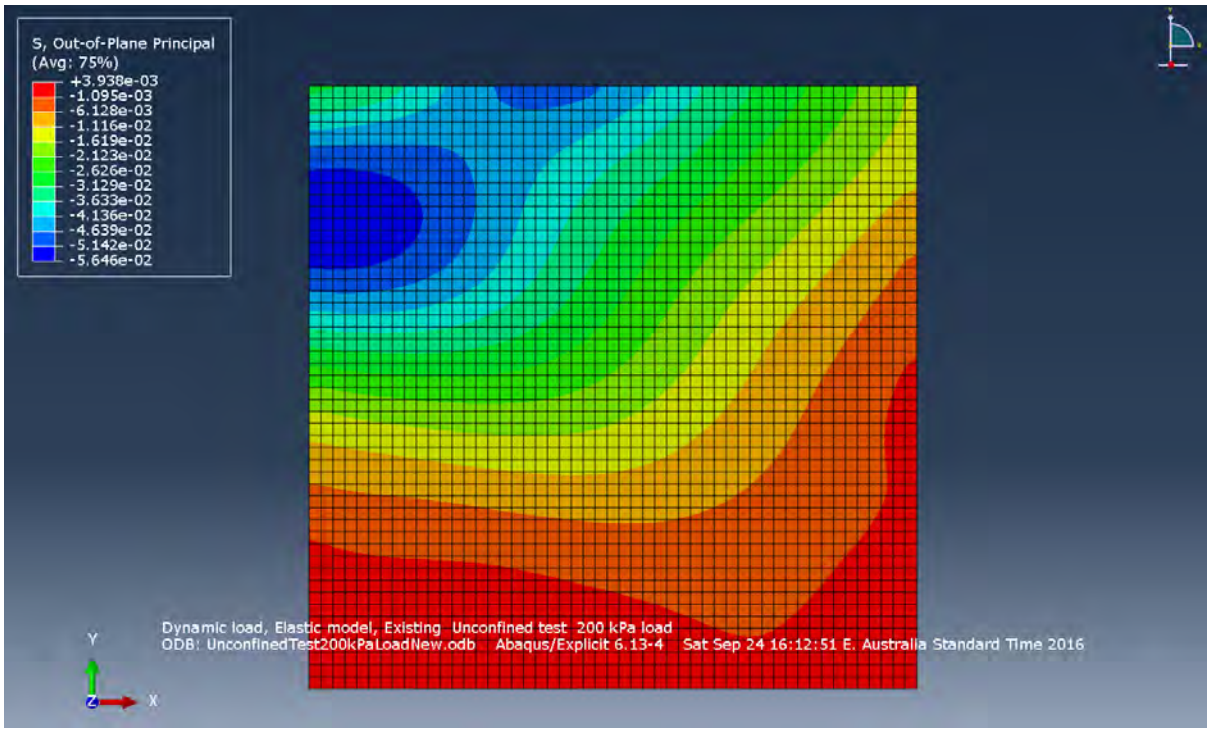

Figure 5: Existing unconfined test for a 100/ 100mm section (200 kPa load) – Out-of-Plane Principal stress.

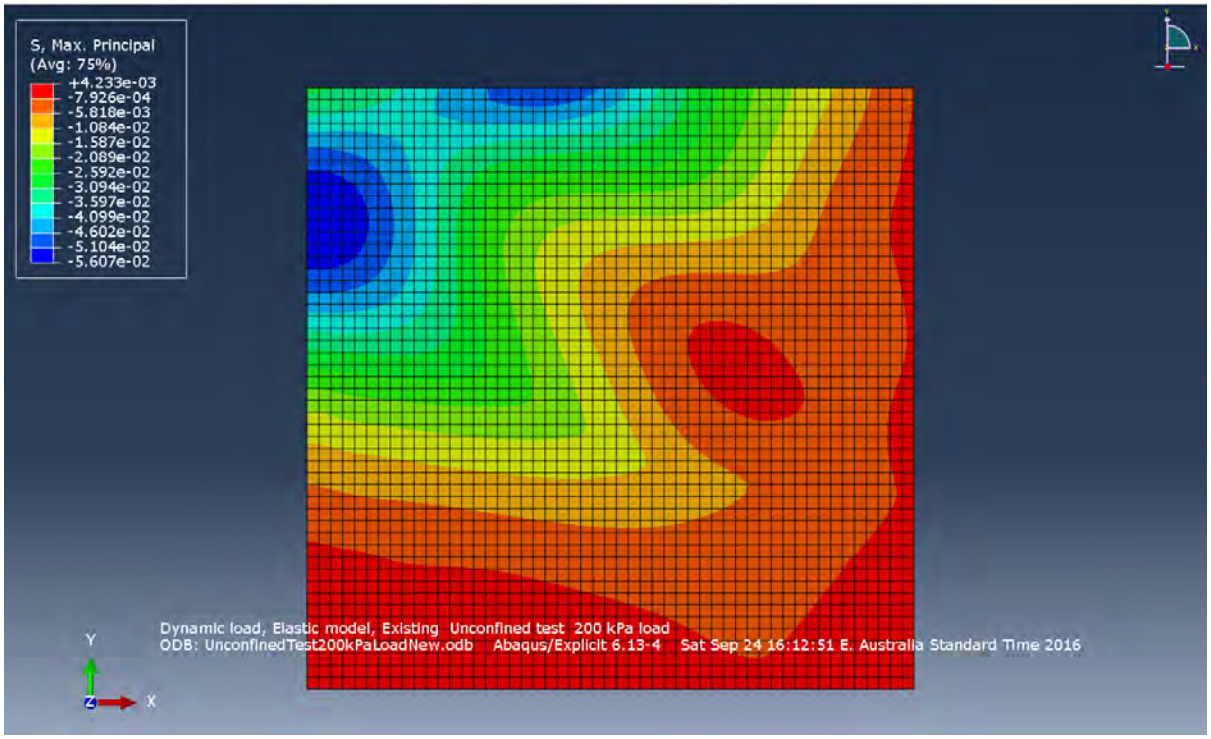

Figure 6: Existing unconfined test for a 100/ 100mm section (200 kPa load) – Max, Principal stress.

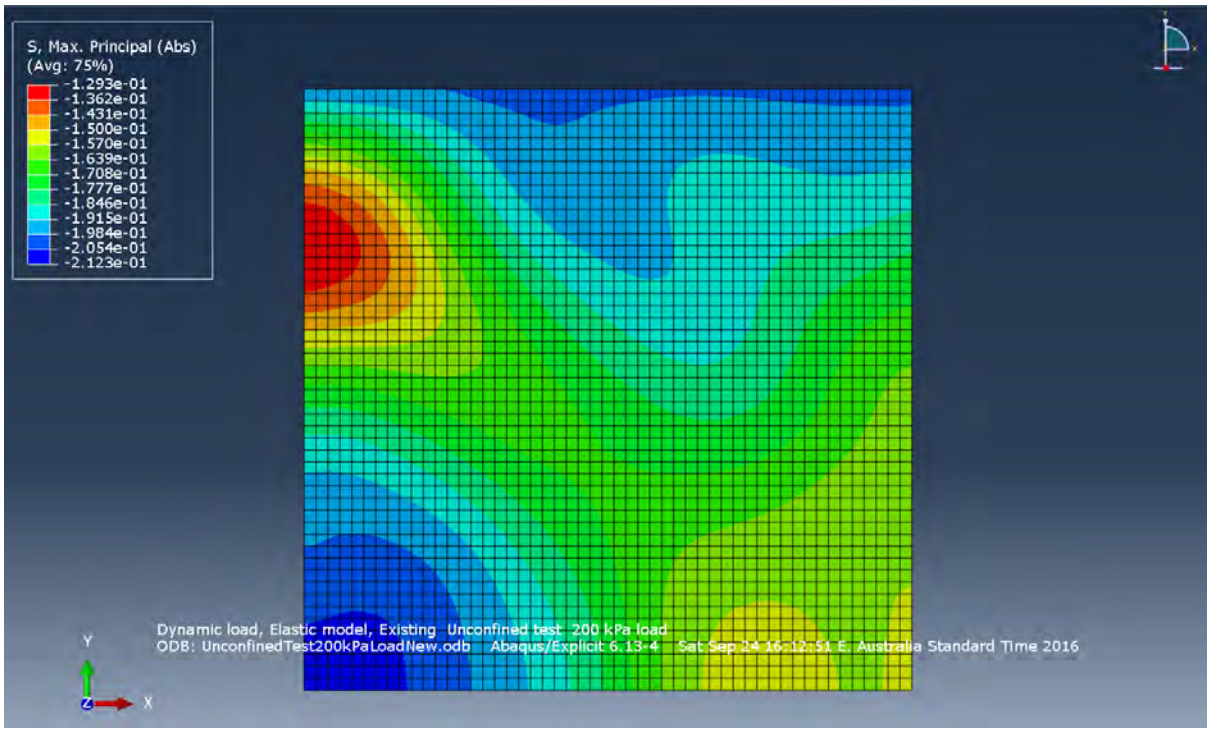

Figure 7: Existing unconfined test for a 100/ 100mm section (200 kPa load) – Max, Principal (Abs) stress.

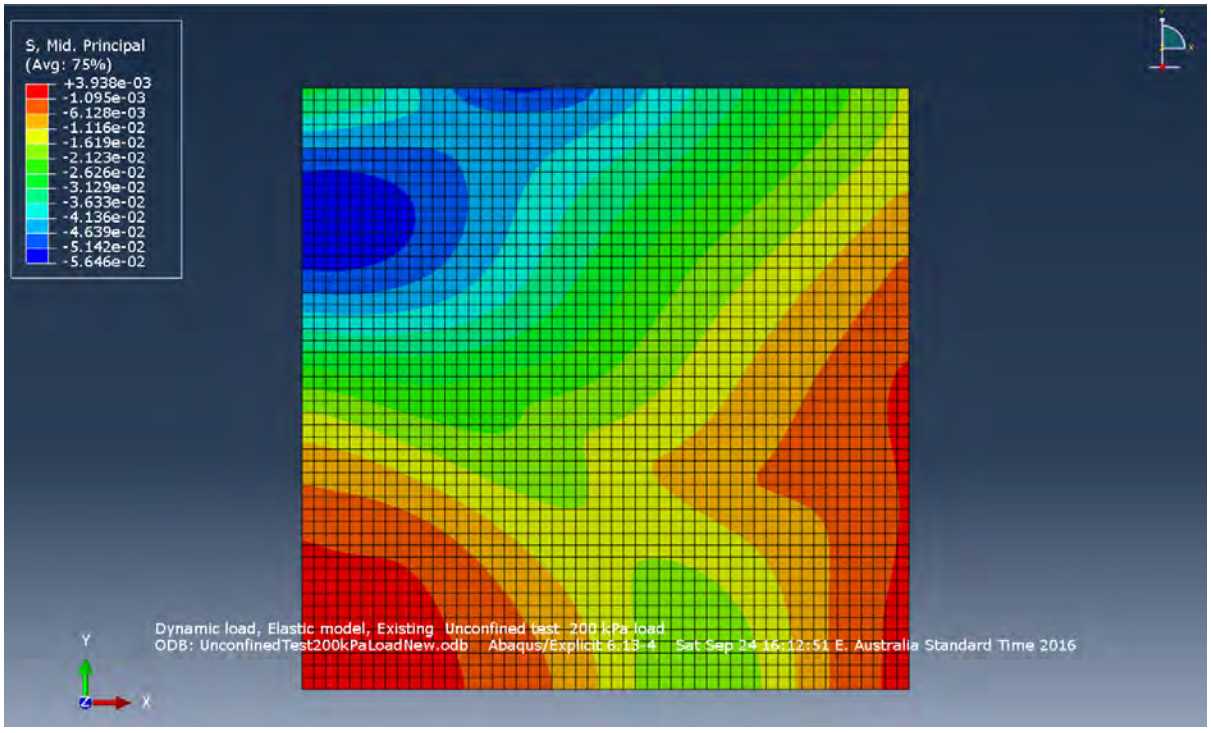

Figure 8: Existing unconfined test for a 100/ 100mm section (200 kPa load) –Mid. Principal stress.

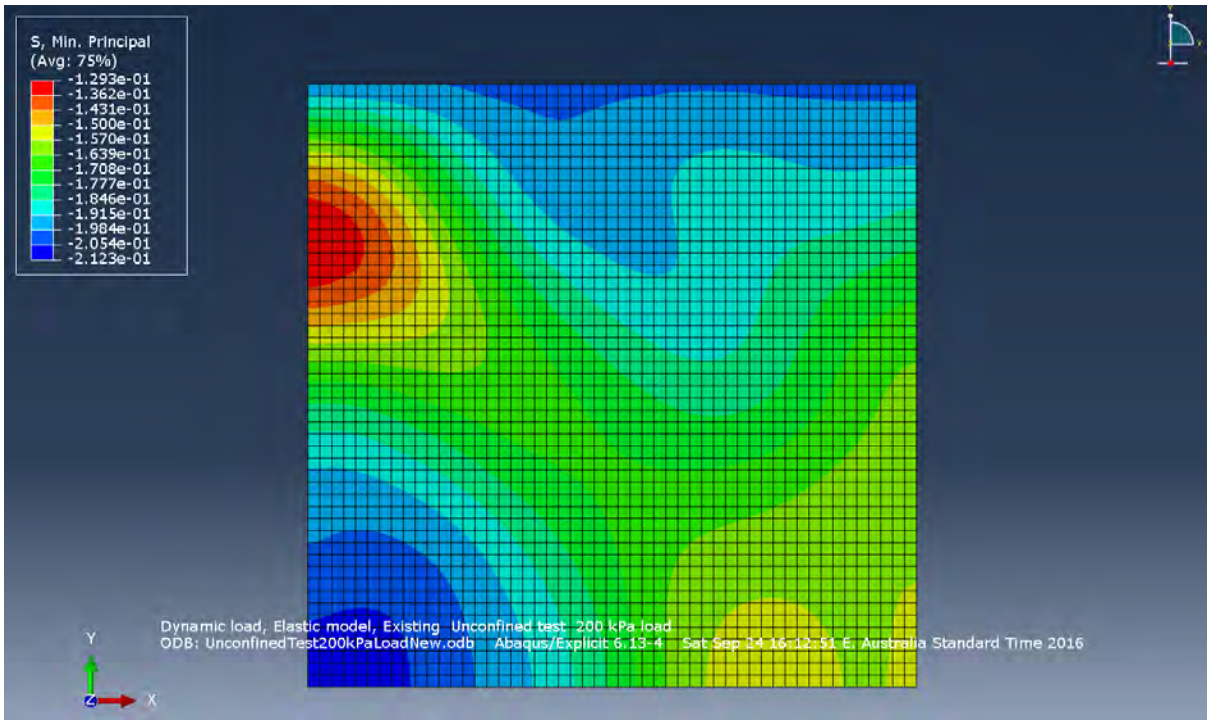

Figure 9: Existing unconfined test for a 100/ 100mm section (200 kPa load) – Min. Principal stress.

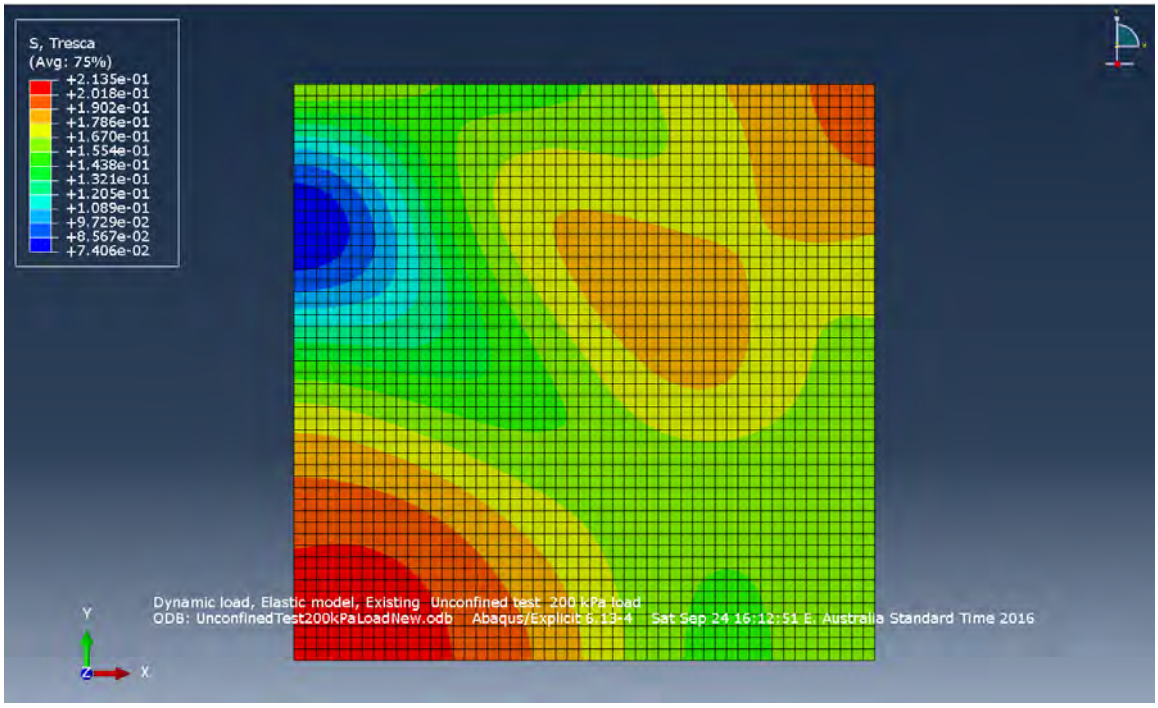

Figure 10: Existing unconfined test for a 100/ 100mm section (200 kPa load) – Tresca stress.

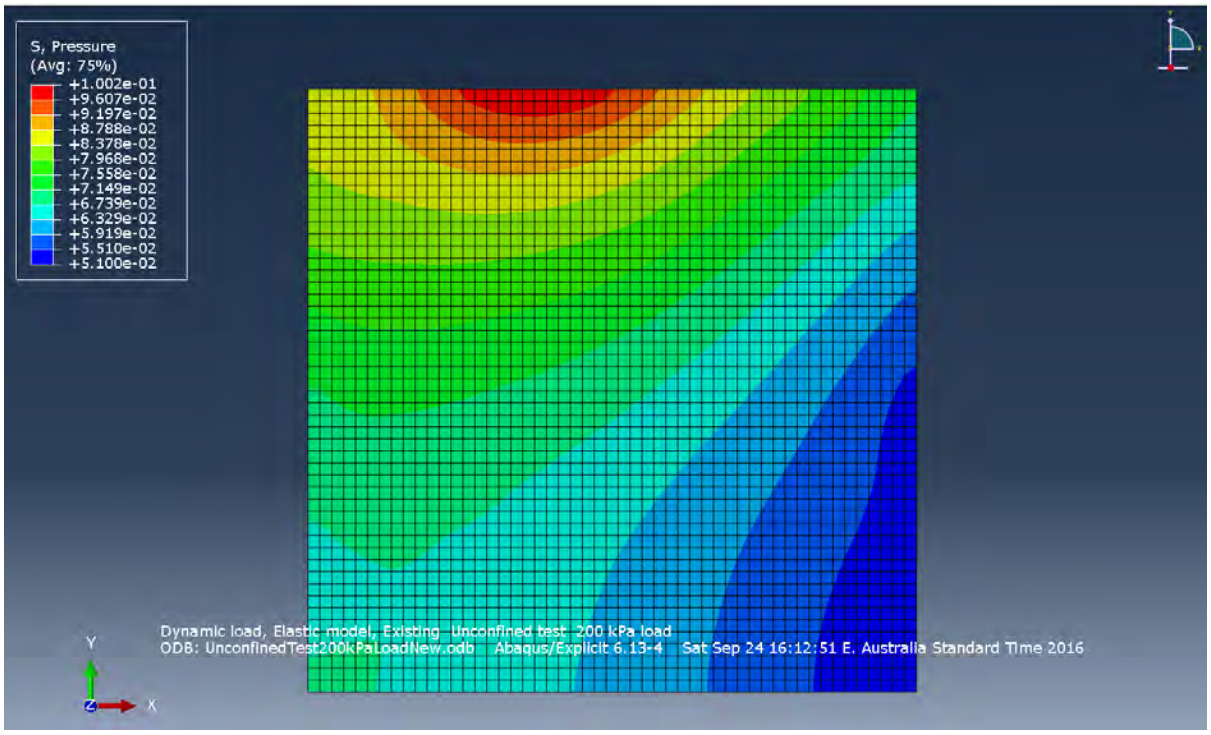

Figure 11: Existing unconfined test for a 100/ 100mm section (200 kPa load) – Pressure.

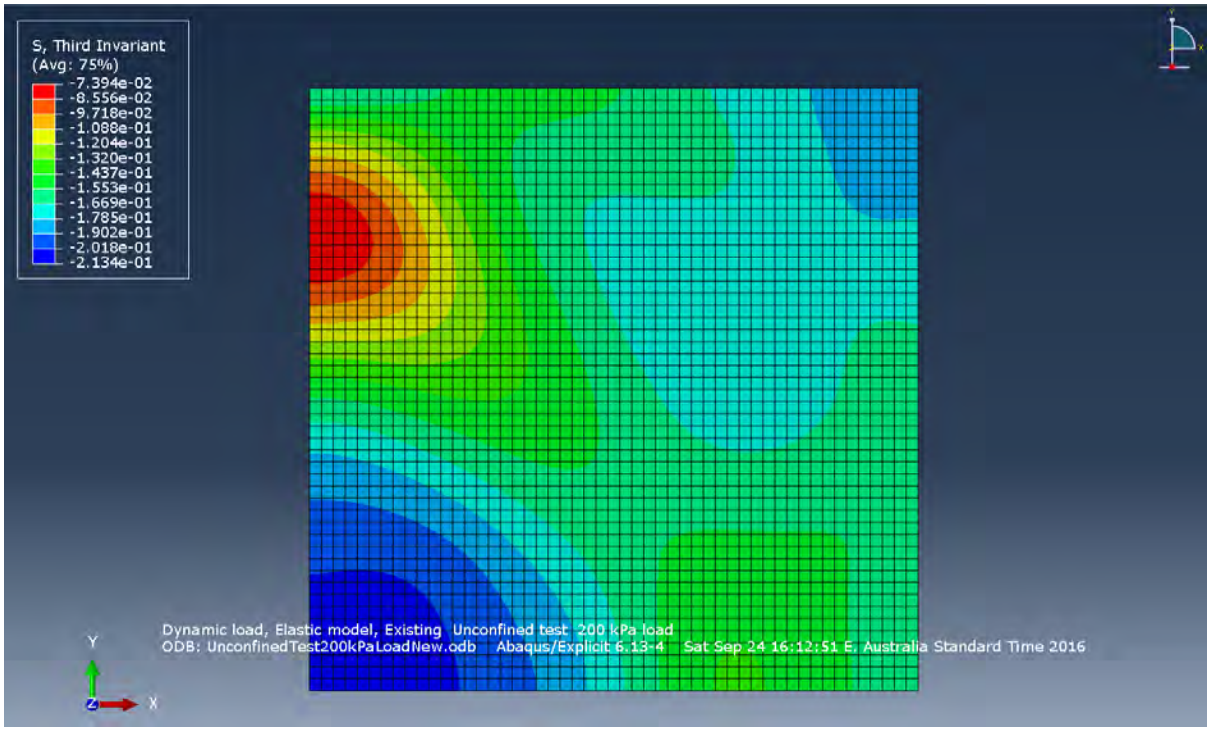

Figure 12: Existing unconfined test for a 100/ 100mm section (200 kPa load) –Third Invariant stress.

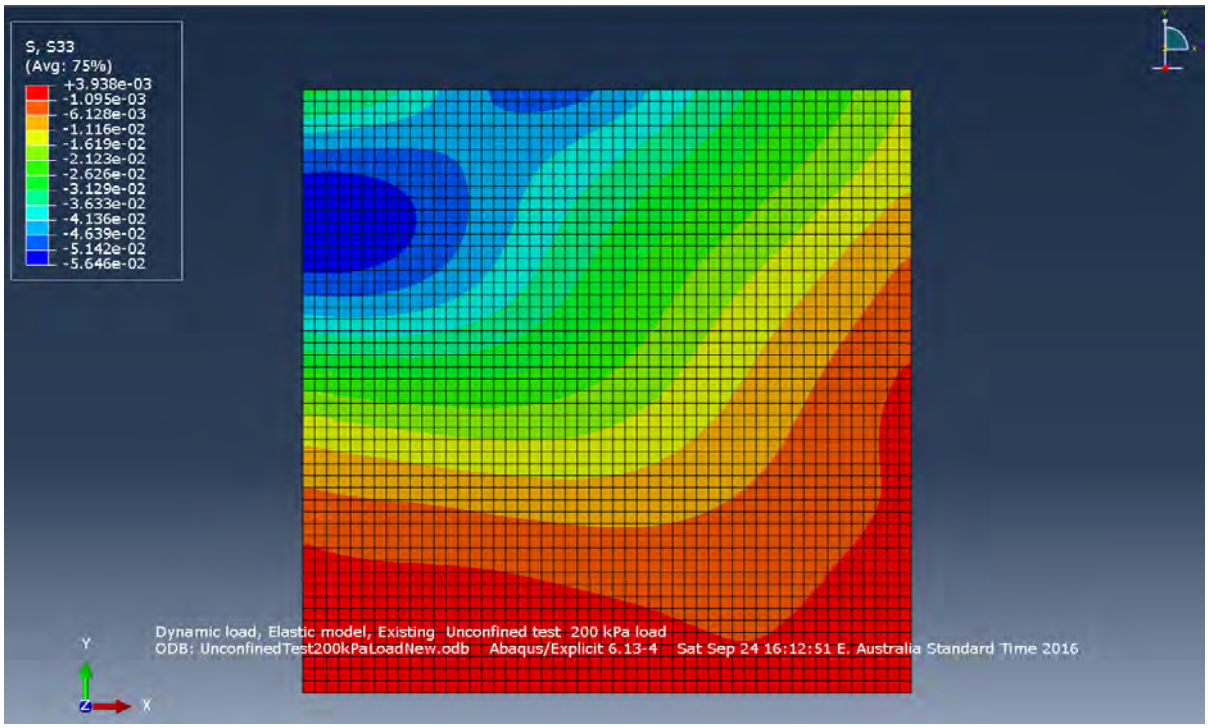

Figure 13: Existing unconfined test for a 100/ 100mm section (200 kPa load) – S33 stress (stress in the Z direction).

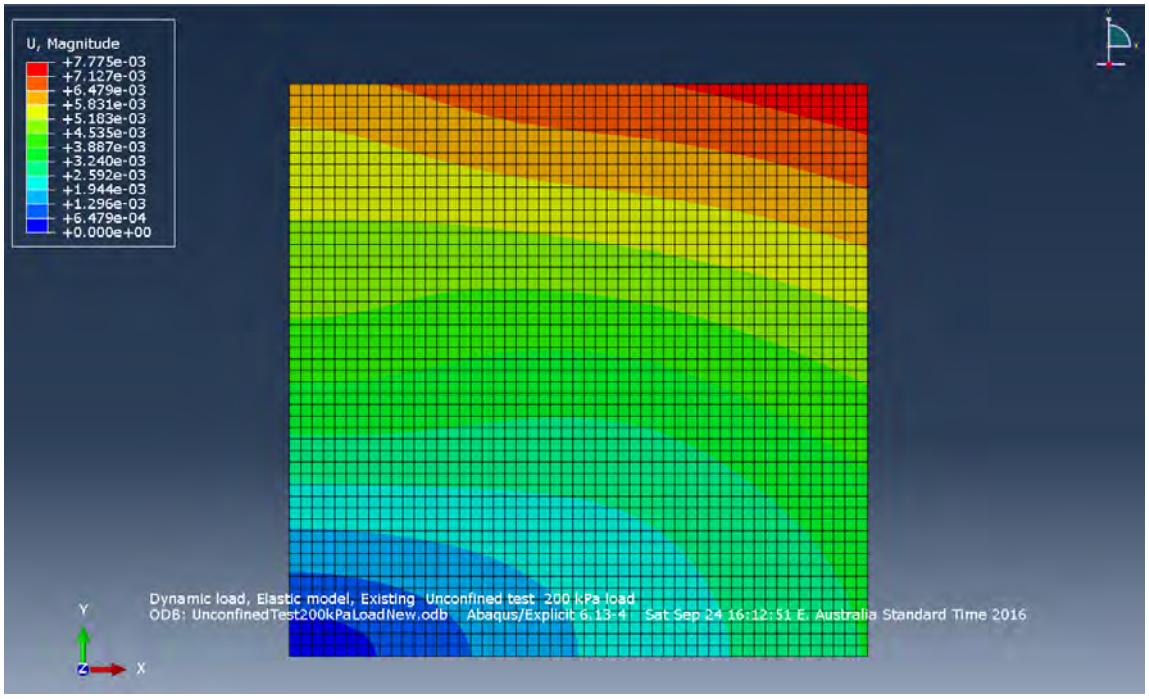

Figure 14: Existing unconfined test for a 100/ 100mm section (200 kPa load) – U (deformation) Magnitude.

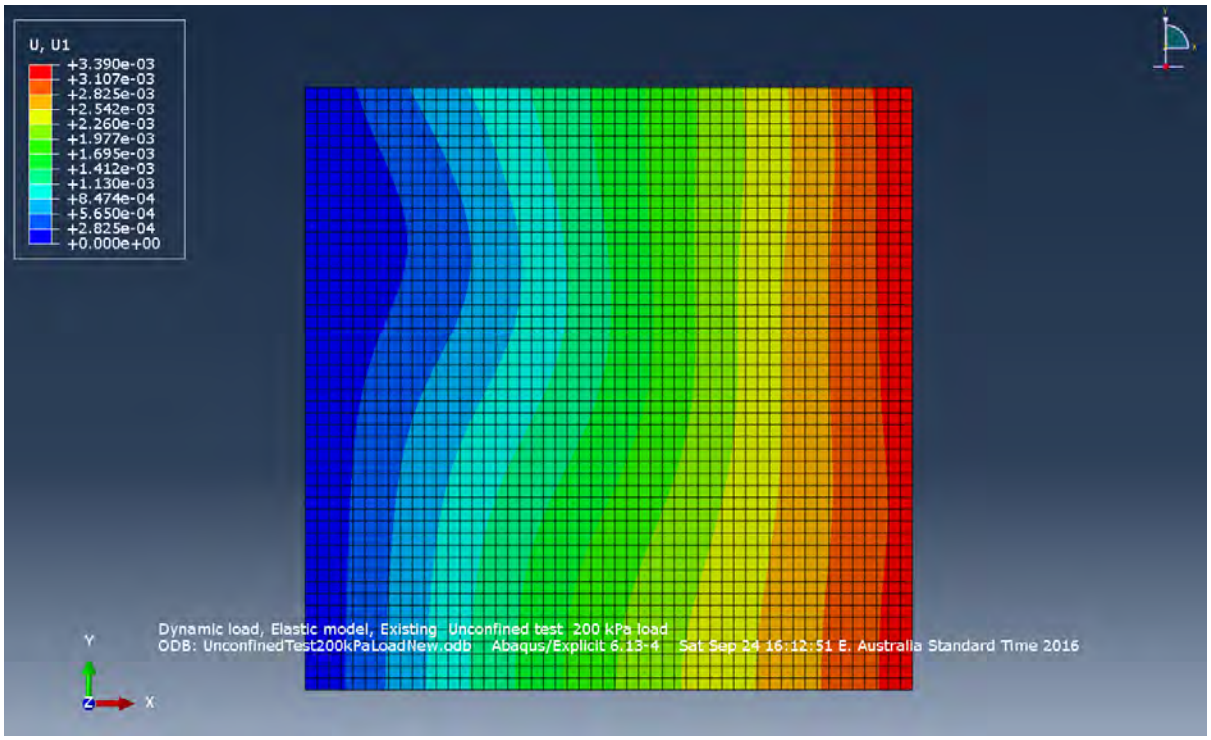

Figure 15: Existing unconfined test for a 100/ 100mm section (200 kPa load) – U1 (deformation in the X direction).

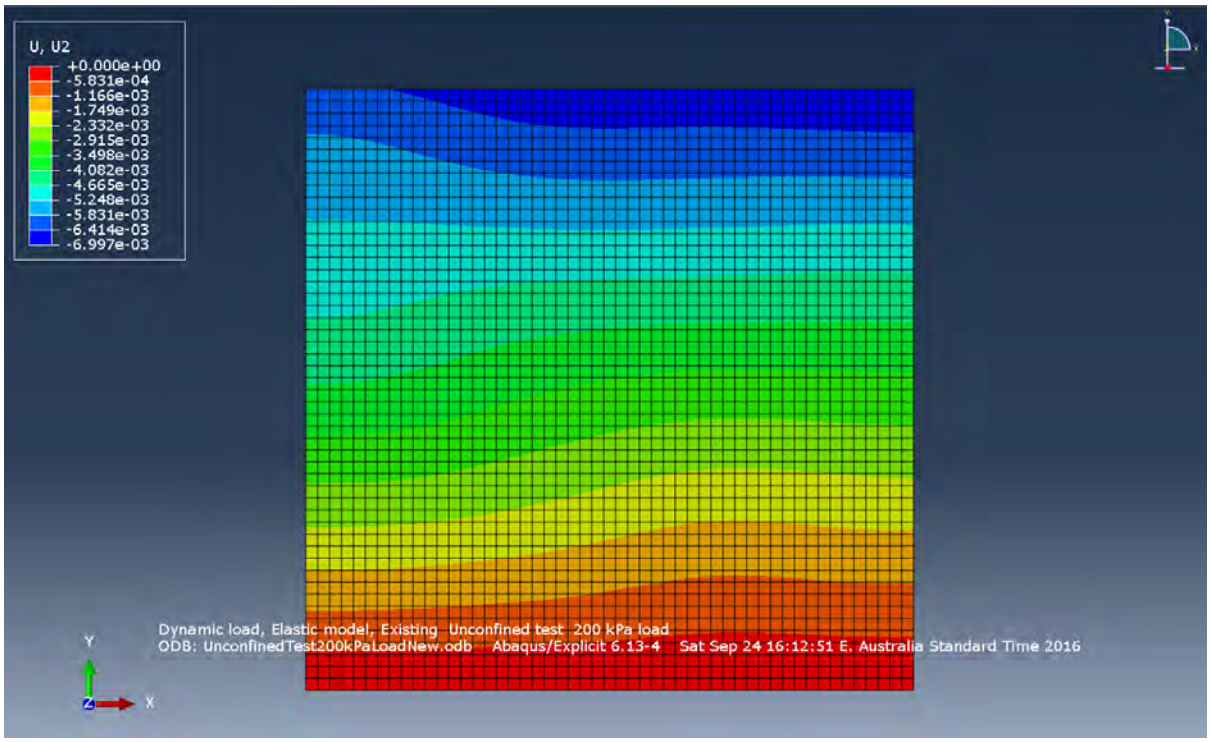

Figure 16: Existing unconfined test for a 100/ 100mm section (200 kPa load) – U2 (deformation in the Y direction).

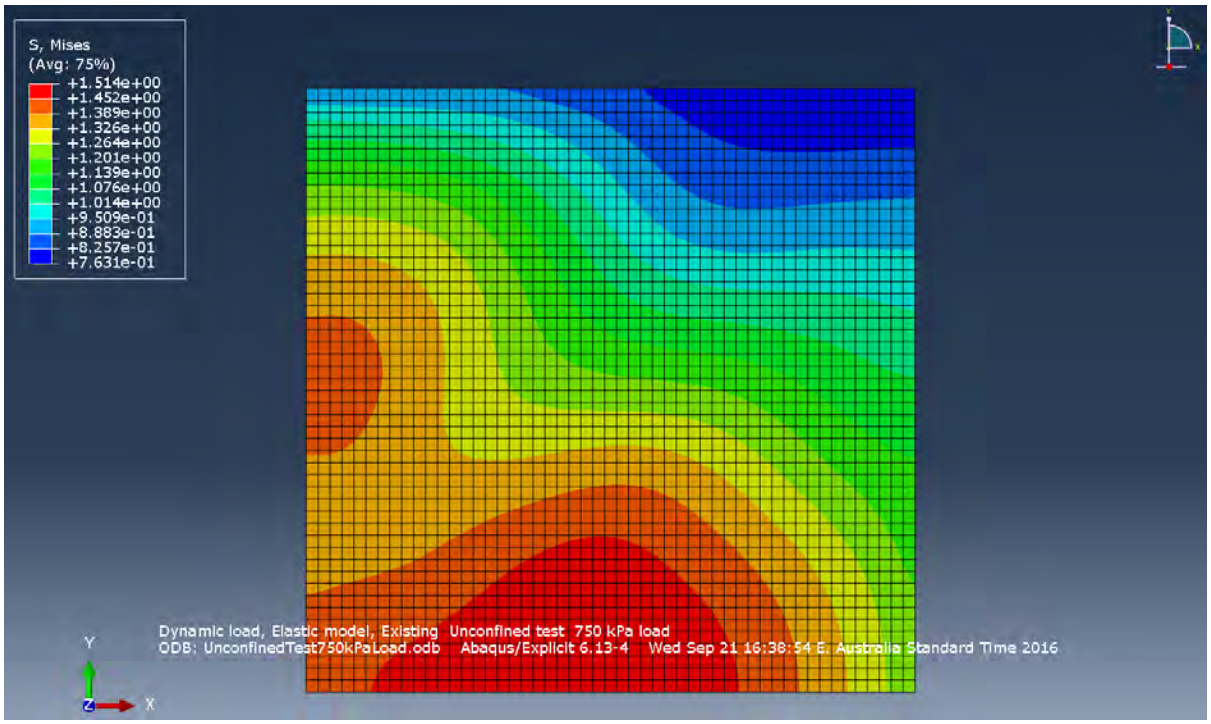

Figure 17: Existing unconfined test for a 100/ 100mm section (750 kPa load) – Mises stress.

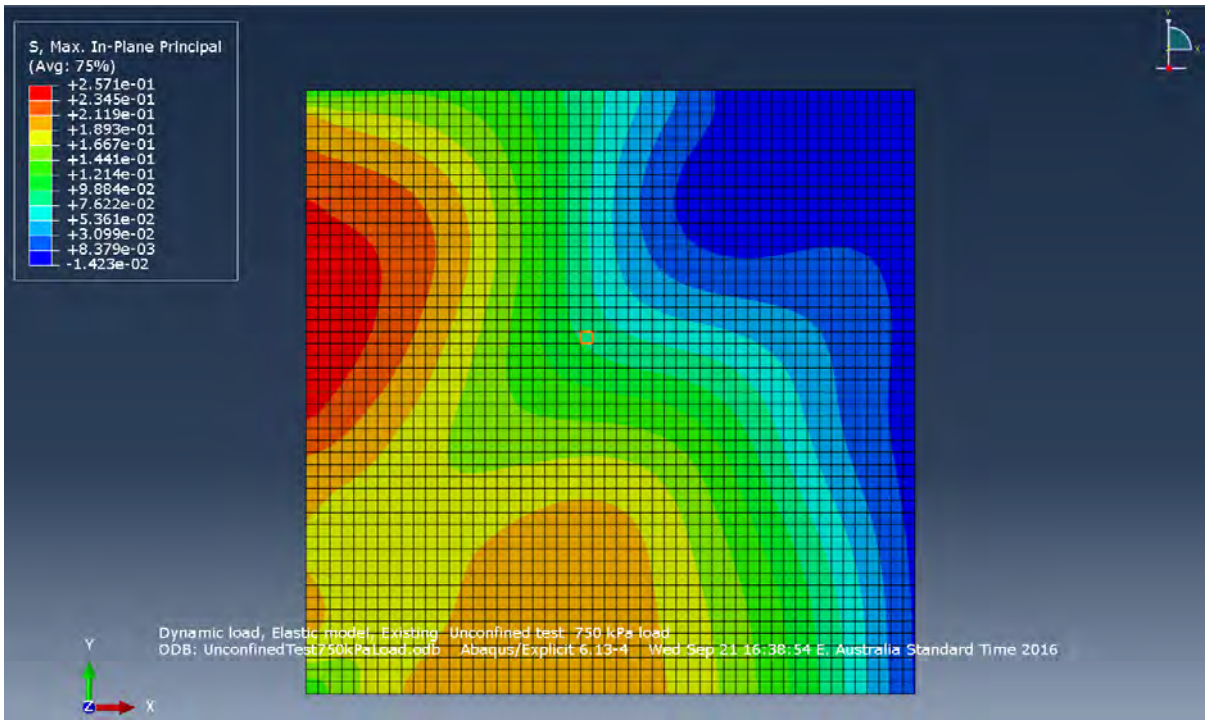

Figure 18: Existing unconfined test for a 100/ 100mm section (750 kPa load) – Max, In-Plane Principal stress.

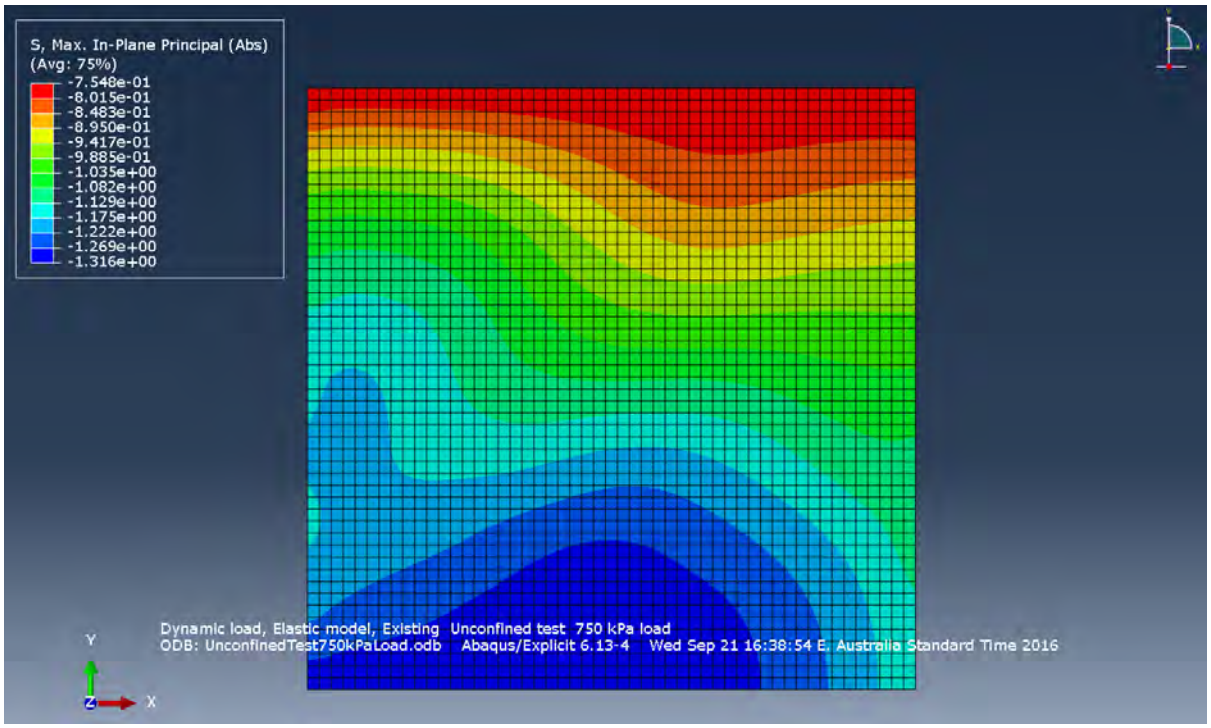

Figure 19: Existing unconfined test for a 100/ 100mm section (750 kPa load) – Max, In-Plane Principal (Abs) stress.

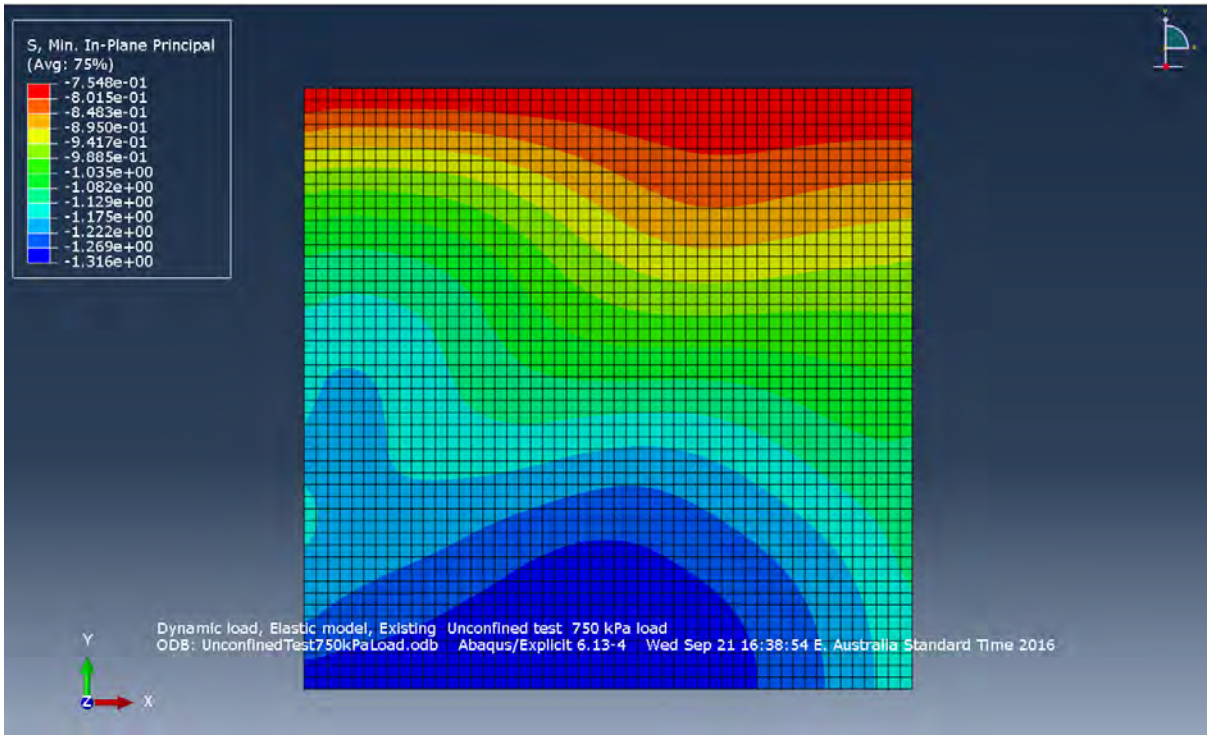

Figure 20: Existing unconfined test for a 100/ 100mm section (750 kPa load) – Min, In-Plane Principal stress.

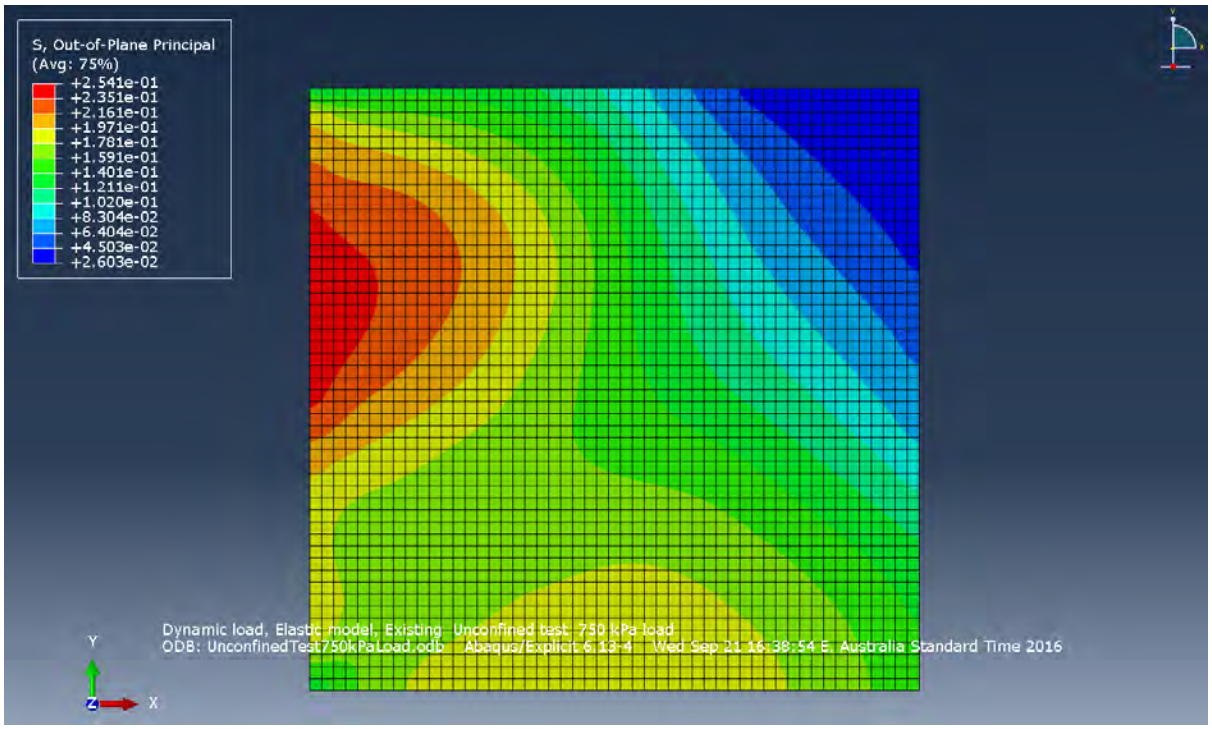

Figure 21: Existing unconfined test for a 100/ 100mm section (750 kPa load) – Out-of-Plane Principal stress.

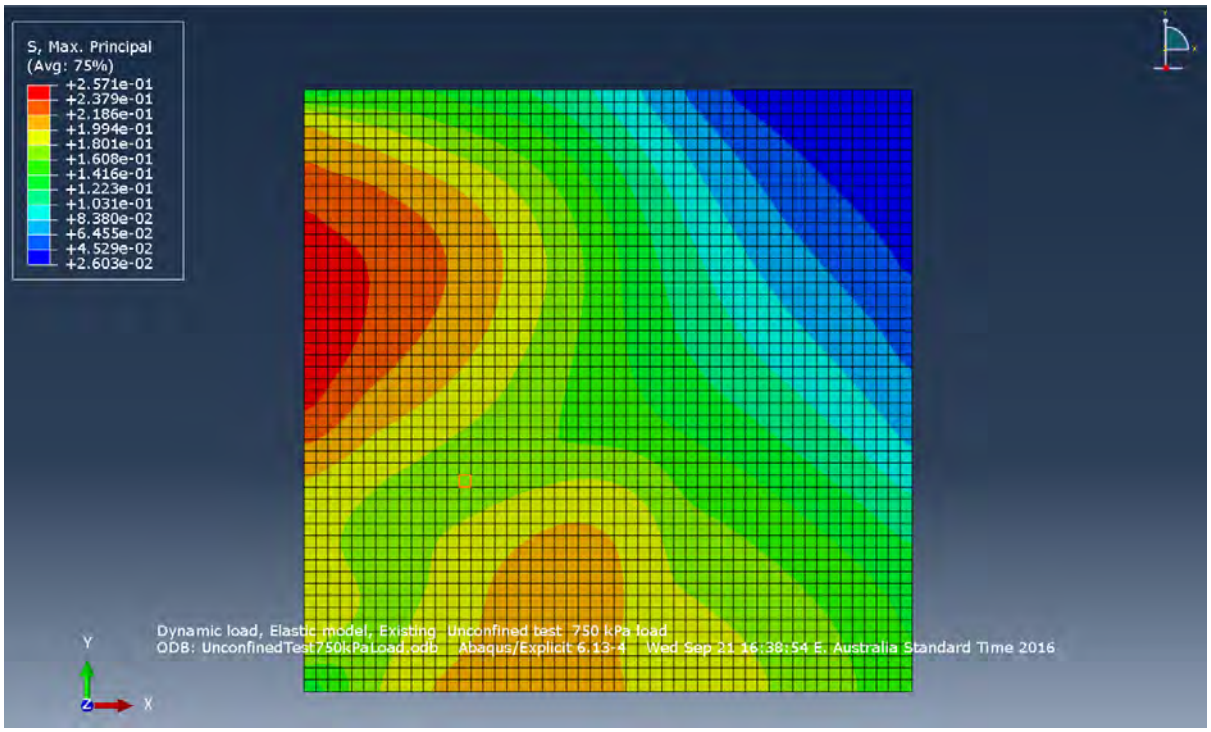

Figure 22: Existing unconfined test for a 100/ 100mm section (750 kPa load) – Max, Principal stress.

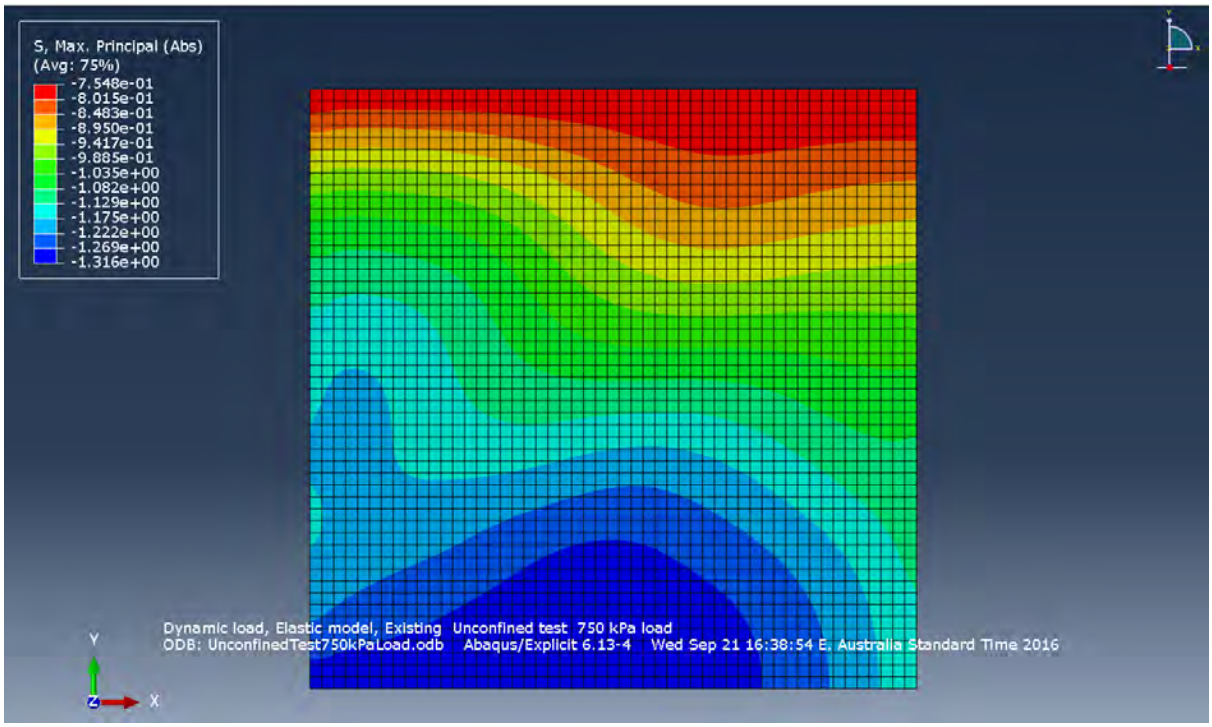

Figure 23: Existing unconfined test for a 100/ 100mm section (750 kPa load) – Max, Principal (Abs) stress.

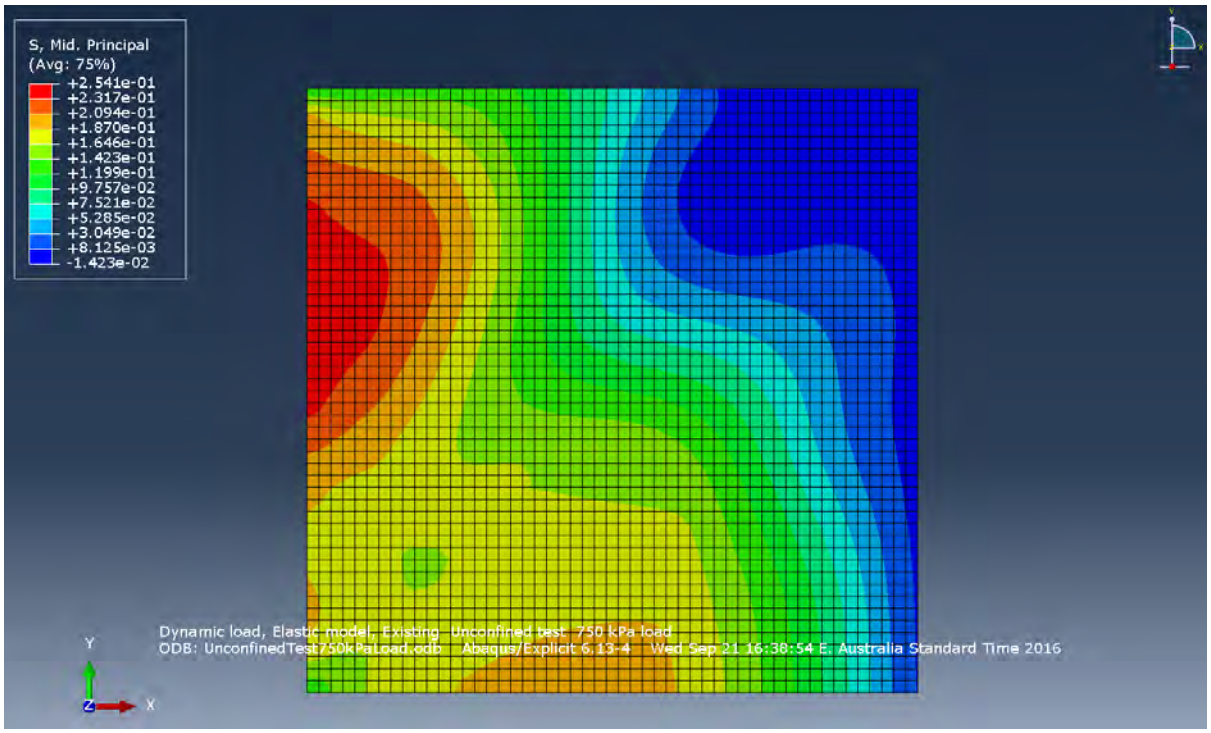

Figure 24: Existing unconfined test for a 100/ 100mm section (750 kPa load) –Mid. Principal stress.

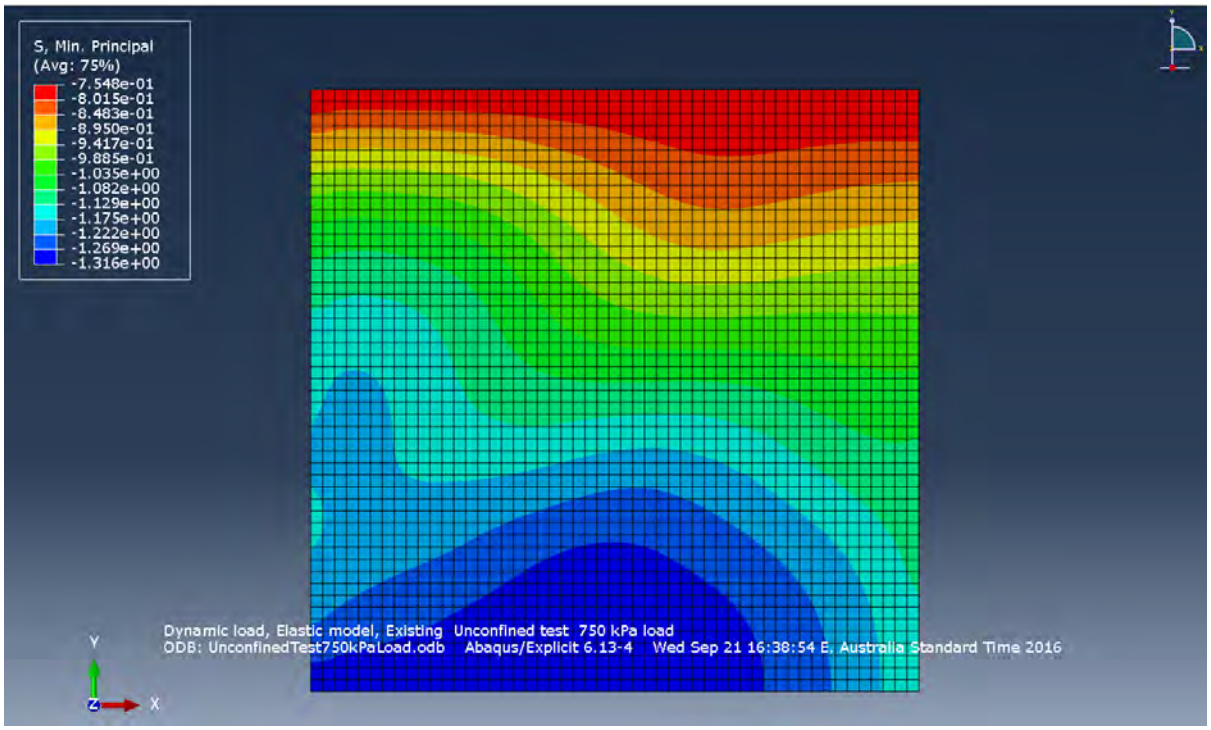

Figure 25: Existing unconfined test for a 100/ 100mm section (750 kPa load) – Min. Principal stress.

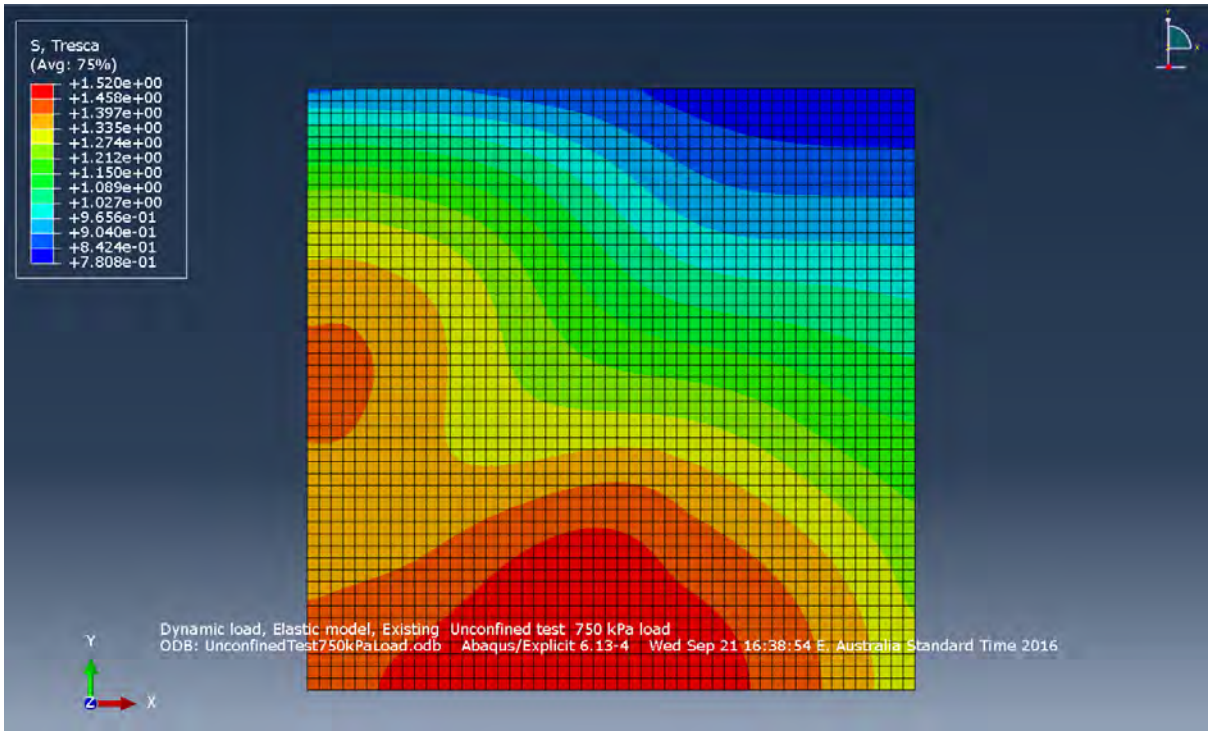

Figure 26: Existing unconfined test for a 100/ 100mm section (750 kPa load) – Tresca stress.

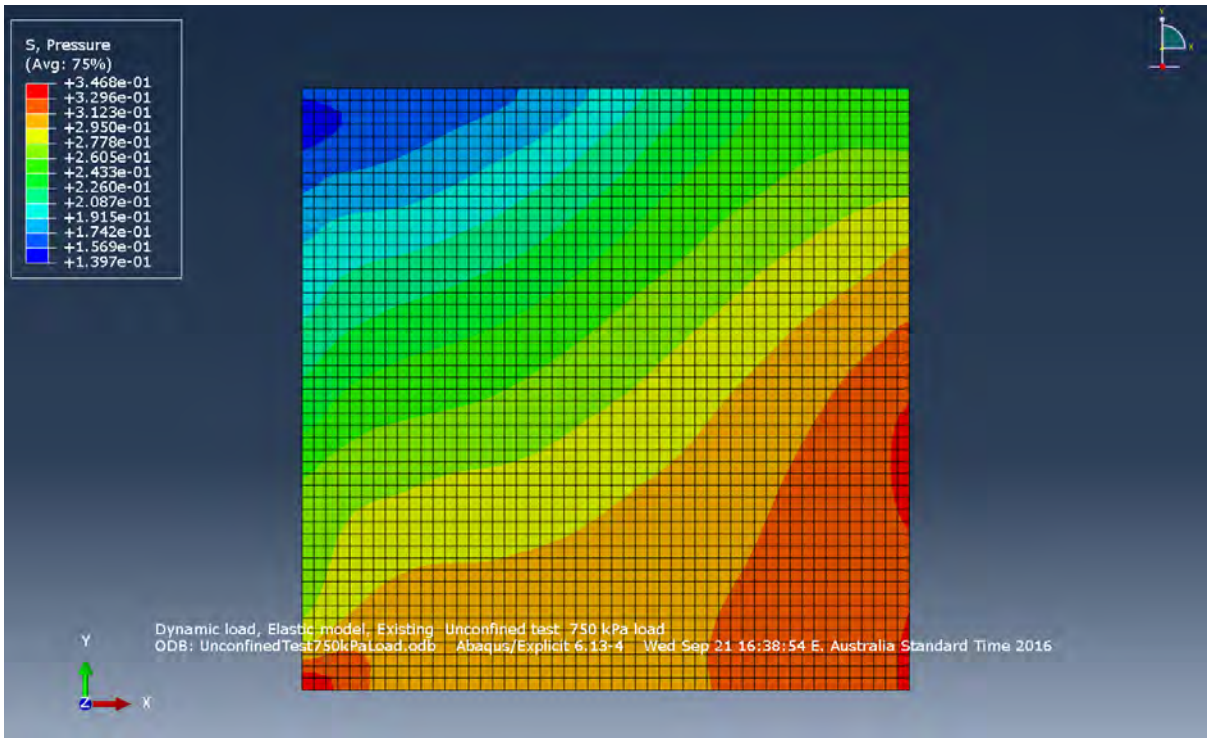

Figure 27: Existing unconfined test for a 100/ 100mm section (750 kPa load) – Pressure.

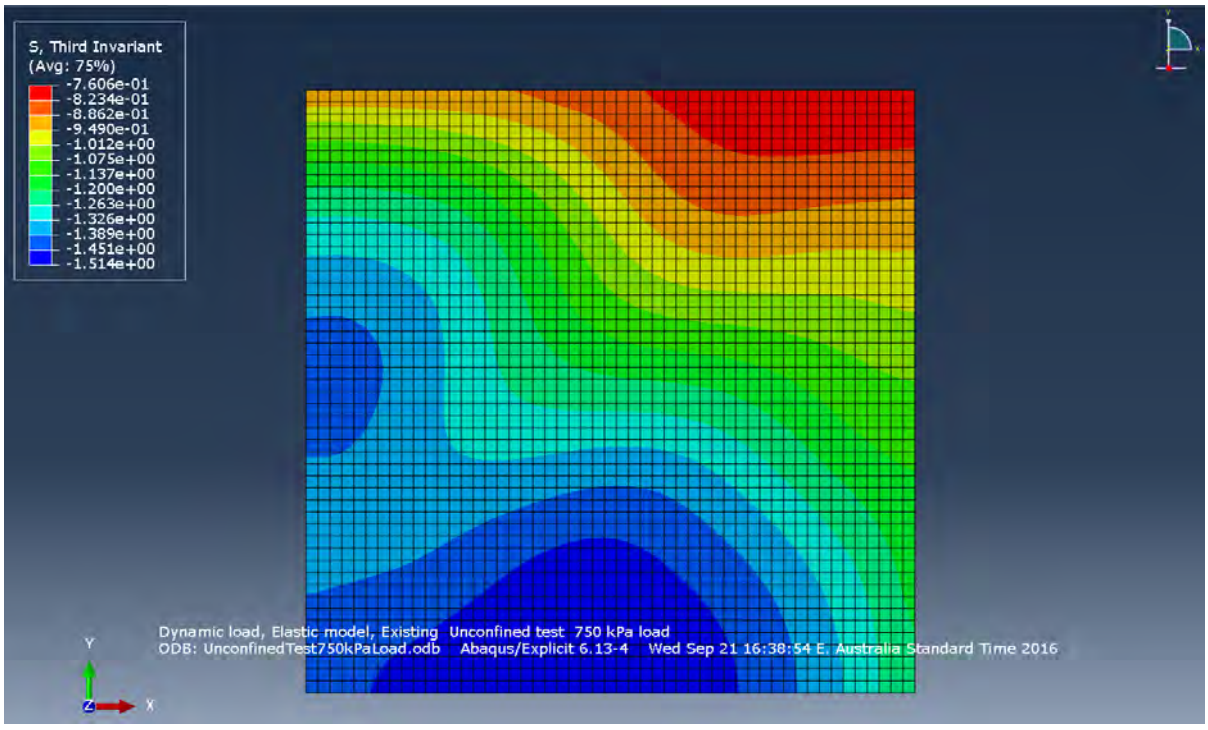

Figure 28: Existing unconfined test for a 100/ 100mm section (750 kPa load) –Third Invariant stress.

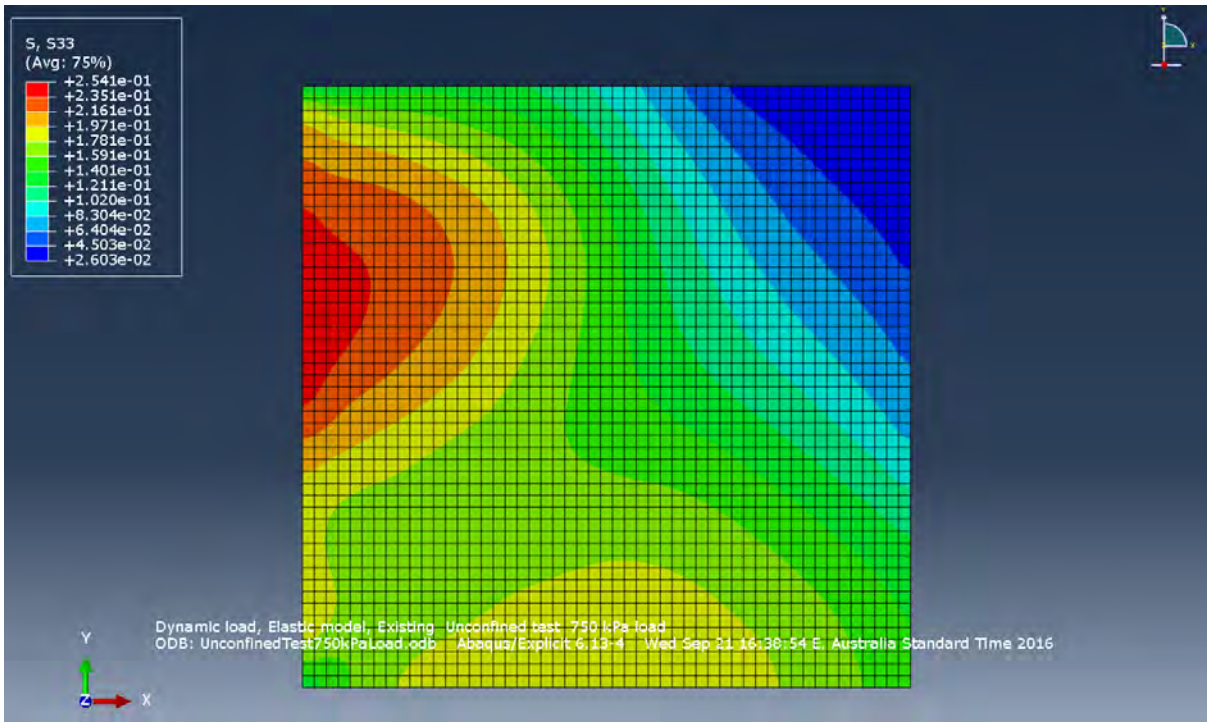

Figure 29: Existing unconfined test for a 100/ 100mm section (750 kPa load) – S33 stress (stress in the Z direction).

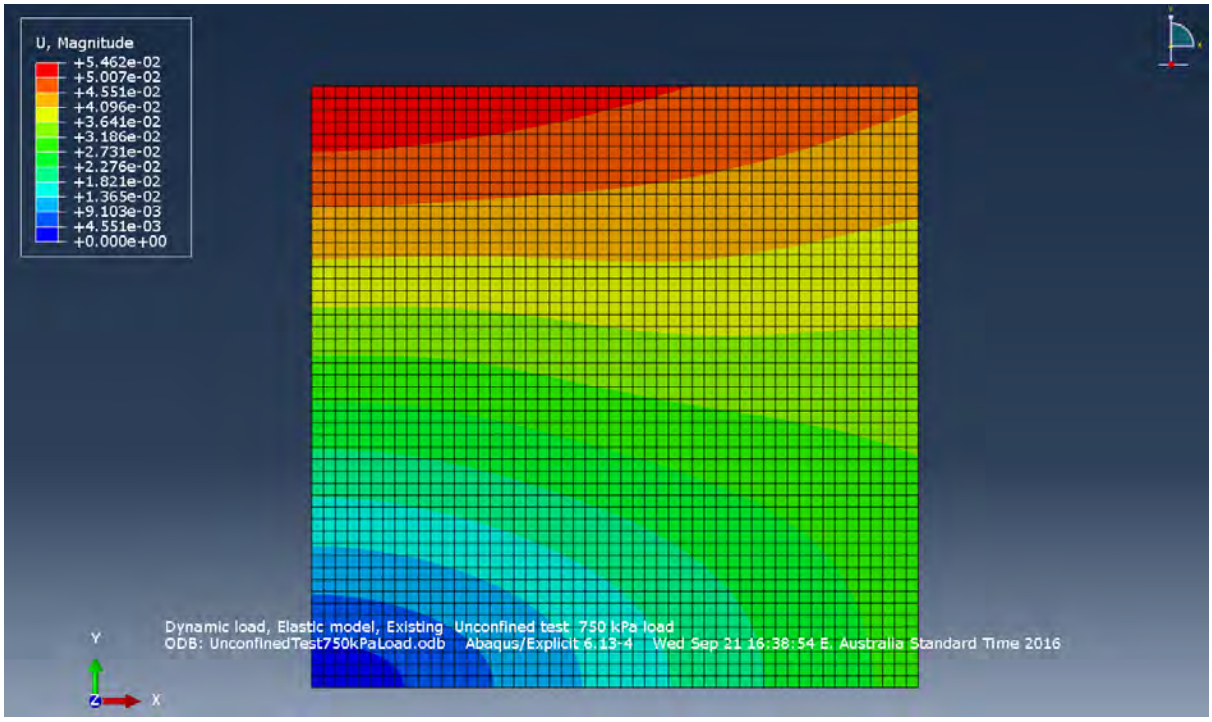

Figure 30: Existing unconfined test for a 100/ 100mm section (750 kPa load) – U (deformation) Magnitude.

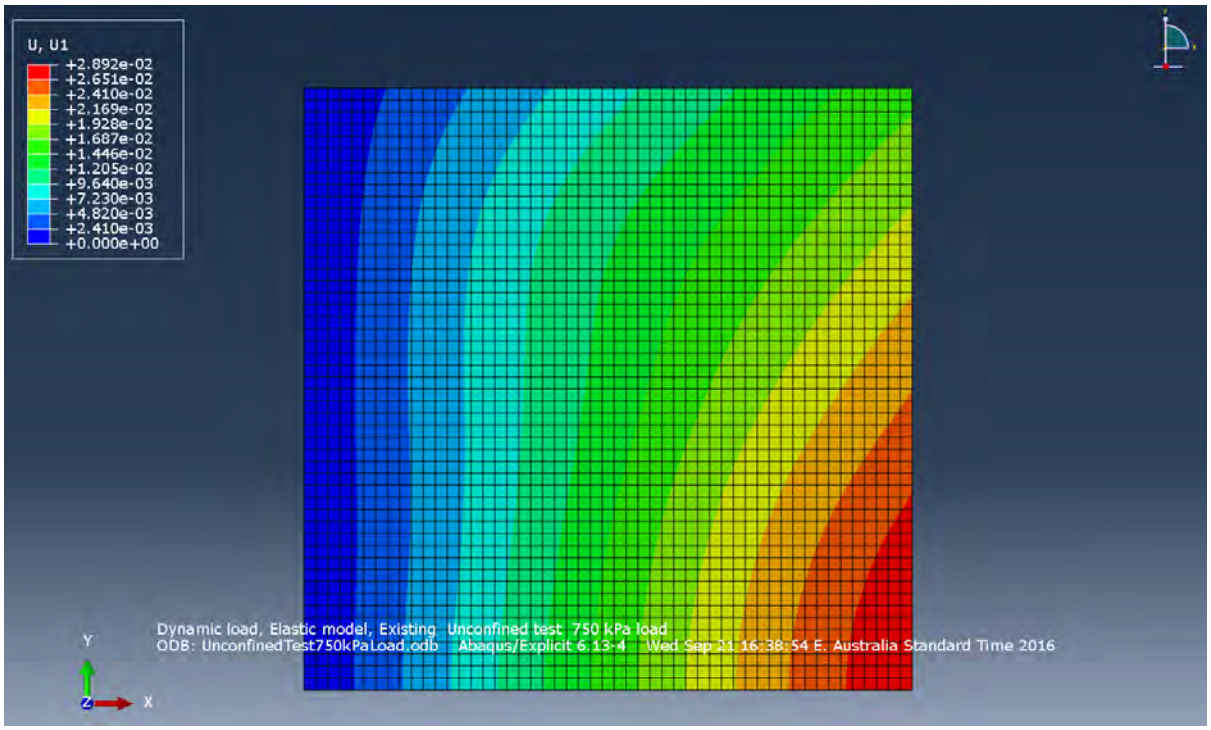

Figure 31: Existing unconfined test for a 100/ 100mm section (750 kPa load) – U1 (deformation in the X direction).

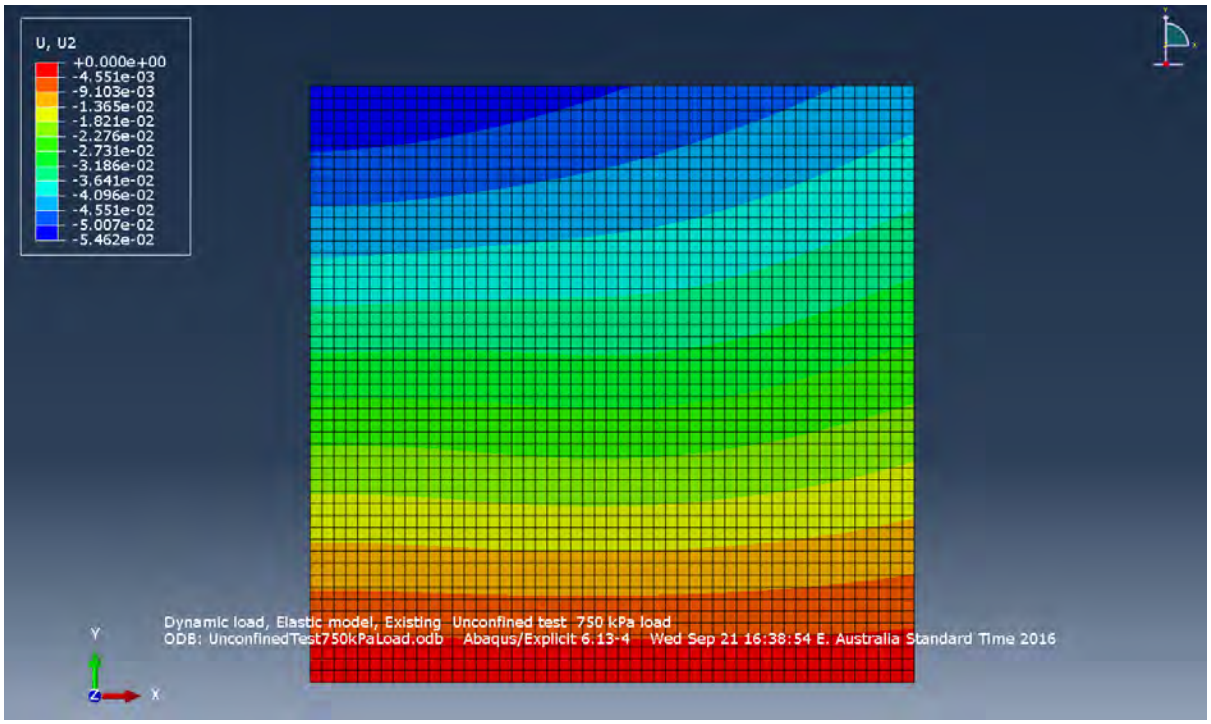

Figure 32: Existing unconfined test for a 100/ 100mm section (750 kPa load) – U2 (deformation in the Y direction).

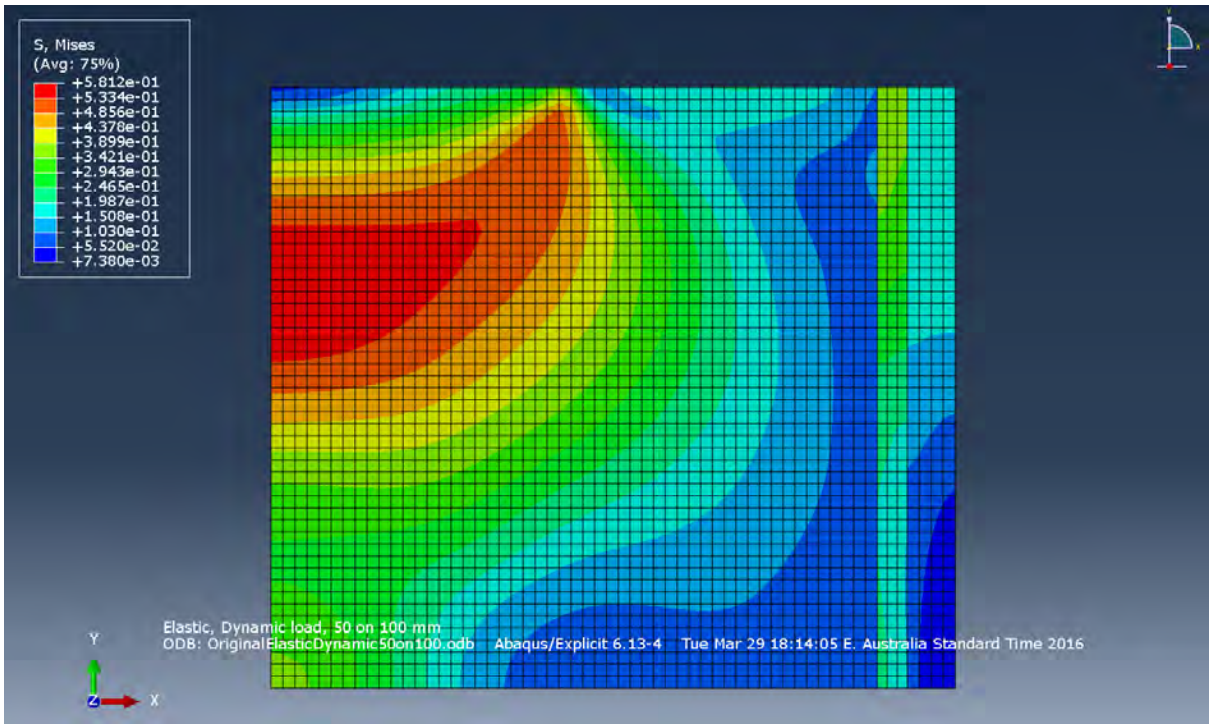

Figure 33: New confined (4mm ring) test for a 50/100mm section – Mises stress.

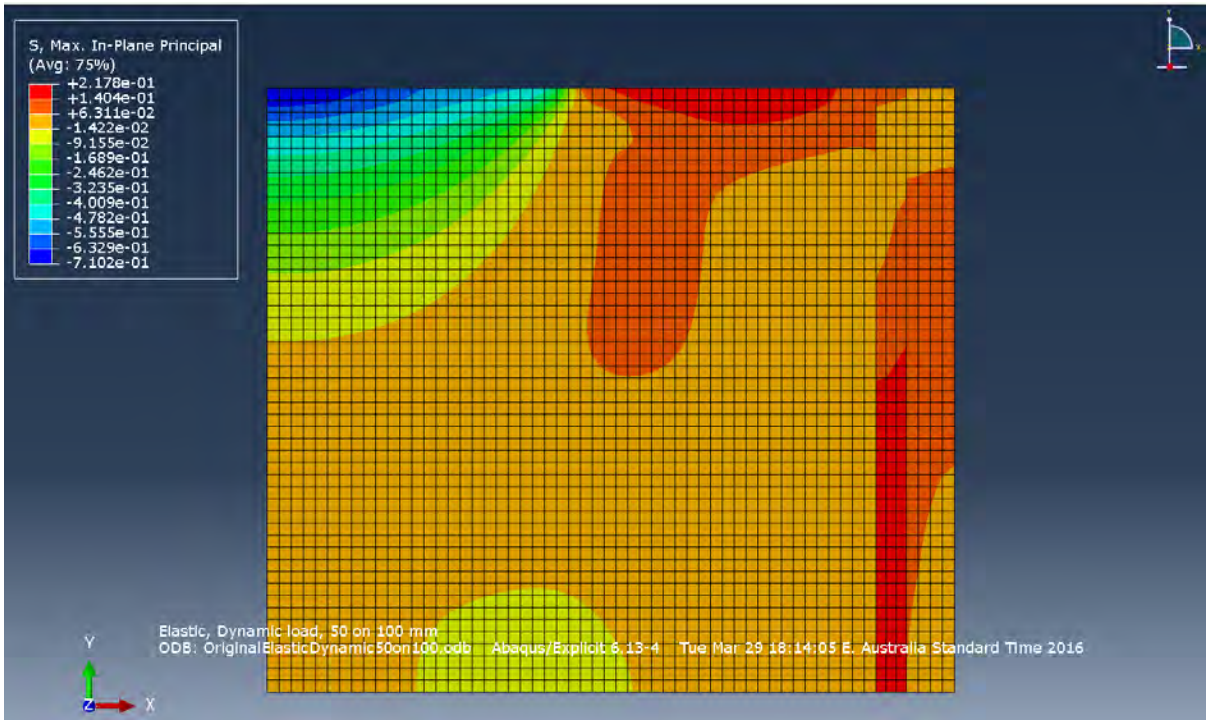

Figure 34: New confined (4mm ring) test for a 50/100mm section – Max, In-Plane Principal stress.

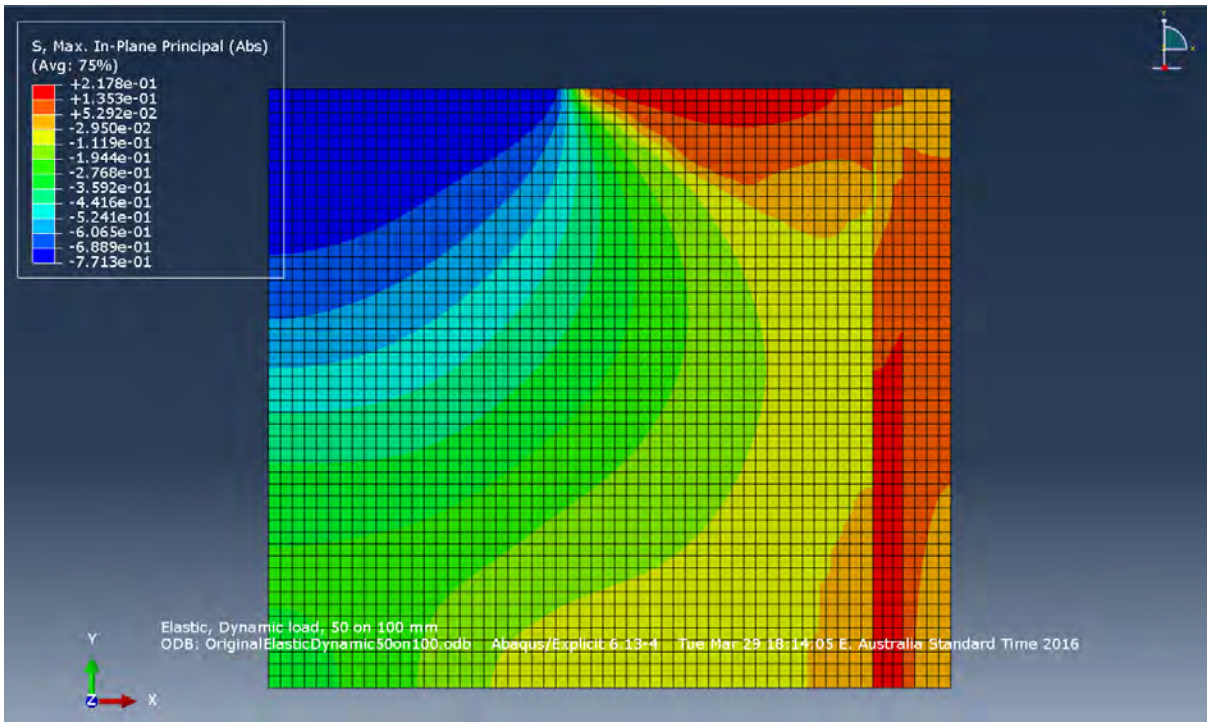

Figure 35: New confined (4mm ring) test for a 50/100mm section – Max, In-Plane Principal (Abs) stress.

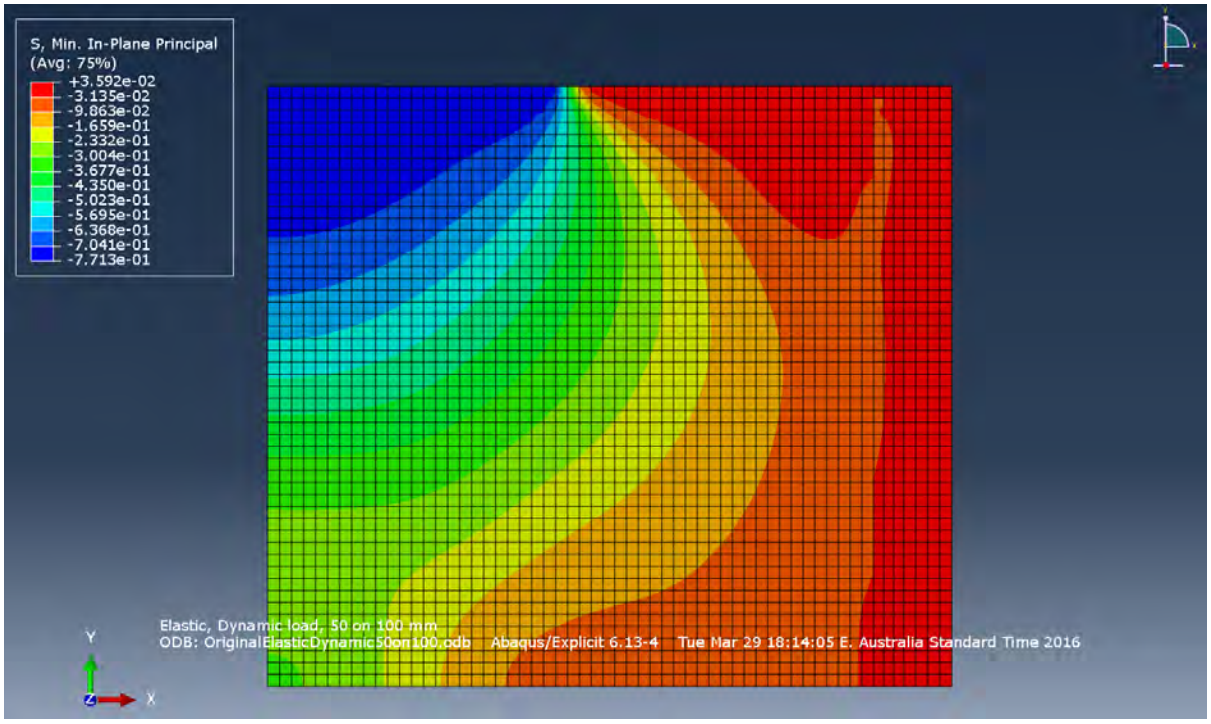

Figure 36: New confined (4mm ring) test for a 50/100mm section – Min, In-Plane Principal stress.

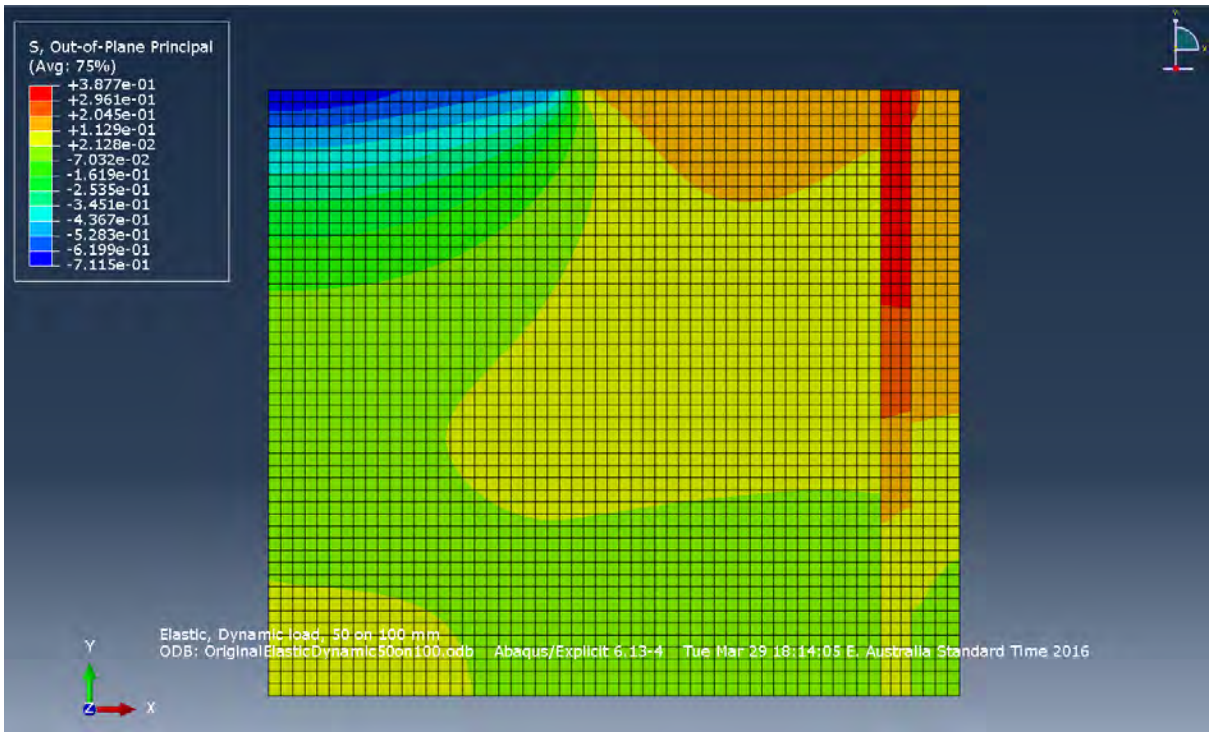

Figure 37: New confined (4mm ring) test for a 50/100mm section – Out-of-Plane Principal stress.

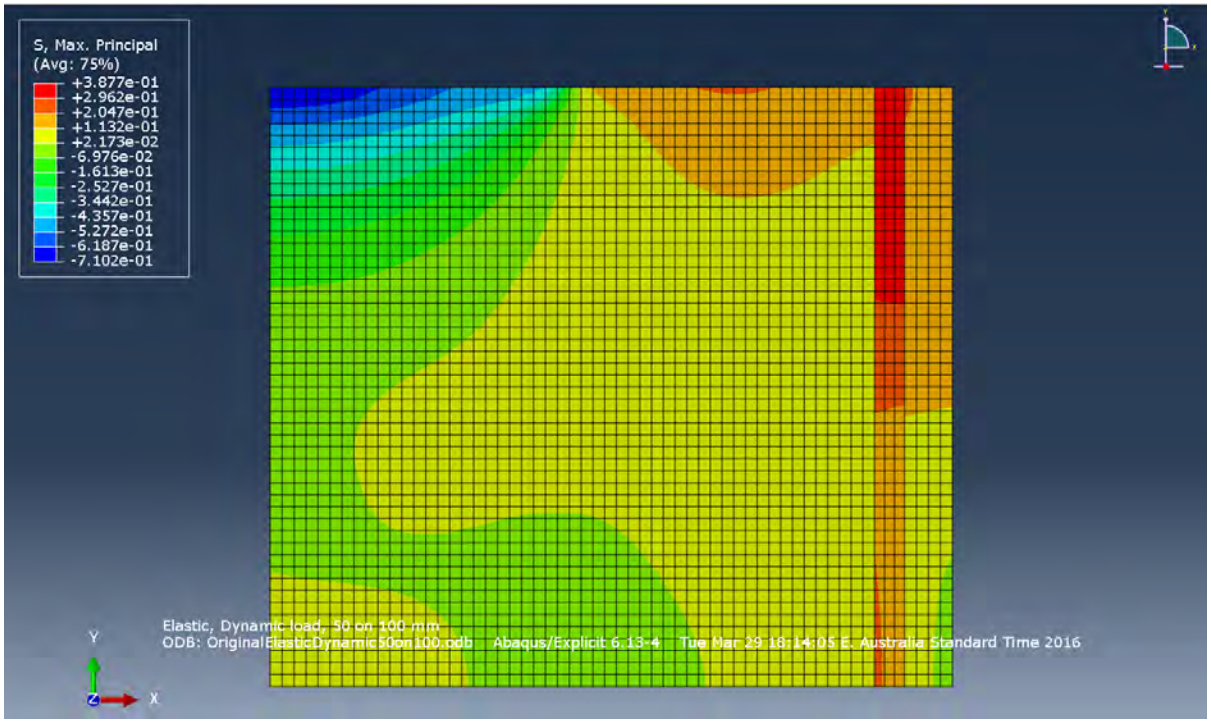

Figure 38: New confined (4mm ring) test for a 50/100mm section – Max, Principal stress.

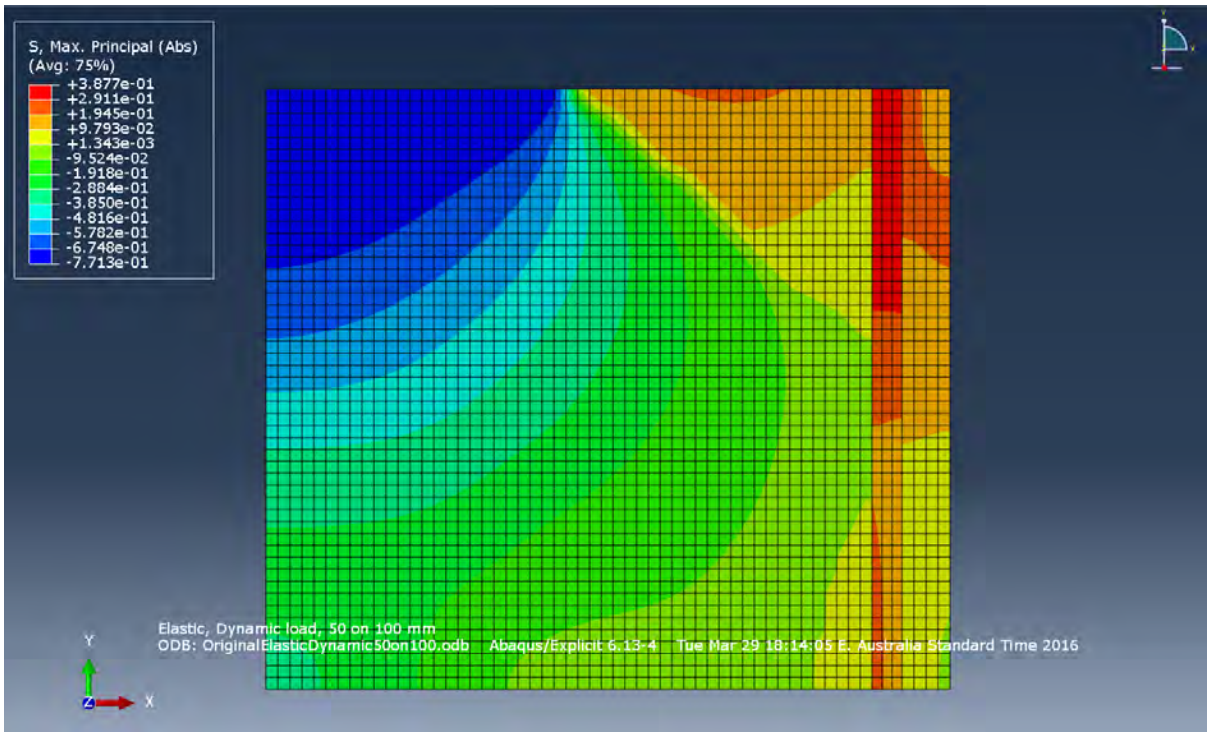

Figure 39: New confined (4mm ring) test for a 50/100mm section – Max, Principal (Abs) stress.

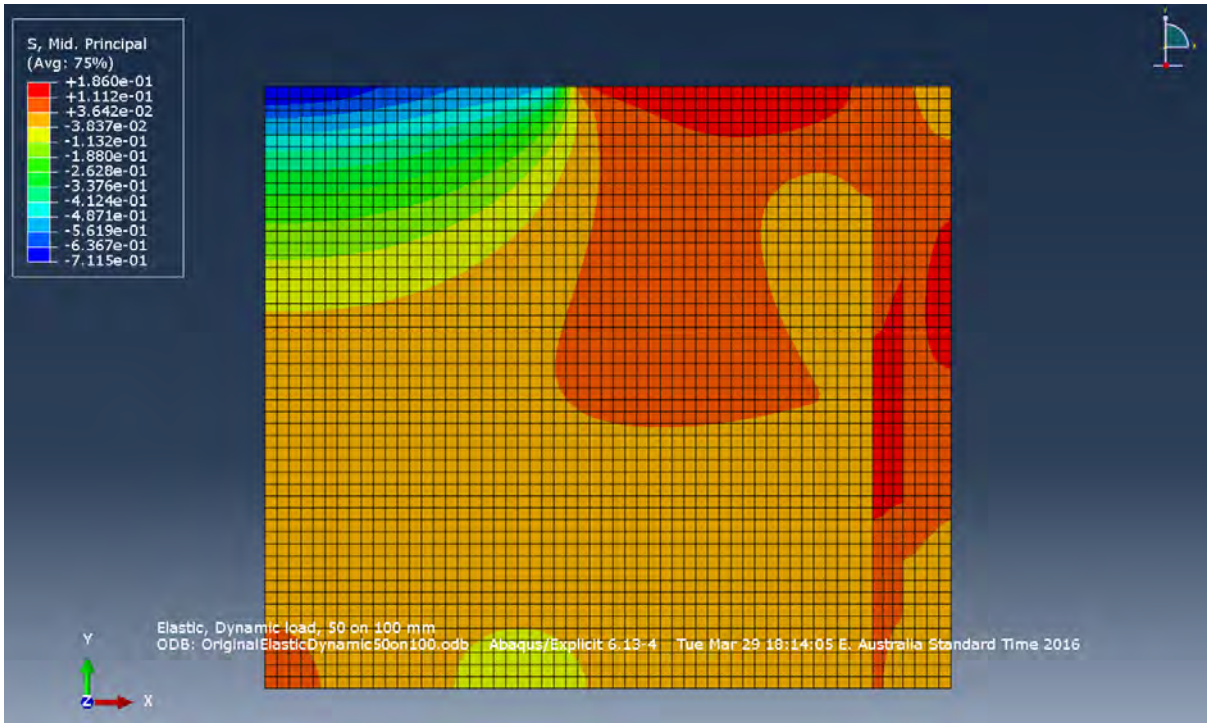

Figure 40: New confined (4mm ring) test for a 50/100mm section –Mid. Principal stress.

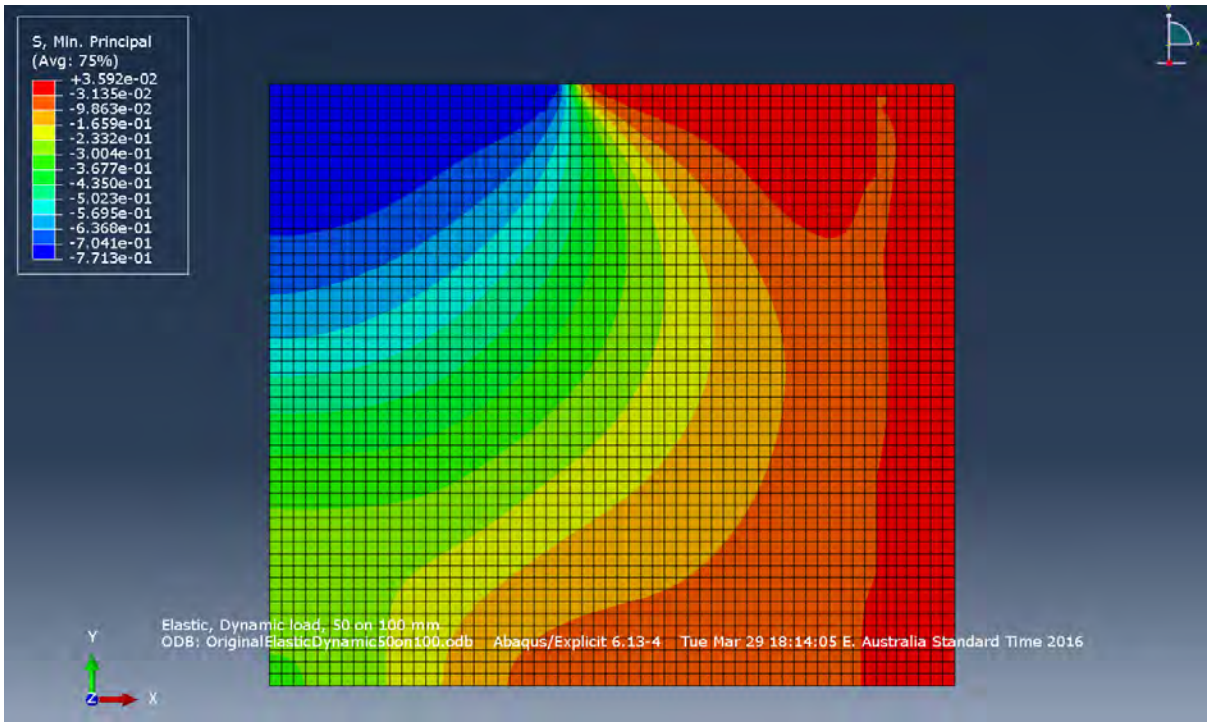

Figure 41: New confined (4mm ring) test for a 50/100mm section – Min. Principal stress.

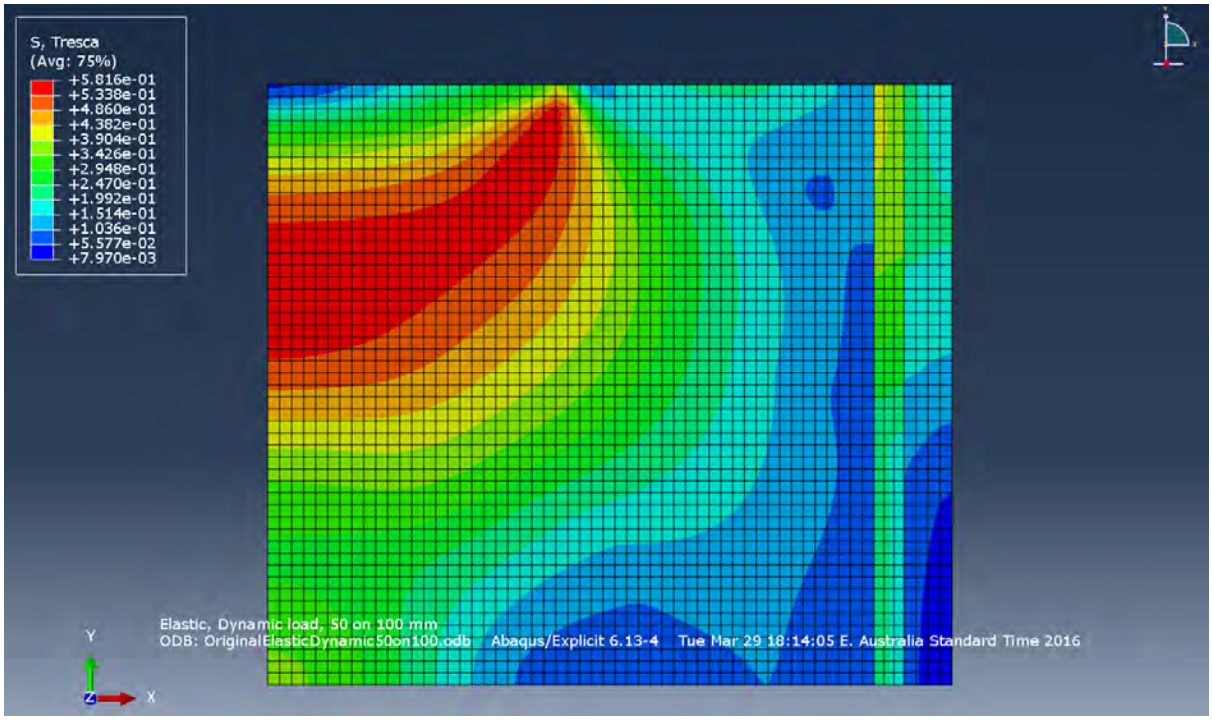

Figure 42: New confined (4mm ring) test for a 50/100mm section – Tresca stress.

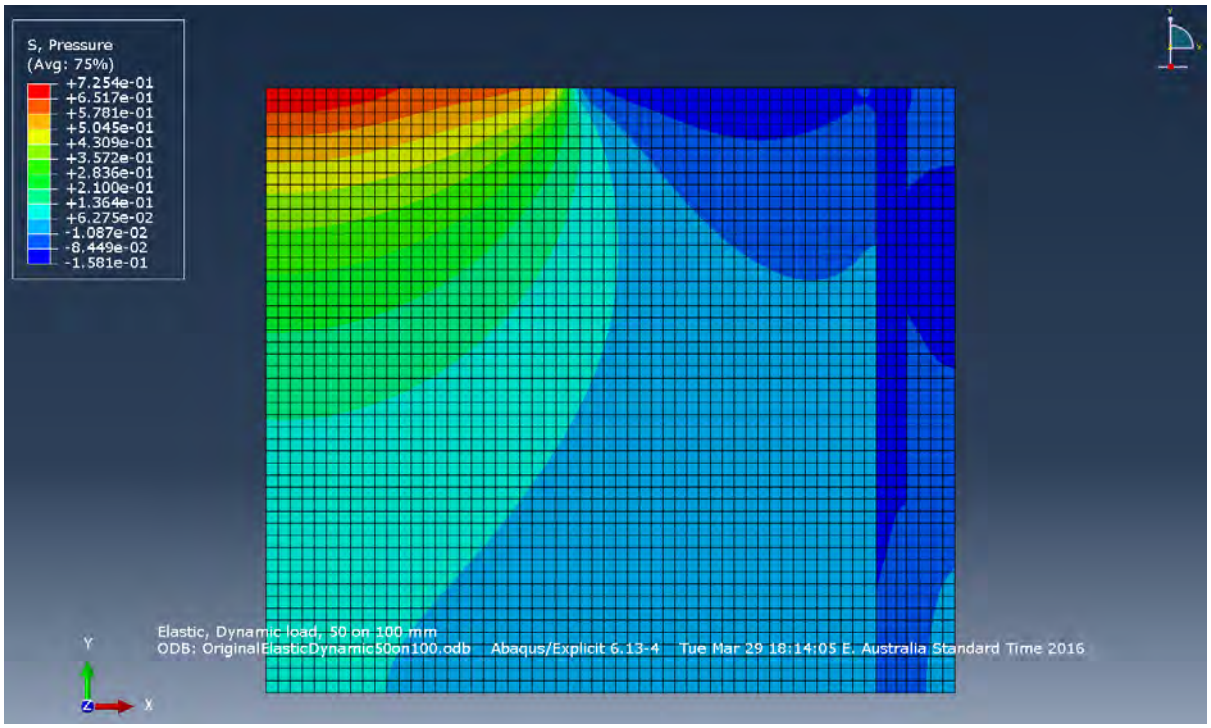

Figure 43: New confined (4mm ring) test for a 50/100mm section – Pressure.

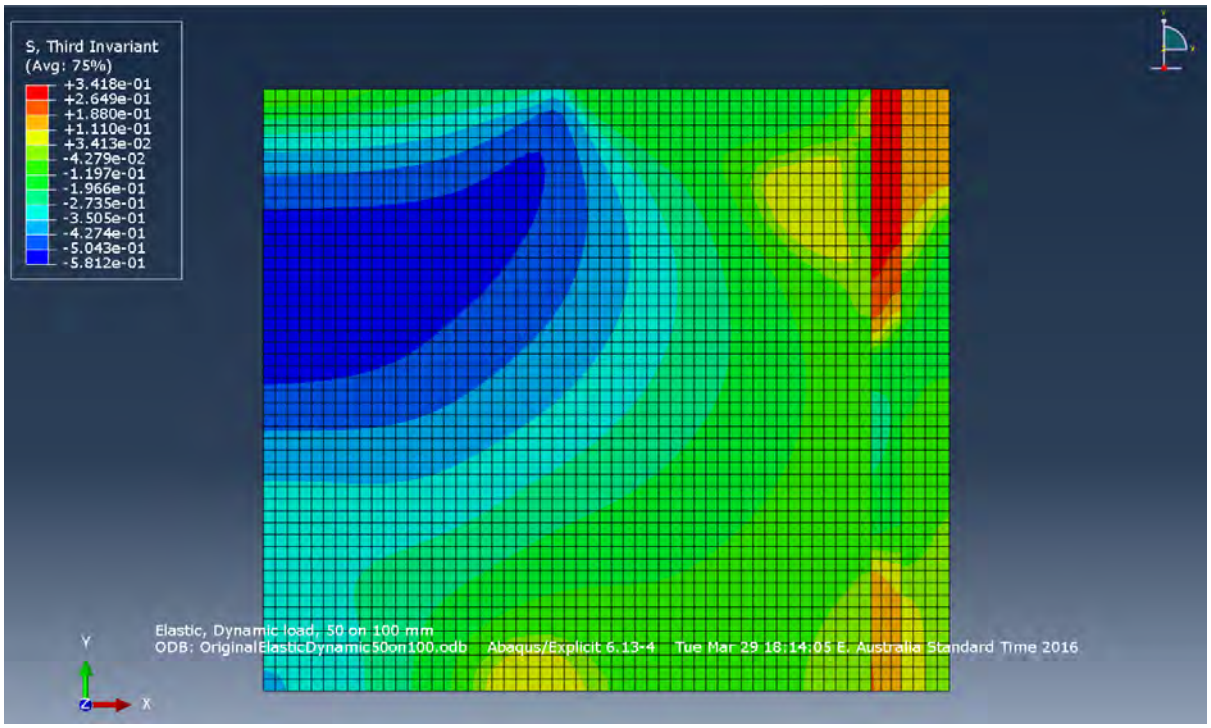

Figure 44: New confined (4mm ring) test for a 50/100mm section –Third Invariant stress.

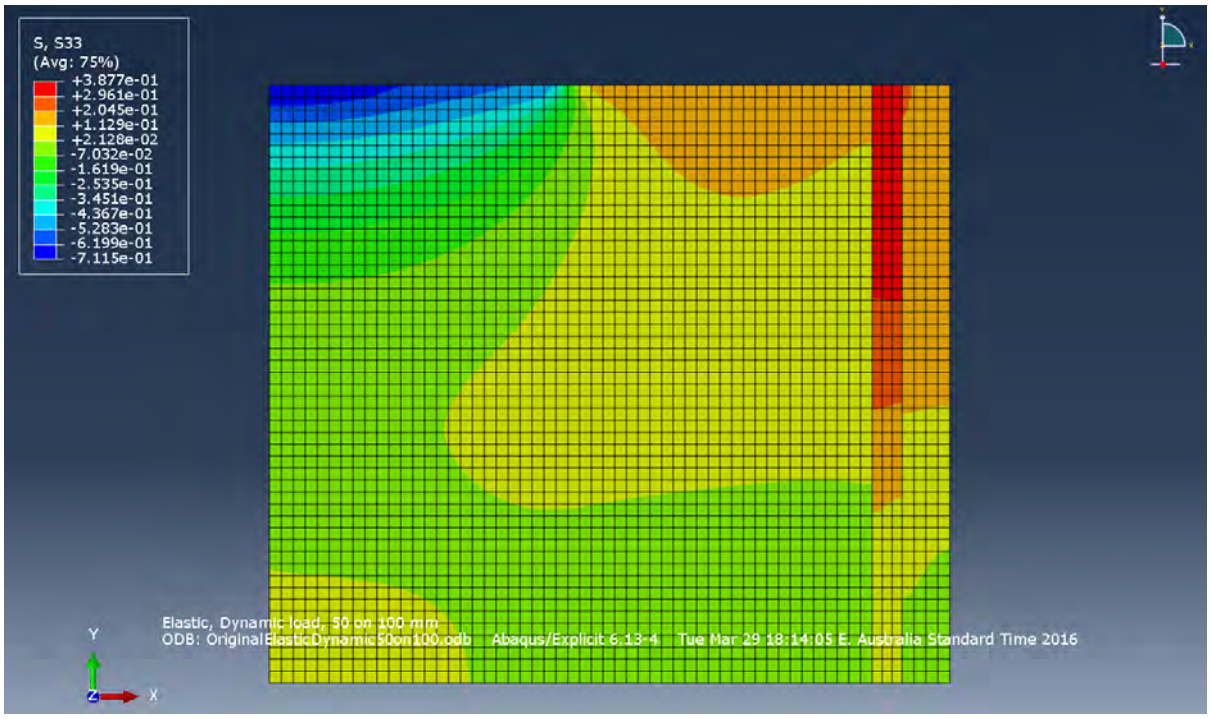

Figure 45: New confined (4mm ring) test for a 50/100mm section – S33 stress (stress in the Z direction).

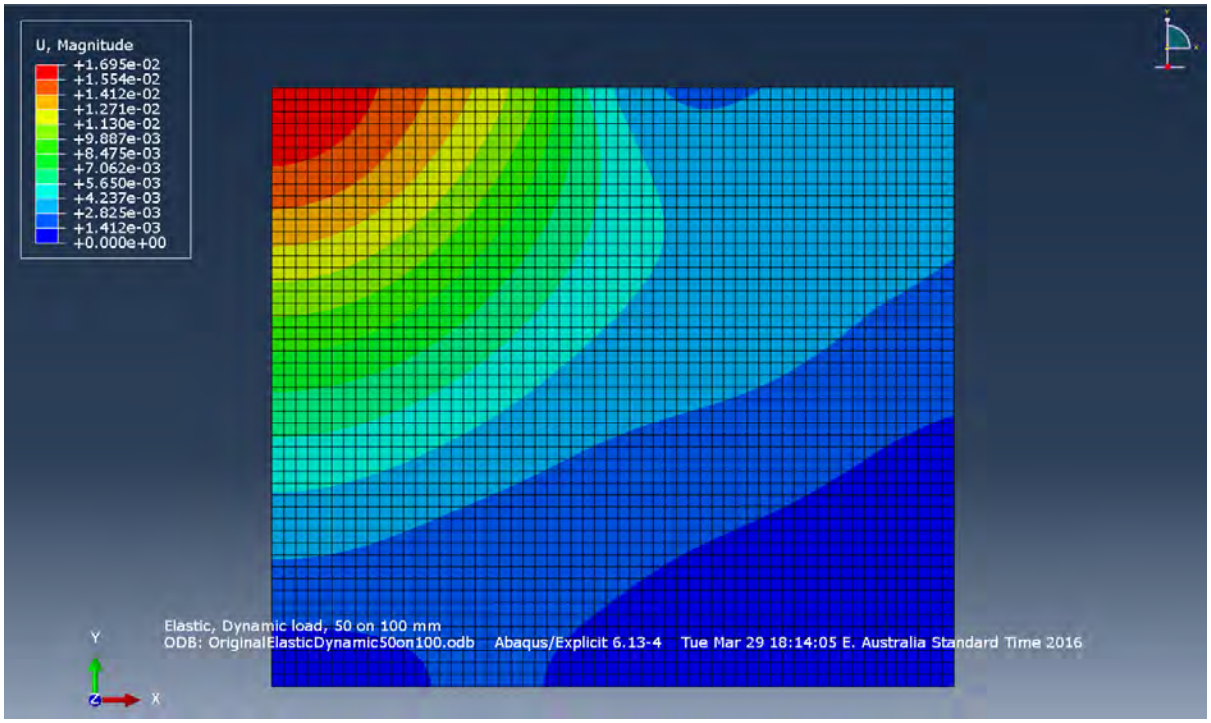

Figure 46: New confined (4mm ring) test for a 50/100mm section – U (deformation) Magnitude.

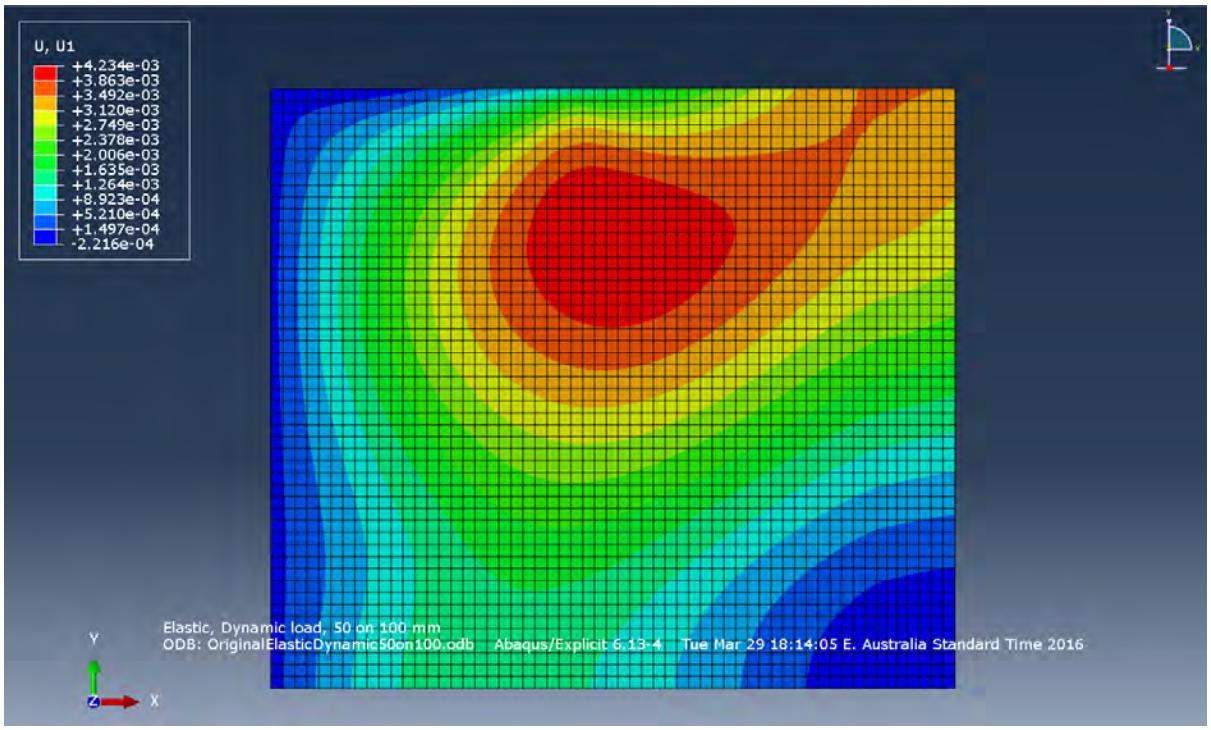

Figure 47: New confined (4mm ring) test for a 50/100mm section – U1 (deformation in the X direction).

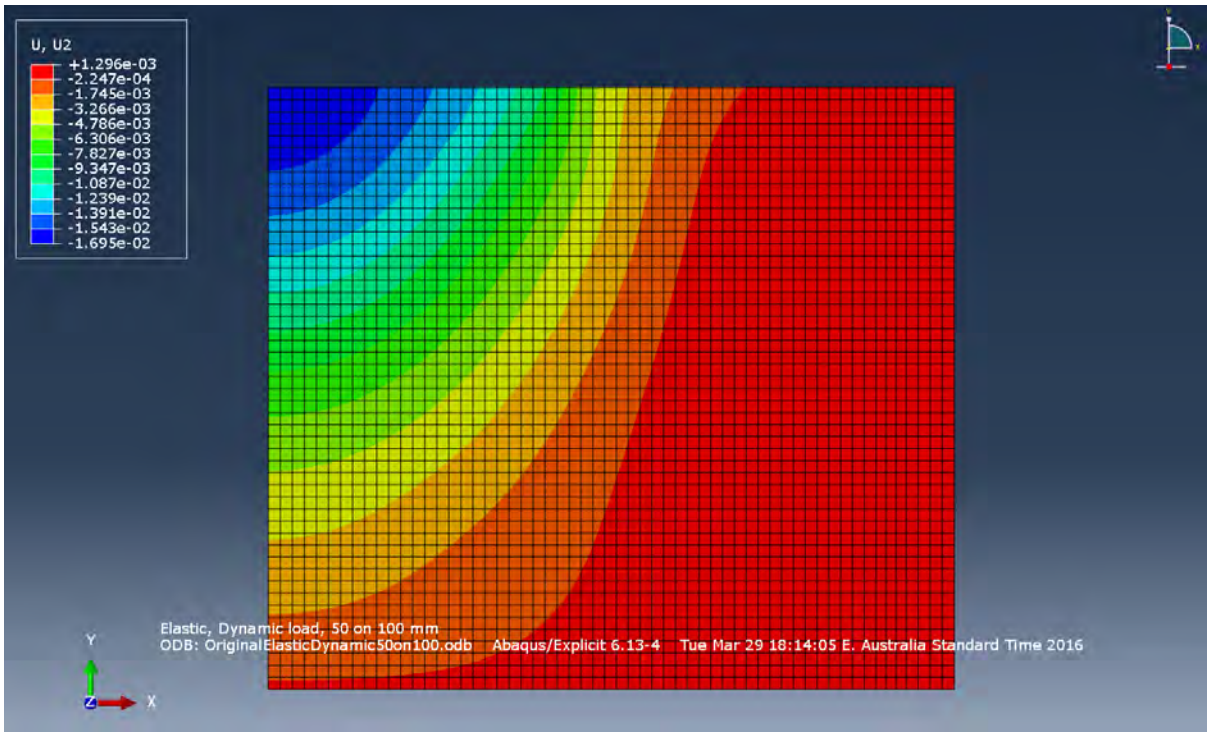

Figure 48: New confined (4mm ring) test for a 50/100mm section – U2 (deformation in the Y direction).

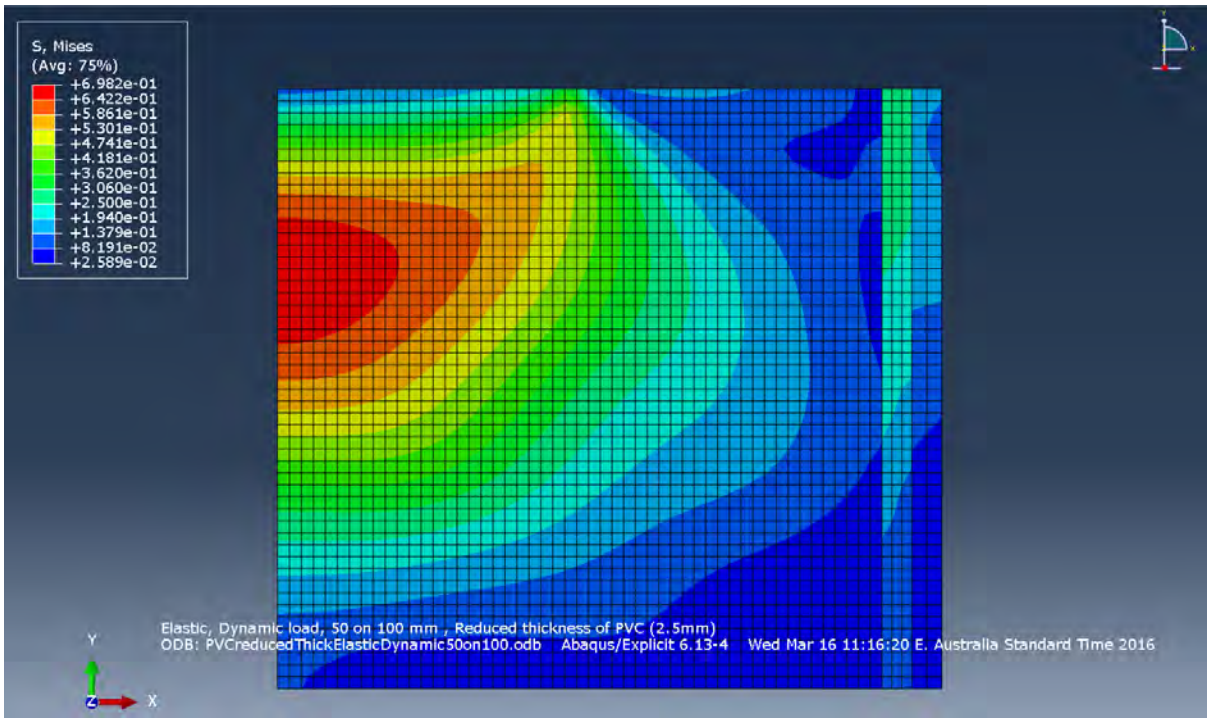

Figure 49: New confined (2.5mm ring) test for a 50/100mm section – Mises stress.

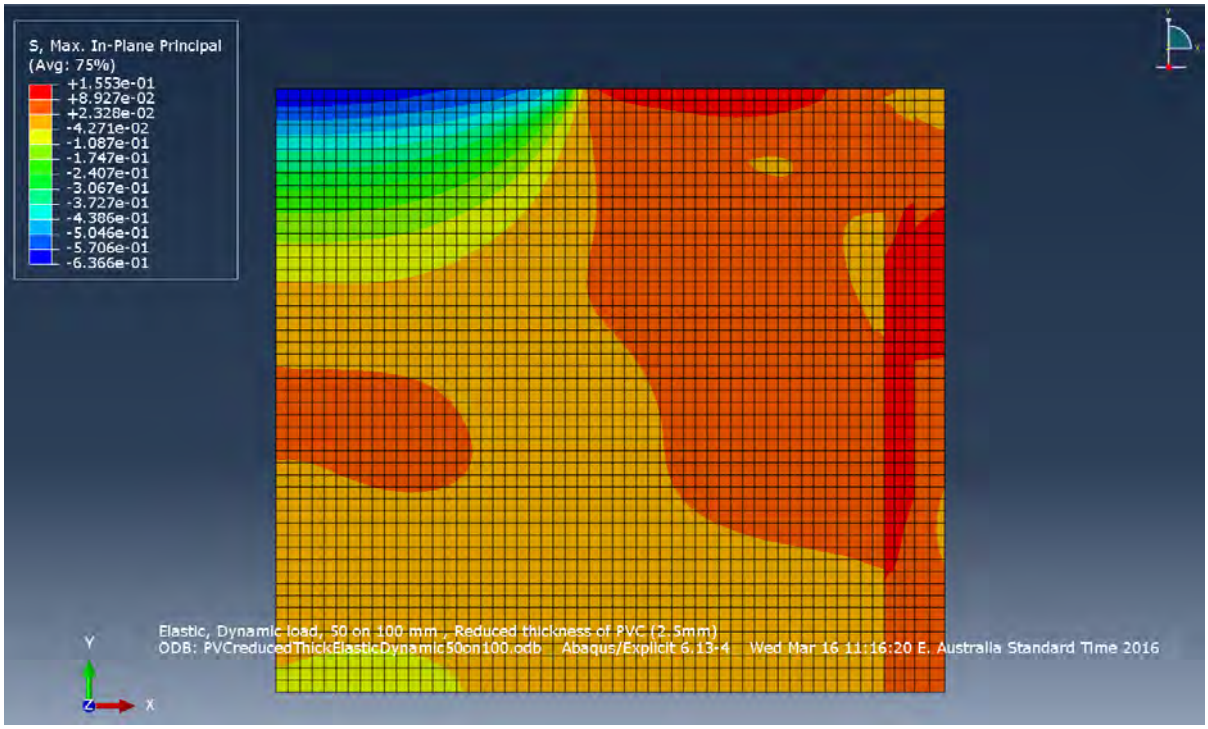

Figure 50: New confined (2.5mm ring) test for a 50/100mm section – Max, In-Plane Principal stress.

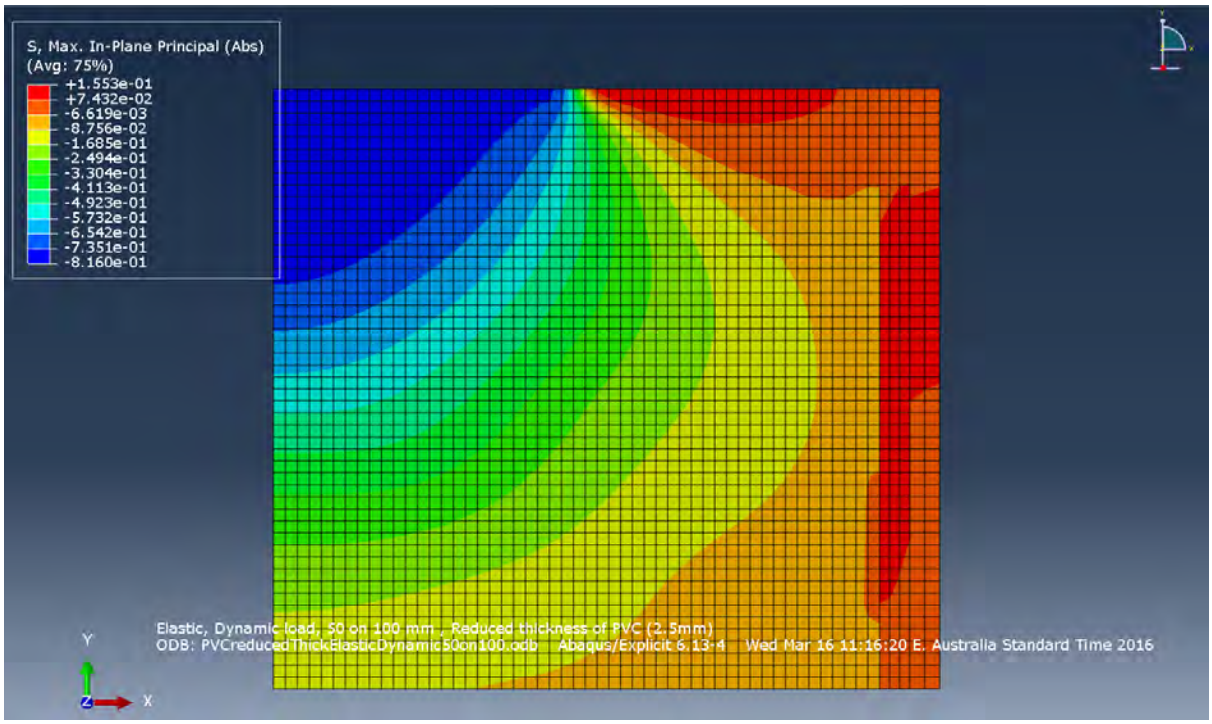

Figure 51: New confined (2.5mm ring) test for a 50/100mm section – Max, In-Plane Principal (Abs) stress.

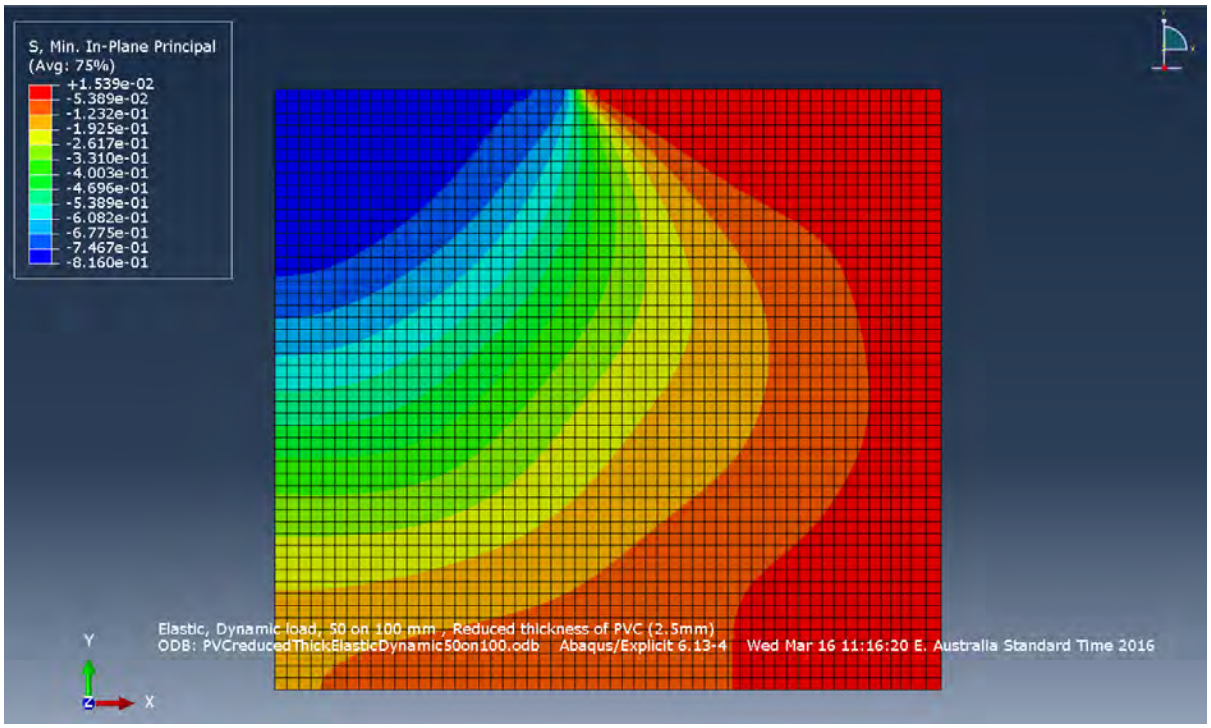

Figure 52: New confined (2.5mm ring) test for a 50/100mm section – Min, In-Plane Principal stress.

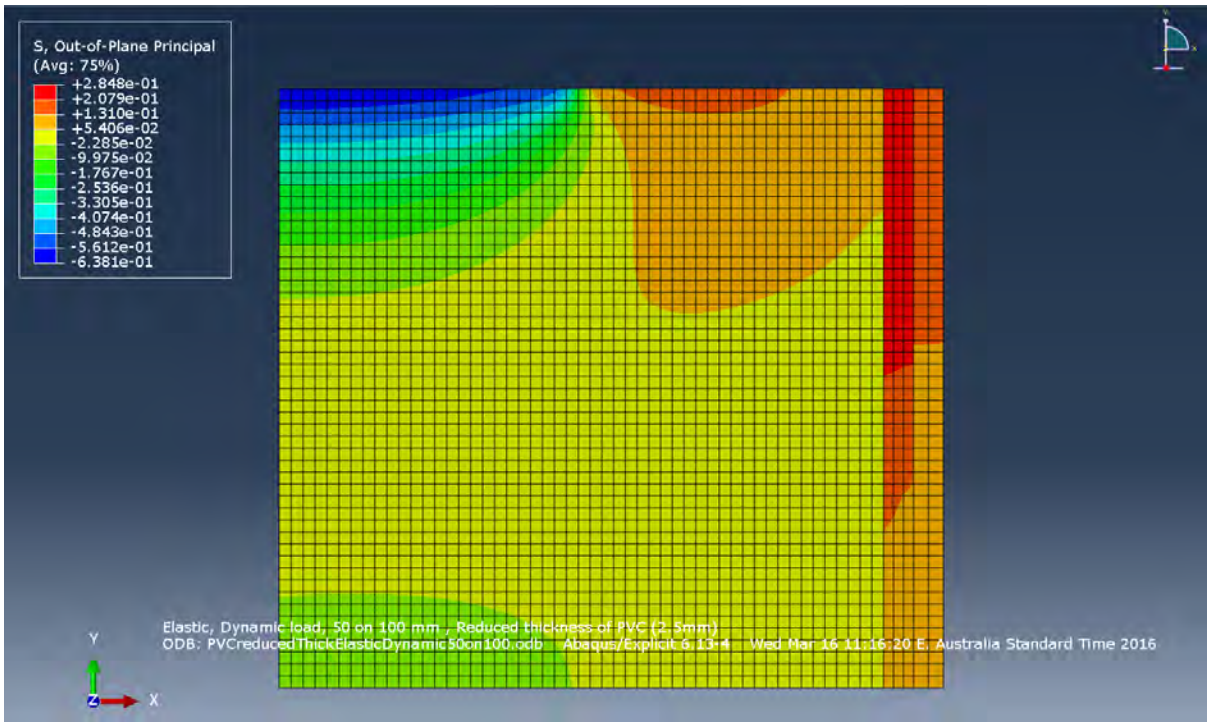

Figure 53: New confined (2.5mm ring) test for a 50/100mm section – Out-of-Plane Principal stress.

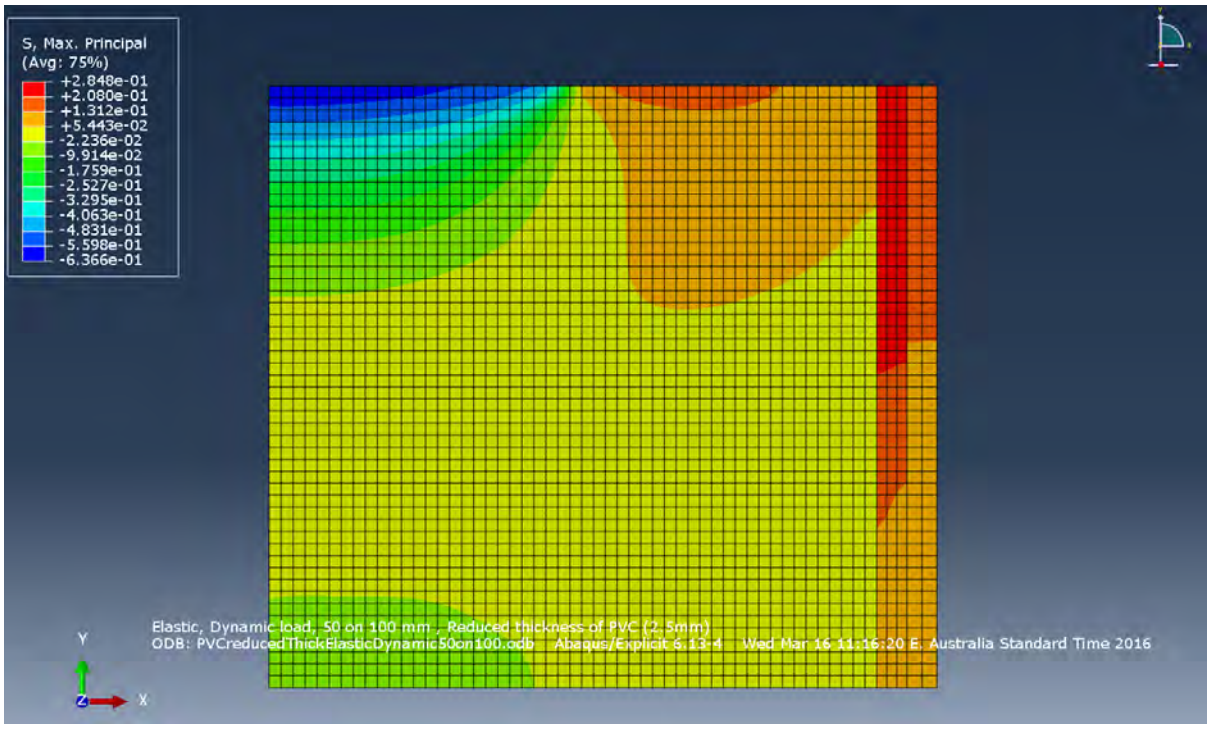

Figure 54: New confined (2.5mm ring) test for a 50/100mm section – Max, Principal stress.

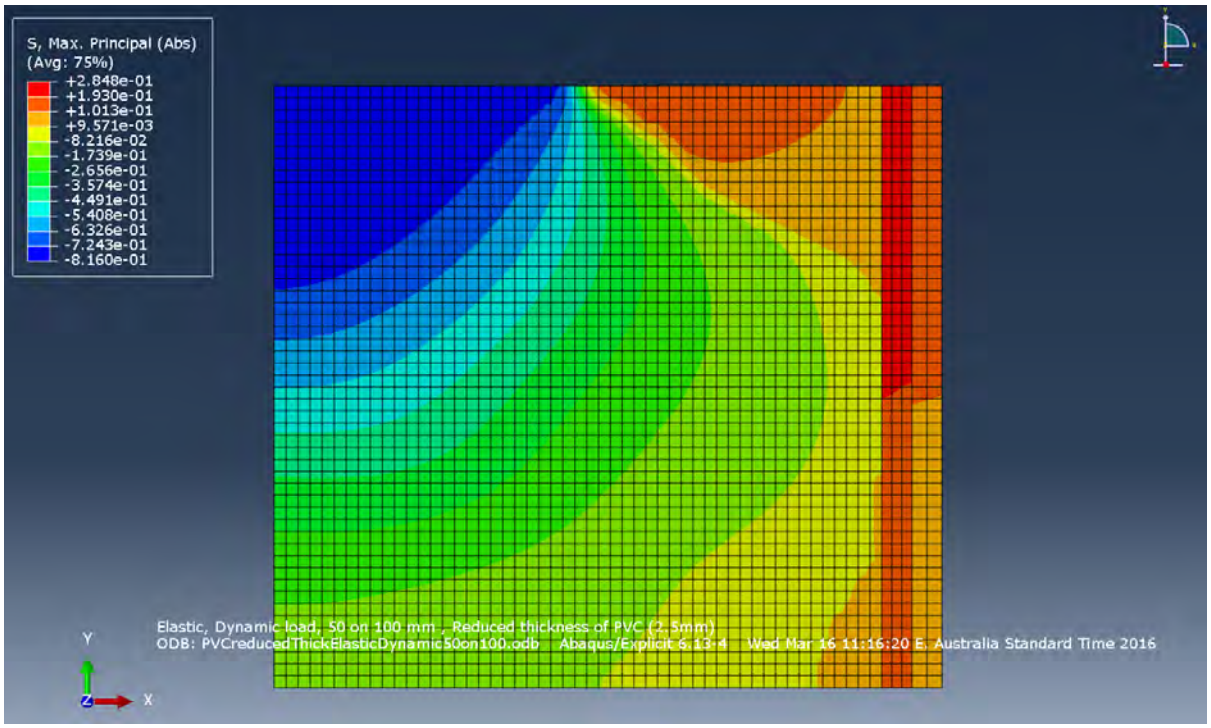

Figure 55: New confined (2.5mm ring) test for a 50/100mm section – Max, Principal (Abs) stress.

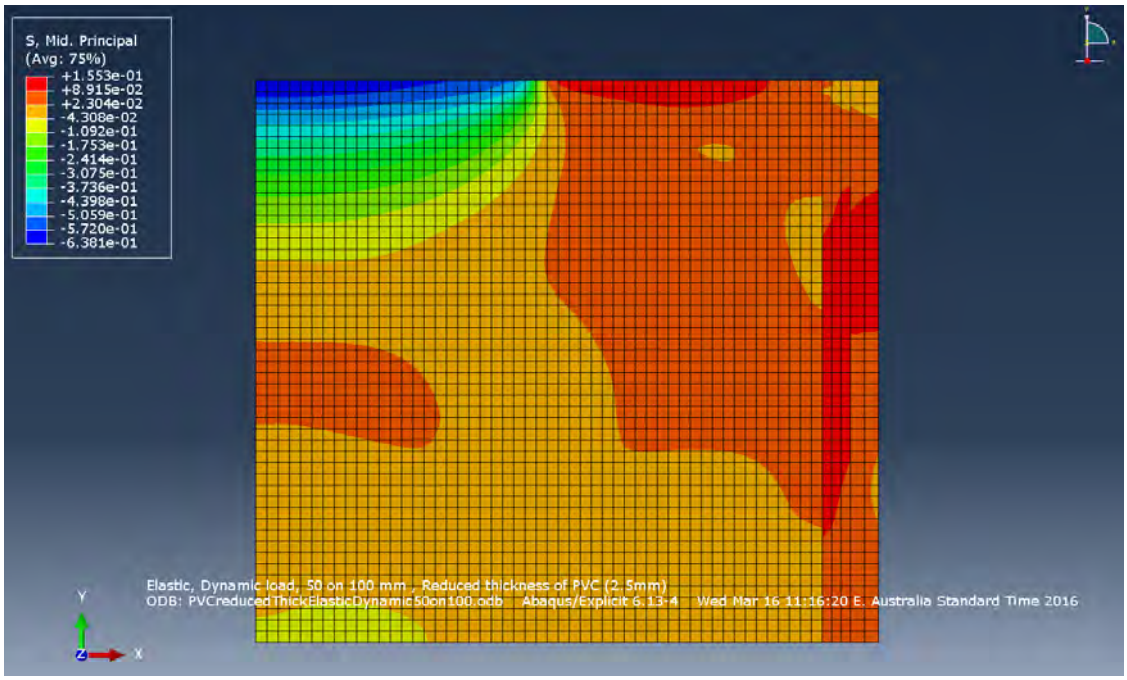

Figure 56: New confined (2.5mm ring) test for a 50/100mm section –Mid. Principal stress.

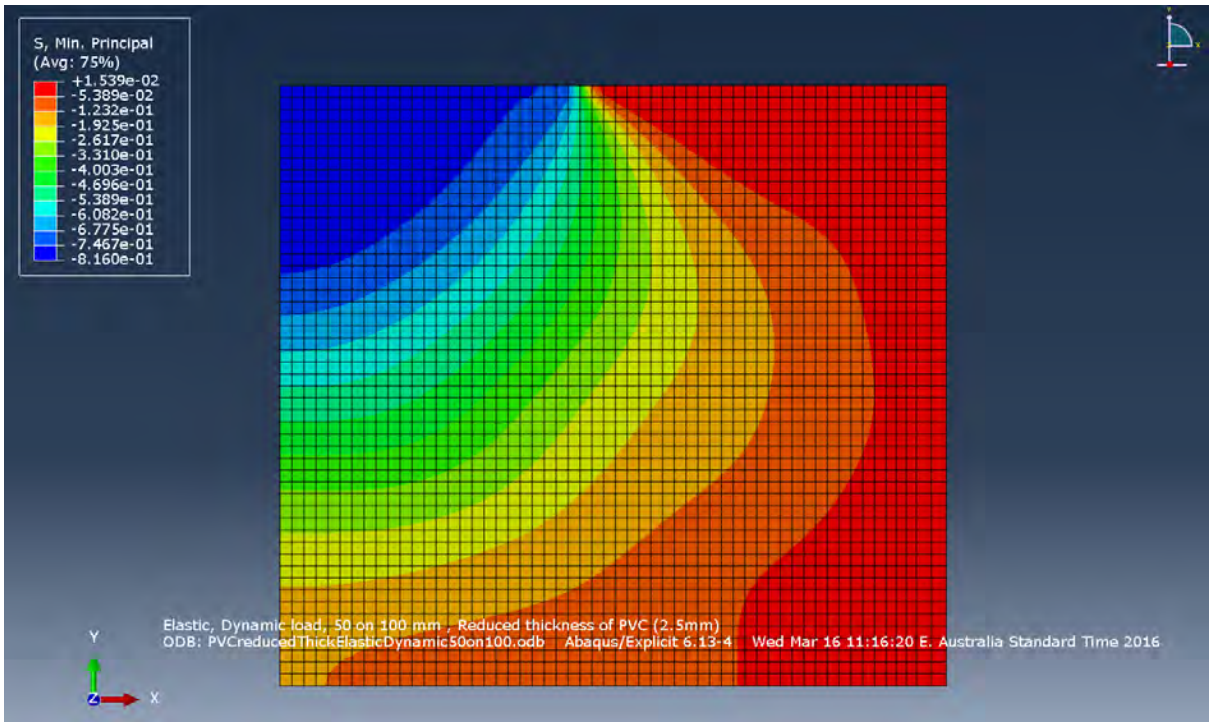

Figure 57: New confined (2.5mm ring) test for a 50/100mm section – Min. Principal stress.

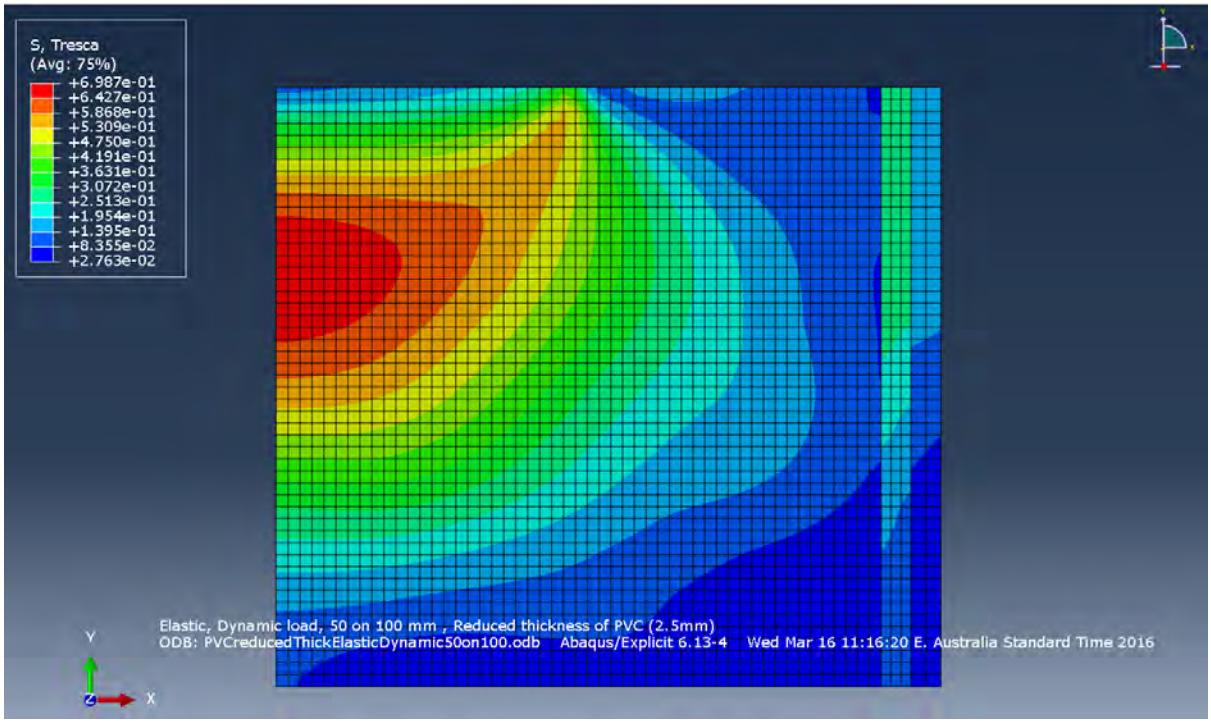

Figure 58: New confined (2.5mm ring) test for a 50/100mm section – Tresca stress.

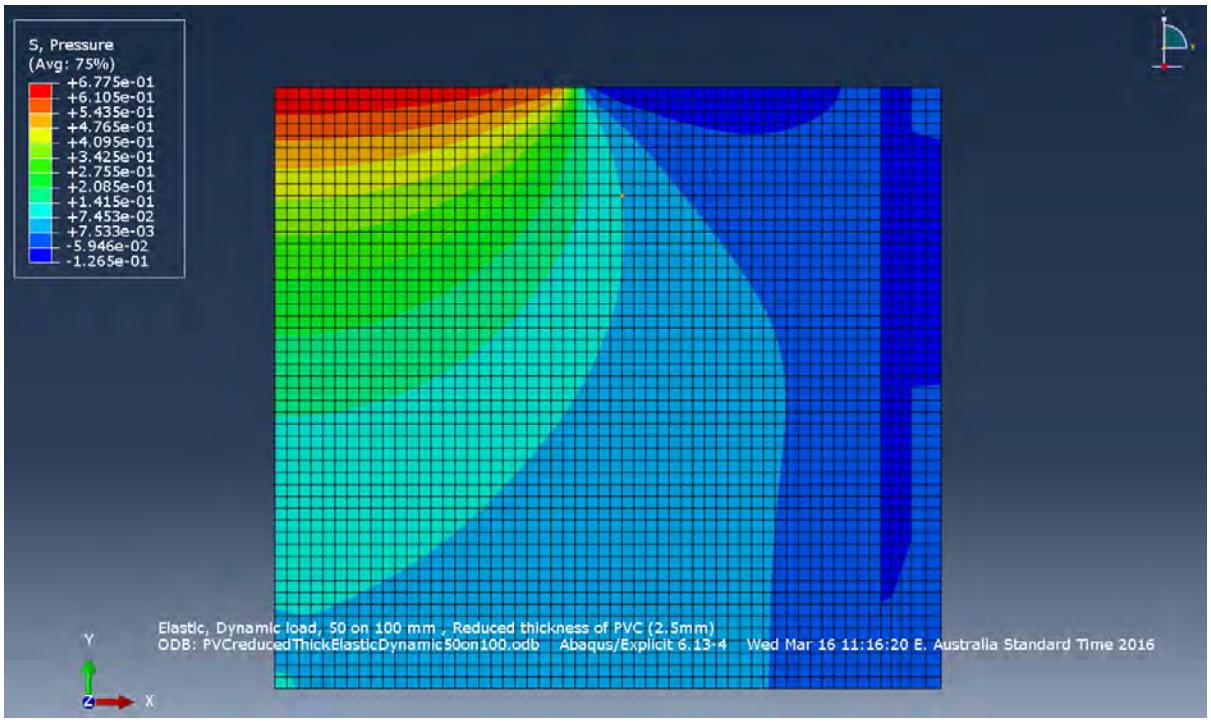

Figure 59: New confined (2.5mm ring) test for a 50/100mm section – Pressure.

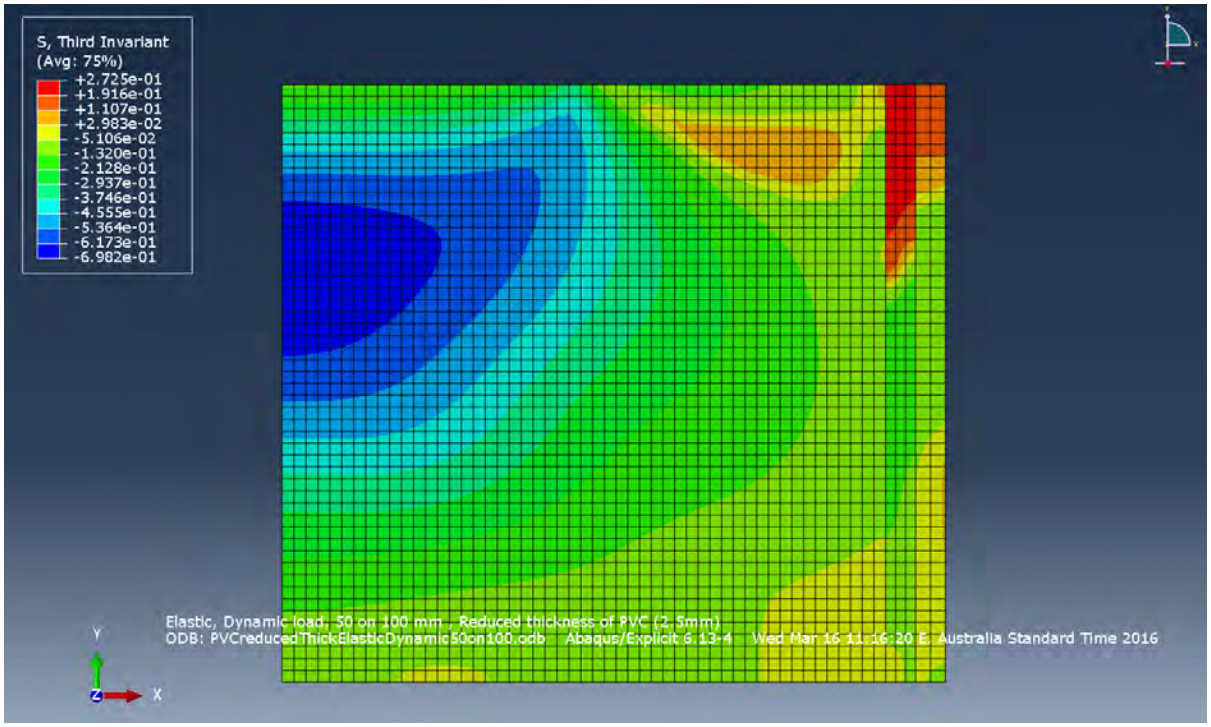

Figure 60: New confined (2.5mm ring) test for a 50/100mm section –Third Invariant stress.

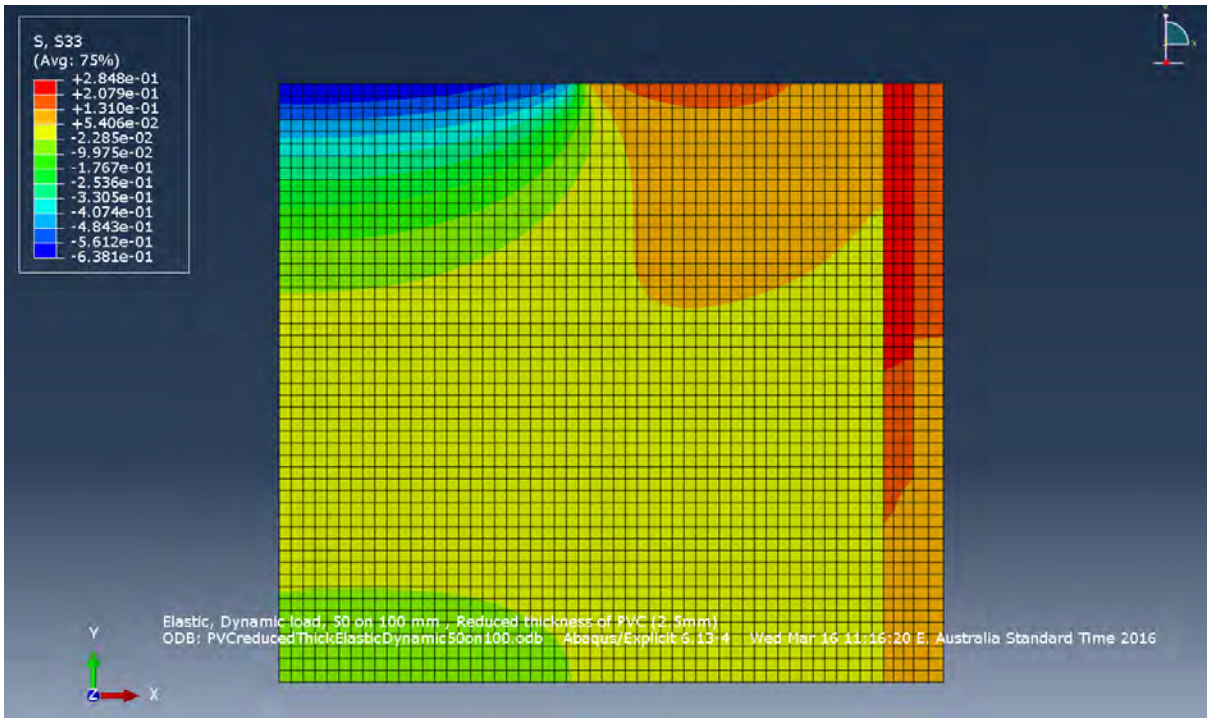

Figure 61: New confined (2.5mm ring) test for a 50/100mm section – S33 stress (stress in the Z direction).

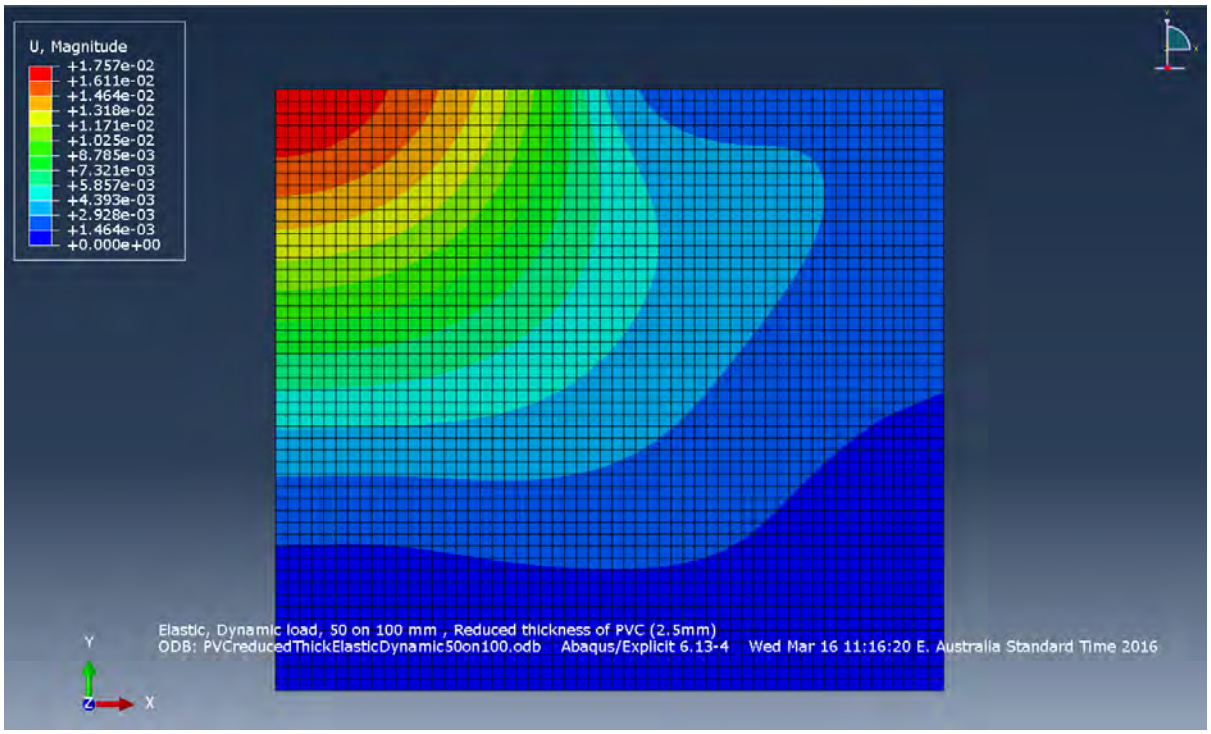

Figure 62: New confined (2.5mm ring) test for a 50/100mm section – U (deformation) Magnitude.

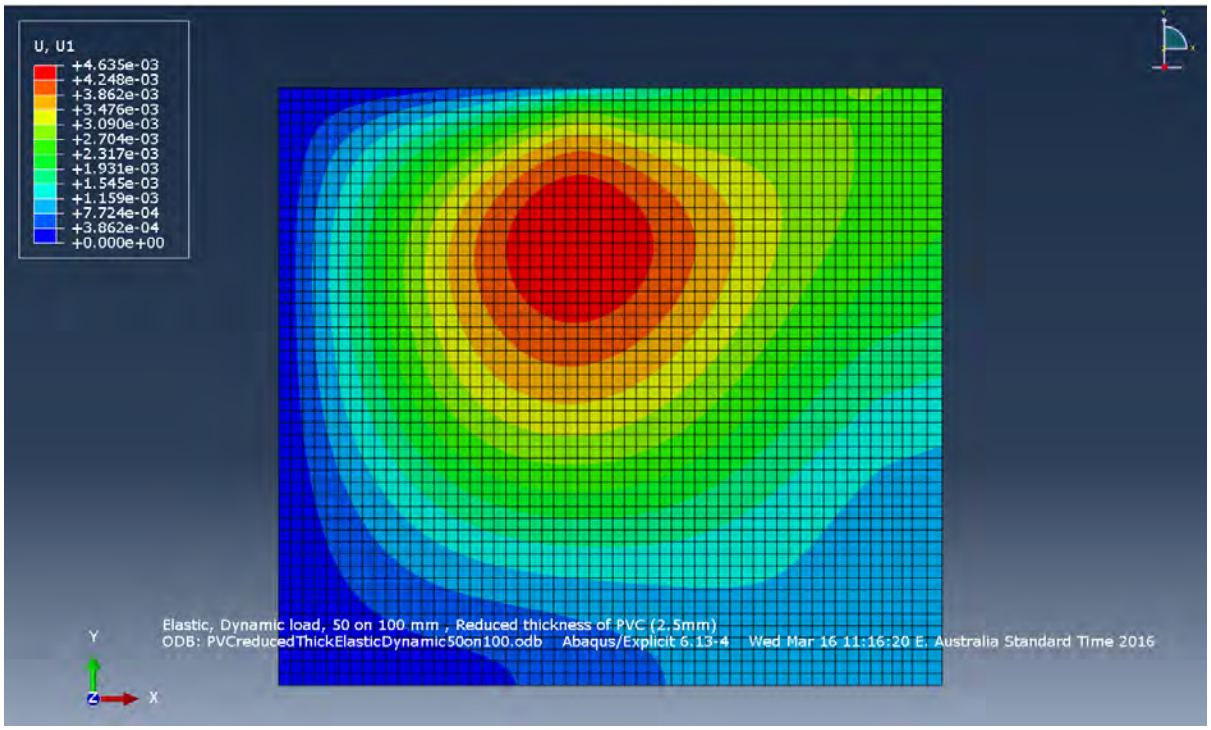

Figure 63: New confined (2.5mm ring) test for a 50/100mm section – U1 (deformation in the X direction).

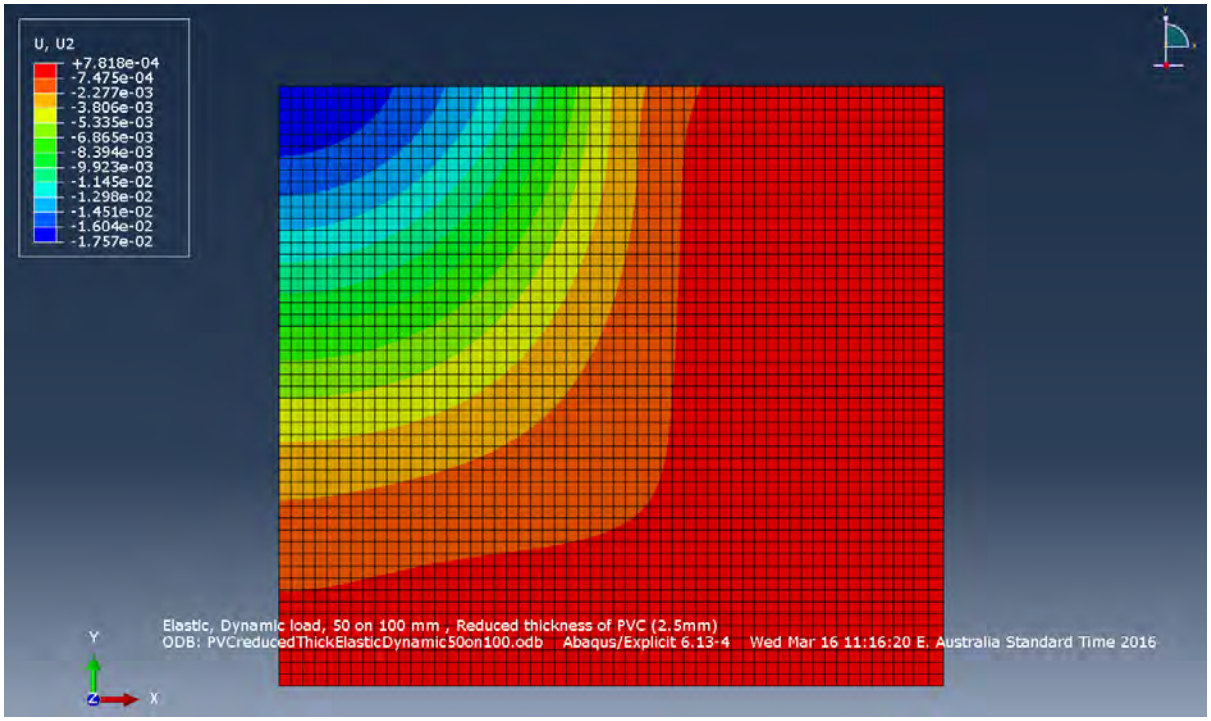

Figure 64: New confined (2.5mm ring) test for a 50/100mm section – U2 (deformation in the Y direction).

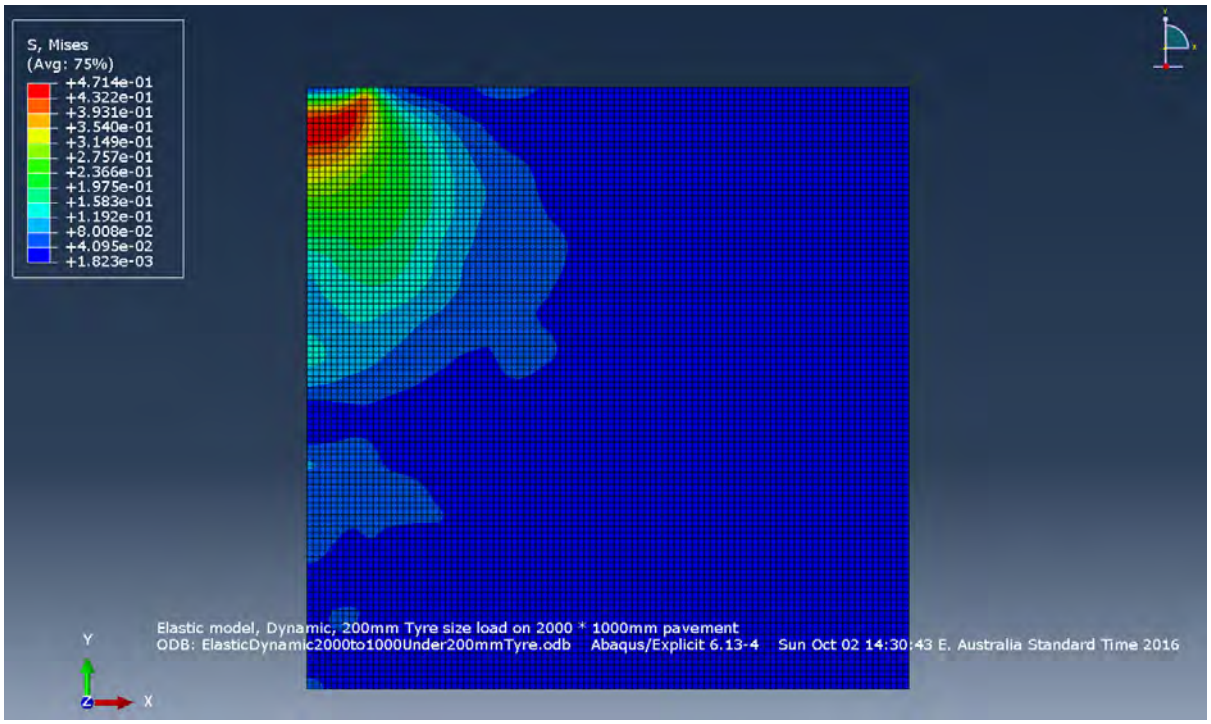

Figure 65: Full depth asphalt pavement, 2000×1000mm section under a 200mm tyre – Mises stress.

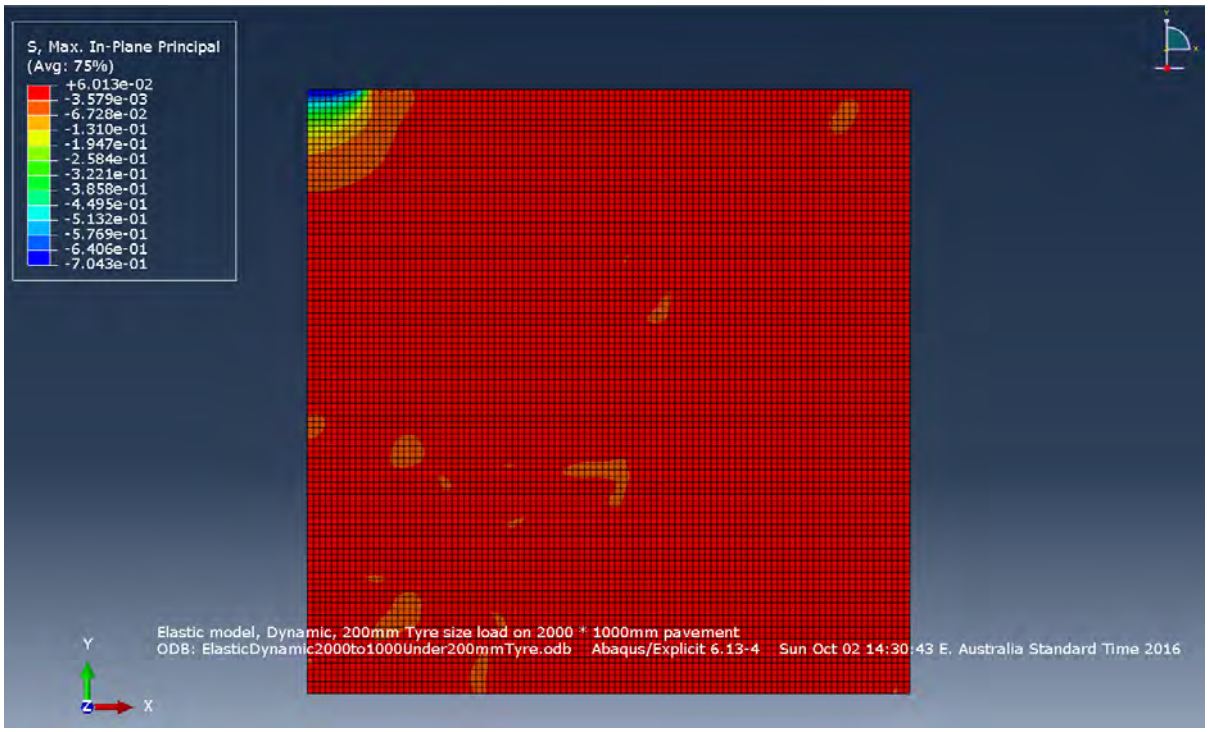

Figure 66: Full depth asphalt pavement, 2000×1000mm section under a 200mm tyre – Max, In-Plane Principal stress.

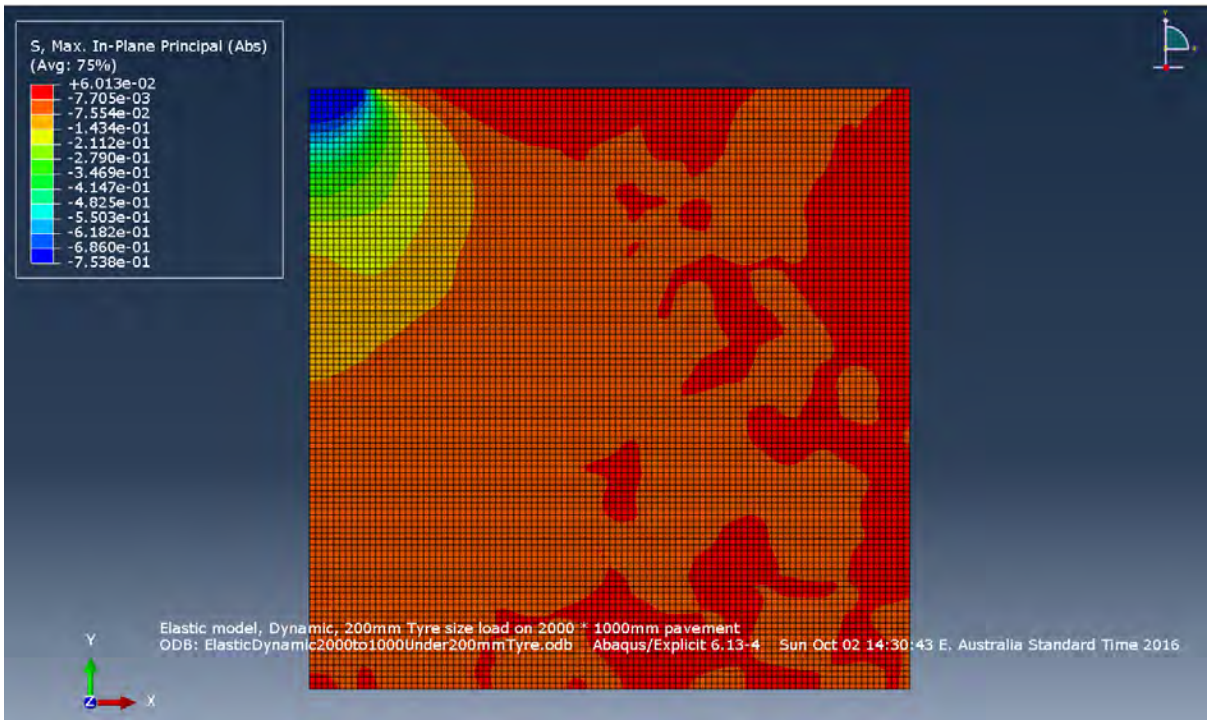

Figure 67: Full depth asphalt pavement, 2000×1000mm section under a 200mm tyre – Max, In-Plane Principal (Abs) stress.

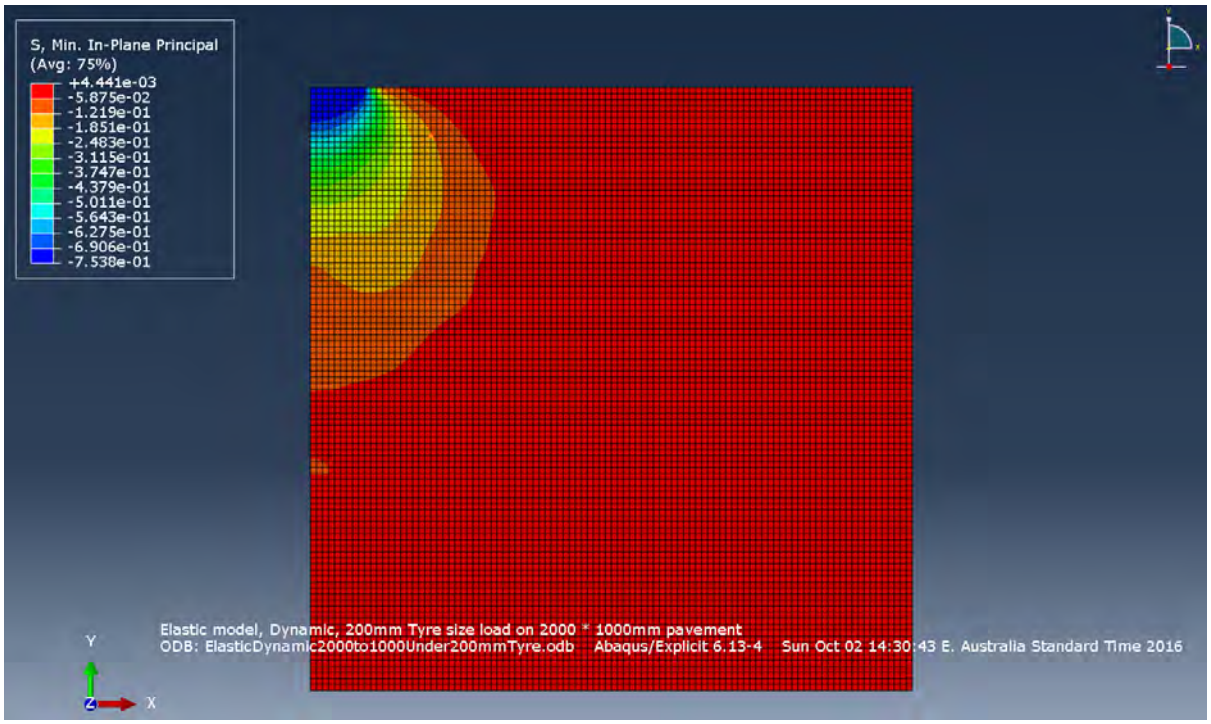

Figure 68: Full depth asphalt pavement, 2000×1000mm section under a 200mm tyre – Min, In-Plane Principal stress.

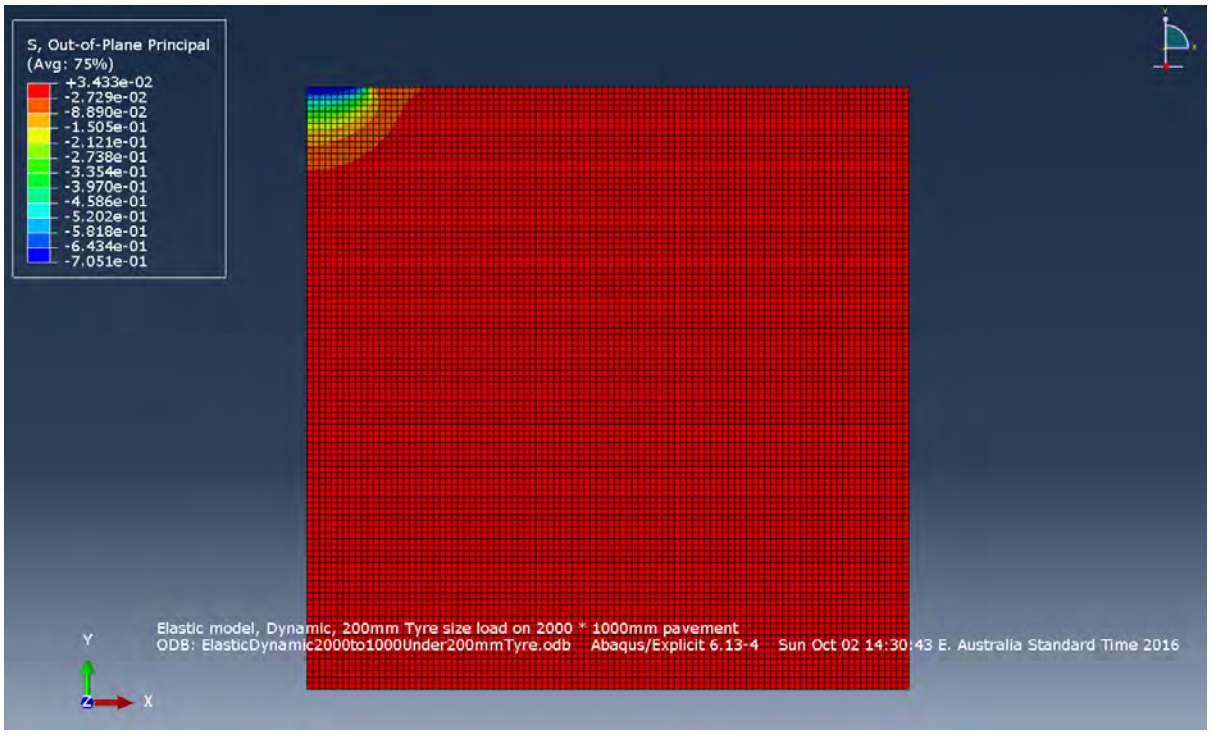

Figure 69: Full depth asphalt pavement, 2000×1000mm section under a 200mm tyre – Out-of-Plane Principal stress.

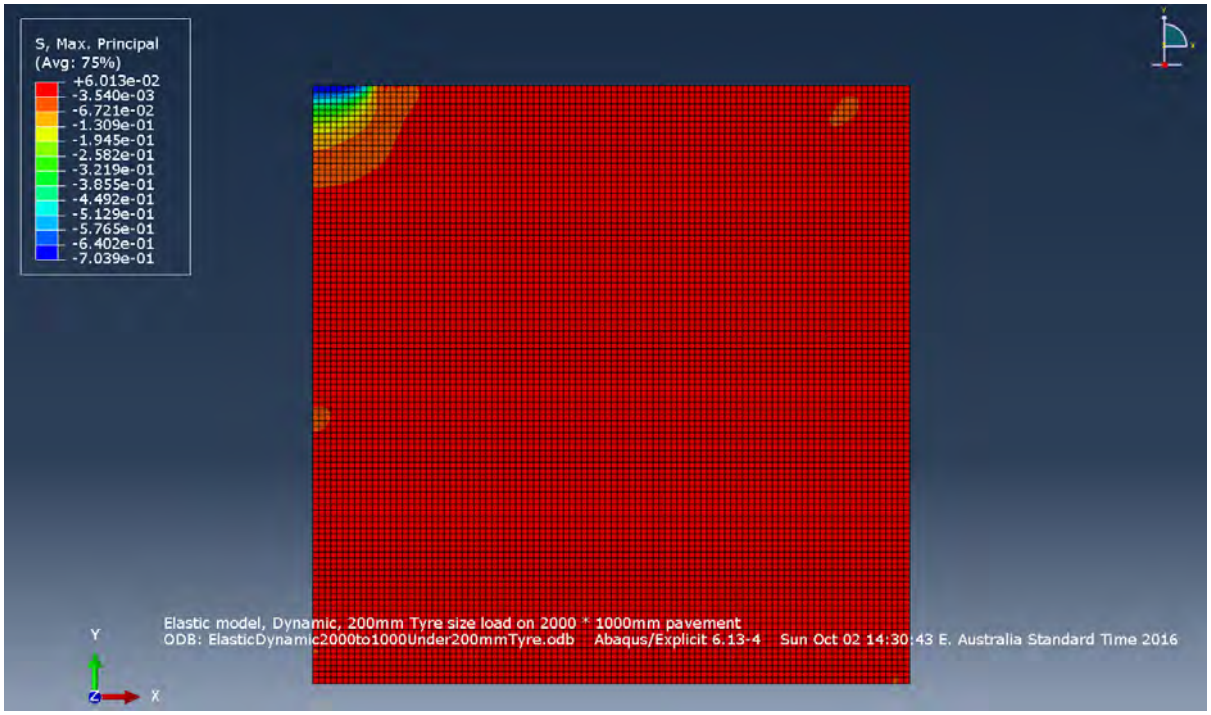

Figure 70: Full depth asphalt pavement, 2000×1000mm section under a 200mm tyre – Max, Principal stress.

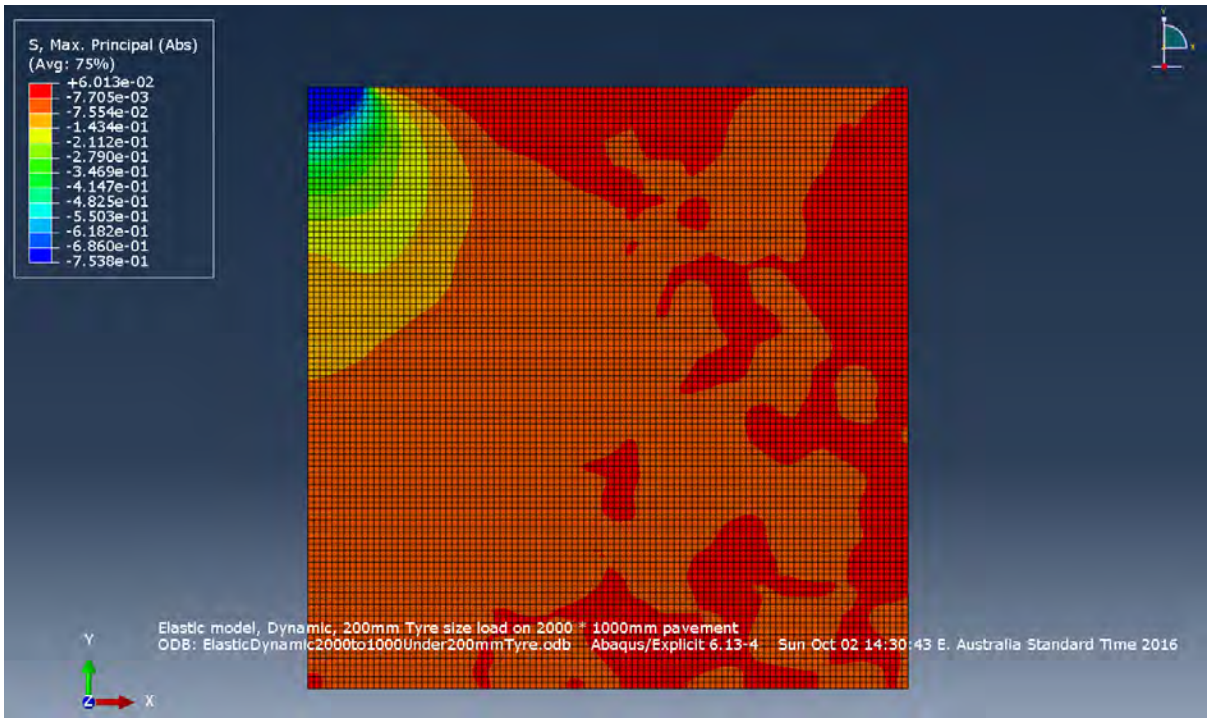

Figure 71: Full depth asphalt pavement, 2000×1000mm section under a 200mm tyre – Max, Principal (Abs) stress.

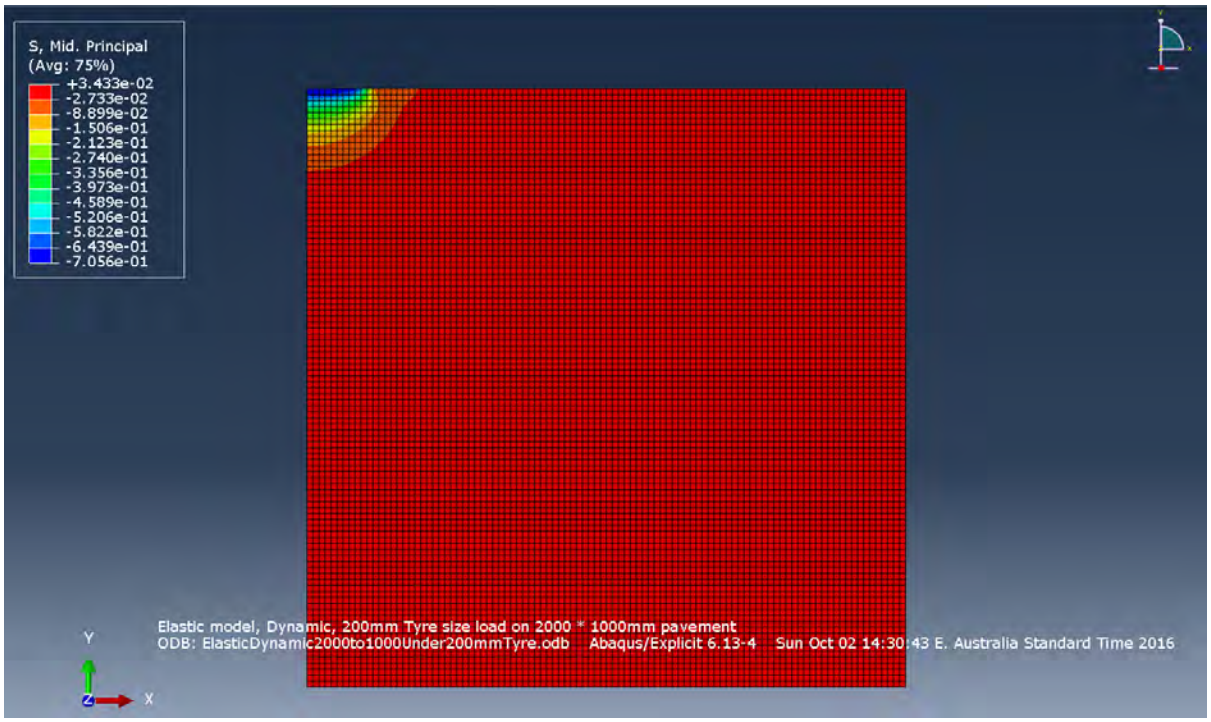

Figure 72: Full depth asphalt pavement, 2000×1000mm section under a 200mm tyre – Mid. Principal stress.

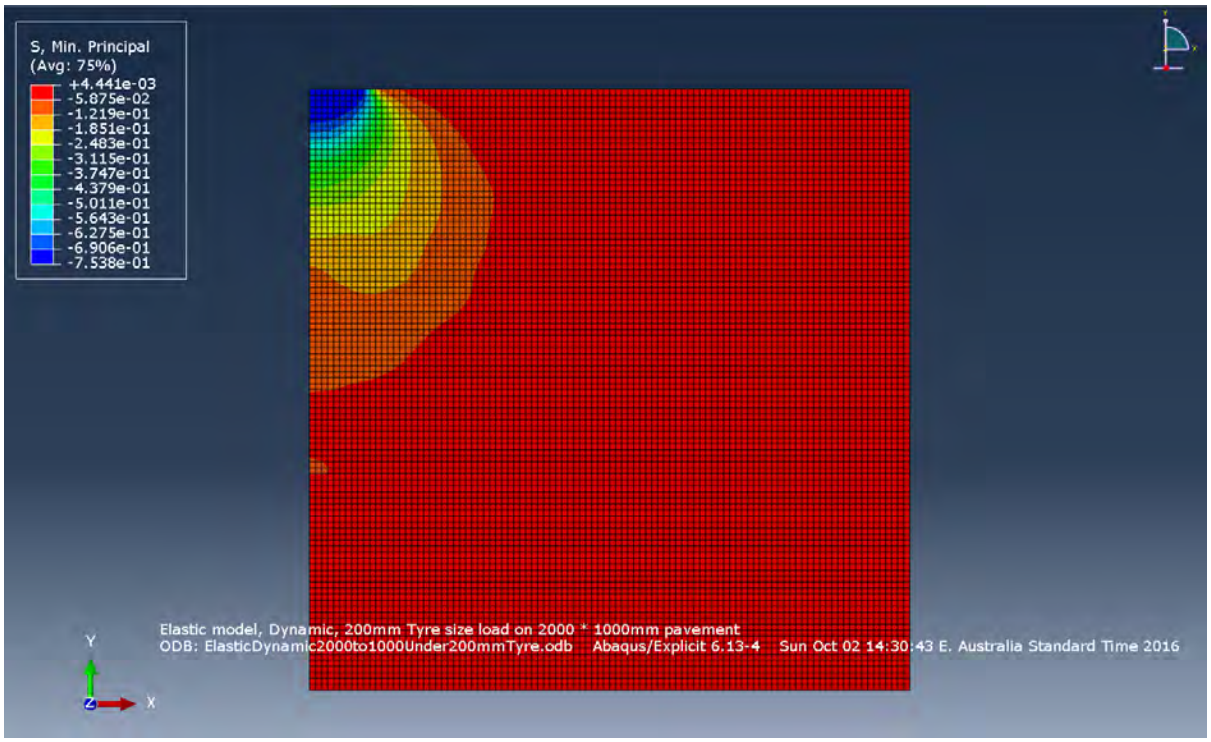

Figure 73: Full depth asphalt pavement, 2000×1000mm section under a 200mm tyre – Min. Principal stress.

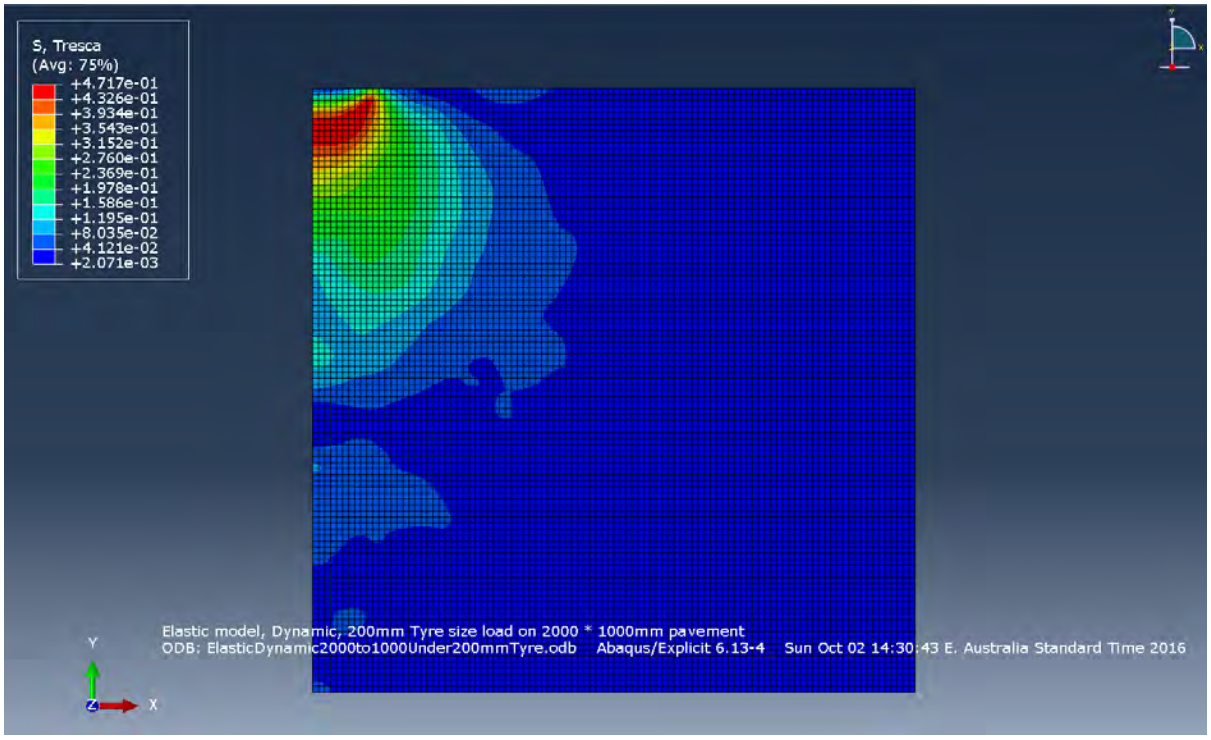

Figure 74: Full depth asphalt pavement, 2000×1000mm section under a 200mm tyre – Tresca stress.

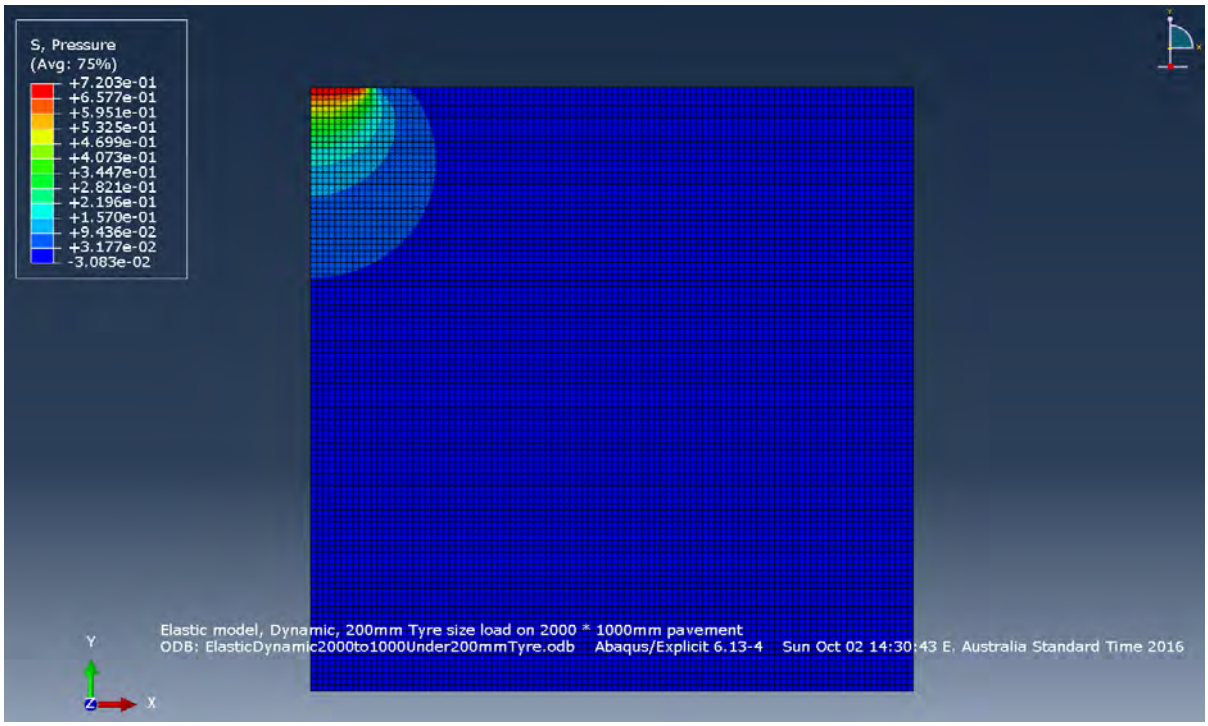

Figure 75: Full depth asphalt pavement, 2000×1000mm section under a 200mm tyre – Pressure.

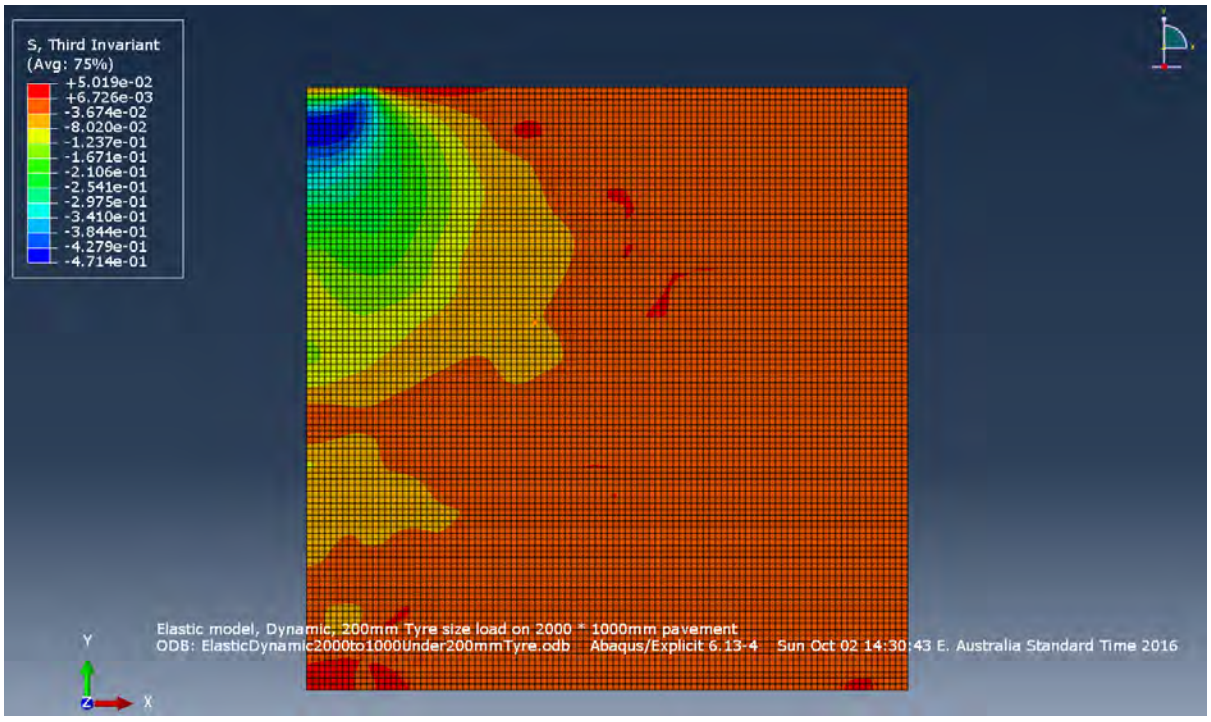

Figure 76: Full depth asphalt pavement, 2000×1000mm section under a 200mm tyre –Third Invariant stress.

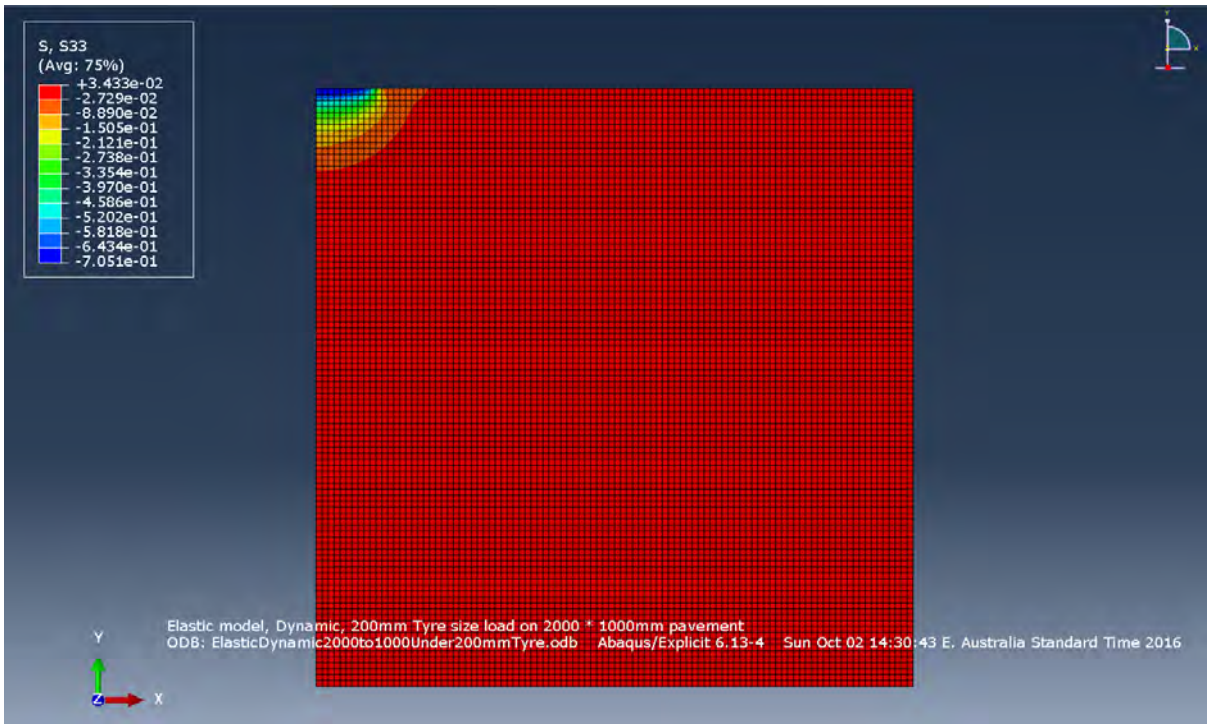

Figure 77: Full depth asphalt pavement, 2000×1000mm section under a 200mm tyre – S33 stress (stress in the Z direction).

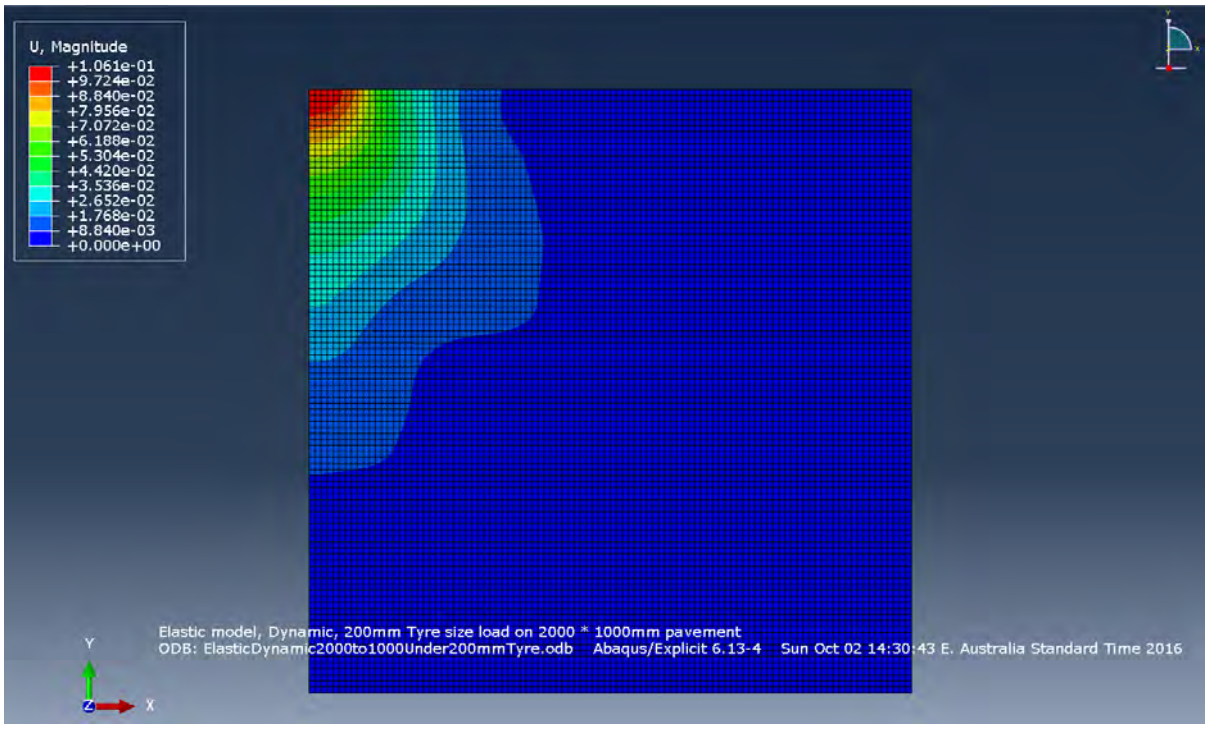

Figure 78: Full depth asphalt pavement, 2000×1000mm section under a 200mm tyre – U (deformation) Magnitude.

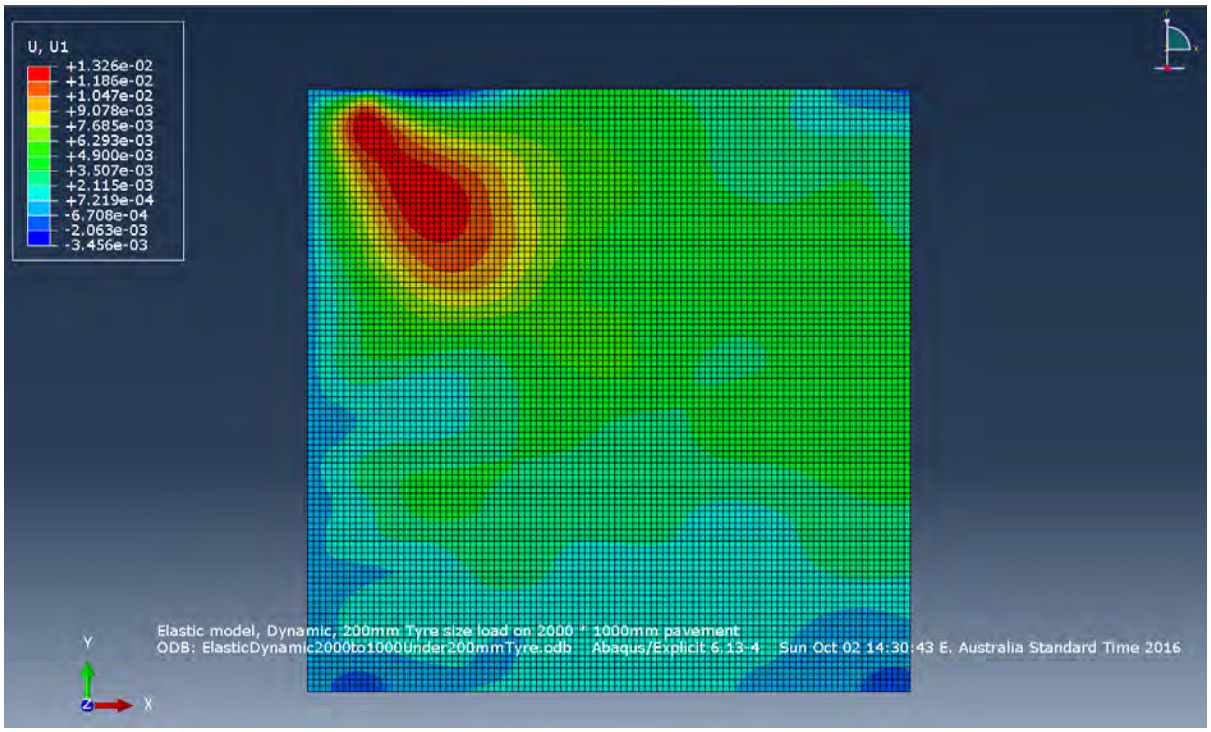

Figure 79: Full depth asphalt pavement, 2000×1000mm section under a 200mm tyre – U1 (deformation in the X direction).

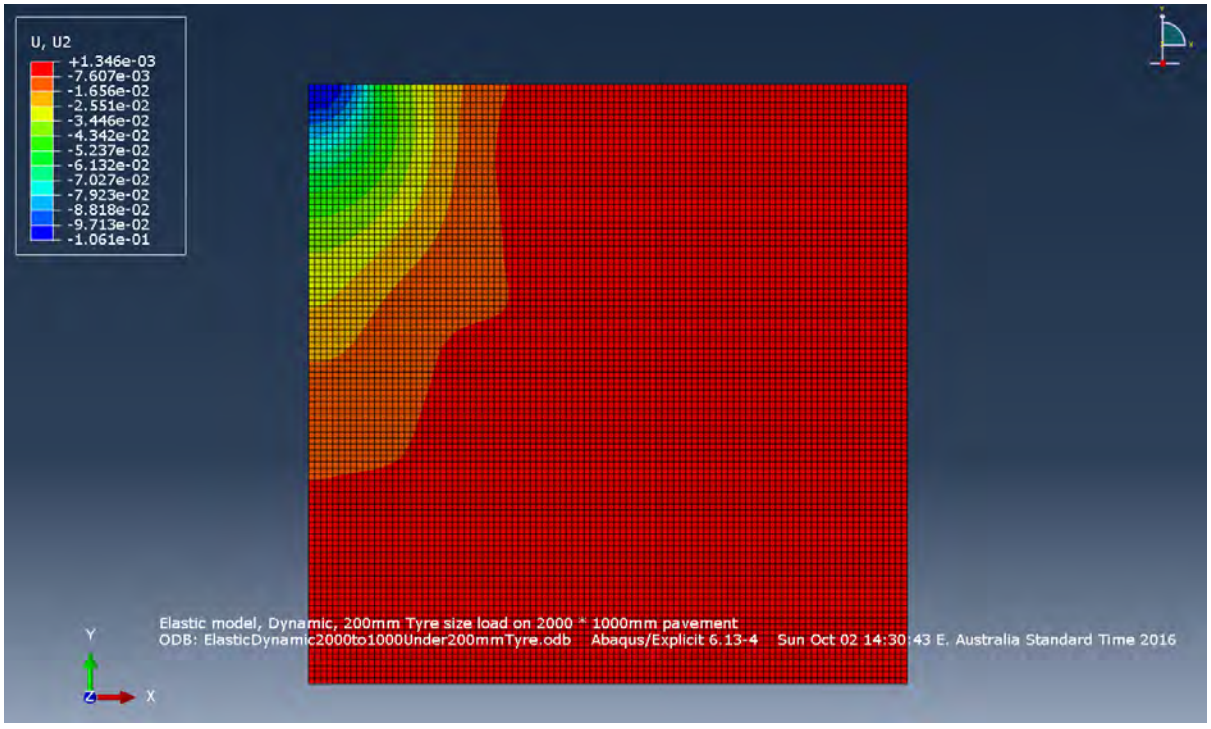

Figure 80: Full depth asphalt pavement, 2000×1000mm section under a 200mm tyre – U2 (deformation in the Y direction).

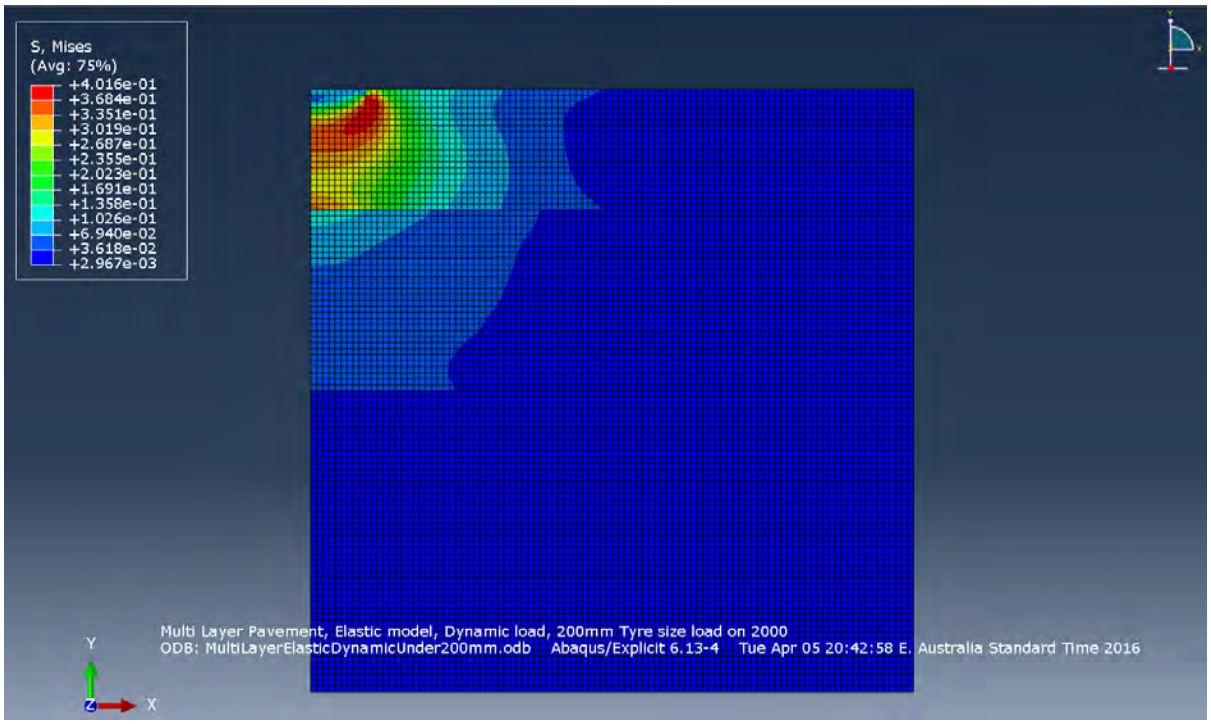

Figure 81: Multi-layer pavement 2000×1000mm section under a 200mm tyre – Mises stress.

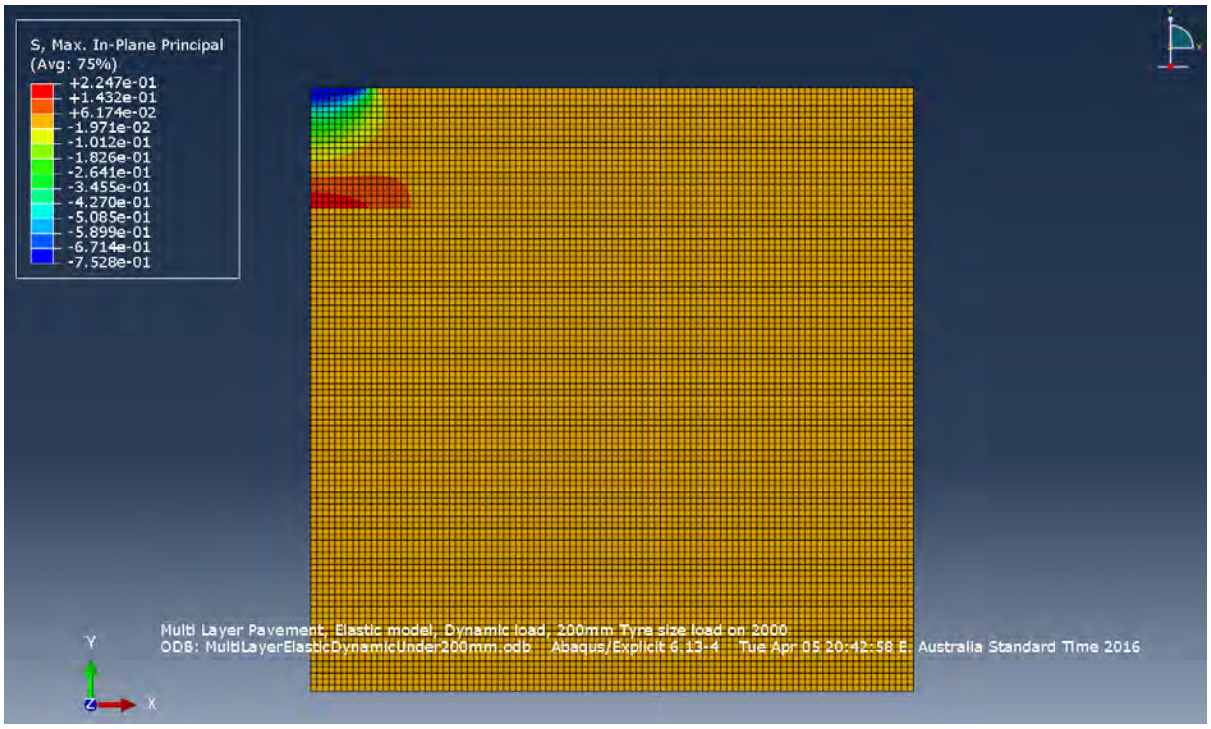

Figure 82: Multi-layer pavement 2000×1000mm section under a 200mm tyre – Max, In-Plane Principal stress.

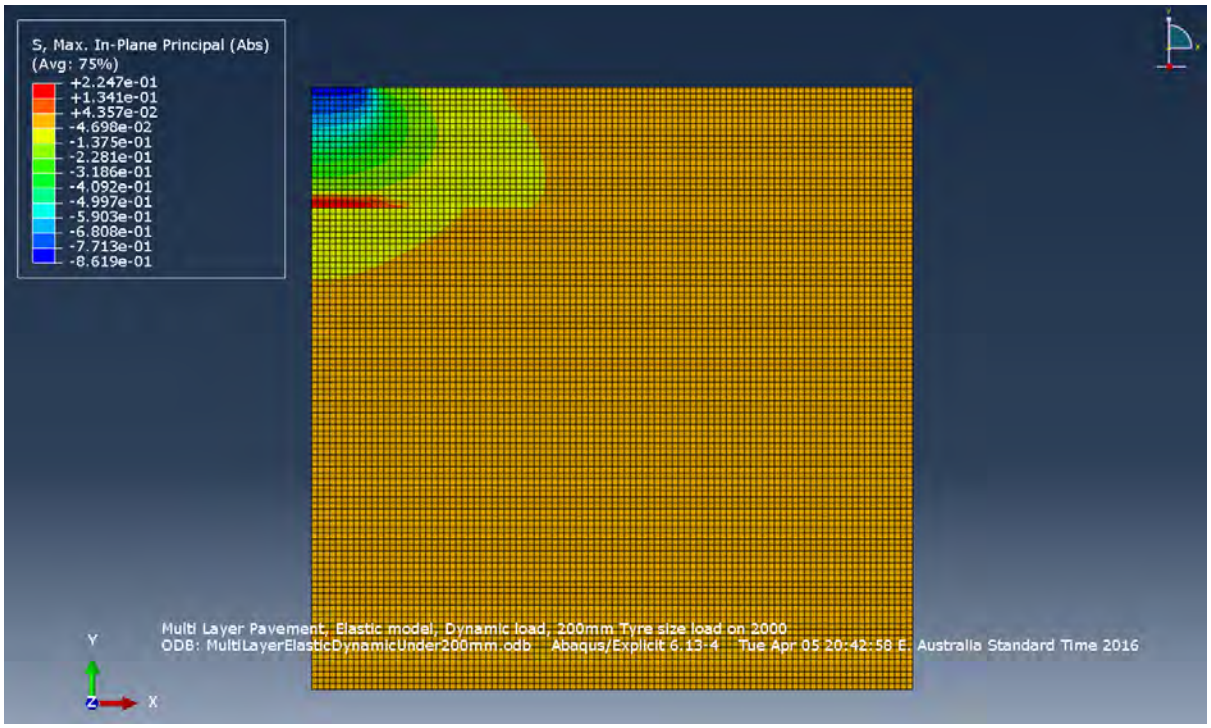

Figure 83: Multi-layer pavement 2000×1000mm section under a 200mm tyre – Max, In-Plane Principal (Abs) stress.

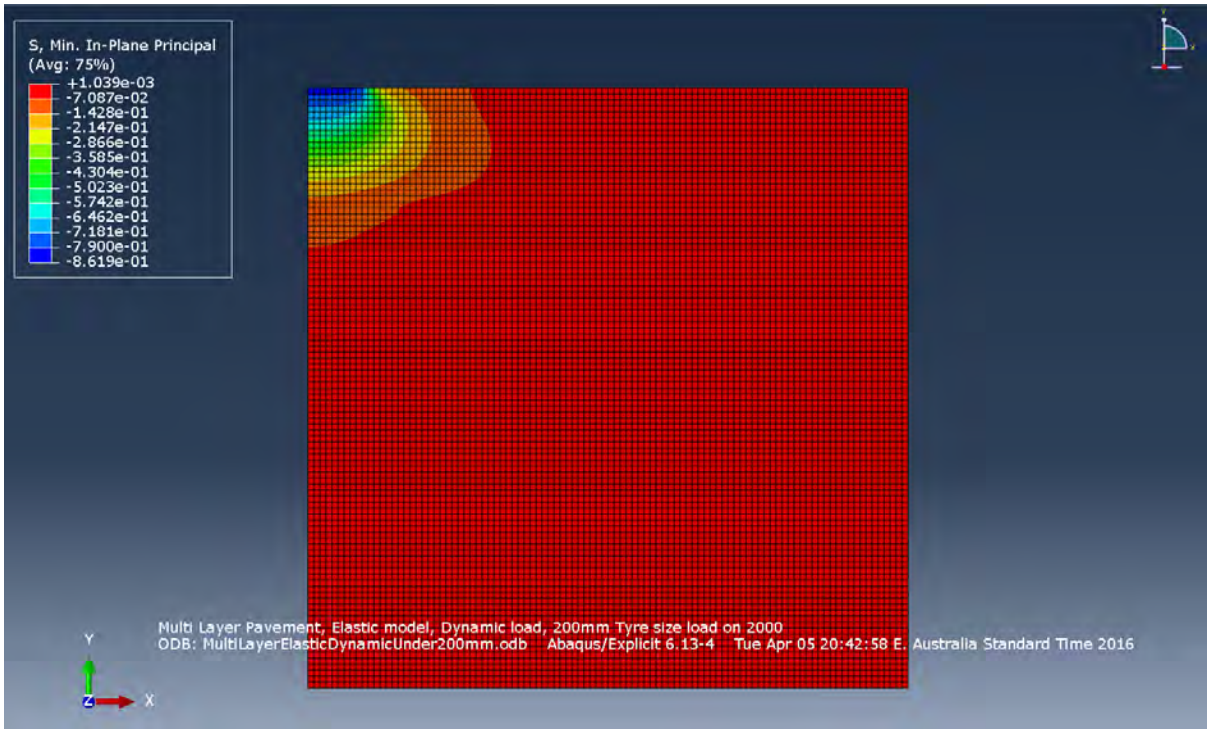

Figure 84: Multi-layer pavement 2000×1000mm section under a 200mm tyre – Min, In-Plane Principal stress.

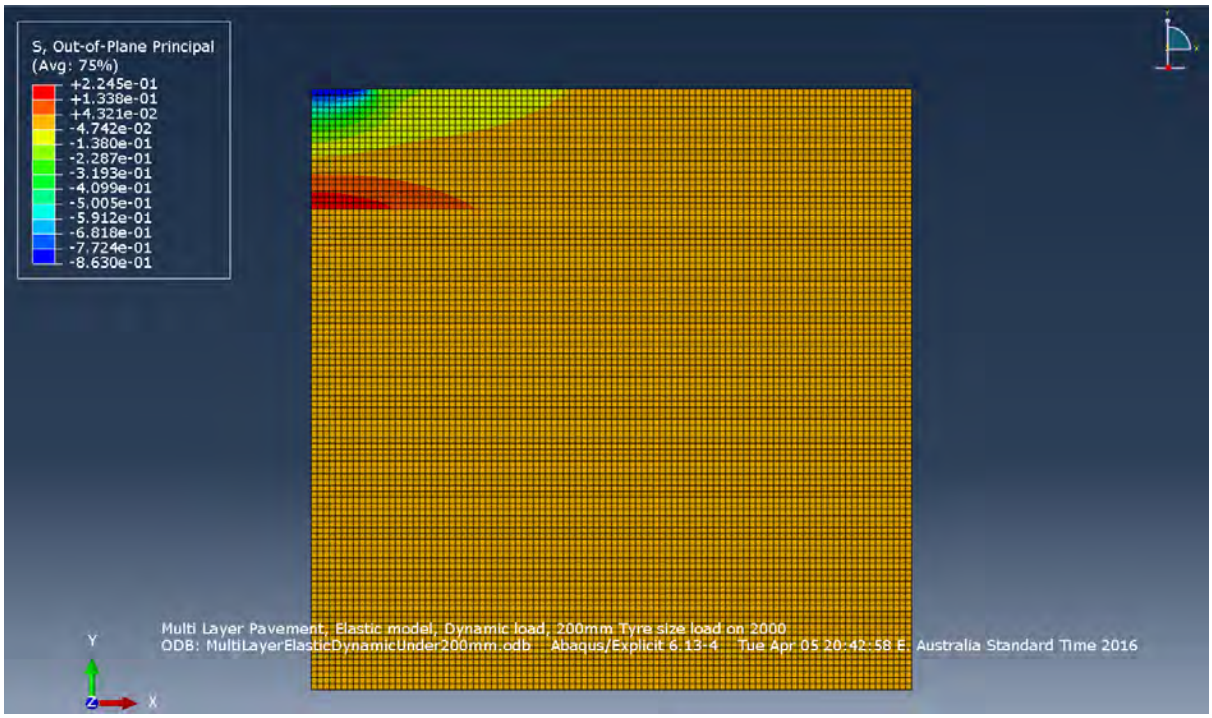

Figure 85: Multi-layer pavement 2000×1000mm section under a 200mm tyre – Out-of-Plane Principal stress.

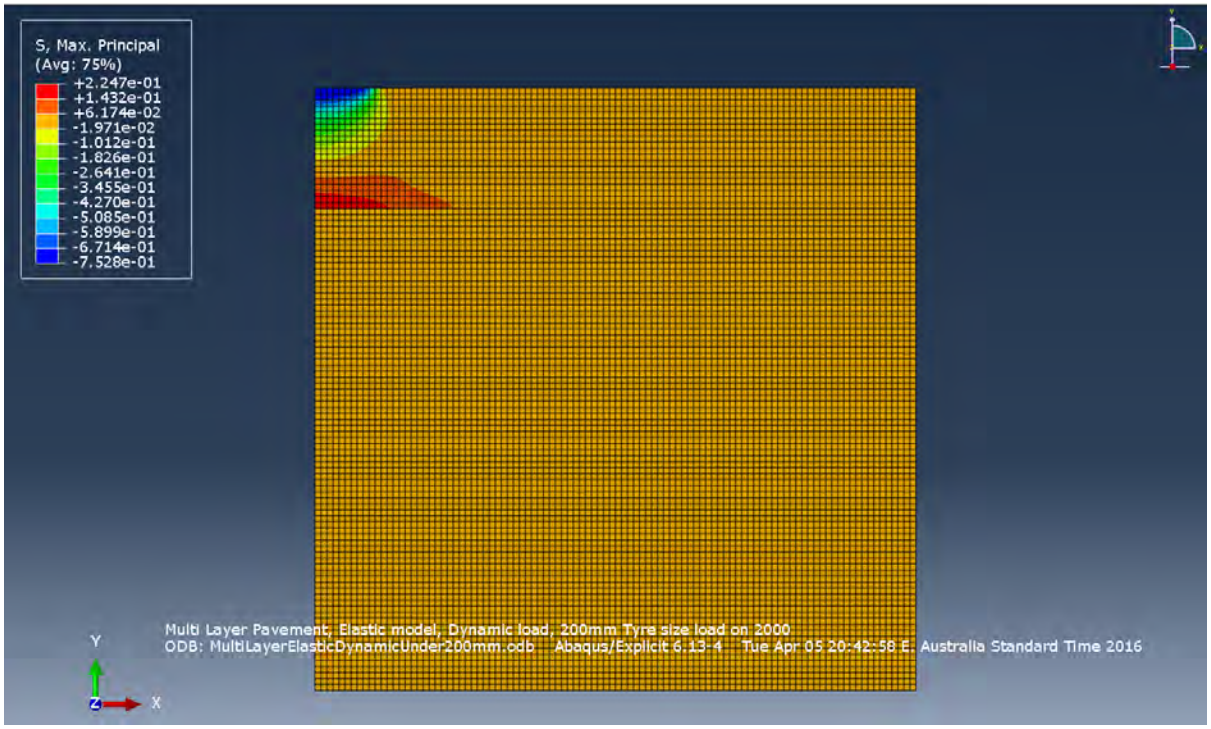

Figure 86: Multi-layer pavement 2000×1000mm section under a 200mm tyre – Max, Principal stress.

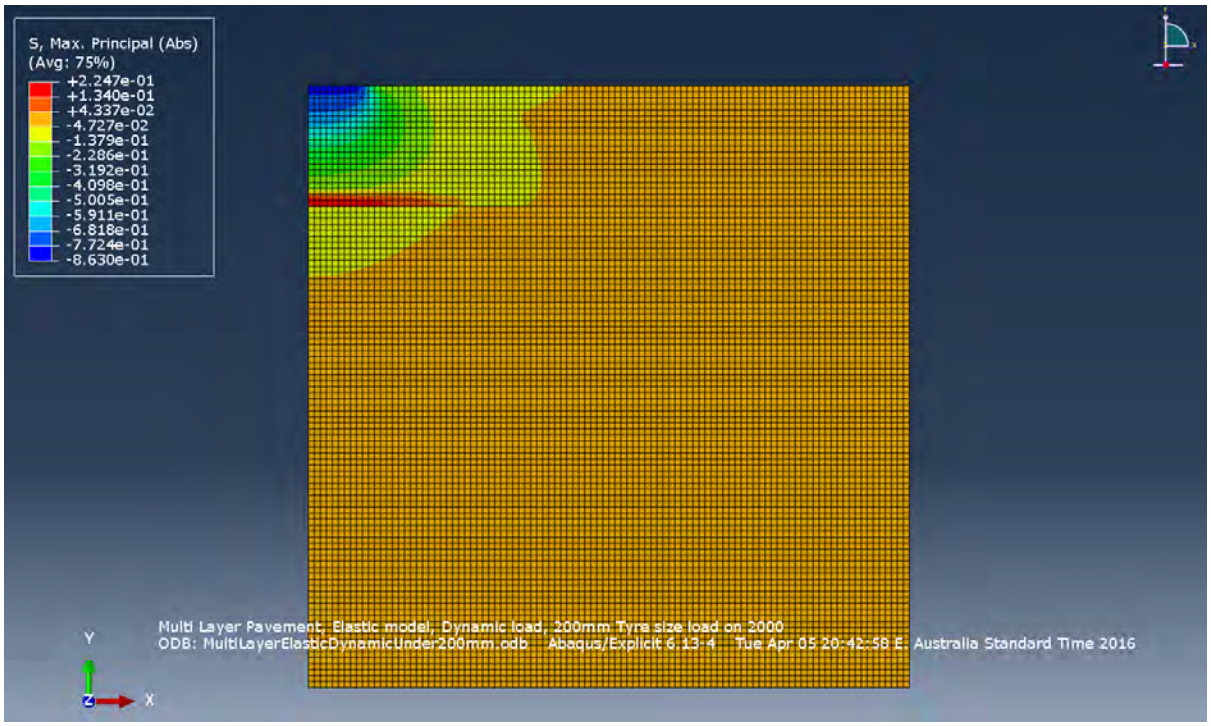

Figure 87: Multi-layer pavement 2000×1000mm section under a 200mm tyre – Max, Principal (Abs) stress.

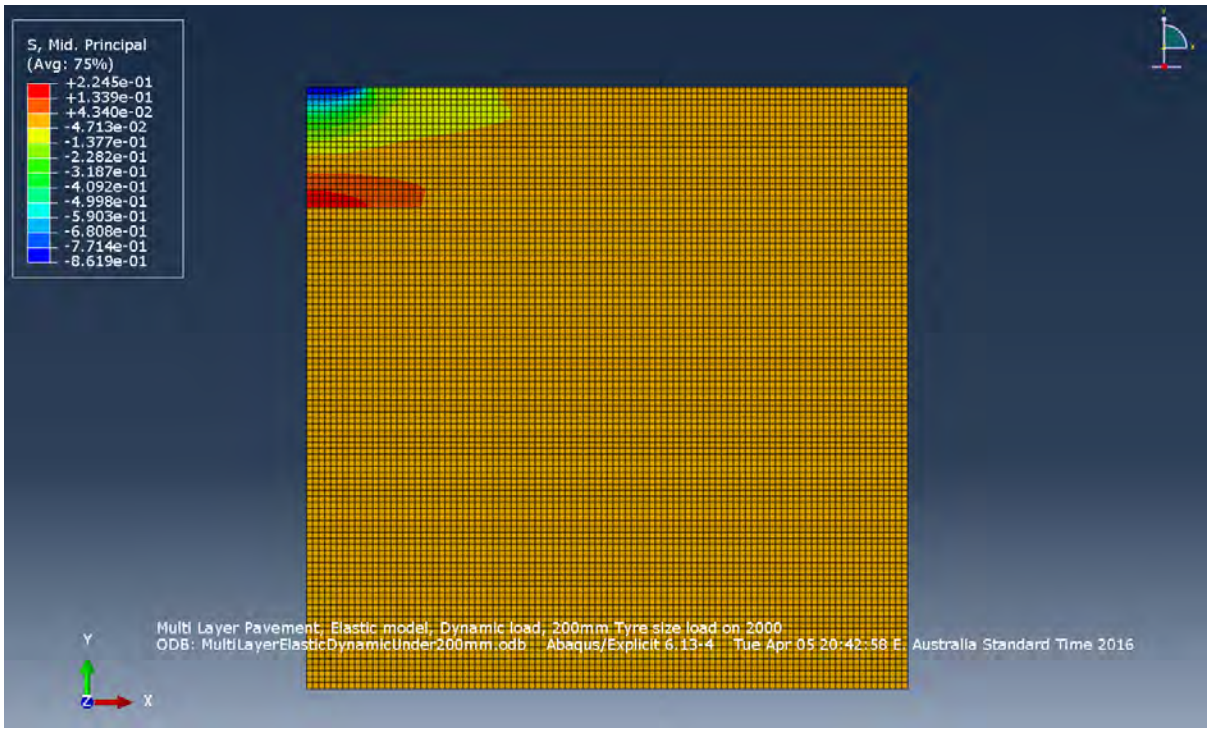

Figure 88: Multi-layer pavement 2000×1000mm section under a 200mm tyre – Mid. Principal stress.

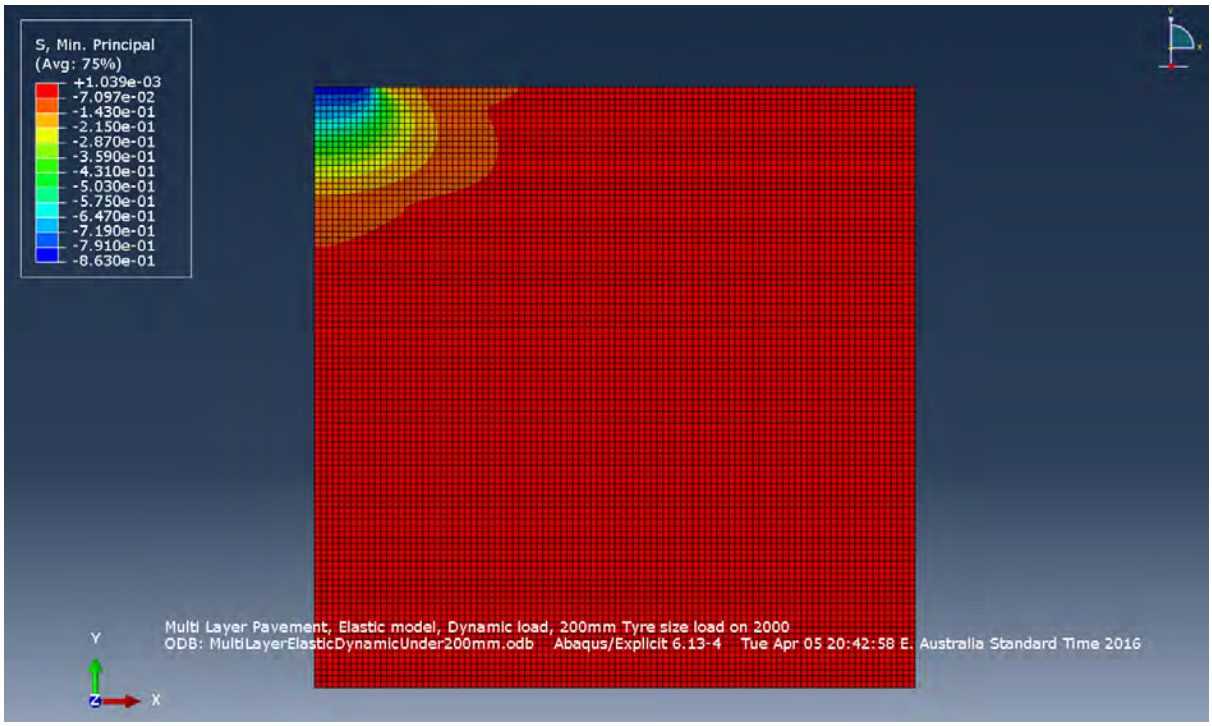

Figure 89: Multi-layer pavement 2000×1000mm section under a 200mm tyre – Min. Principal stress.

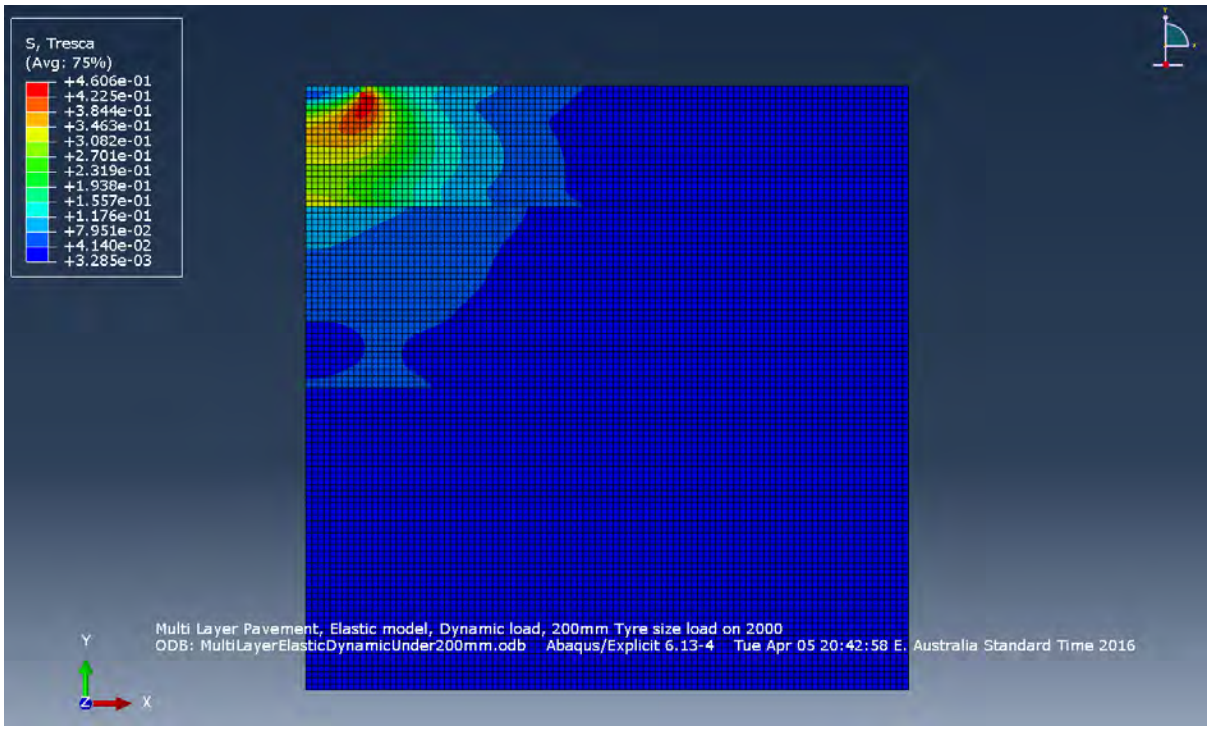

Figure 90: Multi-layer pavement 2000×1000mm section under a 200mm tyre – Tresca stress.

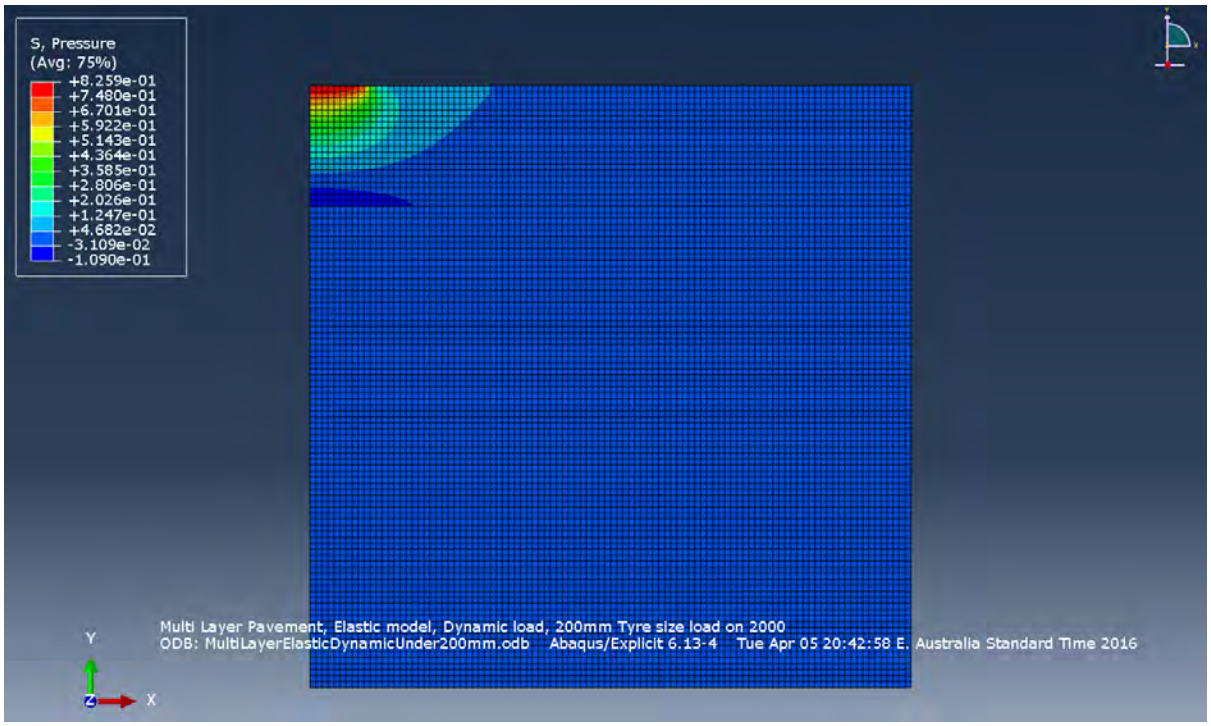

Figure 91: Multi-layer pavement 2000×1000mm section under a 200mm tyre – Pressure.

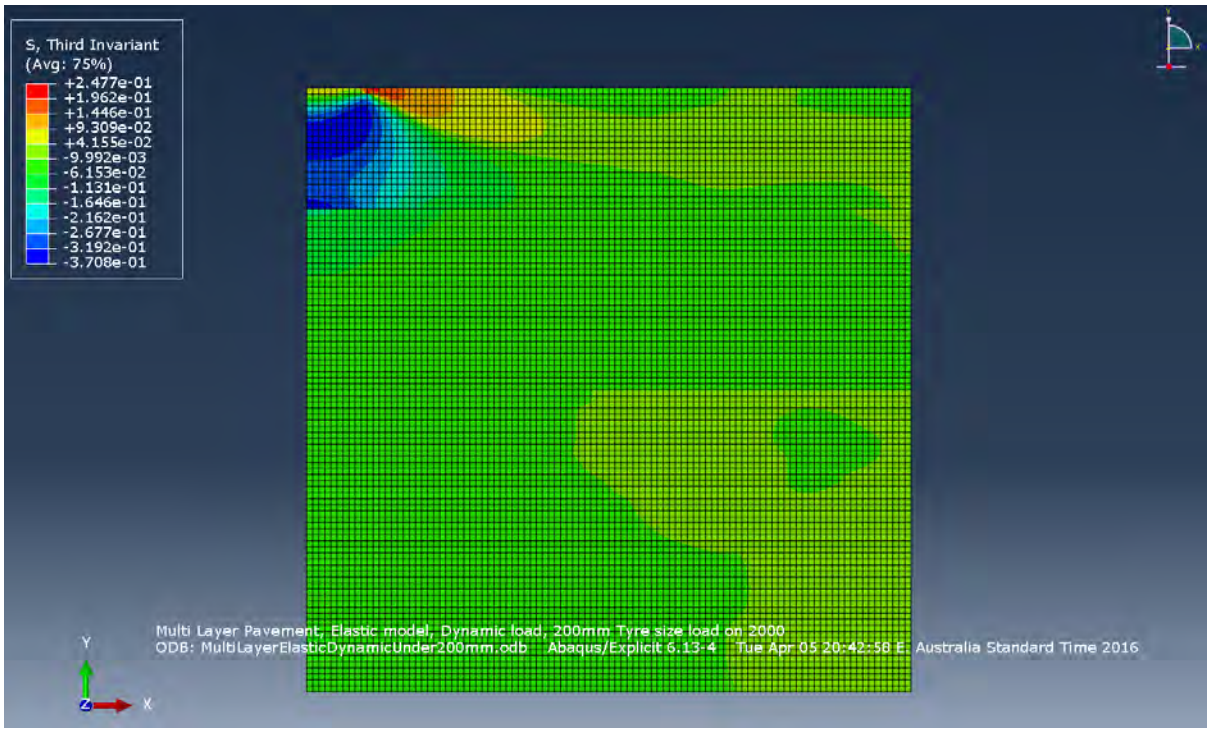

Figure 92: Multi-layer pavement 2000×1000mm section under a 200mm tyre –Third Invariant stress.

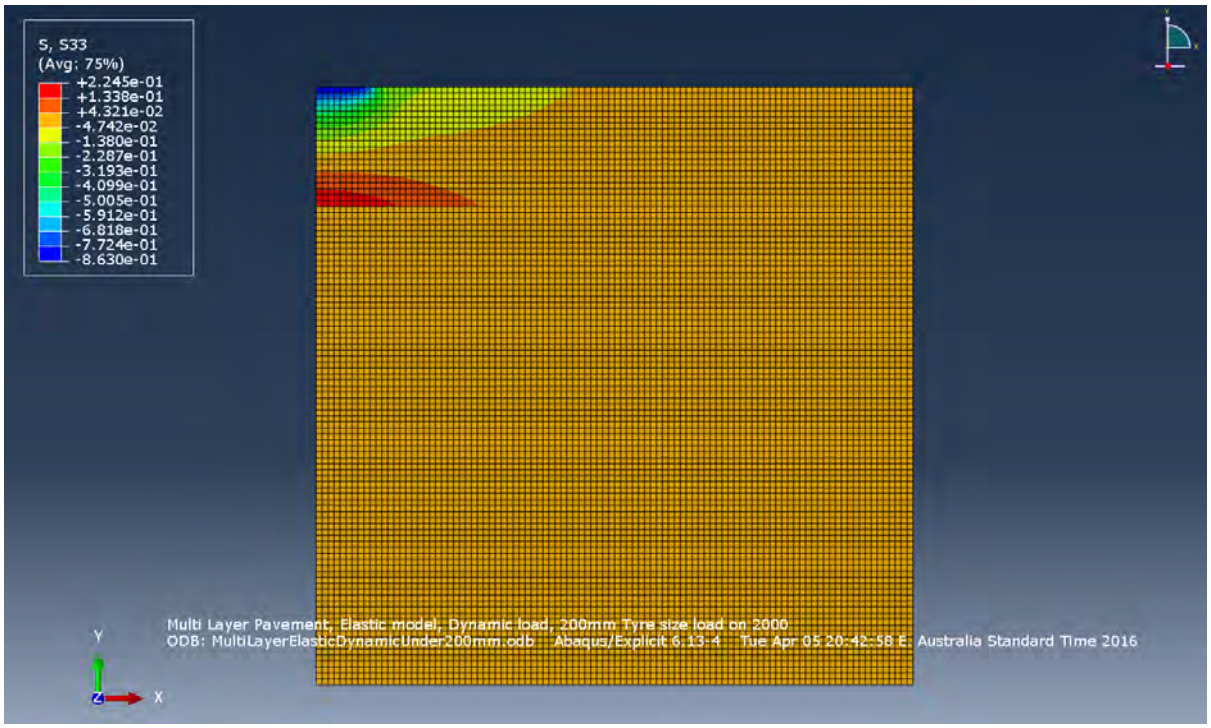

Figure 93: Multi-layer pavement 2000×1000mm section under a 200mm tyre – S33 stress (stress in the Z direction).

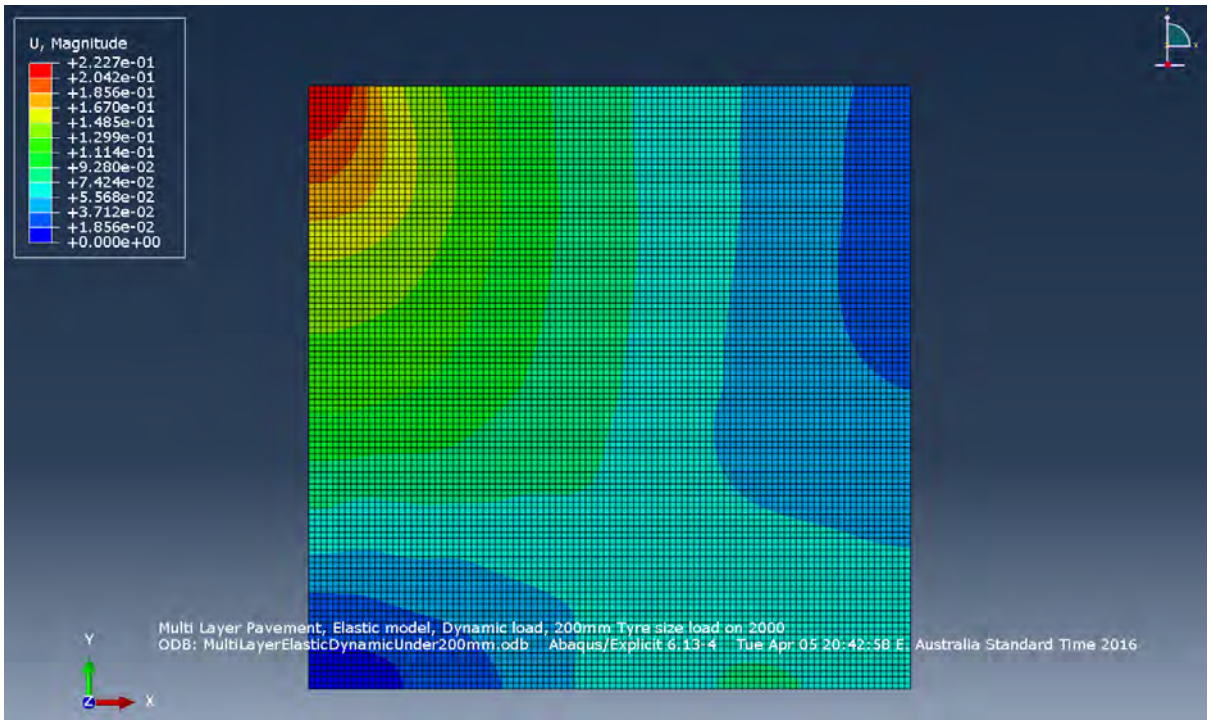

Figure 94: Multi-layer pavement 2000×1000mm section under a 200mm tyre – U (deformation) Magnitude.

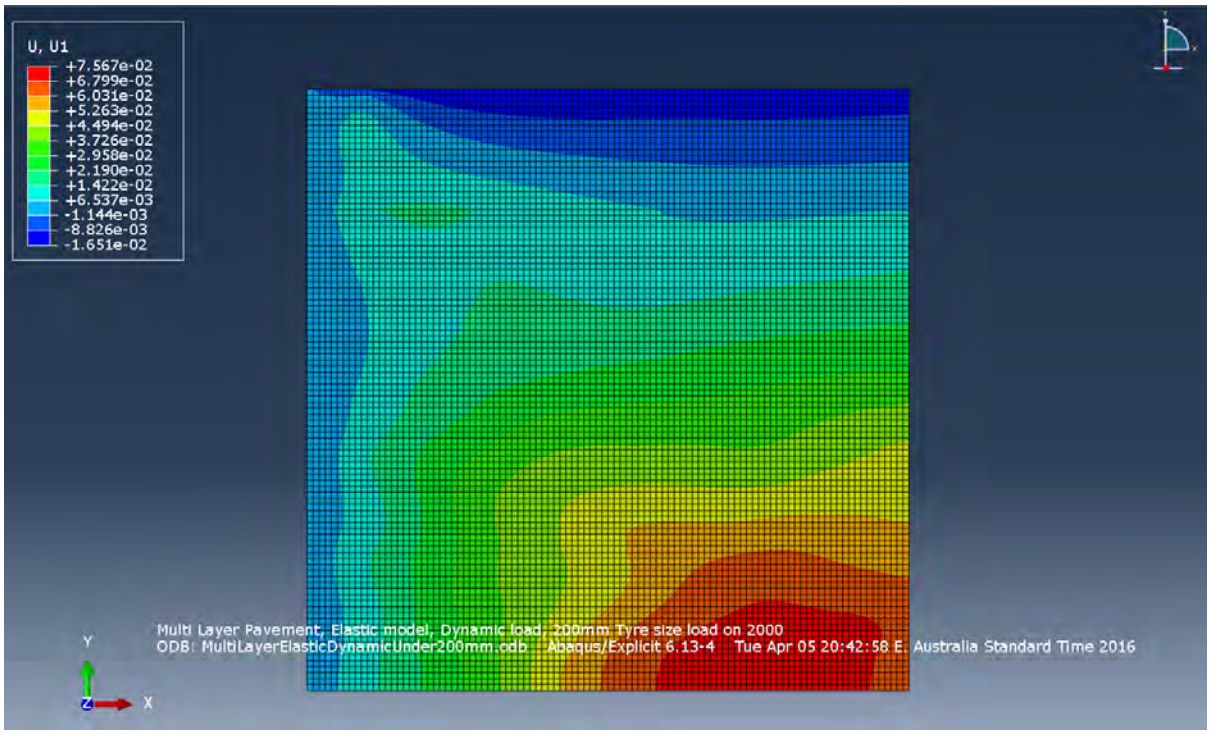

Figure 95: Multi-layer pavement 2000×1000mm section under a 200mm tyre – U1 (deformation in the X direction).

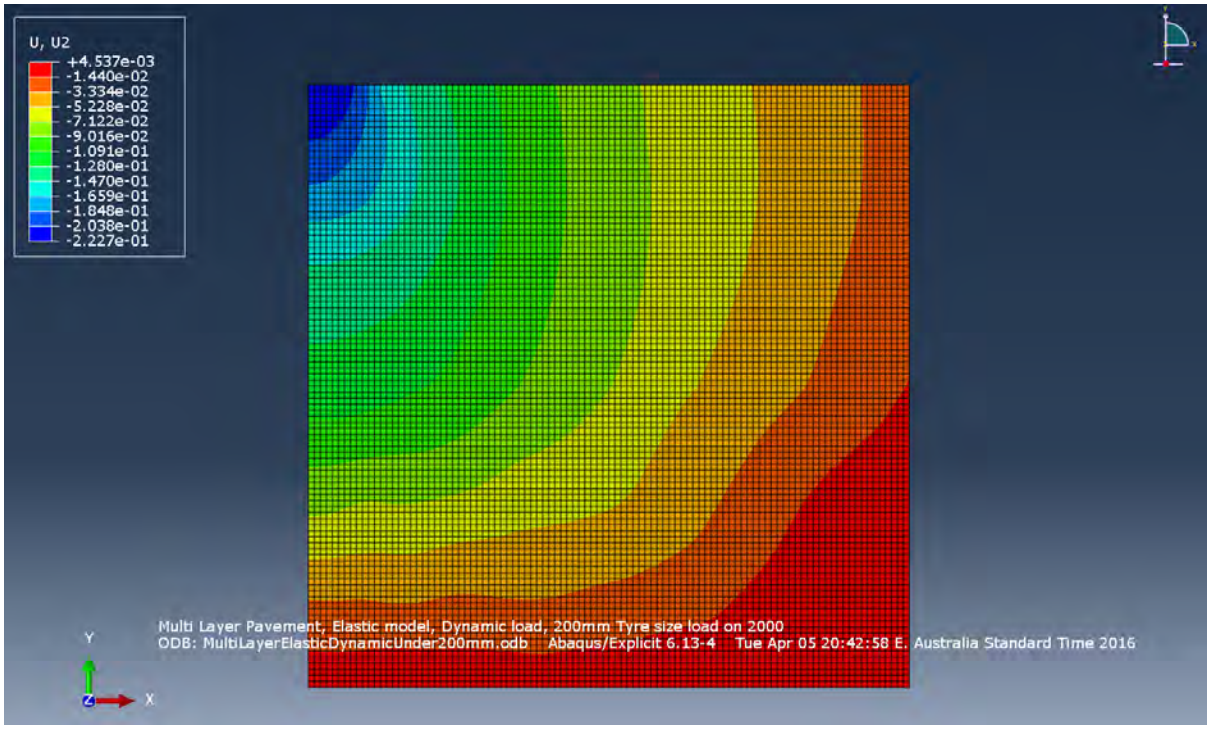

Figure 96: Multi-layer pavement 2000×1000mm section under a 200mm tyre – U2 (deformation in the Y direction).

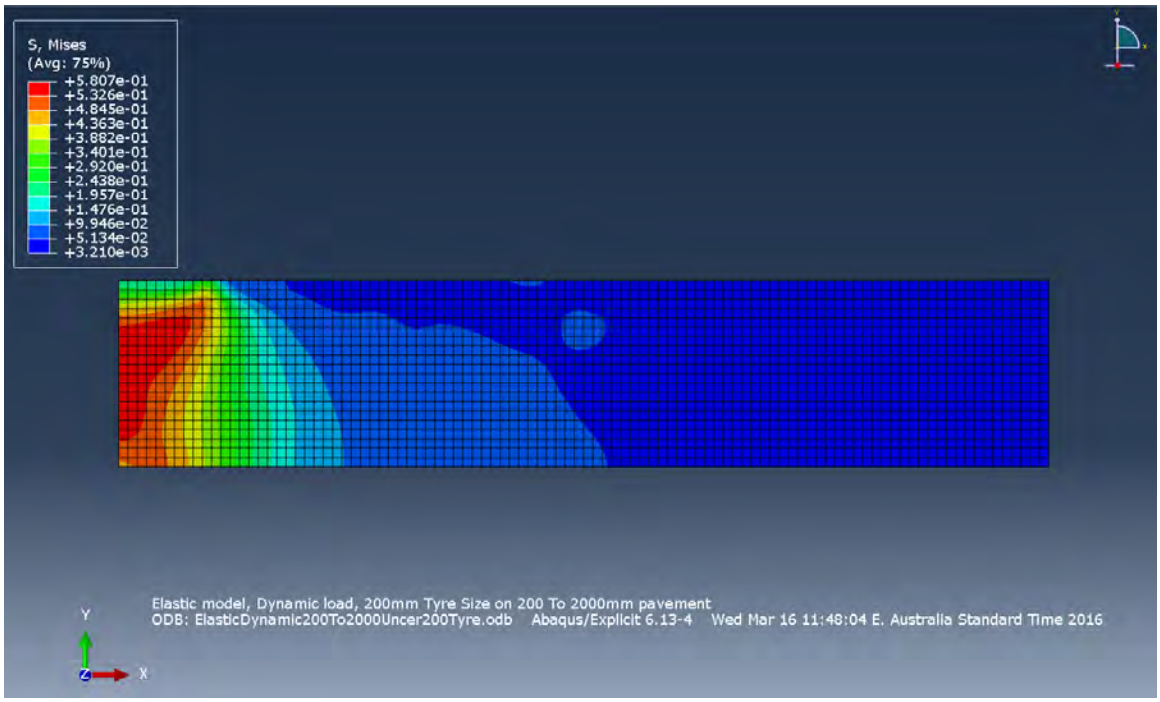

Figure 97: Single asphalt layer 200×2000mm section under a 200mm tyre – Mises stress.

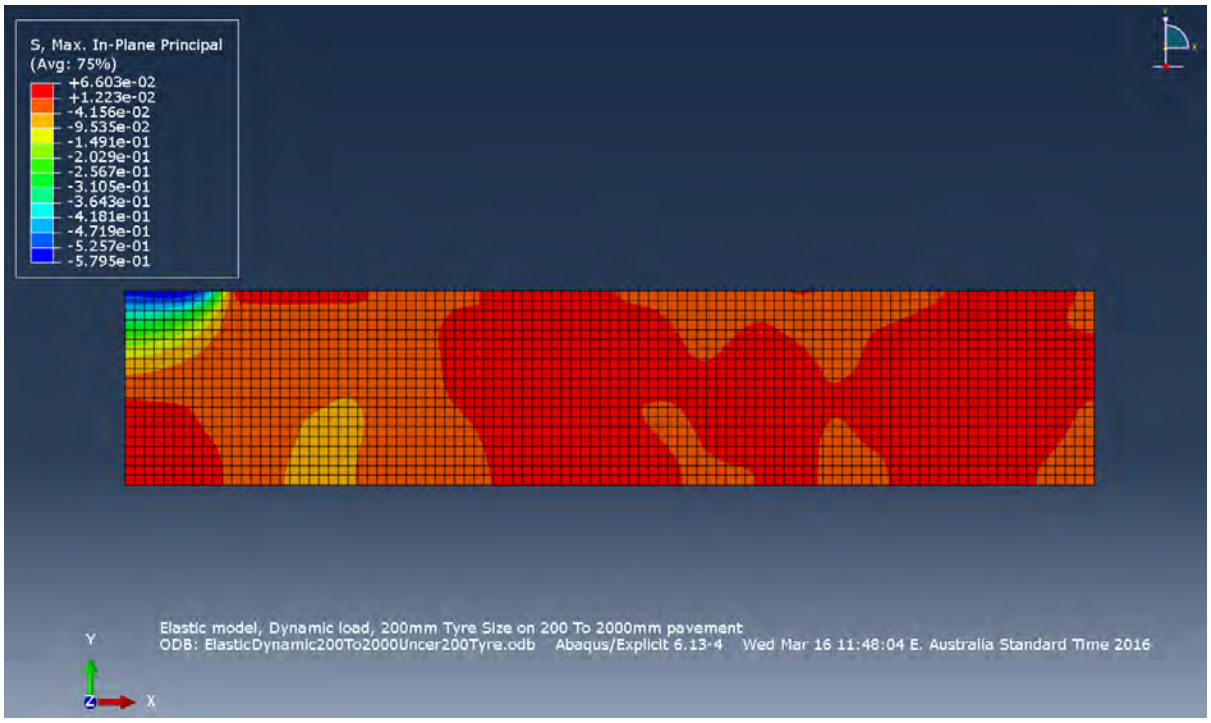

Figure 98: Single asphalt layer 200×2000mm section under a 200mm tyre – Max, In-Plane Principal stress.

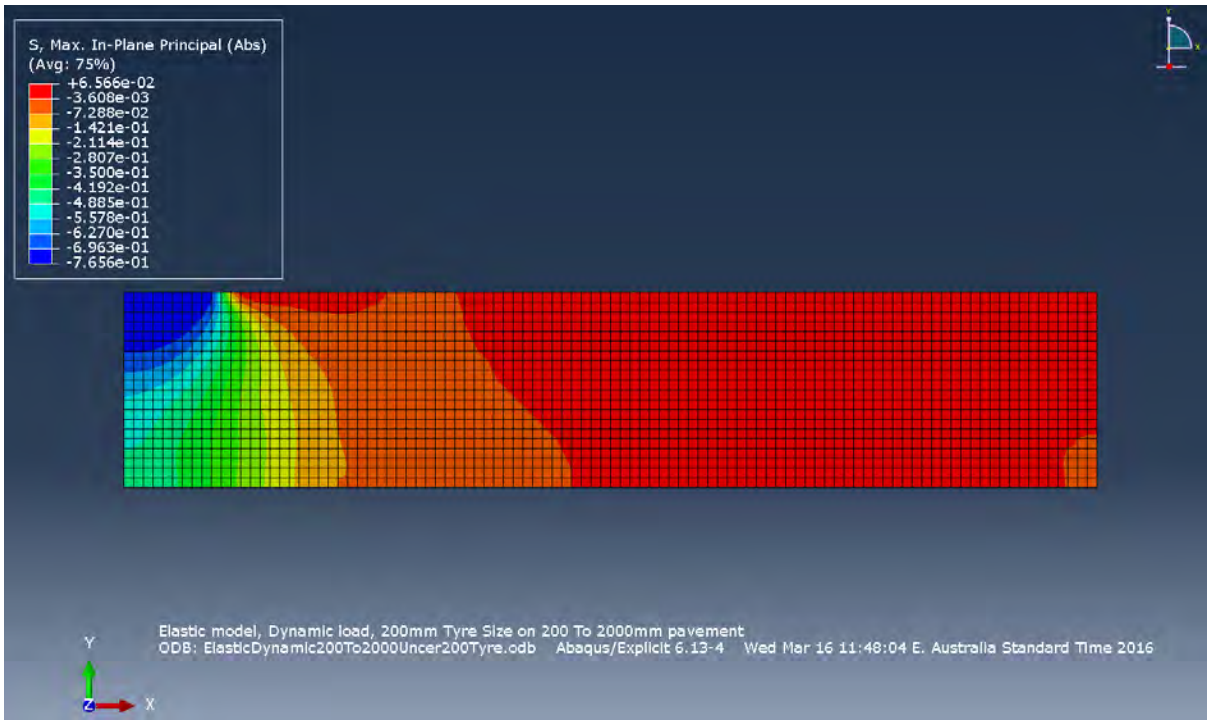

Figure 99: Single asphalt layer 200×2000mm section under a 200mm tyre – Max, In-Plane Principal (Abs) stress.

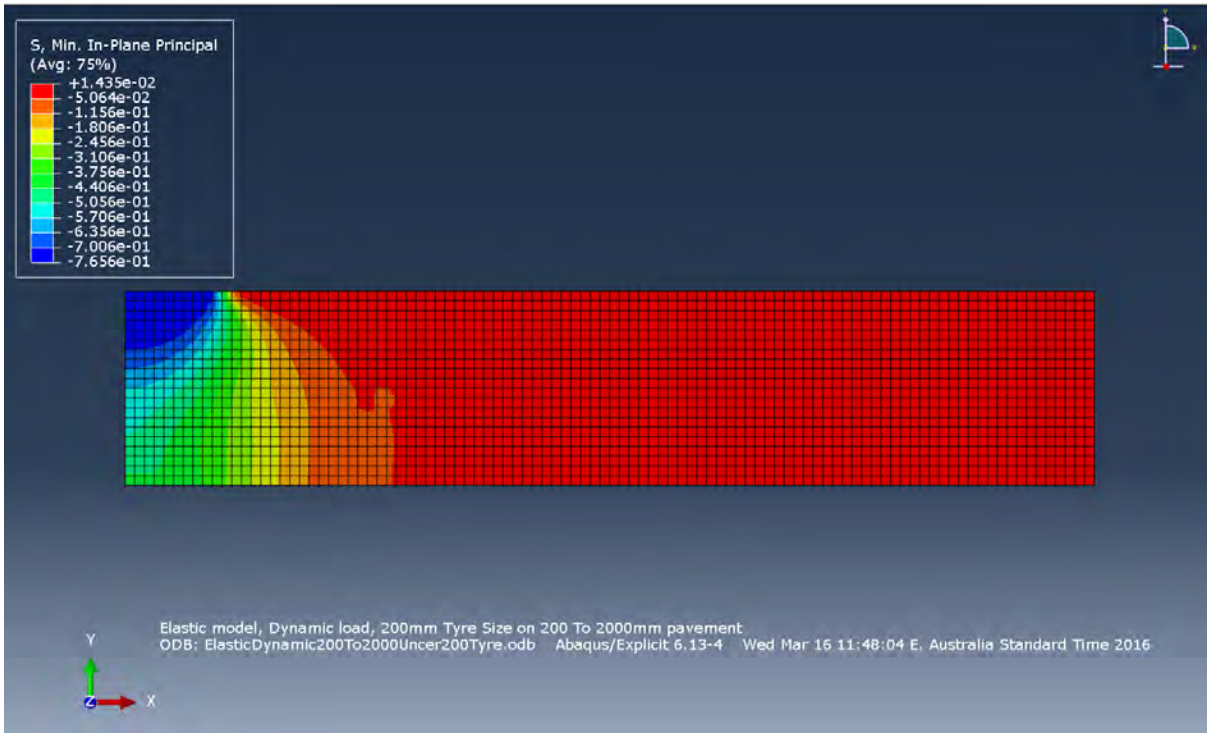

Figure 100: Single asphalt layer 200×2000mm section under a 200mm tyre – Min, In-Plane Principal stress.

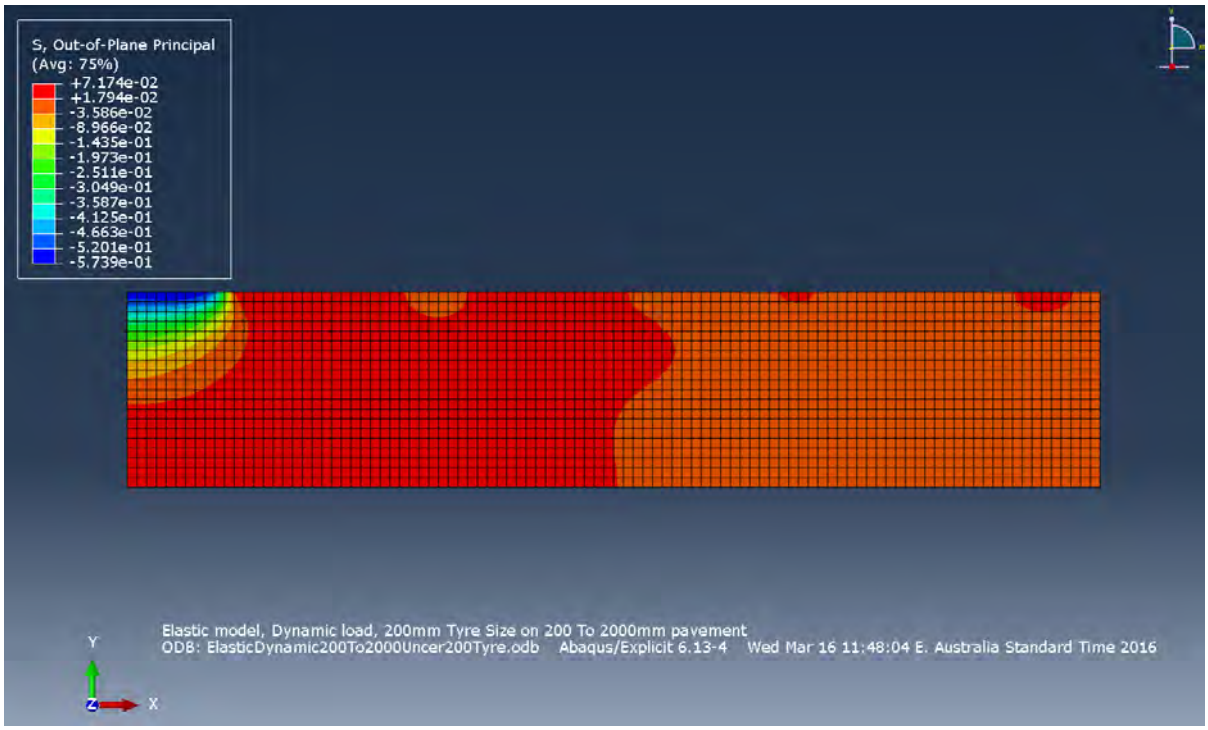

Figure 101: Single asphalt layer 200×2000mm section under a 200mm tyre – Out-of-Plane Principal stress.

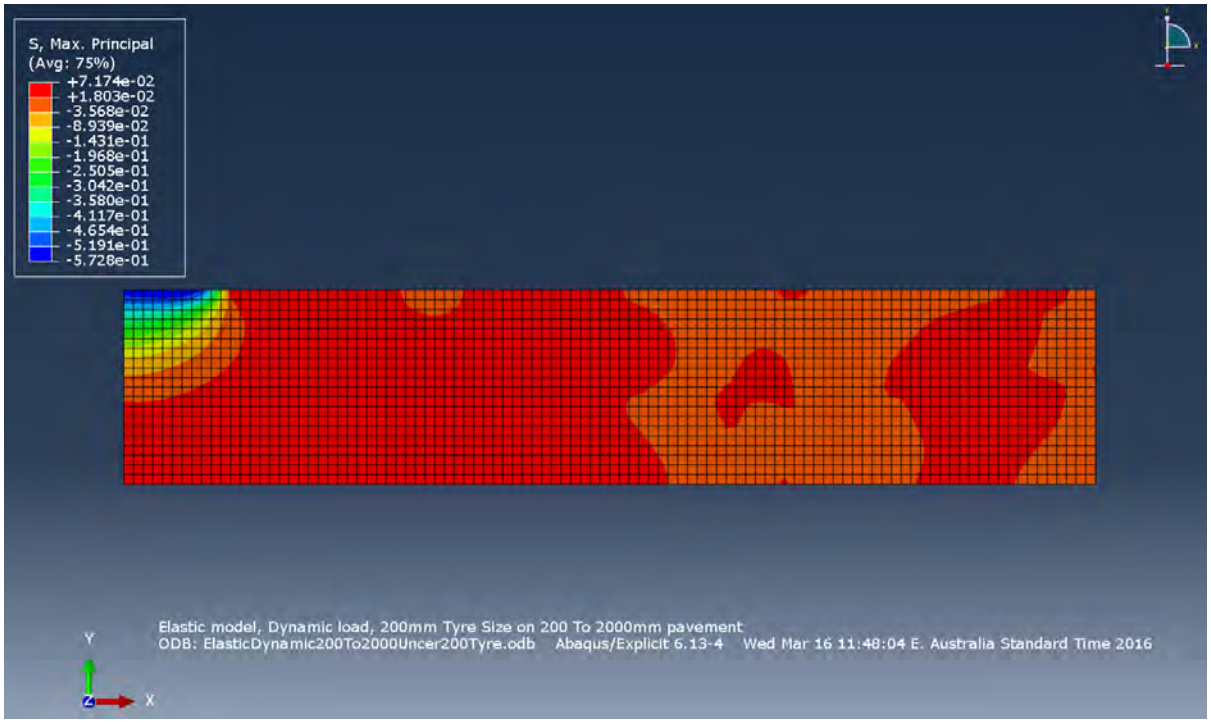

Figure 102: Single asphalt layer 200×2000mm section under a 200mm tyre – Max, Principal stress.

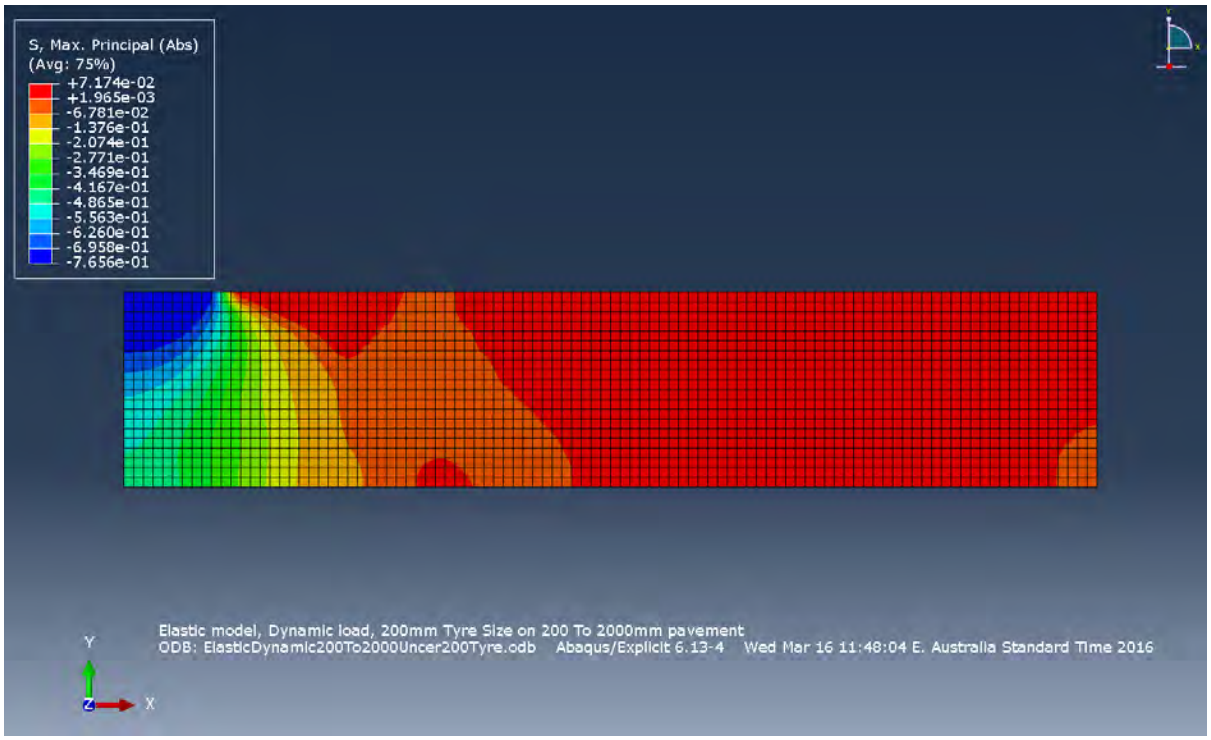

Figure 103: Single asphalt layer 200×2000mm section under a 200mm tyre – Max, Principal (Abs) stress.

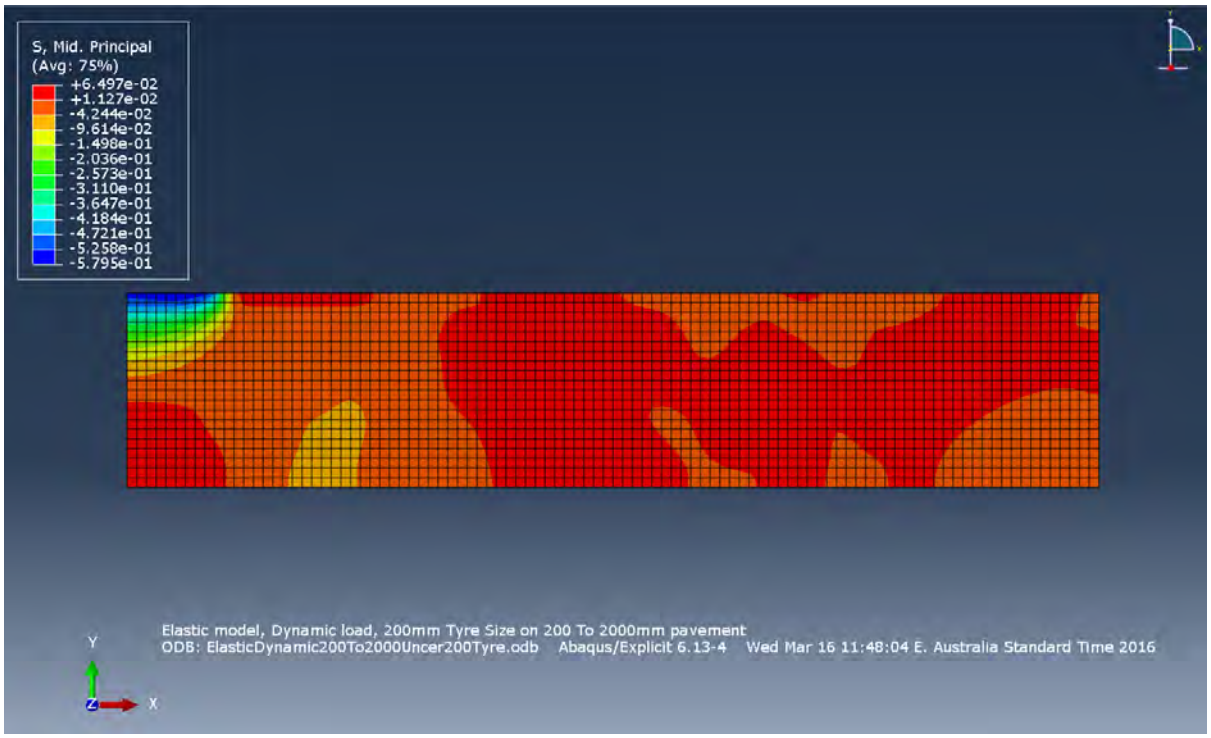

Figure 104: Single asphalt layer 200×2000mm section under a 200mm tyre – Mid. Principal stress.

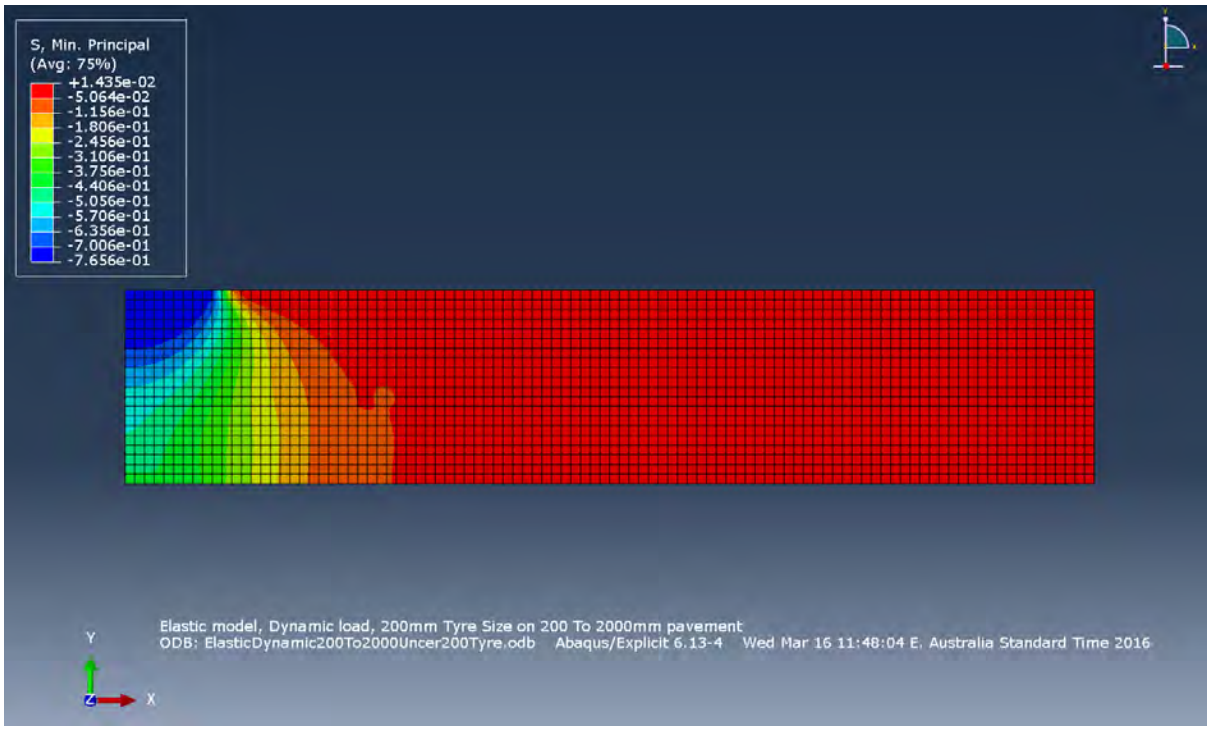

Figure 105: Single asphalt layer 200×2000mm section under a 200mm tyre – Min. Principal stress.

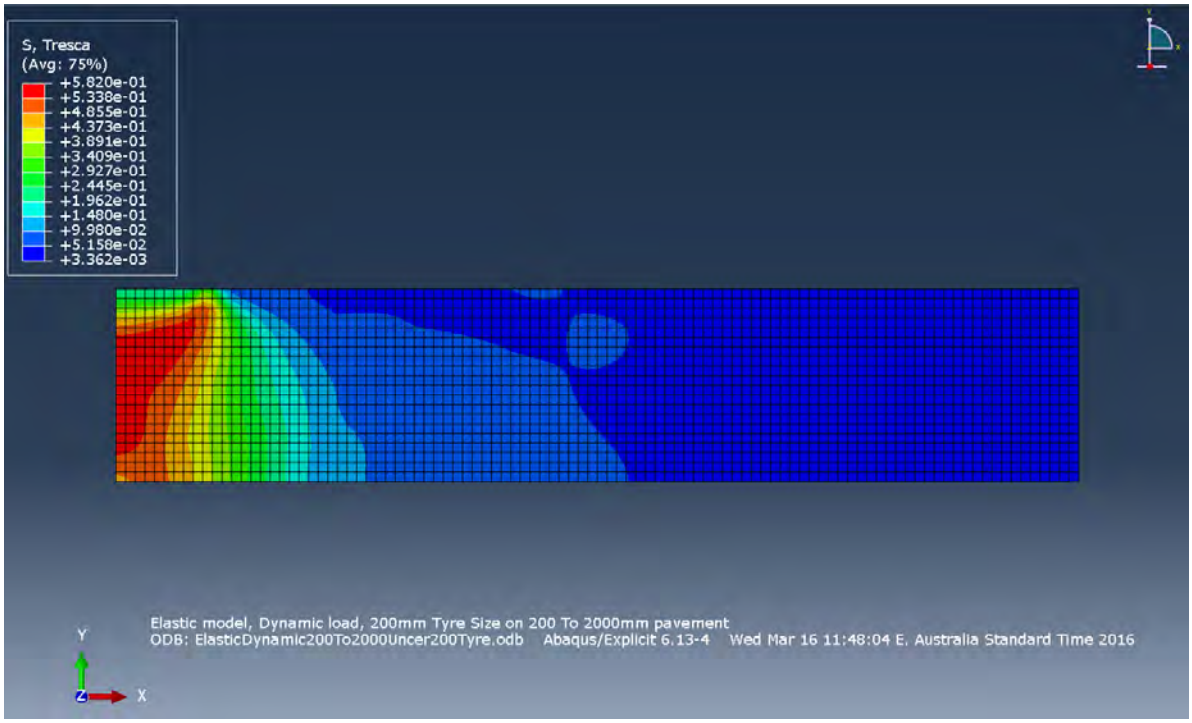

Figure 106: Single asphalt layer 200×2000mm section under a 200mm tyre – Tresca stress.

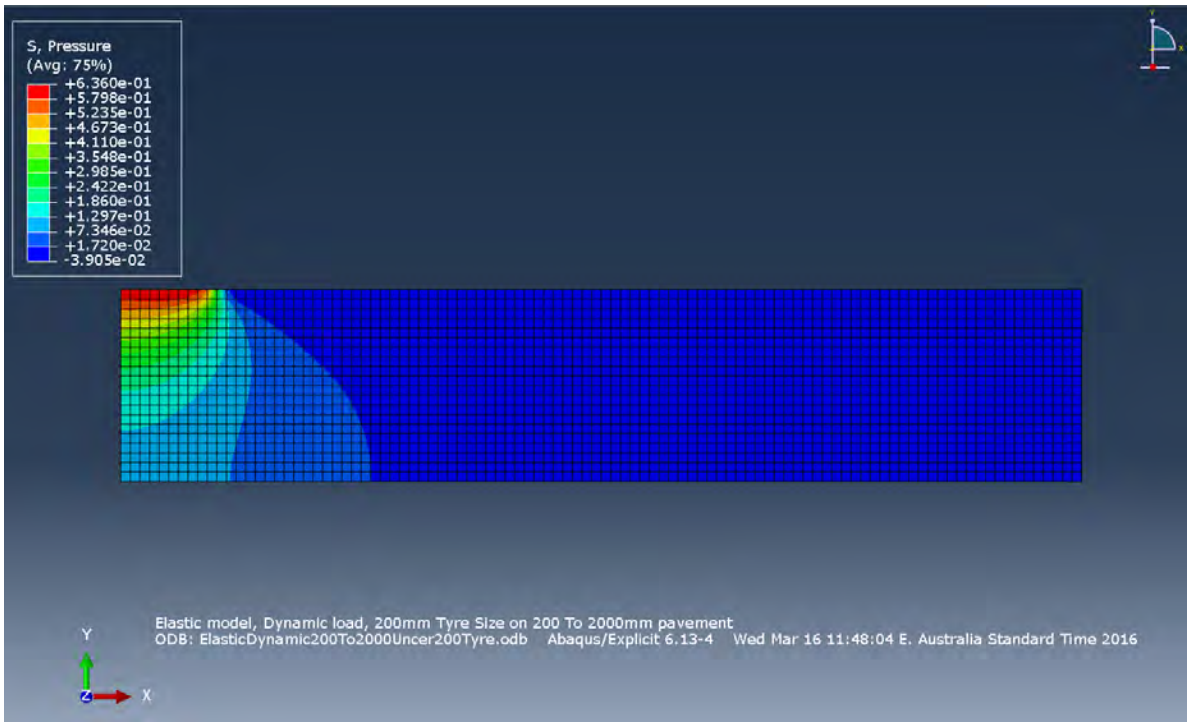

Figure 107: Single asphalt layer 200×2000mm section under a 200mm tyre – Pressure.

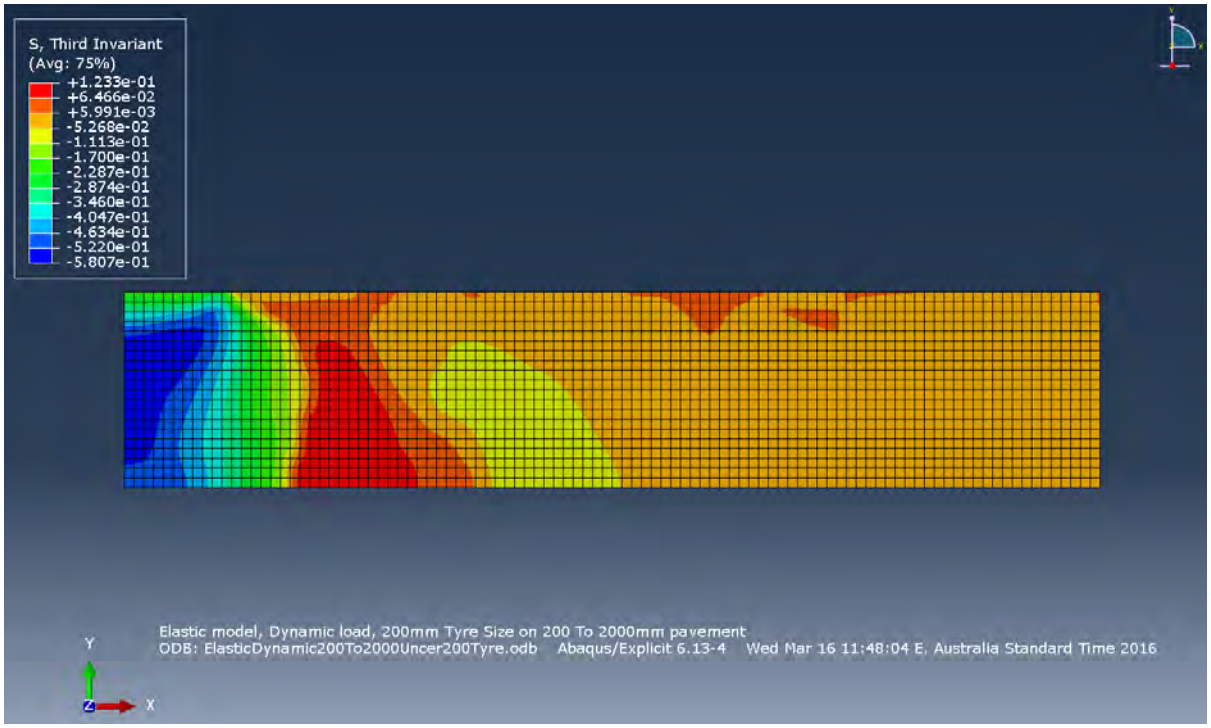

Figure 108: Single asphalt layer 200×2000mm section under a 200mm tyre –Third Invariant stress.

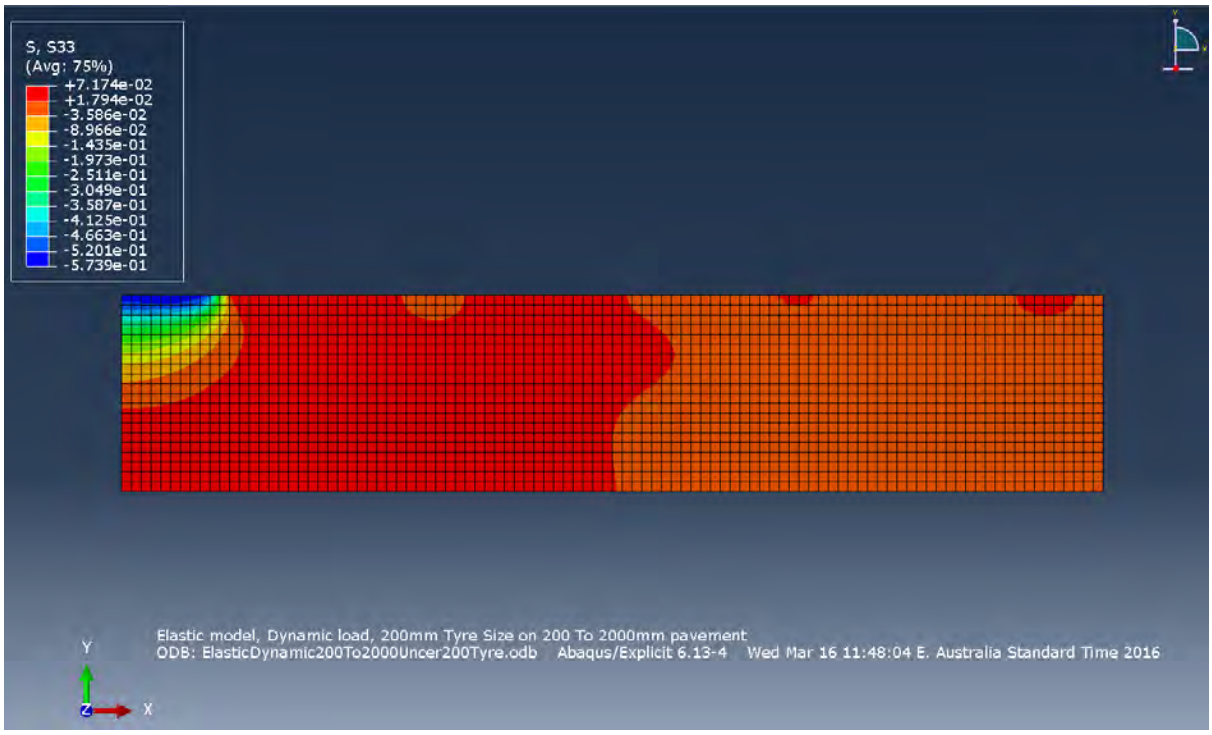

Figure 109: Single asphalt layer 200×2000mm section under a 200mm tyre – S33 stress (stress in the Z direction).

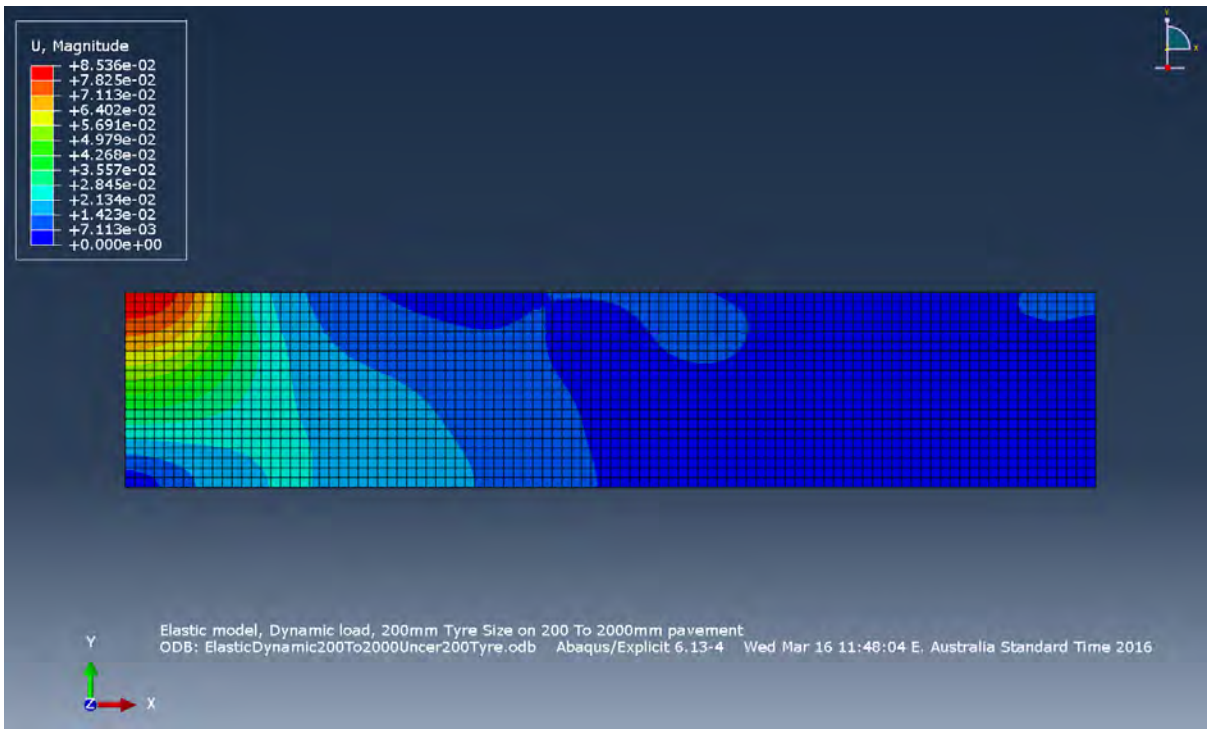

Figure 110: Single asphalt layer 200×2000mm section under a 200mm tyre – U (deformation) Magnitude.

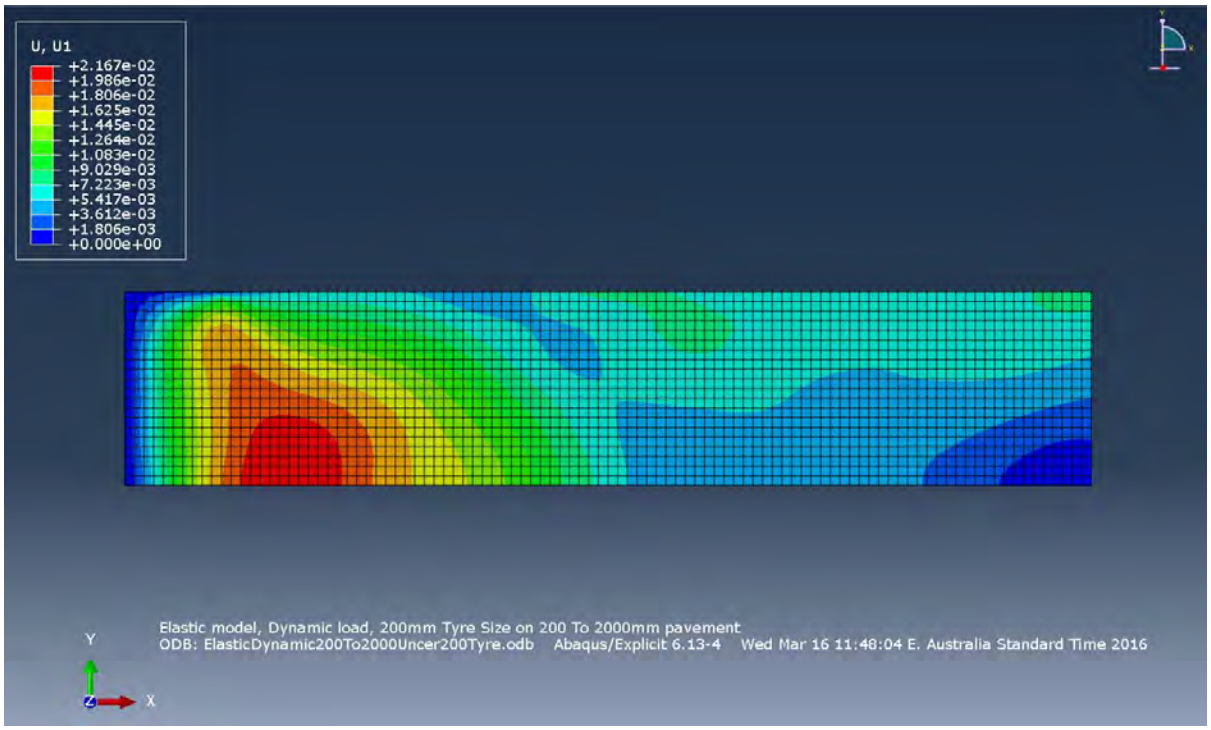

Figure 111: Single asphalt layer 200×2000mm section under a 200mm tyre – U1 (deformation in the X direction).

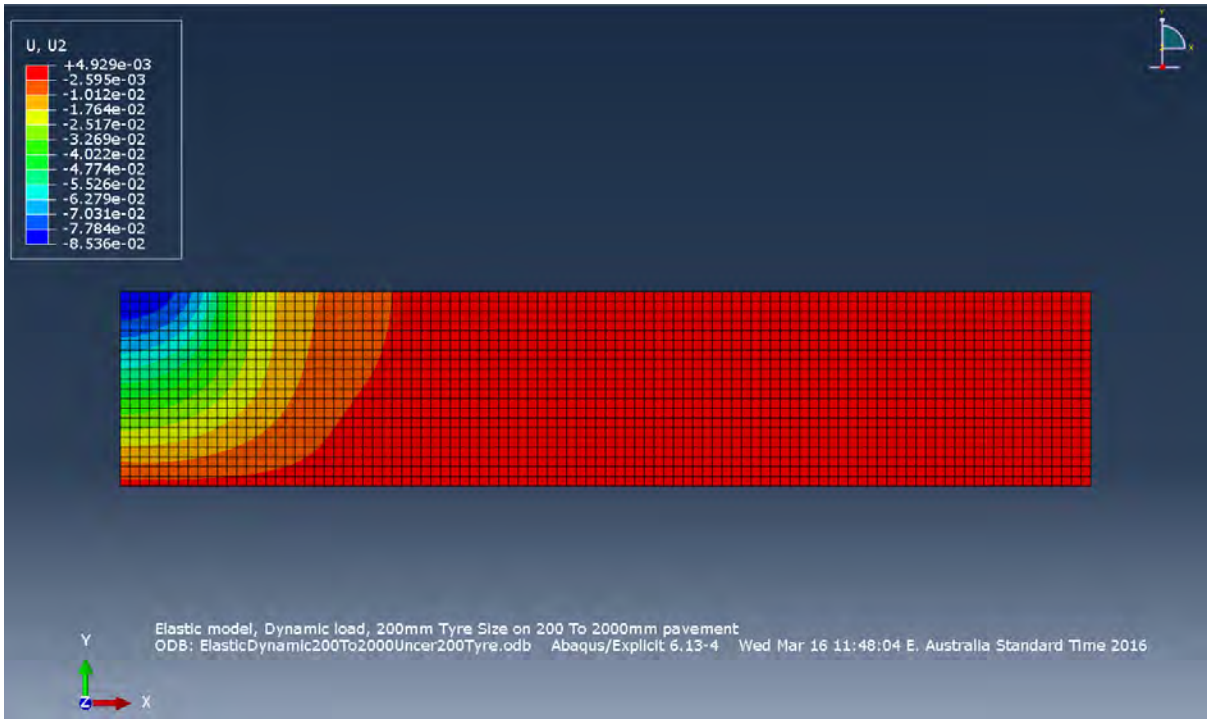

Figure 112: Single asphalt layer 200×2000mm section under a 200mm tyre – U2 (deformation in the Y direction).